technische universität
dortmund

Cosmological Consequences of Lepton Number Violation in the Majoron Model

DISSERTATION

zur Erlangung des akademischen Grades

DR.RER.NAT

TIM BRUNE

geboren in Dortmund

Fakultät Physik

Technische Universität Dortmund

Dortmund, 2025

Erstgutachter: Prof. Dr. Heinrich Päs
Zweitgutachterin: Prof. Dr. Gudrun Hiller
Vorsitzender der Prüfungskomission: JProf. Dr. Armin Lühr
Mitglied der Prüfungskomission: Dr. Dirk Wiedner

Datum des Einreichens der Arbeit: 21.05.2025
Datum der mündlichen Prüfung: 08.07.2025

Publications:

[1] Tim Brune, Thomas W. Kephart, and Heinrich Päs. "Muon $g - 2$ Anomaly from Vector-like Leptons in a 2-Higgs-doublet + Scalar Singlet Model". In: *The European Physical Journal C* 84.12 (Dec. 2024), p. 1254. DOI: 10.1140/epjc/s10052-024-13617-5. arXiv: 2205.05566 [hep-ph].

[2] Tim Brune. "Leptogenesis in Majoron Models without Domain Walls". In: *Physical Review D* 107.9 (May 2023), p. 096023. DOI: 10.1103/PhysRevD.107.096023. arXiv: 2201.12239 [hep-ph].

[3] Tim Brune. "Leptogenesis in a Majoron plus triplet model". In: *Phys. Rev. D* 111.11 (June 2025), p. 115001. DOI: 10.1103/tbsx-7ffr. arXiv: 2501.11529 [hep-ph].

Abstract

In this thesis, we explore two hypothetical extensions of the Standard Model of particle physics. First, we discuss implications of the Majoron model for neutrino mass generation with regard to the appearance of cosmic domain walls before performing an in-depth study of leptogenesis in a Majoron model that is extended by an additional right-handed $SU(2)_L$ triplet. We find that successful leptogenesis in this scenario is in principle possible and that the results partially apply also to the generic Majoron model. Second, we disuss an extension of the Standard Model containing vector-like leptons and new scalars as a solution to the discrepancy between the observed and predicted anomalous magnetic moment of the muon. We find that the model permits contributions to the anomalous magnetic moment that are compatible with experimental data, while simultaneously being in agreement with other experimental bounds on the model parameters.

Kurzfassung

In dieser Arbeit werden Erweiterungen des Standard Modells untersucht. Zunächst werden die Implikationen des Majoron-Modells für die Erzeugung von Neutrinomassen im Hinblick auf das Auftreten von Domänenwänden untersucht. Im Anschluss wird Leptogenese in einem Majoron-Modell diskutiert, welches um ein zusätzliches rechtshändiges $SU(2)_L$-Triplet erweitert wird. Es zeigt sich, dass Leptogenese in diesem Szenario möglich ist und die Ergebnisse teilweilse auf generische Majoron-Modelle übertragbar sind. Außerdem wird eine Erweiterung des Standardmodells um vektorartige Leptonen und zusätzliche Skalare als Lösung für die Diskrepanz zwischen dem gemessenem und dem vorhergesagtem anomalen magnetischen Moment des Muon untersucht. Das Modell erlaubt Beiträge zum anomalen magnetischen Moment des Muons, die mit experimentellen Daten kompatibel sind und gleichzeitig mit anderen experimentellen Beschränkungen der Modellparameter vereinbar sind.

Acknowledgements

This PhD journey has been a remarkable time. I am deeply grateful for all the people who supported me along the way and contributed to this experience.
First, I would like to thank my PhD advisor Prof. Dr. Heinrich Päs for the opportunity to pursue my PhD studies in his group, for his constant support in various research projects from my bachelors thesis until the end of my PhD; and the freedom and independence he gave me as a researcher. Moreover, I would like to thank the *Studienstiftung des deutschen Volkes* for the financial and idealistic support during my PhD.
I am deeply grateful to all the people I met at the department during my time in Dortmund. I want to thank all members of TIII and TIV for the countless insightful discussions, the weekly group meetings, which helped me to maintain a sense of normalcy during the Covid pandemic, and finally, for reviewing parts of my thesis. I fondly remember our coffee breaks, full of serious and unserious discussions as well as the traditional weekly movie night.
A special thanks to Maggi and Dennis, who introduced me to the basics of admin work, and to my office mates, Dominik and Dominik, for always being there to answer random physics and non-physics related questions, and to Dominik for lessening some admin duties, helping the department survive through unprecedented times. I am also thankful to Mathias, who first got me into bouldering, and to the rest of the TIII/TIV climbing crew for the countless memorable hours we shared in the climbing gym together.
I am also incredibly thankful to my friends, to (the other) Mathias, Jana, and Leon for all the hours spent climbing, creating rope messes, and providing much needed distraction from the seriousness of the (physics) world—whether it was at "the tower", in the Frankenjura, in climbing gyms all over the place, or on some mountain in Italy or Spain.
Finally, I want to thank my parents, my sister Lara and my partner Miriam for their immense support, which carried me through my PhD.

Contents

CHAPTER 1

Introduction

Over the past decades, the *Standard Model* (SM) of particle physics has emerged as a theoretical description of the fundamental constituents of matter and their interactions. In particular, the prediction [4, 5] and subsequent discovery [6, 7] of the Higgs boson has been the most groundbreaking success of the SM that manifests its role as the most precise description of nature to date. Together with the theory of *General Relativity* (GR), the SM is an essential foundation for the *Standard Model of cosmology* which plays a crucial role in furthering our understanding of the evolution of the Universe. The latter is based on some of the most notable triumphs of cosmology, such as the discovery that the Universe expands according to Hubble's law [8, 9] as well as the prediction of the *Cosmic Microwave Background* (CMB) [10–12], and successfully predicted e.g. the primordial abundances of light particles [12–16].

In spite of the SM's success, our theoretical understanding of the Universe remains incomplete. Many of its limitations impact both particle physics and cosmology, suggesting the need for solutions that connect both frameworks. For example, the Universe we observe today is maximally baryon asymmetric [17, 18]. It is theorized that rather than being an initial condition, this asymmetry arises at some stage during the evolution of the Universe, requiring that the SM is extended by new particles [19]. Moreover, neutrino oscillations indicate that neutrinos are massive [20–22], yet they are massless in the SM. The most economic model of neutrino mass generation is the *Seesaw mechanism* [23] that postulates the existence of additional heavy neutrinos. Such models are of particular interest for cosmology as the dynamical generation of a baryon asymmetry is an inherent feature of most generic Seesaw models and can therefore elegantly address both shortcomings simultaneously [24]. Further evidence for the existence of *beyond the Standard Model* (BSM) physics stems from the observation that the Universe contains significantly more matter than the visible, luminous matter, hence establishing the existence of a non-luminous matter component, called *dark matter* (DM) [18, 25, 26]. It is widely (though not unanimously) believed that the DM of the Universe consists of a yet unknown, weakly interacting, massive particle, thus implying the existence of BSM physics. Moreover, given the success of the SM in the realm of the unification of the electromagnetic and the weak force at high energies, many BSM models are embedded in the framework of *grand unified theories* (GUTs) which strive for the unification of all forces at even higher energies [27]. Since GUT models predict new particles, it seems obvious to exploit these particles to tackle shortcomings of the SM.

In this thesis, we explore two classes of models in order to address shortcomings in the SM and cosmology from different perspectives. Our main focus is on the *singlet Majoron model* [28–30] and extensions thereof. In the Majoron model, the global $U(1)_{B'-L'}$ symmetry of the SM is spontaneously broken, hence inducing the dynamical generation of neutrino masses and giving rise to a Goldstone boson, the Majoron. Although the main motivation behind the Majoron model is to address the absence of neutrino masses in the SM, Majoron models have also been widely studied with regard to the Majoron as a DM candidate [31–35]. In many aspects, Majoron models are similar to Axion models which are proposed as a solution to the *strong CP problem* [36–38]. However, while Axion models generally suffer from the appearance of topological defects in the form of *domain walls* (DWs), we explore why DWs are absent in Majoron models. Since the Majoron model inherently entails Majorana neutrinos, the majority of this thesis will be concerned with the possibility to create the *baryon asymmetry of the Universe* (BAU) in (extended) Majoron models [3, 39–42]. Additionally, we discuss an extension of the SM that aims to address the observed *anomalous magnetic moment* (AMM) of the muon [43–64] by introducing *vector-like leptons* (VLLs) and new scalars, motivated by the appearance of VLLs in GUT models.

This thesis is structured as follows. In Chapter 2, we briefly discuss the relevance of spontaneously broken symmetries in the realm of particle physics before providing a short introduction to the SM. In Chapter 3, we give an introduction to cosmology. We begin with an overview of the cosmological Standard Model and the concept of equilibrium thermodynamics which we then utilize in the framework of Boltzmann equations. Next, we discuss the relevance of phase transitions throughout the evolution of the Universe. We finish this chapter by briefly outlining the history of the Universe. In Chapter 4, we discuss the evidence for BSM physics in greater detail, focussing on the aspects relevant for this thesis. We also present generic models and frameworks that are often the basis for more evolved BSM models. In Chapter 5, we finally investigate the Majoron model. We begin with a brief review of the generic singlet Majoron model and the implications of a non-vanishing Majoron mass. Next, we discuss the issue of DWs in Majoron models and how the claim that they arise after *spontaneous symmetry breaking* (SSB) has motivated the study of extended Majoron models. In Chapter 6, we present an in-depth analysis of leptogenesis in a Majoron model that is extended by an additional triplet fermion, also addressing the prospects of DM in this model. In Chapter 7, we proceed with the discussion of a model that contains VLLs coupling to muons, a new scalar SU(2) singlet and a scalar SU(2) doublet. We explore the model as an explaination of the discrepancy between the observed and predicted values of the AMM of the muon and study constraints that arise e.g. due to Higgs decays. In Chapter 8, we conclude.

CHAPTER 2

Spontaneous Symmetry Breaking in the Standard Model of Particle Physics and Beyond

SSB is one of the most important concepts in modern particle physics and cosmology. One example is the *electroweak symmetry breaking* (EWSB) where the gauge group of the SM is spontaneously broken from $\mathrm{SU}(3)_C \times \mathrm{SU}(2)_\mathrm{L} \times U(1)_Y$ to $\mathrm{SU}(3)_C \times U(1)_{Q_\mathrm{EM}}$ [65–67]. Moreover, it is believed that symmetries which are spontaneously broken at a low temperature are restored at higher temperatures, similarly to condensed matter systems, and that the Universe underwent a series of phase transitions were different types of symmetries were broken. Broadly speaking, SSB has two implications for particle physics and cosmology: It dynamically generates masses for some particles in the theory, and in the context of cosmology, it gives rise to topological defects. In Secs. 2.1 and 2.2, we focus on the relation between the symmetry that is spontaneously broken and the masses that arise in the model[1] and the application of SSB in the SM, respectively, loosely following [68–75]. Finally, we briefly discuss a more evolved application of SSB in form of the two-Higgs doublet model in Sec. 2.3.

2.1 Spontaneous Symmetry Breaking

2.1.1 Discrete Symmetries

Let us begin with the Lagrangian for a real scalar field ϕ,

$$\mathcal{L} = \frac{1}{2} \left(\partial_\mu \phi\right) \left(\partial^\mu \phi\right) - V(\phi) \,, \tag{2.1.1}$$

where $V(\phi)$ is the potential given by

$$V(\phi) = \frac{\lambda}{4} \left(\phi^2 - v^2\right)^2 \,, \qquad v = \sqrt{\frac{\mu^2}{\lambda}} \,. \tag{2.1.2}$$

It is apparent that the Lagrangian is invariant under *discrete* Z_2 transformations $\phi \to -\phi$. The shape of the potential depends essentially on the signs of μ^2 and λ. First, in order for a stable ground state to exist, we demand that $\lambda > 0$. Next, if $\mu^2 < 0$, the potential

[1] Symmetry restoration and topological defects in the form of domain walls are shortly reviewed in Sec. 3.4 and 3.4.2, respectively.

has a single stable minimum at $\phi = 0$. The more interesting case is $\mu^2 > 0$ which yields a potential with two equivalent *vacuum expectation values* (VEVs) at

$$\langle\phi\rangle = \pm v\,, \tag{2.1.3}$$

and choosing either one of them spontaneously breaks the symmetry. For example, if we take $\langle\phi\rangle = v$, we can expand ϕ around the minimum as

$$\phi(x) = v + \tilde{\phi}(x)\,, \tag{2.1.4}$$

where $\tilde{\phi}$ has a vanishing VEV, $\langle\tilde{\phi}\rangle = 0$. We can now plug (2.1.4) into the Lagrangian (2.1.1), yielding

$$\mathcal{L} = \frac{1}{2}\left(\partial_\mu\tilde{\phi}\right)\left(\partial^\mu\tilde{\phi}\right) - \mu^2\tilde{\phi}^2 - \frac{\lambda}{4}\left(\tilde{\phi}^4 + 4v\tilde{\phi}^3\right)\,, \tag{2.1.5}$$

and we find that $\tilde{\phi}$ obtains a mass $\sqrt{2}\mu$. It is apparent that (2.1.5) is not invariant under $\tilde{\phi} \to -\tilde{\phi}$, i.e. the ground state does not obey the symmetry of the Lagrangian. This is called SSB. Note however that the Z_2 symmetry did not completely disappear. Instead, the symmetry is now realized as a shift symmetry, $\tilde{\phi} \to -\tilde{\phi} - 2v$, and the original Z_2 symmetry is hidden.

2.1.2 Continous Global Symmetries

A simple model that illustrates SSB of a continuous global symmetry is the $U(1)$ model where the Lagrangian for a complex scalar field ϕ,

$$\mathcal{L} = (\partial_\mu\phi)^\dagger\,(\partial^\mu\phi) - V(\phi)\,, \qquad V(\phi) = -\mu^2\phi^\dagger\phi + \lambda(\phi^\dagger\phi)^2\,, \tag{2.1.6}$$

is invariant under a global $U(1)$ transformation,

$$\phi(x) \to e^{i\alpha}\phi(x)\,. \tag{2.1.7}$$

As in the case of a discrete symmetry, we demand $\lambda > 0$ for vacuum stability and find that the potential has a minimum at $\phi = 0$ if $\mu^2 < 0$. If on the other hand $\mu^2 > 0$, the potential has the shape of a mexican hat as shown in Fig. 2.1 and we find an infinite amount of equivalent minima,

$$\langle\phi\rangle = \frac{v}{\sqrt{2}}e^{i\theta}\,, \qquad v = \sqrt{\frac{\mu^2}{\lambda}}\,, \tag{2.1.8}$$

where θ is an arbitrary phase. It is convenient to choose the vacuum with $\theta = 0$ and expand ϕ around two real fields ϕ_1 and ϕ_2 with vanishing VEVs,

$$\phi(x) = \frac{1}{\sqrt{2}}\left(v + \phi_1(x) + i\phi_2(x)\right)\,, \tag{2.1.9}$$

so that (2.1.6) becomes

$$\mathcal{L} = \frac{1}{2}\left(\partial_\mu \phi_1\right)\left(\partial^\mu \phi_1\right) + \frac{1}{2}\left(\partial_\mu \phi_2\right)\left(\partial^\mu \phi_2\right) - \lambda v^2 \phi_1^2 - \lambda v \phi_1 \left(\phi_1^2 + \phi_2^2\right) - \frac{\lambda}{4}\left(\phi_1^2 + \phi_2^2\right)^2 . \tag{2.1.10}$$

It is apparent that the choice of the ground state once again spontaneously breaks the symmetry. Moreover, we find that ϕ_1 obtains a mass $\sqrt{2\lambda v^2}$ while ϕ_2 remains massless. The massless particle is called a *Goldstone* boson, and their appearance is a general feature of spontaneously broken global symmetries.
Aside from the linear representation given in (2.1.9), we can also parametrize ϕ in the polar representation as

$$\phi(x) = \frac{1}{\sqrt{2}}\left(v + \tilde{\phi}_1(x)\right) e^{i\frac{\tilde{\phi}_2(x)}{v}} \tag{2.1.11}$$

and rewrite (2.1.6) as

$$\mathcal{L} = \frac{1}{2}(\partial_\mu \tilde{\phi}_1)(\partial^\mu \tilde{\phi}_1) + \frac{1}{2}\left(1 + \frac{\tilde{\phi}_1}{v}\right)^2 (\partial_\mu \tilde{\phi}_2)(\partial^\mu \tilde{\phi}_2) + \frac{1}{2}\mu^2\left(v + \tilde{\phi}_1^2\right)^2 - \frac{\lambda}{4}\left(v + \tilde{\phi}_1\right)^4 . \tag{2.1.12}$$

In the polar representation, ϕ_1 corresponds to radial excitations of the potenial while ϕ_2 corresponds to tangential excitations, see Fig. 2.1. In the polar representation, it is therefore intuitively clear that ϕ_1 obtains a mass while ϕ_2 remains massless. Moreover, the polar representation is illuminating since it reveals how the symmetry is hidden. While the vacuum $\langle\phi\rangle = v/\sqrt{2}$ does indeed spontaneously break the $U(1)$ symmetry, the symmetry is still realized in terms of a shift symmetry $\tilde{\phi}_2(x) \to \tilde{\phi}_2(x) + v\theta$.

2.1.3 Continous Local Symmetries

In the SM, local (or gauge) symmetries are of particular interest. The simplest model is described by the Lagrangian

$$\mathcal{L} = \left(D_\mu \phi\right)^\dagger \left(D^\mu \phi\right) - \frac{1}{4} F_{\mu\nu} F^{\mu\nu} - V(\phi) , \tag{2.1.13}$$

$$V(\phi) = -\mu^2 \phi^\dagger \phi + \lambda (\phi^\dagger \phi)^2 , \tag{2.1.14}$$

where $F_{\mu\nu}$ and D_μ are the field-strength tensor and the covariant derivative, respectively,

$$F_{\mu\nu} = \partial_\mu A_\nu - \partial_\nu A_\mu , \qquad D_\mu = \partial_\mu + ieA_\mu , \tag{2.1.15}$$

while A_μ is a gauge field. In contrast to the previous section, the Lagrangian is invariant under *local* $U(1)$ gauge transformations given by

$$\phi(x) \to e^{i\alpha(x)}\phi(x) , \qquad A_\mu(x) \to A_\mu(x) - e^{-1}\partial_\mu \alpha(x) . \tag{2.1.16}$$

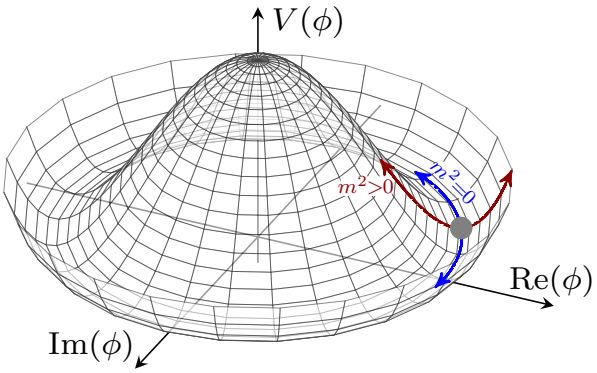

Figure 2.1: Schematical representation of the mexican hat potenial after a continuous symmetry is spontaneously broken. The blue curve corresponds to the radial mode with zero mass, i.e. the Goldstone mode, while the red curve corresponds to the radial mode with mass $m^2 > 0$.

The potential is the same as in (2.1.6), hence the possible ground states are also given by (2.1.8). Thus, inserting (2.1.9) into (2.1.13), we find

$$\begin{aligned}\mathcal{L} = &\frac{1}{2}\left(\partial_\mu\phi_1\right)\left(\partial^\mu\phi_1\right) + \frac{1}{2}\left(\partial_\mu\phi_2\right)\left(\partial^\mu\phi_2\right) - v^2\lambda\phi_1^2 + \frac{1}{2}e^2v^2A_\mu A^\mu - evA_\mu\partial^\mu\phi_2 \\ &- \frac{1}{4}F_{\mu\nu}F^{\mu\nu} + \text{interaction terms}\end{aligned} \tag{2.1.17}$$

and ϕ_1 and A_μ obtain masses,

$$m_{\phi_1} = \sqrt{2\lambda v^2}\,, \qquad m_A = ev\,, \tag{2.1.18}$$

while ϕ_2 remains massless. However, there appear two problems: The Lagrangian in (2.1.17) contains a kinetic mixing term $A_\mu\partial^\mu\phi_2$ and additionally, the degrees of freedom seem to be wrong. Massless gauge bosons have two degrees of freedom while massive gauge bosons have three. Thus, with two degrees of freedom for the complex scalar field, it appears as if we raised the degrees of freedom from four in (2.1.13) to five in (2.1.17). These problems imply that there is one unphysical field in the broken Lagrangian (2.1.17). This is easy so see by switching to the polar representation of ϕ given in (2.1.11). Under a local $U(1)$ transformation, ϕ transforms as

$$\phi(x) \to \phi(x)' = \frac{1}{\sqrt{2}}\left(v + \tilde{\phi}_1(x)\right)e^{i\alpha(x)}e^{i\frac{\tilde{\phi}_2(x)}{v}}\,, \tag{2.1.19}$$

and it is apparent that $\tilde{\phi}_2$ disappears from the Lagrangian if we choose the *unitary gauge* $\alpha(x) = -\tilde{\phi}_2(x)/v$,

$$\mathcal{L} = \frac{1}{2}\left(\partial_\mu\tilde{\phi}_1\right)\left(\partial^\mu\tilde{\phi}_1\right) - v^2\lambda\tilde{\phi}_1^2 + \frac{1}{2}e^2v^2A_\mu A^\mu - \frac{1}{4}F_{\mu\nu}F^{\mu\nu} + \text{interaction terms}\,. \tag{2.1.20}$$

Hence, the massive gauge boson is said to have *eaten* the Goldstone boson to acquire the additional degree of freedom. This is called the *Higgs mechanism*.

2.2 The Standard Model of Particle Physics

There are four fundamental forces known to exist in natue: *gravity*, the *weak force*, the *electromagnetic force* and the *strong force*. While gravity is described by Einstein's theory of GR, the weak, electromagnetic and strong forces are embedded in the SM in the framework of *quantum field theory* (QFT). More precisely, the SM is a gauge theory that explains the interactions of the elementary particles on the basis of their charges under the SM gauge group,

$$G_{\text{SM}} = \text{SU}(3)_C \times \text{SU}(2)_{\text{L}} \times U(1)_Y \,, \tag{2.2.1}$$

where C denotes *color*, L denotes *left* and Y denotes the *weak hypercharge*. The hypercharge Y and the *weak isospin* charge T_3 of a particle can be combined into the corresponding electric charge Q_{EM} as

$$Q_{\text{EM}} = T_3 + Y \,. \tag{2.2.2}$$

The strong force is described in the context of $\text{SU}(3)_C$ and is mediated via eight massless gauge bosons called *gluons*. At high temperatures, the electromagnetic and weak forces are united in the *electroweak gauge group* $\text{SU}(2)_{\text{L}} \times U(1)_Y$, mediated via the gauge bosons B_μ and W^a_μ, $a \in \{1, 2, 3\}$.
Besides the gauge bosons which carry integer spin, the SM contains *fermions* carrying half integer spin. Fermions are *chiral*, i.e. they transform as *left-handed* (LH) or *right-handed* (RH) representations of the Poincaré group. That is, the LH and RH fermions can be obtained from a Dirac fermion by using the projection operators

$$P_{\text{R}} = \frac{1}{2}(1 + \gamma^5) \,, \quad P_{\text{L}} = \frac{1}{2}(1 - \gamma^5) \,, \tag{2.2.3}$$

so that

$$P_{\text{R}}\psi = \psi_{\text{R}} \,, \quad P_{\text{L}}\psi = \psi_{\text{L}} \,, \tag{2.2.4}$$

where γ^5 is the fifth Dirac gamma matrix, see App. A. The SM fermions come in three generations with are indistinguishable based on their charges under G_{SM} and can be further divided into *quarks* and *leptons*. In the SM, the LH particles are the up-type quarks $(u, c, t)_{\text{L}}$ with $Q_{\text{EM}} = 2/3$, the down type quarks $(d, s, b)_{\text{L}}$ with $Q_{\text{EM}} = -1/3$, the charged leptons $(e, \mu, \tau)_{\text{L}}$ with $Q_{\text{EM}} = -1$ and the neutral leptons (neutrinos) $(\nu_e, \nu_\mu, \nu_\tau)_{\text{L}}$ with $Q_{\text{EM}} = 0$. They can be combined into $\text{SU}(2)_{\text{L}}$ quark and leptons doublets Q, L as

$$\underbrace{\begin{pmatrix} u \\ d \end{pmatrix}_{\text{L}}, \quad \begin{pmatrix} c \\ s \end{pmatrix}_{\text{L}}, \quad \begin{pmatrix} t \\ b \end{pmatrix}_{\text{L}}}_{Q}, \quad \underbrace{\begin{pmatrix} \nu_e \\ e \end{pmatrix}_{\text{L}}, \quad \begin{pmatrix} \nu_\mu \\ \mu \end{pmatrix}_{\text{L}}, \quad \begin{pmatrix} \nu_\tau \\ \tau \end{pmatrix}_{\text{L}}}_{L} \,. \tag{2.2.5}$$

The RH particles are the $\text{SU}(2)_{\text{L}}$ up-and down-type quark singlets $U \in (u, c, t)_{\text{R}}$ and $D \in (d, s, b)_{\text{R}}$, respectively, and the $\text{SU}(2)_{\text{L}}$ charged lepton singlets, $E \in (e, \mu, \tau)_{\text{R}}$, which carry the same electric charge Q_{EM} as their LH partners. RH neutrinos are uncharged under the SM gauge group and therefore not included in the SM. The leptons carry an

Table 2.1: Particle content of the SM, along with their transformation properties under the SM gauge group and their charges.

Field		$\mathrm{SU}(3)_C$	$\mathrm{SU}(2)_\mathrm{L}$	Y	B'	L'	Q_EM	T^3
Q	$\begin{pmatrix} u \\ d \end{pmatrix}_\mathrm{L}, \begin{pmatrix} c \\ s \end{pmatrix}_\mathrm{L}, \begin{pmatrix} t \\ b \end{pmatrix}_\mathrm{L}$	**3**	**2**	$1/6$	$1/3$	0	$2/3$ $-1/3$	$1/2$ $-1/2$
L	$\begin{pmatrix} \nu_e \\ e \end{pmatrix}_\mathrm{L}, \begin{pmatrix} \nu_\mu \\ \mu \end{pmatrix}_\mathrm{L}, \begin{pmatrix} \nu_\tau \\ \tau \end{pmatrix}_\mathrm{L}$	**1**	**2**	$-1/2$	0	1	0 -1	$1/2$ $-1/2$
H	$\begin{pmatrix} \phi^+ \\ \phi^0 \end{pmatrix}$	**1**	**2**	$1/2$	0	0	1 0	$1/2$ $-1/2$
U	$u_\mathrm{R}, c_\mathrm{R}, t_\mathrm{R}$	**3**	**1**	$2/3$	$1/3$	0	$2/3$	0
D	$d_\mathrm{R}, d_\mathrm{R}, b_\mathrm{R}$	**3**	**1**	$-1/3$	$1/3$	0	$-1/3$	0
E	$e_\mathrm{R}, \mu_\mathrm{R}, \tau_\mathrm{R}$	**1**	**1**	-1	0	1	-1	0

additional charge called *lepton number* L' and are not charged under $\mathrm{SU}(3)_C$, i.e. they interact only via the electroweak interaction. Quarks interact via both the strong and electroweak interactions and similarly to leptons, they carry an additional charge called *baryon number* B'. Finally, the SM contains the $\mathrm{SU}(2)_\mathrm{L}$ scalar doublet H,

$$H = \begin{pmatrix} \phi^+ \\ \phi^0 \end{pmatrix} \tag{2.2.6}$$

which carries a hypercharge of $Y = 1/2$. The particle content of the SM is summarized in Tab. 2.1.

2.2.1 Electroweak Symmetry Breaking

The SM is a gauge theory, hence we require that the Lagrangian of the SM is invariant under local $\mathrm{SU}(3)_C \times \mathrm{SU}(2)_\mathrm{L} \times U(1)_Y$ transformations of the form

$$\psi \to \exp\left(i\rho_Y(x)Y\right) \exp\left(i\rho^a_\mathrm{L}(x)T^a\right) \exp\left(i\rho^b_C(x)t^b\right)\psi\,, \qquad a \in \{1,2,3\}\,, b \in \{1-8\}\,, \tag{2.2.7}$$

where $Y, T^a = \sigma^a/2, t^b = \lambda^b/2$ are the generators of $U(1)_Y, \mathrm{SU}(2)_\mathrm{L}, \mathrm{SU}(3)_C$, respectively and $\sigma^a(\lambda^a)$ are the Pauli (Gell-Mann) matrices, see App. A.
The dynamics of the gauge bosons are embedded in the term

$$\mathcal{L}_{gauge} = -\frac{1}{4}G^b_{\mu\nu}G^{b\mu\nu} - \frac{1}{4}W^a_{\mu\nu}W^{a\mu\nu} - \frac{1}{4}B_{\mu\nu}B^{\mu\nu}\,, \tag{2.2.8}$$

where the field strength tensors are given by

$$B_{\mu\nu} = \partial_\mu B_\mu - \partial_\nu B_\mu \,, \tag{2.2.9}$$

$$W^a_{\mu\nu} = \partial_\mu W^a_\mu - \partial_\nu W^a_\mu + g\epsilon^{abc} W^b_\mu W^c_\nu \,, \quad a = 1,2,3 \,, \tag{2.2.10}$$

$$G^a_{\mu\nu} = \partial_\mu G^a_\mu - \partial_\nu G^a_\mu + g_s f^{abc} G^b_\mu G^c_\nu \,, \quad a = 1-8 \,. \tag{2.2.11}$$

The structure constants f^{abc} of SU(3) are defined via

$$[t^a, t^b] = i f^{abc} t^c \,, \tag{2.2.12}$$

while ϵ^{abc} is the totally antisymmetric tensor with $\epsilon^{123} = 1$.
The gauge interactions of the fermions are contained in the kinetic terms,

$$\mathcal{L}_{kin} = i\overline{Q}\not{D}Q + i\overline{U}\not{D}U + i\overline{D}\not{D}D + i\overline{L}\not{D}L + i\overline{E}\not{D}E \,, \tag{2.2.13}$$

where D_μ is the covariant derivative,

$$D_\mu = \partial_\mu - ig' B_\mu - igW^a_\mu T^a - ig_s G^a_\mu t^a \,. \tag{2.2.14}$$

We note that so far, all particles are massless, contrary to observations. However, adding a fermion mass term of the form

$$\mathcal{L} \sim m\overline{\psi}\psi = m\left(\overline{\psi_{\mathtt{R}}}\psi_{\mathtt{L}} + \overline{\psi_{\mathtt{L}}}\psi_{\mathtt{R}}\right) \tag{2.2.15}$$

by hand violates $\mathrm{SU}(2)_{\mathtt{L}}$ gauge invariance due to the chiral nature of the fermions and is therefore forbidden. Thus, we need to employ a mechanism that dynamically generates not only the fermion masses but also the masses of the gauge bosons. From the previous section, we know that this can be achieved by means of SSB and the Higgs mechanism. First, we can write down Yukawa interactions between the Higgs doublet and the fermions,

$$\mathcal{L}_{yuk} = -\overline{Q_i} Y^d_{ij} H D_j - \overline{Q_i} Y^u_{ij} \tilde{H} U_j - \overline{L_i} Y^e_{ij} H E_j + \text{h.c.} \,, \tag{2.2.16}$$

where $\tilde{H} = i\sigma_2 H^* = (\phi^0, -\phi^-)^T$ and $Y^k, k = u, d, e$ are 3×3 Yukawa matrices in flavor space, while the indices i and j denote the generations. We note that the Yukawa interactions resemble the chiral nature of (2.2.15) but do not violate gauge invariance due to the non-trivial $\mathrm{SU}(2)_{\mathtt{L}} \times U(1)_Y$ charge of H. Moreover, the kinetic term and the scalar potential for the Higgs are given by

$$\mathcal{L}_{Higgs} = (D_\mu H)^\dagger (D^\mu H) \,, \qquad V(H) = -\mu^2 H^\dagger H + \lambda \left(H^\dagger H\right)^2 \,, \tag{2.2.17}$$

respectively. Similarly to the discussion in Sec. 2, we demand $\lambda > 0$ so that the potential is bounded from below and $-\mu^2 < 0$ so that the minima of the potential are given by

$$|H|^2 = \frac{v_{\mathrm{SM}}^2}{2} \,, \qquad v_{\mathrm{SM}} = \sqrt{\frac{\mu^2}{\lambda}} \,, \tag{2.2.18}$$

where $v_{\mathrm{SM}} = 246\,\mathrm{GeV}$ is the VEV of the Higgs. Analogously to (2.1.8), this corresponds to an infinite number of minima connected via gauge transformations, and choosing one of them spontaneously breaks the symmetry. We can write H in terms of four real scalar

fields $\phi_1, \phi_2, \phi_3, \phi_4$ as

$$H = \frac{1}{\sqrt{2}} \begin{pmatrix} \phi_1 + i\phi_2 \\ \phi_3 + i\phi_4 \end{pmatrix} , \tag{2.2.19}$$

and choose the VEVs of the fields $\phi_1, \phi_2, \phi_3, \phi_4$ so that

$$\langle \phi_3 \rangle = v \, , \quad \langle \phi_1 \rangle = \langle \phi_2 \rangle = \langle \phi_4 \rangle = 0 \, . \tag{2.2.20}$$

Additionally, we introduce a real scalar field h with vanishing VEV, $\langle h \rangle = 0$, so that

$$\phi_3 = v_{\text{SM}} + h \, , \tag{2.2.21}$$

where h represents small fluctuations around the VEV v_{SM}. Hence, we can write H as

$$H = \frac{1}{\sqrt{2}} \begin{pmatrix} \phi_1 + i\phi_2 \\ v_{\text{SM}} + h + i\phi_4 \end{pmatrix} \tag{2.2.22}$$

and rewrite (2.2.17) as

$$V(H) \supset \frac{1}{2} \underbrace{\left(v_{\text{SM}}^2 \lambda - \mu^2 \right)}_{=0} \left(\phi_1^2 + \phi_2^2 + \phi_4^2 \right) + \lambda v_{\text{SM}}^2 h^2 \, , \tag{2.2.23}$$

which indicates that ϕ_1, ϕ_2 and ϕ_4 are massless while h obtains a mass $m_h = \sqrt{2\lambda v_{\text{SM}}^2}$. Moreover, it is illuminating to express H in the polar representation,

$$H = \frac{1}{\sqrt{2}} \exp\left(\frac{i\eta^a \sigma^a}{v_{\text{SM}}} \right) \begin{pmatrix} 0 \\ v_{\text{SM}} + h \end{pmatrix} , \tag{2.2.24}$$

where η^a and h are real fields and $a = 1, 2, 3$. Considering $\text{SU}(2)_{\text{L}}$ gauge transformations of the form

$$H \to \exp\left(i\rho_{\text{L}}^a(x) \frac{\sigma^a}{2} \right) H \tag{2.2.25}$$

and choosing unitary gauge $\rho_{\text{L}}^a(x) = -2\eta^a / v_{\text{SM}}$, we can write H as

$$H = \frac{1}{\sqrt{2}} \begin{pmatrix} 0 \\ v_{\text{SM}} + h \end{pmatrix} , \tag{2.2.26}$$

i.e. we removed the three massless Goldstone bosons η^a (or equivalently ϕ_1, ϕ_2, ϕ_4) by fixing the gauge. Moreover, note that the symmetry is not completely broken as H is electrically neutral and therefore invariant under a $U(1)_{Q_{\text{EM}}}$ gauge transformation

$$H \to e^{i(Y + T^3)\rho(x)} H = e^{i Q_{\text{EM}} \rho(x)} H \, . \tag{2.2.27}$$

Thus, three of the four $\text{SU}(2)_{\text{L}} \times U(1)_Y$ generators T^a, Y break the symmetry while the combination corresponding to Q_{EM} annihilates the vacuum and we find the breaking pattern of EWSB as

$$\text{SU}(3)_C \times \text{SU}(2)_{\text{L}} \times U(1)_Y \to \text{SU}(3)_C \times U(1)_{Q_{\text{EM}}} \, . \tag{2.2.28}$$

Consequently, we expect nine massless gauge bosons, corresponding to the nine generators of the unbroken symmetry group $\text{SU}(3)_C \times U(1)_{Q_{\text{EM}}}$, λ^a and Q_{EM}, and three massive gauge

bosons, corresponding to the generators that break $\mathrm{SU}(2)_\mathrm{L} \times U(1)_Y$.
The masses of the gauge bosons arise from the kinetic term (2.2.17) which we can rewrite in unitary gauge (2.2.26) as

$$(D_\mu H)^\dagger (D^\mu H) \supset \frac{g^2 v_{\mathrm{SM}}^2}{8} \left(W_\mu^1 - iW_\mu^2\right)\left(W^{1\mu} + iW^{2\mu}\right) + \frac{v_{\mathrm{SM}}^2}{8}\sqrt{g^2+g'^2}\left(\frac{gW_\mu^3 - g'B_\mu}{\sqrt{g^2+g'^2}}\right)^2 . \tag{2.2.29}$$

From (2.2.29), we can identify the charged W bosons, Z_μ and the photon A_μ as the linear combinations

$$W_\mu^\pm = \frac{1}{\sqrt{2}}\left(W_\mu^1 \mp iW_\mu^2\right) , \tag{2.2.30}$$

$$Z_\mu = \frac{1}{\sqrt{g^2+g'^2}}\left(gW_\mu^3 - g'B_\mu\right) = c_W W_\mu^3 - s_W B_\mu , \tag{2.2.31}$$

$$A_\mu = \frac{1}{\sqrt{g^2+g'^2}}\left(gW_\mu^3 + g'B_\mu\right) = s_W W_\mu^3 + c_W B_\mu , \tag{2.2.32}$$

where we defined the Weinberg angle θ_W via

$$c_W \equiv \cos\theta_W = \frac{g}{\sqrt{g^2+g'^2}} , \qquad s_W \equiv \sin\theta_W = \frac{g'}{\sqrt{g^2+g'^2}} . \tag{2.2.33}$$

The masses of the gauge bosons $W_\mu^\pm, Z_\mu$ can then be infered from (2.2.29) as

$$m_W^2 = \frac{g^2 v^2}{4} , \qquad m_Z^2 = \frac{(g^2+g'^2)v^2}{4} , \tag{2.2.34}$$

while the photon A_μ and the eigth gluons G_μ^a remain massless. The fermion masses are induced by the Yukawa term (2.2.16) which becomes

$$\mathcal{L}_{yuk} \supset -\overline{u_\mathrm{L}^i}\frac{v_{\mathrm{SM}}Y_{ij}^u}{\sqrt{2}}u_\mathrm{R}^j - \overline{d_\mathrm{L}^i}\frac{v_{\mathrm{SM}}Y_{ij}^d}{\sqrt{2}}d_\mathrm{R}^j - \overline{e_\mathrm{L}^i}\frac{v_{\mathrm{SM}}Y_{ij}^e}{\sqrt{2}}e_\mathrm{R}^j + \mathrm{h.c.} , \tag{2.2.35}$$

$$= -\overline{u_\mathrm{L}^i}\tilde{m}_u^{ij}u_\mathrm{R}^j - \overline{d_\mathrm{L}^i}\tilde{m}_d^{ij}d_\mathrm{R}^j - \overline{e_\mathrm{L}^i}\tilde{m}_e^{ij}e_\mathrm{R}^j + \mathrm{h.c.} , \tag{2.2.36}$$

where we used the shorthand notation $u^i = \{u,c,t\}, d^i = \{d,s,t\}$ and $e^i = \{e,\mu,\tau\}$ and $\tilde{m}_\psi^{ij}, \psi \in$ fermions are the fermion mass matrices. Note that due to the absence of RH neutrinos in the SM, neutrinos do not obtain a mass via the Higgs meachnism and remain massless. In general, the Yukawa and mass matrices, Y^ψ and m_ψ, are not diagonal, i.e. the mass eigenstates do not necessarily correspond to the flavor eigenstates. The mass matrices can be diagonalized via a bi-unitary transformation,

$$m_\psi = V_{\psi\mathrm{L}}\tilde{m}_\psi V_{\psi\mathrm{R}}^\dagger , \tag{2.2.37}$$

resulting in

$$\mathcal{L} \supset -\underbrace{\overline{u_{\mathtt{L}}^i} V_{u\mathtt{L}}^\dagger}_{\overline{u'_{\mathtt{L}}}} \underbrace{V_{u\mathtt{L}} \tilde{m}_u^{ij} V_{u\mathtt{R}}^\dagger}_{m_u} \underbrace{V_{u\mathtt{R}} u_{\mathtt{R}}^j}_{u'_{\mathtt{R}}} - \underbrace{\overline{d_{\mathtt{L}}^i} V_{d\mathtt{L}}^\dagger}_{\overline{d'_{\mathtt{L}}}} \underbrace{V_{d\mathtt{L}} \tilde{m}_u^{ij} V_{d\mathtt{R}}^\dagger}_{m_d} \underbrace{V_{d\mathtt{R}} d_{\mathtt{R}}^j}_{d'_{\mathtt{R}}} - \underbrace{\overline{e_{\mathtt{L}}^i} V_{e\mathtt{L}}^\dagger}_{\overline{e'_{\mathtt{L}}}} \underbrace{V_{e\mathtt{L}} \tilde{m}_u^{ij} V_{e\mathtt{R}}^\dagger}_{m_e} \underbrace{V_{e\mathtt{R}} e_{\mathtt{R}}^j}_{e'_{\mathtt{R}}} + \text{h.c.}\,, \tag{2.2.38}$$

where the corresponding mass eigenstates are given by

$$\psi'_{\mathtt{L}} = V_{\psi\mathtt{L}} \psi_{\mathtt{L}}\,, \qquad \psi'_{\mathtt{R}} = V_{\psi\mathtt{R}} \psi_{\mathtt{R}}\,. \tag{2.2.39}$$

Next, we can rewrite the covariant derivative in terms of the gauge bosons as

$$D_\mu = \partial_\mu - i g_s G_\mu^a t^a - \frac{ig}{\sqrt{2}} \left(W_\mu^+ \sigma^+ + W_\mu^- \sigma^- \right) - \frac{ie}{s_W c_W} Z_\mu \left(T^3 - s_W^2 Q_{\text{EM}} \right) - ie A_\mu Q_{\text{EM}}\,, \tag{2.2.40}$$

where the electromagnetic coupling e is defined as

$$e = \frac{g g'}{\sqrt{g^2 + g'^2}} = g s_W = g' c_W\,, \tag{2.2.41}$$

and $2\sigma^\pm = \sigma^1 \pm i\sigma^2$. The charged-current interactions of quarks can then be rewritten as

$$\mathcal{L}_{CC}^q = \frac{ig}{\sqrt{2}} \left[\overline{u_{\mathtt{L}}^{i\prime}} (V_{u\mathtt{L}} V_{d\mathtt{L}}^\dagger)^{ij} \gamma^\mu d_{\mathtt{L}}^{j\prime} W_\mu^+ \right] + \text{h.c.}\,, \tag{2.2.42}$$

where we introduced the *Cabibbo-Kobayashi-Masukawa* (CKM) matrix [76, 77]

$$V = V_{u\mathtt{L}} V_{d\mathtt{L}}^\dagger = \begin{pmatrix} V_{ud} & V_{us} & V_{ub} \\ V_{cd} & V_{cs} & V_{cb} \\ V_{td} & V_{ts} & V_{tb} \end{pmatrix}\,. \tag{2.2.43}$$

The CKM matrix is not diagonal and consequently, the quark mass eigenstates are not flavor eigenstates and the charged-current interactions of the quarks induce flavor changing transitions. The CKM matrix is unitary and can be parametrized in terms of three mixing angles $\theta'_{12}, \theta'_{13}, \theta'_{23}$ and one $\mathcal{CP}$ violating phase δ' as

$$V = \begin{pmatrix} c_{12} c_{13} & s_{12} c_{13} & s_{13} e^{-i\delta'} \\ -s_{12} c_{23} - c_{12} s_{23} s_{13} e^{i\delta'} & c_{12} c_{23} - s_{12} s_{23} s_{13} e^{i\delta'} & s_{23} c_{13} \\ s_{12} s_{23} - c_{12} c_{23} s_{13} e^{i\delta'} & -c_{12} s_{23} - s_{12} c_{23} s_{13} e^{i\delta'} & c_{23} c_{12} \end{pmatrix} \tag{2.2.44}$$

where $c_{ij} \equiv \cos\theta'_{ij}, s_{ij} \equiv \sin\theta'_{ij}$. Note that δ' is the only source of $\mathcal{CP}$ violation in the SM. A convenient measure of $\mathcal{CP}$ violation is the Jarlskog invariant $\mathcal{J}$ [78] which is defined via

$$\text{Im}\left[V_{ij} V_{kl} V_{il}^* V_{kj}^* \right] = \mathcal{J} \sum_{m,n} \epsilon_{ikm} \epsilon_{jln}\,. \tag{2.2.45}$$

The crucial point is that $\mathcal{J}$ vanishes *only* if there is no $\mathcal{CP}$ violation in the quark sector. In the standard parametrization (2.2.44), $\mathcal{J}$ can be written as

$$\mathcal{J} = s_{13} s_{23} s_{31} c_{12} c_{23} c_{31}^2 \sin\delta'\,, \tag{2.2.46}$$

and with the SM parameters given in Tab. C.1, we find $\mathcal{J} \sim \mathcal{O}(10^{-5})$.
Next, the charged current interactions of leptons are given by

$$\mathcal{L}^{\ell}_{CC} = \frac{ig}{\sqrt{2}} \left[\overline{\nu^{i}_{\mathrm{L}}} (V^{\dagger}_{e\mathrm{L}})^{ij} \gamma^{\mu} e^{j\prime}_{\mathrm{L}} W^{+}_{\mu} \right] + \mathrm{h.c.}\,, \tag{2.2.47}$$

and since the neutrinos are massless in the SM, we can reabsorb the matrix $V_{e\mathrm{L}}$ in the definition of the neutrino fields,

$$\nu^{i}_{\mathrm{L}} \to V^{ij}_{e\mathrm{L}} \nu^{j}_{\mathrm{L}}\,. \tag{2.2.48}$$

Thus, we can work in the basis where charged lepton mass eigenstates correspond to the flavor eigenstates,

$$\mathcal{L}^{\ell}_{CC} = \overline{\nu_{\mathrm{L}}}^{i} \gamma^{\mu} e^{i\prime}_{\mathrm{L}} W^{+}_{\mu} + \mathrm{h.c.}\,. \tag{2.2.49}$$

Note that the redefinition (2.2.48) is only possible as long as neutrinos are massless and consequently, introducing neutrino masses results in the appearance of a mixing matrix in the lepton sector called the *Pontecorvo-Maki-Nakagawa-Sakata* (PMNS) matrix, which we will discuss in greater detail in Sec. 4.2.
Finally, the can write the neutral current interactions of a generic LH or RH SM fermion ψ as

$$\mathcal{L}_{NC} = \frac{3}{s_W} c_W Z_{\mu} \overline{\psi} \left(T^{3}(\psi) - s^{2}_{W} Q_{\mathrm{EM}}(\psi) \right) \psi + e A_{\mu} \overline{\psi} Q_{\mathrm{EM}}(\psi) \psi\,, \tag{2.2.50}$$

with $T^3(\psi)$ and $Q_{\mathrm{EM}}(\psi)$ according to Tab. 2.1. Thus, the neutral-current interactions are not affected by the mixing between the mass and flavor eigenstates and *flavor changing neutral currents* (FCNCs) on tree level are forbidden in the SM.
To conclude this section, let us count the parameters of the SM that are not predicted by the theory and need to be measued by experiment. They are e.g.

- 2 parameters for the scalar potential, v_{SM} and m_h,
- 3 couplings that describe the strength of gauge interactions, g, g', g_s,
- 6 quark masses $m_u, m_d, m_c, m_s, m_t, m_b$ (or 6 Yukawa couplings),
- 3 charged lepton masses m_e, m_μ, m_τ (or 3 Yukawa couplings),
- 3 CKM angles $\theta'_{12}, \theta'_{13}, \theta'_{23}$,
- 1 phase δ',

i.e. in total 18 parameters.[2] Numerical values for the SM parameters are summarized in App. C.

[2] An additional paramters, θ_{QCD}, arises due to Instanton effects, see App. E.

2.3 Two-Higgs Doublet Models

In the previous section, we discussed how the masses of the SM particles arise via SSB with a minimal scalar sector, i.e. *one* Higgs doublet. Although a minimal Higgs sector is appealing due to its simplicity, it remains plausible that more than one $\mathrm{SU}(2)_\mathrm{L}$ scalar exists, and models with extended scalar sectors are easy to envisage. One extension that has been extensively studied is the *two-Higgs doublet model* (2HDM) where a second $\mathrm{SU}(2)_\mathrm{L}$ doublet is introduced. 2HDMs have interesting theoretical implications, e.g. with regard to vaccum stability, and have a rich phenomenology. While a detailed phenomenological discussion is beyond the scope of this work, in the following, we will give a brief overview how the scalar mass spectrum and Higgs couplings to gauge bosons and fermions in the 2HDM are affected compared to the SM and discuss the vacuum structure of the model, following [69, 79–84].
The most general scalar potential of 2HDMs is given by

$$\begin{aligned} V(\Phi_1,\Phi_2) = {} & m_{11}^2\left(\Phi_1^\dagger\Phi_1\right) + m_{22}^2\left(\Phi_2^\dagger\Phi_2\right) - \left[m_{12}^2\Phi_1^\dagger\Phi_2 + \mathrm{h.c.}\right] + \frac{\lambda_1}{2}\left(\Phi_1^\dagger\Phi_1\right)^2 \\ & + \frac{\lambda_2}{2}\left(\Phi_2^\dagger\Phi_2\right)^2 + \lambda_3\left(\Phi_1^\dagger\Phi_1\right)\left(\Phi_2^\dagger\Phi_2\right) + \lambda_4\left(\Phi_1^\dagger\Phi_2\right)\left(\Phi_2^\dagger\Phi_1\right) \\ & + \left[\frac{\lambda_5}{2}\left(\Phi_1^\dagger\Phi_2\right)^2 + \lambda_6\left(\Phi_1^\dagger\Phi_1\right)\left(\Phi_1^\dagger\Phi_2\right) + \lambda_7\left(\Phi_2^\dagger\Phi_2\right)\left(\Phi_1^\dagger\Phi_2\right) + \mathrm{h.c.}\right] \end{aligned} \tag{2.3.1}$$

where Φ_1 and Φ_2 are the complex Higgs doublets,

$$\Phi_1 = \begin{pmatrix} \phi_1^+ \\ \frac{1}{\sqrt{2}}\left(v_1 + \phi_1 + i\rho_1\right) \end{pmatrix}, \qquad \Phi_2 = \begin{pmatrix} \phi_2^+ \\ \frac{2}{\sqrt{2}}\left(v_2 + \phi_2 + i\rho_2\right) \end{pmatrix}, \tag{2.3.2}$$

and $v_{1,2}$ are the VEVs of $\Phi_{1,2}$. We have assumed that the vacuum is charge and $\mathcal{CP}$ conserving (see Sec. 2.3.1) and all parameters are real. In this most simple realization of the 2HDM, the SM fermions couple both to Φ_1 and Φ_2, which induces problematic tree-level FCNCs. However, several modifications of 2HDMs exist that eliminate the dangerous FCNCs. For example, imposing a discrete Z_2 symmetry under which Φ_2 is odd and all other fields are even, the SM fermions couple only to Φ_1 and no FCNCs exist. Moreover, the Z_2 symmetry implies that $\lambda_6 = \lambda_7 = 0$ while the soft breaking parameter m_{12} can be non-zero. Defining

$$t_\beta \equiv \tan\beta = \frac{v_2}{v_1}, \qquad v^2 \equiv v_1^2 + v_2^2, \qquad \lambda_{345} = \lambda_3 + \lambda_4 + \lambda_5, \tag{2.3.3}$$

we can write the conditions that minimize the potential as

$$m_{11} = m_{12}^2 t_\beta - \frac{v^2}{2}\left(\lambda_1 c_\beta^2 + \lambda_{345} s_\beta^2\right), \qquad m_{22} = m_{12}^2 t_\beta^{-1} - \frac{v^2}{2}\left(\lambda_2 s_\beta^2 + \lambda_{345} c_\beta^2\right), \tag{2.3.4}$$

where $s_\beta \equiv \sin\beta$ and $c_\beta \equiv \cos\beta$. SSB gives rise to non-diagonal mass terms in the Higgs sector as

$$V = \begin{pmatrix}\phi_1 & \phi_2\end{pmatrix} M_\phi \begin{pmatrix}\phi_1 \\ \phi_2\end{pmatrix} + \begin{pmatrix}\rho_1 & \rho_2\end{pmatrix} M_\rho \begin{pmatrix}\rho_1 \\ \rho_2\end{pmatrix} + \begin{pmatrix}\phi_1^+ & \phi_2^+\end{pmatrix} M_{\phi^\pm} \begin{pmatrix}\phi_1^- \\ \phi_2^-\end{pmatrix}, \tag{2.3.5}$$

with mass matrices given by

$$M_\phi = \begin{pmatrix} m_{12}^2 t_\beta + \lambda_1 v^2 c_\beta^2 & -m_{12}^2 + \frac{\lambda_{345}}{2} v^2 s_{2\beta} \\ -m_{12}^2 + \frac{\lambda_{345}}{2} v^2 s_{2\beta} & m_{12}^2 t_\beta^{-1} + \lambda_2 v^2 s_\beta^2 \end{pmatrix} \equiv \begin{pmatrix} M_{11} & M_{12} \\ M_{12} & M_{22} \end{pmatrix}, \tag{2.3.6}$$

$$m_\rho = \left[m_{12}^2 - \frac{\lambda_5}{2} v_{s2\beta}^2 \right] \begin{pmatrix} t_\beta & -1 \\ -1 & t_\beta^{-1} \end{pmatrix}, \tag{2.3.7}$$

$$M_{\Phi^\pm} = \left[m_{12}^2 - \frac{\lambda_4 + \lambda_5}{4} v_{s2\beta}^2 \right] \begin{pmatrix} t_\beta & -1 \\ -1 & t_\beta^{-1} \end{pmatrix}. \tag{2.3.8}$$

Thus, we find the mass eigenstates of the $\mathcal{CP}$ even Higgs fields by performing a rotation by an angle α,

$$\begin{pmatrix} \tilde{h} \\ \tilde{H} \end{pmatrix} = \underbrace{\begin{pmatrix} c_\alpha & s_\alpha \\ -s_\alpha & c_\alpha \end{pmatrix}}_{\equiv U_\alpha} \begin{pmatrix} \phi_1 \\ \phi_2 \end{pmatrix}, \tag{2.3.9}$$

while the corresponding mass eigenstates are

$$m_{\tilde{h}}^2 = \frac{M_{11} + M_{22}}{2} + \frac{1}{2}\sqrt{(M_{11} - M_{22})^2 + M_{12}^2}, \tag{2.3.10}$$

$$m_{\tilde{H}}^2 = \frac{M_{11} + M_{22}}{2} - \frac{1}{2}\sqrt{(M_{11} - M_{22})^2 + M_{12}^2}. \tag{2.3.11}$$

Moreover, the mass eigenstates of the $\mathcal{CP}$ odd and charged Higgs fields are read

$$\begin{pmatrix} G^0 \\ A \end{pmatrix} = \begin{pmatrix} c_\beta & s_\beta \\ -s_\beta & c_\beta \end{pmatrix} \begin{pmatrix} \rho_1 \\ \rho_2 \end{pmatrix}, \qquad \begin{pmatrix} G^\pm \\ H^\pm \end{pmatrix} = \begin{pmatrix} c_\beta & s_\beta \\ -s_\beta & c_\beta \end{pmatrix} \begin{pmatrix} \phi_1^\pm \\ \phi_2^\pm \end{pmatrix}, \tag{2.3.12}$$

where G_0 and $G^\pm$ are the massless Goldstone bosons, while A and $H^\pm$ acquire masses given by

$$m_A^2 = \frac{m_{12}^2}{s_\beta c_\beta} - \lambda_5 v^2, \qquad m_{H^\pm}^2 = \frac{m_{12}^2}{s_\beta c_\beta} - \frac{1}{2}(\lambda_4 + \lambda_5) v^2. \tag{2.3.13}$$

We can now express the couplings of the gauge and fermions fields to the mass eigenstates $\tilde{h}, \tilde{H}$ in a convenient form. The kinetic term of the Higgs fields,

$$\mathcal{L}_{kin}^\Phi = (D_\mu \Phi_1)^\dagger (D^\mu \Phi_1) + (D_\mu \Phi_2)^\dagger (D^\mu \Phi_2), \tag{2.3.14}$$

gives to rise trilinear gauge couplings,

$$\mathcal{L} \supset \frac{g^2}{2}(v_1\phi_1 + v_2\phi_2) W_\mu^+ W^{-\mu} + \frac{g^2 + g'^2}{4}(v_1\phi_1 + v_2\phi_2) Z_\mu Z^\mu. \tag{2.3.15}$$

Using

$$v_1 = v\cos\beta\,, \quad v_2 = v\sin\beta\,, \tag{2.3.16}$$

we can reexpress the gauge couplings in a similar form to the SM,

$$\begin{aligned}\mathcal{L} \supset \frac{g^2 v}{2}\cos(\alpha-\beta)\,\tilde{h}W^+_\mu W^{-\mu} + \frac{(g^2+g'^2)\,v}{4}\cos(\alpha-\beta)\,\tilde{h}Z_\mu Z^\mu \\ + \frac{g^2 v}{2}\sin(\beta-\alpha)\tilde{H}W^+_\mu W^{-\mu} + \frac{(g^2+g'^2)\,v}{4}\sin(\beta-\alpha)\tilde{H}Z_\mu Z^\mu\,.\end{aligned} \tag{2.3.17}$$

Moreover, a generic fermion f in its mass eigenstate with a Yukawa coupling y_f interacts with ϕ_1 via

$$\mathcal{L}_f = -y_f \overline{f}\phi_1 f \tag{2.3.18}$$

and obtains a mass

$$m_f = \frac{y_f v_1}{\sqrt{2}} = \frac{y_f v\cos\beta}{\sqrt{2}}\,. \tag{2.3.19}$$

Thus, we can rewrite (2.3.18) as

$$\mathcal{L}_f = -\frac{m_f}{v}\left[\cos(\alpha-\beta) + t_\beta\sin(\alpha-\beta)\right]\tilde{h} + \frac{m_f}{v}\left[\sin(\alpha-\beta) + t_\beta\cos(\alpha-\beta)\right]\tilde{H}\,. \tag{2.3.20}$$

It is now evident that the decay widths of $\tilde{h}$ and $\tilde{H}$ to a pair of gauge bosons or fermions depend on α and β. Moreover, note that we can recover a $\mathcal{CP}$ even scalar mass eigenstate with the same tree-level couplings as the SM Higgs if we impose the *alignment limit* where either

$$\cos(\alpha-\beta) = 1\,, \quad \sin(\beta-\alpha) = 0\,, \tag{2.3.21}$$

so that $\tilde{h}$ is SM-like or

$$\cos(\alpha-\beta) = 0\,, \quad \sin(\beta-\alpha) = 1\,, \tag{2.3.22}$$

where $\tilde{H}$ is SM-like. This is even more striking if we rotate the Higgs fields to the *Higgs basis* where only one of the doublet obtaines a VEV,

$$\Phi_1 c_\beta + \Phi_2 s_\beta = \begin{pmatrix} G^+ \\ \frac{1}{\sqrt{2}}\left(v + \phi_1 c_\beta + \phi_2 s_\beta + iG^0\right)\end{pmatrix} \equiv \begin{pmatrix} G^+ \\ \frac{1}{\sqrt{2}}\left(v + \hat{h} + iG^0\right)\end{pmatrix}\,, \tag{2.3.23}$$

$$-\Phi_1 s_\beta + \Phi_2 c_\beta = \begin{pmatrix} H^+ \\ \frac{1}{\sqrt{2}}\left(-\phi_1 s_\beta + \phi_2 c_\beta + iA\right)\end{pmatrix} \equiv \begin{pmatrix} G^+ \\ \frac{1}{\sqrt{2}}\left(\hat{H} + iA\right)\end{pmatrix}\,, \tag{2.3.24}$$

so that

$$\begin{pmatrix}\hat{h}\\ \hat{H}\end{pmatrix} = \underbrace{\begin{pmatrix} c_\beta & s_\beta \\ -s_\alpha & c_\beta\end{pmatrix}}_{\equiv U_\beta}\begin{pmatrix}\phi_1\\ \phi_2\end{pmatrix} = U_\beta U_\alpha^T\begin{pmatrix}\tilde{h}\\ \tilde{H}\end{pmatrix}\,. \tag{2.3.25}$$

Thus, we find a relation between the scalars in the Higgs basis, i.e. $\hat{h}$ and $\hat{H}$, and the mass eigenstates, i.e. $\tilde{h}$ and $\tilde{H}$, given by

$$\hat{h} = \cos(\alpha-\beta)\,\tilde{h} - \sin(\alpha-\beta)\,\tilde{H}\,, \qquad \hat{H} = \sin(\alpha-\beta)\,\tilde{h} + \cos(\alpha-\beta)\,\tilde{H}\,. \tag{2.3.26}$$

2.3.1 Vacuum Stability

In the discussion above, we assumed that the potential (2.3.1) has a global minimum. However, the existence of a global minimum is non-trivial since it requires that the potential is bounded from below, i.e. the quartic terms in (2.3.1) have to be positive for arbitrarly large values of $\Phi_{1,2}$. This requirement induces conditions on the parameters of the scalar potential, given by

$$\lambda_{1,2} \geq 0\,, \quad \lambda_3 \geq -\sqrt{\lambda_1\lambda_2}\,, \quad \lambda_3+\lambda_4-|\lambda_5| \geq -\sqrt{\lambda_1\lambda_2}\,. \tag{2.3.27}$$

Moreover, the vaccum structure in 2HDMs is much richer compared to SM where only two types of vacua are possible, the trivial one with $\langle\phi\rangle = 0$ and the non-trivial one which breaks $\mathrm{SU}(2)_{\mathrm{L}}$, $\langle\phi\rangle \sim v$. In 2HDMs on the other hand, several types of vacua can occur. We can have the "normal" charge- and $\mathcal{CP}$ conserving vacuum,

$$\langle\Phi_1\rangle_N = \begin{pmatrix} 0 \\ \frac{v_1}{\sqrt{2}} \end{pmatrix}\,, \quad \langle\Phi_2\rangle_N = \begin{pmatrix} 0 \\ \frac{v_2}{\sqrt{2}} \end{pmatrix}\,, \tag{2.3.28}$$

the $\mathcal{CP}$ violating vacuum,

$$\langle\Phi_1\rangle_{\mathcal{CP}} = \begin{pmatrix} 0 \\ \frac{\bar{v}_1}{\sqrt{2}}e^{i\theta} \end{pmatrix}\,, \quad \langle\Phi_2\rangle_{\mathcal{CP}} = \begin{pmatrix} 0 \\ \frac{\bar{v}_2}{\sqrt{2}} \end{pmatrix}\,, \tag{2.3.29}$$

where θ is a phase, or the charge breaking vacuum,

$$\langle\Phi_1\rangle_C = \begin{pmatrix} \frac{\alpha}{\sqrt{2}} \\ \frac{\tilde{v}_1}{\sqrt{2}} \end{pmatrix}\,, \quad \langle\Phi_2\rangle_C = \begin{pmatrix} 0 \\ \frac{\tilde{v}_2}{\sqrt{2}} \end{pmatrix}\,, \tag{2.3.30}$$

where $\tilde{v}_{1,2}$ and α are real numbers. It is evident that the coexistence of different types of minima would be a recipe for disaster. However, it can be shown that minima of different types cannot coexist and consequently, tunneling from e.g. a normal vauum to an energetically lower charge breaking vacuum is impossible [82]. Nevertheless, two normal minima can coexist, resulting in a potential scenario where besides the minimum with $v = \sqrt{v_1^2+v_2^2} = 246\,\mathrm{GeV}$, another minimum with $\hat{v} = \sqrt{\hat{v}_1^2+\hat{v}_2^2} \neq 246\,\mathrm{GeV}$ could exist. The mass spectrum in the second minimum evidently differs from the mass spectrum of the first minimum and it is therefore desirable to impose a condition to ensure that the first minumum is the global minimum, which can be written as [79]

$$m_{12}^2\left(m_{11}^2 - \sqrt{\frac{\lambda_1}{\lambda_2}}m_{22}^2\right)\left(t_\beta - \sqrt[4]{\frac{\lambda_1}{\lambda_2}}\right) > 0\,. \tag{2.3.31}$$

CHAPTER 3

Cosmology

So far, we have only discussed the fundamental forces in particle physics that can be described in the formalism of QFT. However, in order to understand the evolution of the Universe, we need to take the fourth fundamental force, gravity, into account. Therefore, modern cosmology is not only build on the SM but also on Einstein's theory of GR. The expansion of the Universe is determined by Einstein's field equations,

$$R_{\mu\nu} - \frac{1}{2} g_{\mu\nu} R - \Lambda g_{\mu\nu} = 8\pi G \tilde{T}_{\mu\nu} \,, \tag{3.0.1}$$

which relate the geometry of the spacetime (LHS) to the matter content of the Universe (RHS). Here, $R_{\mu\nu}$ is the Ricci Tensor, R is the Ricci scalar (see App. A), $G(\Lambda)$ is the gravitational(cosmological) constant and the matter content is described by means of the stress-energy tensor $\tilde{T}_{\mu\nu}$. In the next section, we will give a short introduction to the Hot Big Bang model, which can be considered as the Standard Model of cosmology, followed by an an overview of the most relevant theoretical tools necessary to dicuss the evolution of the Universe in Secs. 3.3, 3.4 and 3.4.2. In Sec. 3.5, we provide a short summary of the history of the Universe alongside a discussion of constraints on cosmological parameters from *Big Bang Nucleosynthesis* (BBN) and the CMB. For details, we refer the reader to Refs. [72, 87–93].

3.1 Cosmological Standard Model

In the Standard Model of cosmology, the Einstein equations are solved under the assumption that the *Cosmological Principle* holds. It states the Universe is homogenous and isotropic on large scales and therefore looks the same in every direction from every point in space. In this case, the geometry of the Universe is described by the *Friedmann-Robertson-Walker* (FRW) metric, which can be written in the form

$$\mathrm{d}s^2 = \mathrm{d}t^2 - a^2(t) \left\{ \frac{\mathrm{d}r^2}{1 - kr^2} + r^2 \mathrm{d}\vartheta^2 + r^2 \sin^2 \vartheta \mathrm{d}\phi^2 \right\} . \tag{3.1.1}$$

Here, $a(t)$ is the scale factor and $k = -1, 0, 1$ is the curvature parameter which determines the geometry of spacetime,

$$\begin{aligned} k = -1 \quad &\Rightarrow \quad \text{hyperbolical}\,, \\ k = 0 \quad &\Rightarrow \quad \text{flat}\,, \\ k = 1 \quad &\Rightarrow \quad \text{spherical}\,. \end{aligned}$$

Note that the coordinates in (3.1.1) are comoving coordinates, i.e. if two objects are separated by a coordinate distance l_{coord}, the corresponding physical distance is given by

$$l_{\text{phys}} = a(t) l_{\text{coord}}\,. \tag{3.1.2}$$

Thus, objects recede from each other with a velocity

$$v = \frac{\dot{a}(t)}{a(t)} l_{\text{phys}} \equiv \mathcal{H} l_{\text{phys}}\,, \tag{3.1.3}$$

where $\mathcal{H}$ is the *Hubble parameter* and overdots denote time derivatives. The equation above is known as the *Hubble law* after Edwin Hubble who observed that distant galaxies move away from us, establishing that the Universe indeed expands [8, 9]. The Hubble parameter is often expressed as

$$h \equiv \frac{\mathcal{H}_0}{100\,\text{km}\,\text{s}^{-1}\,\text{Mpc}^{-1}}\,, \tag{3.1.4}$$

where $\mathcal{H}_0$ is the Hubble parameter today with current limits on h from Planck [18] given by

$$h = 0.674 \pm 0.0005\,. \tag{3.1.5}$$

Moreover, due to the expansion of the Universe, light that is emitted at a time t_e with a wavelength λ_e is redshifted according to the relation

$$1 + z \equiv \frac{a(t_0)}{a(t_e)} = \frac{\lambda_0}{\lambda_e}\,, \tag{3.1.6}$$

where λ_0 is the wavelength observed today and z is the *redshift*.
Concerning the RHS of (3.0.1), it is commonly assumed that the energy content of the Universe behaves like a perfect fluid with an energy density $\tilde{\rho} = \rho_M + \rho_R$ and a pressure $\tilde{p} = p_M + p_R$, where the indices M and R denote matter and radiation, respectively, yielding the stress-energy tensor[1]

$$\tilde{T}^{\mu}{}_{\nu} = \text{diag}\left[\tilde{\rho}(t), -\tilde{p}(t), -\tilde{p}(t), -\tilde{p}(t)\right]\,. \tag{3.1.7}$$

Analogously, the Λ-term on the LHS of (3.0.1) is equivalent to including a stress-energy tensor of the form

$$\hat{T}^{\mu}{}_{\nu} = \text{diag}\left[\rho_\Lambda, -\rho_\Lambda, -\rho_\Lambda, -\rho_\Lambda\right]\,, \qquad \rho_\Lambda = \frac{\Lambda}{8\pi G} \tag{3.1.8}$$

[1]For simplicity, we restrict ourselves here to contributions to the stress-energy tensor from matter and radiation and neglect contributions from e.g. cosmic strings and DWs as their energy densities are believed to be small.

on the RHS of (3.0.1). In this form, it is transparent that the cosmological constant Λ can be interpreted as a vacuum energy. Hence, we can rewrite (3.0.1) as

$$R_{\mu\nu} - \frac{1}{2} g_{\mu\nu} R = 8\pi G \left(\tilde{T}_{\mu\nu} + \hat{T}_{\mu\nu} \right) \equiv 8\pi G T_{\mu\nu} \,, \tag{3.1.9}$$

and define the total energy density and pressure of the Universe as

$$\rho \equiv \rho_M + \rho_R + \rho_\Lambda \,, \qquad p \equiv p_M + p_R + p_\Lambda \,. \tag{3.1.10}$$

The law of energy conservation,

$$\Delta_\mu T^{0\mu} = 0 \,, \tag{3.1.11}$$

where Δ_μ is the covariant derivative (A.0.11), then yields the equation

$$\dot{\rho}(t) + 3 \frac{\dot{a}(t)}{a(t)} \left(p(t) + \rho(t) \right) = 0 \,. \tag{3.1.12}$$

Moreover, combining (3.1.1), (3.1.7) and (3.1.9) we find the Friedmann equations [2]

$$\mathcal{H}(t)^2 = \frac{8\pi G}{3} \rho(t) - \frac{k}{a(t)^2} \,, \tag{3.1.13}$$

$$\frac{\ddot{a}(t)}{a(t)} = -\frac{4\pi G}{3} \left(\rho(t) + 3p(t) \right) \,. \tag{3.1.14}$$

They describe the expansion of the Universe on the basis of the cosmological principle and are therefore a crucial ingredient in modern cosmology. In order to study the effect of different curvature parameters, it is convenient to rewrite (3.1.13) in another form,

$$\frac{k^2}{\mathcal{H}^2 a^2} = \frac{\rho}{\rho_c} \equiv \Omega - 1 \,, \tag{3.1.15}$$

where Ω is the density parameter and the *critical energy density* ρ_c,

$$\rho_c \equiv \frac{3\mathcal{H}^2}{8\pi G} \,, \tag{3.1.16}$$

is precisely the energy density of a flat Universe. Moreover, from (3.1.12), it is easy to deduce how the respective energy densities evolve with a. With the equation of state

$$p = \omega \rho \tag{3.1.17}$$

where ω is a constant that depends on the type of energy that is considered and (3.1.12), we find

$$\rho(t) \sim a(t)^{-3(1+\omega)} \,. \tag{3.1.18}$$

[2] Note that (3.1.12), (3.1.13) and (3.1.14) are not independent as they are related by Bianchi identities.

Consequently, the energy densities of matter, radiation and vacuum energy evolve as

matter:	$\omega_M = 0\,,$	$\rho_M \sim a^{-3}\,,$
radiation:	$\omega_R = \dfrac{1}{3}\,,$	$\rho_R \sim a^{-4}\,,$
vacuum energy:	$\omega_\Lambda = -1\,,$	$\rho_\Lambda \sim \text{const}\,.$

This behavior can easily be understood: A given density of non-relativistic matter is diluted proportionally to the volume factor a^3 while the radiation density is diluted proportionally to a^4 as the photon energy is additionally redshifted due to the expansion of the Universe. We can further express (3.1.13) in terms of $\Omega_i = \rho_i/\rho_c$ as

$$\mathcal{H}^2 = \mathcal{H}_0^2 \left[\Omega_R^0 \left(\frac{a_0}{a}\right)^4 + \Omega_M^0 \left(\frac{a_0}{a}\right)^3 + \Omega_k^0 \left(\frac{a_0}{a}\right)^2 + \Omega_\Lambda^0\right]\,, \tag{3.1.19}$$

where $\rho_k \equiv -3k/8\pi G a^2$ and the index 0 denotes the value of the quantity today. From the time scale dependence of ρ_i (or equivalently Ω_i) we can draw the conclusion that different forms of energy dominated throughout the history of the Universe. Current experimental bounds on $\Omega_{R,M,\Lambda,k}$, to be discussed in Sec. 3.5.2, indicate that the Universe is currently dominated by the vacuum energy. However, going back in time, i.e. to smaller scale factors a, the vacuum energy density stays constant while the radiation and matter densities increase. Thus, in the very early Universe, radiation dominated the energy density, until an era was reached where matter was dominant, which was eventually superseded by the vacuum energy.

Moreover, another important concept in cosmology is *causality*. That is, if two objects are separated by more than twice the *particle horizon*,

$$d_H(t) = a(t) \int_0^t \frac{dt'}{a(t')}\,, \tag{3.1.20}$$

they can never have been in contact and are causally disconnected. From (3.1.13) we can deduce the time dependence of the scale factor $a(t)$ as

$$\omega \neq -1:\ a(t) \sim t^{\frac{2}{3(1+\omega)}}\,, \qquad \omega = -1:\ a(t) \sim e^{\sqrt{\frac{\Lambda}{3}}t}\,, \tag{3.1.21}$$

which yields the particle horizons in a matter or radiation dominated Universe as

$$d_H^M = 3t\,, \qquad d_H^R = 2t\,, \tag{3.1.22}$$

respectively.

Finally, note that for $a = t = 0$, a spacetime singularity is reached, known as the *Big Bang*. In the Big Bang model, the time dependence of the scale factor is used to estimate the age of the Universe to be around $t_U \sim 14\,\text{Gyr}$. However, this is to be treated with caution: At temperatures higher than the Planck mass M_Pl, quantum corrections to GR become important and a theory of *quantum gravity* is necessary. Since gravity is non-renormalizable and non-pertrubative, it is not trivial to quantize and consequently, an accepted theory of quantum gravity does not yet exist.

3.2 Equilibrium Thermodynamics

Throughout its early evolution, it is commonly assumed that the Universe evolved through sequences of states where at each stage, the constituents are described by equilibrium distributions. This assumption greatly simplifies the theoretical description of the thermal history of the Universe as it reduces the parameters that describe the state of matter to the temperature and the chemical potentials of the particles. In the following, we will give a short overview of equilibrium thermodynamics before discussing how to treat deviations from equilibrium in the next section.
The kinetic equilibrium distribution of a species i at a temperature T is given by

$$f_i(\vec{p_i}) = \frac{1}{e^{\frac{E_i-\mu_i}{\mathsf{T}}} \pm 1}\,, \tag{3.2.1}$$

where the plus sign is for fermions and the minus for bosons, $E_i = \sqrt{|\vec{p_i}^2| + m_i^2}$ is the energy of i while m_i and μ_i are the mass and the chemical potential, respectively. Using (3.2.1), we can determine the number density n_i, energy density ρ_i and pressure p_i for a species i with g_i internal degrees of freedom as

$$n_i = \frac{g_i}{(2\pi)^3}\int d^3p f_i(\vec{p_i})\,, \tag{3.2.2}$$

$$\rho_i = \frac{g_i}{(2\pi)^3}\int d^3p E_i(\vec{p_i}) f_i(\vec{p_i})\,, \tag{3.2.3}$$

$$p_i = \frac{g_i}{(2\pi)^3}\int d^3p \frac{|\vec{p_i}|^2}{3E_i} f_i(\vec{p_i})\,. \tag{3.2.4}$$

Although the chemical potentials play an important role in the evolution of the Universe, their numerical values appearing in (3.2.1) are generally assumed to be small enough to neglect them. In this case, (3.2.2)-(3.2.4) can be written as

$$n_i = \begin{cases} \frac{\zeta(3)}{\pi^2} g_i \mathsf{T}^3\,, & \text{bosons}\,, \\ \frac{3\zeta(3)}{4\pi^2} g_i \mathsf{T}^3\,, & \text{fermions}\,, \end{cases} \qquad \rho_i = \begin{cases} \frac{\pi^2}{30} g_i \mathsf{T}^4\,, & \text{bosons}\,, \\ \frac{7}{8}\frac{\pi^2}{30} g_i \mathsf{T}^4\,, & \text{fermions}\,, \end{cases} \qquad p_i = \frac{\rho}{3}\,. \tag{3.2.5}$$

in the relativistic limit $\mathsf{T} \gg m_i$ and as

$$n_i = g_i \left(\frac{m\mathsf{T}}{2\pi}\right)^{\frac{3}{2}} e^{-\frac{m_i}{\mathsf{T}}}\,, \quad \rho_i = m_i n_i\,, \quad p_i = n_i \mathsf{T}\,. \tag{3.2.6}$$

in the non-relativistic limit $\mathsf{T} \ll m_i$. Here, $\zeta(x)$ is the Riemann zeta function with $\zeta(3) \approx 1.20206$. From (3.2.6), it is apparent that the number and energy densities of a non-relativistic species are exponentially suppressed compared to a relativistic species, see (3.2.5). This is called *Boltzmann suppression*. Hence, when calculating the *total* energy density ρ and pressure p of all particles in equilibrium, it is generally a good approximation to include only the contributions from *relativistic* species. Introducing the total number

of effectively massless degrees of freedom,

$$g_* = \sum_{i\in\text{bosons}} g_i \left(\frac{\mathsf{T}_i}{\mathsf{T}}\right)^4 + \frac{7}{8}\sum_{i\in\text{fermions}} g_i \left(\frac{\mathsf{T}_i}{\mathsf{T}}\right)^4 , \tag{3.2.7}$$

we find the total energy density and pressure of all relativistic species as

$$\rho_\text{rel} = \frac{\pi^2}{30} g_* \mathsf{T}^4 , \qquad p_\text{rel} = \frac{\pi^2}{90} g_* \mathsf{T}^4 , \tag{3.2.8}$$

respectively. The number of effectively massless degrees of freedom g_* is a function of temperature as only the degrees of freedom of particles that are relativistic contribute, i.e. it changes when a species falls out of equilibrium. At high temperatures $\mathsf{T} \gtrsim 300\,\text{GeV}$, all SM species are relativistic and we find

$$g_* = 106.75 . \tag{3.2.9}$$

Another useful quantity is the *entropy density*,

$$s(\mathsf{T}) \equiv \frac{\rho(\mathsf{T}) + p(\mathsf{T})}{\mathsf{T}} \approx \frac{\rho_\text{rel}(\mathsf{T}) + p_\text{rel}(\mathsf{T})}{\mathsf{T}} = \frac{2\pi^2}{45} g_{*s} \mathsf{T}^3 , \tag{3.2.10}$$

where

$$g_{*s} = \sum_{i\in\text{bosons}} g_i \left(\frac{\mathsf{T}_i}{\mathsf{T}}\right)^3 + \frac{7}{8}\sum_{i\in\text{fermions}} g_i \left(\frac{\mathsf{T}_i}{\mathsf{T}}\right)^3 , \tag{3.2.11}$$

which is numerically equivalent to (3.2.7) at high temperatures. From the conservation of the entropy,

$$S = Vs = a^3 s , \tag{3.2.12}$$

we can deduce that $s \sim a^{-3}$, which prompts us to define the *abundance* Y_i as

$$Y_i = \frac{n_i}{s} \sim n_i a^3 . \tag{3.2.13}$$

The abundance Y_i is useful since in the absence of particle-number changing interactions of a species i, it is constant. Using (3.2.13), we can further define a *charge asymmery* as

$$Y_{\Delta q} \equiv \frac{n_q - n_{\overline{q}}}{s} , \tag{3.2.14}$$

which can be related to chemical potentials by taking the concept of *chemical equilibrium* into account. If a reaction $i + j \leftrightarrow k + l$ is in chemical equilibrium, the chemical potentials of the species i, j, k and l are related via

$$\mu_i + \mu_j = \mu_k + \mu_l , \tag{3.2.15}$$

which implies that the chemical potential of a species whose particle number is not conserved, e.g. photons, has to vanish. Considering a particle i with an corresponding antiparticle $\bar{i}$ and $i + \bar{i} \leftrightarrow \gamma$ in chemical equilibrium, this further implies that

$$\mu_i + \mu_{\bar{i}} = 0 \tag{3.2.16}$$

and hence

$$\mu_i \equiv \mu_i = -\mu_{\bar{i}}\,, \tag{3.2.17}$$

i.e. the chemical potenials of particles and antiparticles differ only by the sign. In the relativistic limit $\mathsf{T} \gg m_i$, we can use (3.2.2) and (3.2.17) to find a simple expression for the difference between the particle and antiparticle number densities,

$$n_i - n_{\bar{i}} \approx \begin{cases} \frac{g_i \mathsf{T}^2}{6}\mu_i\,, & i \in \text{fermions}\,, \\ \frac{g_i \mathsf{T}^2}{3}\mu_i\,, & i \in \text{bosons}\,. \end{cases} \tag{3.2.18}$$

The charge asymmetry $Y_{\Delta q}$ can then be written in terms of the chemical potentials as

$$Y_{\Delta q} \approx \frac{\mathsf{T}^2}{6s}\left[\sum_{k\in\text{fermions}} q_k g_k \mu_k + 2\sum_{k\in\text{bosons}} q_k g_k \mu_k\right], \tag{3.2.19}$$

where q_k is the charge of a species i. The charge asymmery is a useful quantity since e.g. the conservation of the Q_{EM} implies that $Y_{\Delta Q_{\text{EM}}} = 0$, which imposes relations between the chemical potentials of the particles that contribute to $Y_{\Delta Q_{\text{EM}}}$.

3.3 Boltzmann Equations

Although the assumption that the Universe evolves through sequences of states close to thermal equilibrium proves reasonable, it is the intermedient departures of the particle content from equilibrium that invoke interesting effects. Thus, in order to study those deviations from equilibrium, we need a formalism that describes the evolution of the different particles species, taking both the expansion of the Universe and the interactions in the plasma into account. This is achieved by means of *Boltzmann equations*.[3] It greatly simplifies the Boltzmann equations to assume that kinetic equilibrium holds and that the phase space densities of the relevant particles can be approximated as Maxwell-Boltzmann distributions,

$$f_i \approx e^{\frac{\mu_i}{\mathsf{T}}} e^{-\frac{E_i}{\mathsf{T}}} \equiv e^{\frac{\mu_i}{\mathsf{T}}} f_i^{\text{eq}}\,, \tag{3.3.1}$$

yielding the number density of a species l as

$$n_i = e^{\frac{\mu_i}{\mathsf{T}}} n_i^{\text{eq}}\,. \tag{3.3.2}$$

Here, the chemical equilibrium number density is given by

$$n_i^{\text{eq}} = g_i \int \frac{d^3 p_i}{(2\pi)^3} f_i^{\text{eq}} = \frac{g_i m_i \mathsf{T}}{2\pi^2}\mathrm{K}_2\Big(\frac{m_i}{\mathsf{T}}\Big) \approx \begin{cases} g_i \frac{\mathsf{T}^3}{\pi^2}\,, & \mathsf{T} \gg m_i\,, \\ g_i \left(\frac{m_i \mathsf{T}}{2\pi}\right) \frac{3}{2} e^{-\frac{m_i}{\mathsf{T}}}\,, & \mathsf{T} \gg m_i\,, \end{cases} \tag{3.3.3}$$

and $K_n(x)$ is the modified Bessel function of the second kind. Further defining

$$z_X \equiv \frac{m_X}{\mathsf{T}}\,, \tag{3.3.4}$$

[3] See App. F for details.

the Boltzmann equation for a particle X can be written as [94]

$$s\mathcal{H}z_X\frac{dY_X}{dz_X} = -\sum_{\text{processes}}\left[Xa... \leftrightarrow ij...\right] , \tag{3.3.5}$$

where the sum runs over all processes that change the number density of X. For example, for the $2 \to 2$ scattering $Xa \leftrightarrow ij$, we have

$$\left[Xa \leftrightarrow ij\right] \equiv \left[\delta_X\delta_a\gamma^{\text{eq}}\left(Xa \to ij\right) - \delta_i\delta_j\gamma^{\text{eq}}\left(ij \to Xa\right)\right] , \qquad \delta_l \equiv \frac{n_l}{n_l^{\text{eq}}} , \tag{3.3.6}$$

where $\gamma^{\text{eq}}\left(Xa \to ij\right)$ is the *thermal rate* that depends on the matrix elements of $Xa \to ij$ scatterings and the equilibrium distributions of X and a, see (F.1.17). If the process $Xa \leftrightarrow ij$ is $\mathcal{CP}$ invariant,

$$\gamma^{\text{eq}}\left(Xa \to ij\right) \overset{\mathcal{CP}}{=} \gamma^{\text{eq}}\left(ij \to Xa\right) , \tag{3.3.7}$$

we can simplify (3.3.6) further, yielding

$$\left[Xa \leftrightarrow ij\right] = \left[\delta_X\delta_a - \delta_i\delta_j\right]\gamma^{\text{eq}}\left(ij \leftrightarrow Xa\right) . \tag{3.3.8}$$

From (3.3.5), we can derive a qualitative estimate when a species is in equilibrium. For simplicity, we assume that X only interacts via a $\mathcal{CP}$ conserving scattering process with $Xa \leftrightarrow ij$ with a, i and j in equilibrium, yielding the Boltzmann equation for the evolution of X as

$$s\mathcal{H}z_X\frac{dY_X}{dz} = -\left(\delta_X - 1\right)\gamma^{\text{eq}}\left(Xa \leftrightarrow ij\right) . \tag{3.3.9}$$

Clearly, the LHS of (3.3.9) is of order $n_X\mathcal{H}$ and thus, if the reaction rate

$$\Gamma_{Xa\leftrightarrow ij} \equiv \frac{\gamma^{\text{eq}}\left(Xa \leftrightarrow ij\right)}{n_X} \tag{3.3.10}$$

is much larger than the expansion rate $\mathcal{H}$, the only way to maintain equality in (3.3.9) is that $\delta_X = 1$, i.e. the species X is in equilibrium. Hence, a useful rule of thumb is that a process P is effective at keeping a species X in equilibrium if

$$\Gamma_P \gg \mathcal{H} \tag{3.3.11}$$

holds. On the other hand, if

$$\Gamma_P \ll \mathcal{H} , \tag{3.3.12}$$

the process P is ineffective at establishing equilibrium.
In this work, we restrict ourselves to Boltzmann equations including decays and $2 \to 2$ scatterings. For brevity, we will use the notation

$$\gamma_{ab,ij} \equiv \gamma^{\text{eq}}\left(ab \leftrightarrow ij\right) \tag{3.3.13}$$

if $ab \leftrightarrow ij$ conserves $\mathcal{CP}$ and

$$\gamma_{ab\to ij} \equiv \gamma^{\text{eq}}\left(ab \to ij\right) , \qquad \gamma_{ij\to ab} \equiv \gamma^{\text{eq}}\left(ij \to ab\right) \tag{3.3.14}$$

if $ab \leftrightarrow ij$ violates $\mathcal{CP}$.

3.4 Phase Transitions

In Sec. 2, we have discussed SSB at zero temperature. However, as discussed in this Chapter, we have excellent reason to believe that the Universe was initially very hot and subsequently cooled down to lower temperatures. Thus, we expect that similarly to condensed matter systems, spontaneously broken symmetries are restored at higher temperatures. Moreover, in the context of cosmology, SSB has implications beyond the generation of particle masses. Depending on the symmetry that is spontaneously broken, different types of topological defects arise that can have crucial effects on the evolution of the Universe and constrain particle physics models based on the (un-)observed signatures. After reviewing the mechanism of symmetry restoration, we will briefly discuss topological defects, in particular focussing on DWs, following Refs. [75, 89, 92, 95–98].

3.4.1 Symmetry Restoration

At zero temperature, the equilibrium value of a field ϕ is determined by minimizing the tree-level potenial $V(\phi)$ or, more precisely the effective potenial V_{eff}, which includes higher-order corrections,

$$V_{\text{eff}}(\phi) = V(\phi) + V_1(\phi) + V_2(\phi) + \dots\,, \tag{3.4.1}$$

where $V_n(\phi)$ are the n-loop contributions to the potenial. On the other hand, at non-zero temperature, the equilibrium value of a scalar ϕ is determined by minimizing the free energy,

$$F(\phi, \mathsf{T}) = E(\phi) - S(\phi)\mathsf{T}\,, \tag{3.4.2}$$

or the *finite-temperature effective potential*,

$$V_{\text{eff}}(\phi, \mathsf{T}) = \frac{F(\phi, \mathsf{T})}{\mathcal{V}} = V(\phi) + V_1(\phi) + \sum_i \mathcal{F}_i(\phi, \mathsf{T})\,, \tag{3.4.3}$$

$$\mathcal{F}_i(\phi, \mathsf{T}) = \pm\frac{g_i \mathsf{T}^4}{2\pi^2}\int dx x^2 \ln\left[1 \mp \exp\left(-\sqrt{x^2 + \frac{m_i(\phi)^2}{\mathsf{T}^2}}\right)\right]\,, \tag{3.4.4}$$

where $\mathcal{V}$ is the volume, $\mathcal{F}_i$ and g_i are the free energy density and the spin degrees of freedom of a particle i, respectively, $m_i(\phi)$ is the ϕ-dependent mass of i and the upper (lower) sign is for bosons(fermions). At high temperatures $\mathsf{T} \gg m_i(\phi)$, the free energy can be simplified to

$$\mathcal{F}_i = \begin{cases} -\frac{\pi^2\mathsf{T}^4}{90} + \frac{m_i(\phi)^2\mathsf{T}^2}{24}\,, & i \in \text{bosons}\,, \\ -\frac{7\pi^2\mathsf{T}^4}{720} + \frac{m_i(\phi)^2\mathsf{T}^2}{48}\,, & i \in \text{fermions}\,. \end{cases} \tag{3.4.5}$$

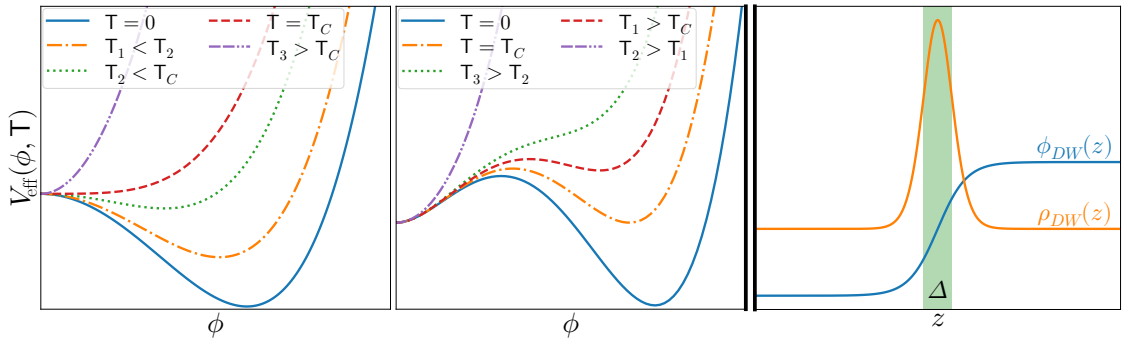

Figure 3.1: Temperature dependence of the finite-temperature effective potential $V_{\text{eff}}(\mathsf{T}, \phi)$ for a second order phase transition (left) and a first order phase transition (right).

Figure 3.2: The DW solution $\phi_{\text{DW}}(z)$ and energy density $\rho_{\text{DW}}(z)$ for a DW with characteristic width Δ.

Considering for example the simple case of the Z_2 symmetric Lagrangian discussed in Sec. 2.1.1, the effective potential is given by

$$V_{\text{eff}}(\phi, \mathsf{T}) = V(\phi) + V_1(\phi) - \frac{\pi^2 \mathsf{T}^4}{90} + \frac{M(\phi)^2 \mathsf{T}^2}{24} \tag{3.4.6}$$

$$= -\frac{1}{2}\mu^2(\mathsf{T})\phi^2 + \frac{\lambda}{4}\phi^4 - \frac{\pi^2 \mathsf{T}^4}{90} - \frac{\mu^2 \mathsf{T}^2}{24} + \frac{\lambda v^4}{4} + \ldots \tag{3.4.7}$$

where

$$\mu^2(\mathsf{T}) \equiv \mu^2 - \frac{\lambda}{4}\mathsf{T}^2\,, \qquad M(\phi) = \frac{\partial^2 V}{\partial \phi^2} = -\mu^2 + 3\lambda\phi^2\,. \tag{3.4.8}$$

It is apparent that $\mu^2(\mathsf{T})$ is negative as long as $\mathsf{T}^2 > \frac{4\mu^2}{\lambda}$ and changes sign at the *critical temperature*, $\mathsf{T}_C \equiv 2\mu/\sqrt{\lambda}$. This implies that for $\mathsf{T} > \mathsf{T}_C$, $\langle\phi\rangle = 0$ is a stable minimum and the Z_2 symmetry is manifest. On the other hand, for $\mathsf{T} \leq \mathsf{T}_C$, $\langle\phi\rangle = 0$ becomes a local maximum and the symmetry is spontaneously broken, with the two equivalent ground states being given by (2.1.3). This behavior is characteristic for a *second order* phase transition where $\langle\phi\rangle$ is continuous at the critical temperature, as illustrated in Fig. 3.1. The other possibility are *first order* phase transitions, also shown in Fig. 3.1. At high temperatures, $\langle\phi\rangle = 0$ is the only minimum but as the temperature decreases, two additional minima develop at $|\langle\phi\rangle| \neq 0$. At $\mathsf{T} = \mathsf{T}_C$, the minima become degenerate and as the temperature decreases further, the non-symmetric minima become smaller than the symmetric minimum. Depending on the theory, the minimum at $\langle\phi\rangle = 0$ either vanishes at some temperature T^* or persists, as is the case here, until $\mathsf{T} = 0$.

3.4.2 Domain Walls and other Topological Defects

DWs [99] are topological defects that are associated with the SSB of discrete symmetries. A simple example for a theory where a DW arises is the Z_2 invariant model discussed in

Sec. 2.1.1 with a Lagrangian given by

$$\mathcal{L} = \frac{1}{2}\left(\partial_\mu \phi\right)\left(\partial^\mu \phi\right) - V(\phi)\,, \qquad V(\phi) = \frac{\lambda}{4}\left(\phi^2 - v^2\right)^2\,. \tag{3.4.9}$$

So far, we assumed that ϕ acquires the same VEV, either $\langle\phi\rangle = v$ or $\langle\phi\rangle = -v$, everywhere in space when a symmetry is spontaneously broken. However, let us now consider the possibility that ϕ takes on different values at distinct regions in space, for example

$$\phi(z=\infty) = v\,, \qquad \phi(z=-\infty) = -v\,, \tag{3.4.10}$$

where we assumed that ϕ does not depend on y and z. By solving the static equation of motion for ϕ,

$$-\frac{\partial \phi^2}{\partial z^2} + \lambda\phi(\phi^2 - v^2) = 0\,, \tag{3.4.11}$$

we find that there is indeed a solution that interpolates between $\phi(z=\infty) = v$ and $\phi(z=-\infty) = -v$, given by

$$\phi_{\rm DW}(z) = v\tanh\left(\frac{v\sqrt{\lambda}z}{2}\right)\,. \tag{3.4.12}$$

It is apparent that a smooth transition from $\phi(x=\infty) = v$ to $\phi(x=-\infty) = -v$ implies that we have $\phi(x=0) = 0$ and $V(\phi(x=0)) \neq 0$, i.e. the field configuration (3.4.12) has non-zero energy. The transition region between the minima with a characteristic width $\Delta \equiv \sqrt{2/\lambda v^2}$ is called the DW in the $x-y$ plane, see Fig. 3.2. The stress-energy tensor for the DW is given by

$$T_{\mu\nu} = \frac{\lambda}{v^4} 2 \frac{1}{\cosh^4\left(\frac{x}{\Delta}\right)} \mathrm{diag}\left(1,-1,-1,0\right)\,, \tag{3.4.13}$$

and we can identify the T_{00} component, which is centered around $z=0$, as the energy density $\rho(z)$, see Fig. 3.2. Moreover, note that the pressures in the x- and y-directions are negative, i.e. the DW *repells* test particles. From (3.4.13), we find the surface energy density of the DW as

$$\sigma_{\rm DW} \equiv \int dz\, T_{00} = \frac{2\sqrt{2}}{3}\sqrt{\lambda} v^3\,. \tag{3.4.14}$$

One important property of the configuration (3.4.12) is the existence of a conserved current,

$$j^\mu = \frac{1}{2v}\epsilon^{\mu\nu}\partial_\nu \phi\,, \tag{3.4.15}$$

which implies the presence of a conserved topological charge,

$$Q = \int dz\, j^0 = \phi(z=\infty) - \phi(z=-\infty). \tag{3.4.16}$$

It is easy to see that the trivial vacua $\phi = \pm v$ have $Q=0$ while the DW has $Q=1$. Thus, the DW configuration lies in a different topological sector than the trivial vacua,

ensuring its stability.[4]

Let us now discuss the implications of DWs in the context of cosmology. In cosmology, DWs are produced via the *Kibble mechanism* [100, 101] in phase transitions if the vacuum state has disconnected components, as discussed above. In contrast to the simplified discussion though, the Kibble mechanism takes into account that the correlation length ζ of the Higgs field during the phase transitions is finite, leading to a system of domains with arbitrary vacua. The correlation length depends on the details of the phase transition, but a simple estimate based on causality exists. As regions that are separated by more than the particle horizon d_H, given in (3.1.20), are causally disconnected, we can apply the particle horizon as the upper bound on the correlation length,

$$\zeta \lesssim d_H(\mathsf{T}_C)\,, \tag{3.4.17}$$

where T_C is the critical temperature where the phase transition takes place.[5] In fact, this argument implies that at any time after the phase transition, the characteristic domain size has to be smaller than the particle horizon and we expect *at least* one DW per horizon. Thus, we can give a lower limit on the energy densities of the DWs at a time t as

$$\rho_{\mathrm{DW}} \gtrsim \frac{\sigma}{d_H(t)} \sim \sigma\mathcal{H}\,. \tag{3.4.18}$$

which we can compare to the critical energy density,

$$\Omega_{\mathrm{DW}} \equiv \frac{\rho_{\mathrm{DW}}}{\rho_c} \gtrsim \frac{G\sigma}{\mathcal{H}} \sim G\sigma t\,. \tag{3.4.19}$$

Using $\sigma \sim v^3$ and requiring that the energy density of the network of DWs does not exceed the critical energy density today, we can find an upper bound on the VEV v,

$$v \sim \left(\frac{{\mathrm{M_{Pl}}}^2}{t_0}\right)^{\frac{1}{3}} \sim 100\,\mathrm{MeV}\,, \tag{3.4.20}$$

where $t_0 \approx 10^{17}\,\mathrm{s}$. Thus, if DWs exist today, the associated energy scale needs to be very low.

Another model that implies the appearance of DWs is the sine-Gordon model, where the potential in the Lagrangian (3.4.9) is given by

$$V(\phi) = \frac{m^4}{\lambda}\left(1 - \cos\left(\frac{\sqrt{\lambda}}{m}\phi\right)\right)\,. \tag{3.4.21}$$

The potential (3.4.23) is periodic and therefore has an infinite number of degenerate vacua with $\langle\phi\rangle = 2\pi m N \lambda^{-1/2}$, where N is an integer. Similarly to the Z_2-model, DWs arise if the field settles into distinct vacua at different locations in space. For example, if ϕ settles

[4] In principle, DWs can be rendered unstable, for example if a subsequent symmetry breaking sufficiently alters the vacuum structure of the theory. However, this possibility is not relevant here.

[5] More precisely, T_C should be replaced with the Ginzburg temperature $\bar{\mathsf{T}}_C$ which is slightly smaller than T_C.

into neighboring vacua at $z = \pm\infty$, a domain wall with a surface energy density

$$\sigma_{SG} = \frac{8m^3}{\lambda} \tag{3.4.22}$$

arises. A special case of the sine-Gordon model appears e.g. in Axion models [36–38][6] where the field $\phi \equiv \mathtt{a}$ is the Goldstone boson of a spontaneously broken $U(1)$ symmetry. In such models, the Axion obtains a potential,

$$V(\mathtt{a}) = \frac{m_{\mathtt{a}}^2 f_{\mathtt{a}}^2}{N_{\mathrm{DW}}^2}\left(1 - \cos\left(\frac{N_{\mathrm{DW}}}{f_{\mathtt{a}}}\mathtt{a}\right)\right), \tag{3.4.23}$$

due to QCD Instanton effects. Here, the integer N_{DW} is the DW number which is related to the chiral anomaly, while $m_{\mathtt{a}}$ is the Axion mass and $f_{\mathtt{a}}$ is the VEV that breaks $U(1)$. Interpreting $\mathtt{a}$ as a 2π periodic phase (see Sec. 2.1.2), we find that the potential posseses a discrete $Z_{N_{\mathrm{DW}}}$ symmetry with N_{DW} discrete minima [110] and consequently, DWs with a surface energy density of order

$$\sigma_{\mathtt{a}} \sim m_{\mathtt{a}} f_{\mathtt{a}}^2 \,. \tag{3.4.24}$$

appear in generic Axion models [110–112].

There exist a variety of other topological defects that can potentially arise throughout the evolution of the Universe, depending on the symmetry that is broken. Two notable examples are *strings* and *magnetic monopoles.*
Strings arise if the vacuum manifold[7] has non-contractible, one-dimensional closed paths. An example for this scenario is a model where a $U(1)$ is completely broken so that the corresponding vacuum manifold is a circle.
Magnetic monopoles appear when the vacuum manifold has non contractible two spheres or, in other words, when the unbroken subgroup has non contractible paths. This situation occurs e.g. whenever the unbroken subgroup contains an explicit factor of $U(1)$. This implies that *any* GUT[8] that breaks to the electroweak gauge group $\mathrm{SU}(2)_{\mathtt{L}}\times U(1)_Y$ predicts the existence of magnetic monopoles.[9] These monopoles are highly problematic as they would contribute sizably to the energy density of the Universe, contrary to observations.

[6] See e.g. [102–110] for detailed reviews on Axion physics.
[7] If a theory that is invariant under transformations by elements of a group G is broken due to the VEV of a scalar field, a subgroup H of G remains unbroken. The vacuum manifold, i.e. the space of non-trivial transformations, is denoted as G/H and can be considered as the space of distinct ground states.
[8] See App. D for details on GUTs.
[9] EWSB does not predict magnetic monopoles since the SM gauge group is not simply connected[75].

3.5 A Brief History of the Universe

After having discussed the basic theoretical concepts relevant for cosmology, we now provide a very brief overview of the thermal history of the Universe, focussing on stages relevant for this thesis.

- $\mathsf{T} \gtrsim 10^{19}\,\mathrm{GeV}$:
  At temperatures above the Planck scale, gravity is strong and hence the theory of GR invalid. Thus, a theory of quantum gravity is necessary which does not yet exist.

- $10^{19}\,\mathrm{GeV} \gtrsim \mathsf{T} > 10^{2}\,\mathrm{GeV}$:
  The energy scales in this era are far above experimental access and consequently, we can only speculate how the Universe evolved at this stage. There are, however, some well-motivated theories. For example, one assumption is that around $\mathsf{T} \sim 10^{16}\,\mathrm{GeV}$, the gauge interactions of the SM combine to form a GUT. Moreover, it is possible that the origin of the baryon asymmetry of the Universe lies in this era. This will be discussed in greater detail in Sec. 4.3. It is also widely believed that *Inflation* took place in this era. The yet hypothetical Inflation mechanism postulates a period of rapid expansion in the very early Universe, thereby addressing several problems of the Big Bang model, such as the absence of magnetic monopoles predicted by GUTs, the *flatness problem*[10] and the *horizon problem*[11].

- $\mathsf{T} \sim 174\,\mathrm{GeV}$: EWSB
  At a temperature around $\mathsf{T}_{\mathrm{EWSB}} \approx 174\,\mathrm{GeV}$, EWSB takes place. Before EWSB, the particles in the plasma only have thermal masses while after EWSB, they obtain masses via the Higgs mechanism, as discussed in Sec. 2.2.1.

- $\mathsf{T} \sim 200\,\mathrm{MeV}$: QCD phase transition
  After EWSB, the temperature is still too high for bound states to form and quarks form a *quark gluon plasma*. Once confinement sets in around $\mathsf{T}_{QCD} \sim 200\,\mathrm{MeV}$, quarks are bound into baryons and mesons.

- $\mathsf{T} \sim 1\,\mathrm{MeV}$: Neutrino decoupling
  Neutrinos fall out of equilibrium as the weak interaction rate becomes slower than the expansion of the Universe. After decoupling, neutrinos free-stream the Universe with a temperature that is related to the photon temperature T_γ as

  $$\mathsf{T}_\nu = \left(\frac{4}{11}\right)^{\frac{1}{3}} \mathsf{T}_\gamma\,.$$

  Today, these neutrinos are predicted to form the cosmic neutrino background, yet direct detection remains elusive.

[10] Today, we have an almost perfectly flat Univere with $\Omega \approx 1$. This requires that Ω is fine-tuned even close to 1 in the Planck epoch, $|\Omega - 1| \lesssim 10^{-60}$.

[11] The Universe is very homogenous, even over distances that can never have been in thermal contact according to the Hot Big Bang model.

- $1\,\mathrm{MeV} \gtrsim \mathsf{T} \gtrsim 0.05\,\mathrm{MeV}$: BBN
  At about 1 MeV, the temperature of the plasma is low enough to allow protons and neutrons to form the first light primordial nuclei, ^{2}He, ^{3}He, ^{4}He and ^{7}Li. BBN corresponds to the earliest stage of the Universe which has accesible observational signatures.
- $\mathsf{T} \sim 1\,\mathrm{eV}$: Matter-radiation equality
  Matter begins to dominate the energy density of the Universe over radiation, allowing structure formation to start.
- $\mathsf{T} \sim 0.3\,\mathrm{eV}$: Recombination and photon decoupling
  At $\mathsf{T} \gtrsim 0.3\,\mathrm{eV}$, photons are coupled to the plasma via elastic Thomson scattering off free electrons. Around $\mathsf{T} \sim 0.3\,\mathrm{eV}$, electrons and protons combine to form hydrogen, thus significantly decreasing the electron density and resulting in the decoupling of photons from the plasma. After decoupling, the photons freely propagate in the Universe and form the CMB.

Observations of the CMB and the light elements formed during BBN are valuable tools to constrain cosmological parameters. In the following, we will shortly discuss these stages in more detail.

3.5.1 Big Bang Nucleosynthesis

At high temperatures, neutrons are coupled to the plasma via weak interactions such as

$$n + \nu_e \leftrightarrow p + e^- \tag{3.5.1}$$

and kinetic equilibrium implies that the neutron-proton ratio follows

$$\frac{n_n}{n_p} \sim e^{-\frac{m_n - m_p}{\mathsf{T}}}\,, \tag{3.5.2}$$

where we assume that the chemical potentials can be neglected. Eventually, at $\mathsf{T}_n^{\mathrm{dec}} \sim 1\,\mathrm{MeV}$, the rate of the weak interactions in Eq. (3.5.1) drops below the expansion of the Universe and neutrons decouple, freezing the neutron abundance in at a ratio $n_n/n_p \sim 0.2$. As the temperature decreases further, the synthesis of a light element i with nucleon (proton) number $A_i(Z_i)$ and nuclear mass m_{A_i} becomes favored over free protons and neutrons. Consequently, the first light elements ^{2}He, ^{3}He, ^{4}He and ^{7}Li are formed through chains like

$$\begin{aligned} p + n &\leftrightarrow {}^2\mathrm{He} + \gamma \\ {}^2\mathrm{He} + {}^2\mathrm{He} &\leftrightarrow {}^3\mathrm{He} + n \\ {}^3\mathrm{He} + {}^2\mathrm{He} &\leftrightarrow {}^4\mathrm{He} + p\,. \end{aligned} \tag{3.5.3}$$

The temperature where the production of an element i can start is not only determined by the corresponding nuclear binding energy,

$$B_i = Z_i m_p + (A_i - Z_i)\, m_n - m_{A_i}\,, \tag{3.5.4}$$

but also depends on the baryon-to-photon ratio

$$\eta_{B'} \equiv \frac{n_{B'} - n_{\overline{B'}}}{n_\gamma}\,, \tag{3.5.5}$$

and is given by

$$\mathsf{T}_i \approx \frac{B_i}{A_i - 1} \frac{1}{\ln\left(\eta_{B'}^{-1} + \frac{3}{2}\ln\left(\frac{m_p}{\mathsf{T}}\right)\right)}\,. \tag{3.5.6}$$

However, since the synthesis of the heavier elements ${}^3\mathrm{He}$, ${}^4\mathrm{He}$ and ${}^7\mathrm{Li}$ requires a sufficent abundance of ${}^2\mathrm{He}$, see (3.5.3), primordial nucleosynthesis starts only for $\mathsf{T} < \mathsf{T}_{{}^2\mathrm{He}}$, even though $\mathsf{T}_{{}^2\mathrm{He}} < \mathsf{T}_{{}^3\mathrm{He},{}^4\mathrm{He},{}^7\mathrm{Li}}$. This is often called the *deuterium bottleneck*. The abundances of the light elements that are subsequently produced essentially depend only on one single parameter, the baryon-to-photon ratio $\eta_{B'}$. From observations, the primordial abundances of the light elements can be infered which allows to predict a range for $\eta_{B'}$ that is consistent with all four abundances, [17]

$$\eta_{B'}^{BBN} = (6.04 \pm 0.12) \times 10^{-10}\,. \tag{3.5.7}$$

3.5.2 Cosmic Microwave Background

The CMB radiation reaching us today corresponds to the surface where photons last scattered and has a nearly perfect black body spectrum with a temperature of [113]

$$\mathsf{T}_0 \approx (2.7255 \pm 0.0006)\,\mathrm{K}\,. \tag{3.5.8}$$

It is remarkably uniform with anisotropies of order 10^{-5}, yielding evidence for the large-scale isotropy and homogeneity of the Universe. However, precisely these anisotropies are imprints of the conditions at recombination and can be used to constrain various cosmological parameters. Notably, the general shape of the anisotropy spectrum, shown in Fig. 3.3, can be almost entirely explained by considering the acoustic oscillations of the photon-baryon fluid before recombination.[12] Roughly, the perturbations of the photon temperature θ obey a differential equation of the form [88, 114]

$$\ddot{\theta} + k^2 c_s^2 \theta = F\,, \tag{3.5.9}$$

where k is the wave number, F is a driving force that takes gravity effects into account, c_s is the speed of sound in the photon-baryon fluid,

$$c_s = \frac{1}{\sqrt{3\left(1 + \frac{3\rho_{B'}}{4\rho_\gamma}\right)}}\,, \tag{3.5.10}$$

[12] In a detailed analysis, other effects need to be taken into account, such as the Sachs-Wolfe effect (CMB photons are gravitationally redshifted) and the Sunyaev-Zeldovich effect (distortion of the CMB spectrum due to photons beung scatterd by hot gas when passing through clusters).

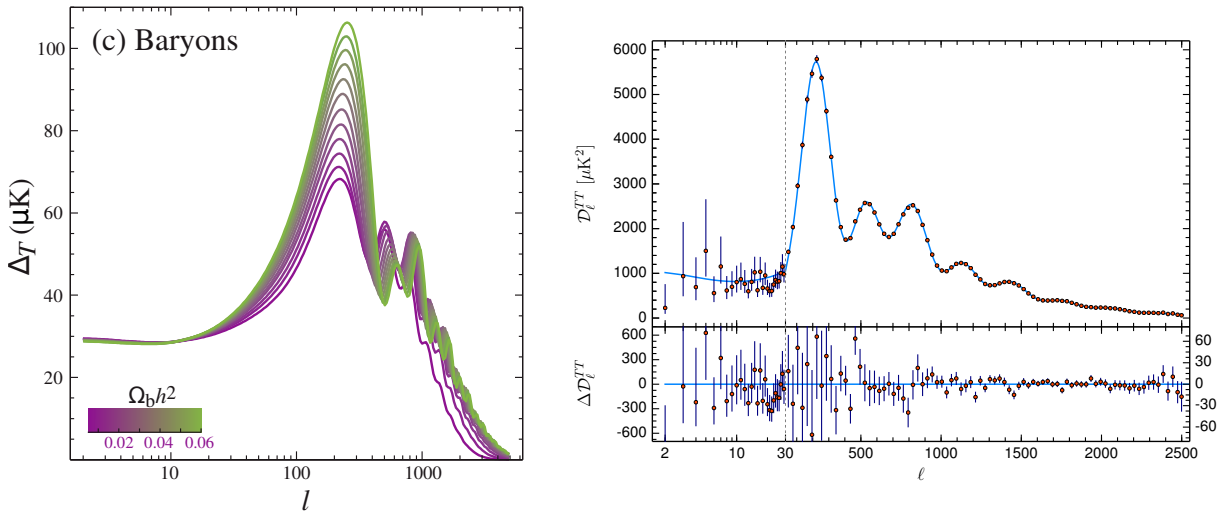

Figure 3.3: *Left:* The acoustic temperature spectrum for different values of $\Omega_{B'}h^2$. It is evident that the disparity of even and odd peaks is enhanced for larger values of $\Omega_{B'}h^2$. Figure taken from Ref. [114]. *Right:* CMB temperature power spectrum from measurements by Planck [18].

and derivatives are with respect to conformal time,

$$\eta \equiv \int_0^t \frac{dt'}{a(t')} \,. \tag{3.5.11}$$

Clearly, this is the differential equation for a forced harmonic oscillator, and the corresponding squared solutions $\theta^2(\eta)$ have a characteristic spectrum with even and odd peaks of different height. The disparity between even and odd peaks depends on c_s, and hence on the baryon number. For larger $\rho_{B'}$, the speed of sound decreases and the effect of the external force, i.e. gravity, becomes more relevant. In other words, baryons provide an additional source of gravity that enhances the disparity between even and odd peaks, corresponding to variations in temperature. An additional effect that needs to be accounted for is that during the era of recombination, the mean free path of photons, and therefore also the mean distance traveled by photons in a Hubble time, is finite, $\lambda_D \sim 1/\sqrt{n_e}$. Consequently, oscillations on scales smaller than the mean distance, or equivalently at large k, are damped. Moreover, during recombination, the electron number density is proportional to the baryon number density, and consequently, a larger baryon number implies a *smaller* mean distance and thus the dampings sets in at *larger* k.

Taking these two effects into account, we can predict a spectrum of inhomogenities on scales k at recombination, which is then projected onto the anisotropies on angular scales l we can observe today, roughly following the relation [88, 114]

$$l \approx k\,(\eta_0 - \eta_*) \,, \tag{3.5.12}$$

where $(\eta_0 - \eta_*)$ is the comoving distance between us and the surface of last scattering. In Fig. 3.3 (left), we show the predicted anisotropy spectrum for different baryon energy

Table 3.1: Cosmological parameters from CMB measurements.

Parameter	Value	Reference	Parameter	Value	Reference
h	0.674 ± 0.005	[18]	Ω_k	0.0007 ± 0.0019	[18]
Ω_R	$(5.38 \pm 0.15) \times 10^{-5}$	[113]	$\Omega_{B'} h^2$	0.0224 ± 0.0001	[18]
Ω_M	0.315 ± 0.007	[18]	$\Omega_{\rm DM} h^2$	0.1200 ± 0.0012	[18]
Ω_Λ	0.685 ± 0.007	[18]	$\sum m_\nu$	$< 0.12\,\text{eV}$	[18]

densities while in Fig. 3.3 (right), we show the results from Planck [18]. Note that today, we obseve the baryonic acoustic observations at angular scales $100 \leq l \leq 1000$ while the effects of diffusion damping appear at $l \geq 1000$. Since the disparity of even and odd peaks and the damping tail are very sensitive to the baryon energy density, comparisons between the predicted spectrum and the observed spectrum can be used to place tight constraints on its value, with the most stringent bounds being provided by the Planck collaboration [18],

$$\Omega_{B'}^{\rm CMB} h^2 = 0.0224 \pm 0.0001\,. \tag{3.5.13}$$

Besides the energy density of the baryons, the anisotropy spectrum of the CMB is very sensitive to a number of other parameters such as the curvature Ω_k, the matter density Ω_M, and the energy density of the cosmological constant Ω_Λ. In Tab. 3.1, we present bounds on several parameters relevant for this thesis.

CHAPTER 4

Evidence and Frameworks for BSM physics

Despite the success of the SM and the cosmological Standard Model, there is ample evidence that both models are not yet complete. In the following, we will outline several shortcomings of the SM and the cosmological Standard Model with a focus on the topics relevant for this thesis.

4.1 Dark Matter

Based on observations of the velocities of galaxies in the Coma cluster, Fritz Zwicky [25] postulated in 1933 the existence of a non-luminous matter component, called DM. Many years later, in the 1970s, the measurements of the rotation curves of galaxies further increased the evidence for the existence of non-luminous matter [115]. Kepler's third law implies that the orbital velocities of gas clouds and stars around the core of the galaxies should decrease with the radial distance r,

$$v(r) = \sqrt{\frac{G_N M(r)}{r}}\,, \tag{4.1.1}$$

where $M(r)$ is the mass contained in a sphere of radius r. If the mass of a galaxy is mainly given by visible objects such as stars, the mass far away from the visible galaxy becomes constant, implying $v(r) \sim r^{-1/2}$ at large r. However, according to observations, the velocity at large r becomes constant, indicating that $M(r) \sim r$, i.e. there is non-luminous matter far beyond the visible disc.
Further evidence for the existence of DM comes from observations of the Bullet cluster [26], which is composed of two clusters that passed through each other. Gravitational lensing studies of the cluster indicate that a sizable mass component stems from dark objects that are weakly interacting and hence were not significantly affected by the collision, in contrast to the strongly interacting baryonic matter that was significantly slowed down in the collision. This observation strongly supports the existence of DM, while other theories that attempt to explain e.g. the flattening of the rotation curves of galaxies as consequences of a modified theory of gravity generally fail to explain the displacement of the matter components in the Bullet cluster.
Moreover, DM plays an important role for the formation of structures in the early universe. Before recombination, baryons are coupled to photons in a baryon-photon plasma, preventing density perturbations from growing. Only once baryons and photons decouple, density perturbations can start to grow as overdense regions attract surrounding matter.

The density contrast δ is defined as

$$\delta \equiv \frac{\delta\rho}{\rho} = \frac{\rho' - \rho}{\rho}\,, \tag{4.1.2}$$

where ρ is the mean energy density and ρ' is the overdensity. The density contrast evolves as $\delta(t) \sim a(t)$, allowing us to give an estimate of the density contrast today,

$$\delta_0 \sim \frac{a(t_0)}{a(t_{rec})}\delta_{rec} \sim 10^{-2}, \tag{4.1.3}$$

where we used $\delta_{rec} \sim 10^{-5}$ and $a(t_0)/a(t_{rec}) \sim 10^3$ [18]. This is in stark contrast to observations, as the existence of structures such as galaxies implies a density contrast many orders of magnitudes larger. As DM particles can decouple from the plasma significantly earlier than baryons (or never were coupled to the plasma in the first place), the associated density perturbations can start to grow significantly earlier as well. Once baryons eventually decouple, they fall in the gravitational wells formed by DM, allowing structures like galaxies to form. The way structure formation proceeds depends significantly on the mass of the DM particle. If it is relativistic when structure formation starts, a large free-streaming length implies that structure forms top-down, i.e. large structures are formed before small structures. However, observations indicate a hierarchical structure formation, where smaller structures are formed first, requiring DM to be non-relativistic at the onset of structure formation.[1]
Finally, as discussed in Sec. 3.5.2, CMB measurements are very sensitive to the matter density Ω_M and the baryon density $\Omega_{B'}$, which indicate that $\Omega_M \gg \Omega_{B'}$ (see Tab. 3.1), impliying that DM is non-baryonic. Moreover, CMB measurements are also sensitive to the DM relic density itself, with the most current bound being provided by the Planck collaboration, [18]

$$\Omega_{\rm DM}h^2 = 0.1200 \pm 0.0012\,. \tag{4.1.4}$$

To summarize, observations indicate the need for at least one DM particle that is electrically neutral, weakly interacting, non-relativistic at the onset of structure formation, non-baryonic and sufficiently stable.[2] These observations have motivated intense efforts to build a wide range of models that can account for the DM relic density. Moreover, DM candidates appear naturally in many models and hence provide constraints on the model parameters as to avoid e.g. overproduction of DM or a sizable hot DM contribution to the relic density. In many models, be it decicated DM models or models with "accidentally" appearing DM candidates, the relic density arises either via the *freeze-in* [34] and or the *freeze-out* mechanism [116–118], both of which we will shortly discuss below.

[1] Strictly speaking, these bounds only hold if the DM particle has established kinetic equilibrium at some point. If it is never in kinetic equilibrium, it can lead to a hierarchical structure formation even if it has a very small mass. An example for this scenario is the Axion.

[2] While it is often assumed that DM is stable based on the absence of decay channels, it is in principle viable that a DM particle has decay channels, provided that the lifetime is at least of order of the age of the Universe.

4.1.1 Freeze-In and Freeze-Out

In order to illustrate the freeze-in and the freeze-out mechanisms, let us consider the Boltzmann equation for a species X with a mass m_X that interacts with a single other massless species A. For simplicity, we assume that X is stable and interacts with A only via $\mathcal{CP}$ conserving scatterings $XX \leftrightarrow AA$ while A has interactions with other particles in the plasma, keeping it in equilibrium. The Boltzmann equation for this scenario is given by

$$s\mathcal{H}z_X \frac{dY_X}{dz_X} = -2\left(\delta_X^2 - 1\right)\gamma_{XX,AA}\,, \tag{4.1.5}$$

where the factor of 2 appears since the scattering processes change the abundance of X by *two* units. The thermal rate $\gamma_{XX,AA}$ is determined using (G.1.1) and we assume that the cross section scales as $\sigma \sim g^2/s$, where g is the corresponding coupling constant.
In the freeze-out mechanism, interactions between X and A are initially fast, i.e. $\gamma_{XX,AA} > \mathcal{H}n_X$, hence X is coupled to the plasma and in equilibrium. However, as the temperature drops and $z_X \gtrsim 1$, the number density $n_X^{\rm eq} \sim e^{-z_X}$ becomes Boltzmann suppressed and the thermal rate $\gamma_{XX,AA} \sim \left(n_X^{\rm eq}\right)^2$ drops rapidly (see Fig. 4.1). At some $z_X^{\rm fo}$, the rate $\gamma_{XX,AA}/n_X^{\rm eq}$ drops below $\mathcal{H}$ and the X particles cease to find partners to annihilate with. Thus, the abundance Y_X becomes constant and *freezes out*. One characteristic feature of the freeze out mechanism is the dependence on the coupling g. As shown in Fig. 4.1, a larger g corresponds to a larger thermal rate and a larger $z_X^{\rm fo}$, keeping X longer in equilibrium. Due to the exponential drop of $Y_X^{\rm eq}$, this implies that the frozen abundance decreases as g increases.
In contrast, the interactions of X with A in the freeze-in scenario are so weak that it never reaches equilibrium. Moreover, as $Y_X \ll Y_X^{\rm eq}$, we can simplify the Boltzmann equation (4.1.5) to

$$s\mathcal{H}z_X \frac{dY_X}{dz_X} \approx 2\gamma_{XX,AA}\,. \tag{4.1.6}$$

Thus, for small $z_X \lesssim 1$, annihilations of A produce a small number density of X. However, as soon as the temperature drops below the mass of X, i.e. $z_X \gtrsim 1$, the production of X becomes ineffective and the abundance of X becomes constant, i.e. it *freezes in*. Contrary to the freeze-out mechanism, the frozen abundance in the freeze-in mechanism increases with the coupling g since a larger thermal rate implies a faster production of X, see Fig. 4.1.
Defining the frozen abundance produced either via freeze-in or freeze-out as Y_X^f, the corresponding relic density today can be calculated as

$$\Omega_{RD} = \frac{Y_X^f m_X s_0}{\rho_c}\,, \tag{4.1.7}$$

where s_0 is the entropy density today.

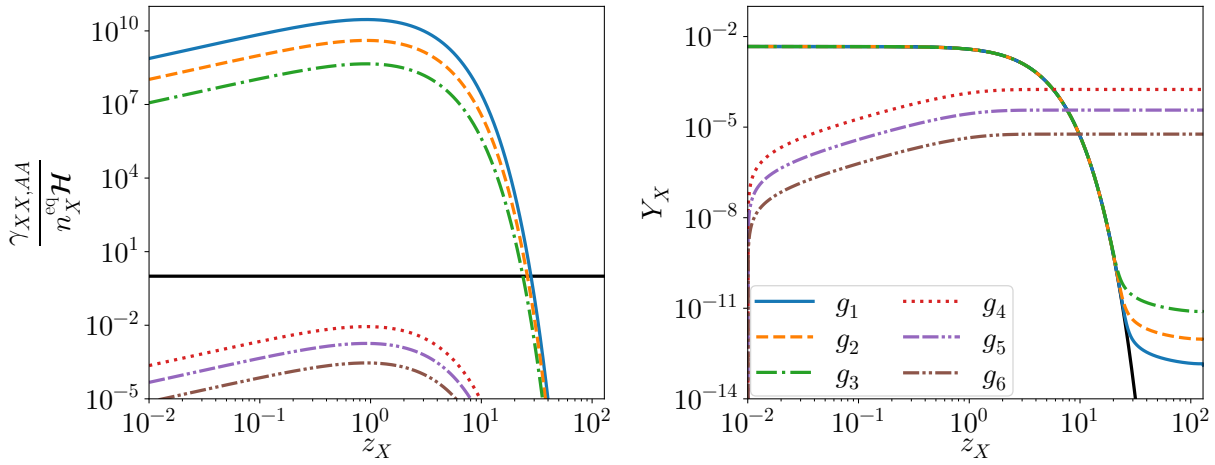

Figure 4.1: Thermal rates of $XX \leftrightarrow AA$ scatterings (left) and the evolution of the abundance $Y_X(z_X)$ (right) for $g_1 > g_2 > g_3 \gg g_4 > g_5 > g_6$ where $g_{1,2,3}(g_{4,5,6})$ correspond to the freeze-out (freeze-in) scenario. In the left figure, the solid black line denotes $\gamma_{XX,AA}/n_X^{eq}H = 1$ while in the right figure, the solid black line denotes Y_X^{eq}.

4.2 Neutrino Masses

The observation of neutrino oscillations [20–22] has been a groundbreaking discovery, and since oscillations imply that the corresponding particle is massive, it remains to this day one of the clearest hints that the SM is not complete. However, neutrino masses are not part of the SM as the RH neutrino required for the Higgs mechanism to work is not part of the SM. Besides the bare existence of neutrino masses, the current bounds on the values of the masses are well below the masses of the other SM fermions, see Fig. 4.2, raising additional questions. Below, we will briefly review neutrino oscillations and present current bounds on the neutrino masses and the mixing angles, followed by a discussion of possible mass generating mechanisms in the next section.
The relation between the flavor- and mass-eigenstates of the neutrinos can be written as

$$|\nu_\alpha\rangle = U_{\alpha i}\,|\nu_i\rangle\ , \qquad |\nu_i\rangle = U^*_{\alpha i}\,|\nu_\alpha\rangle\ , \tag{4.2.1}$$

where U is the unitary PMNS matrix, $\alpha = e, \mu, \tau$ denote the flavor eigenstates while $i = 1, 2, 3$ denote the mass eigenstates. Similarly to the CKM matrix, (2.2.44), the PMNS matrix [124, 125] can be parametrized as

$$U = \begin{pmatrix} c_{12}c_{13} & s_{12}c_{13} & s_{13}e^{-i\delta} \\ -s_{12}c_{23} - c_{12}s_{23}s_{13}e^{i\delta} & c_{12}c_{23} - s_{12}s_{23}s_{13}e^{i\delta} & s_{23}c_{13} \\ s_{12}s_{23} - c_{12}c_{23}s_{13}e^{i\delta} & -c_{12}s_{23} - s_{12}c_{23}s_{13}e^{i\delta} & c_{23}c_{12} \end{pmatrix} \mathrm{diag}\left(e^{i\rho}, e^{i\sigma}\right) \tag{4.2.2}$$

where $c_{ij} \equiv \cos\theta_{ij}, s_{ij} \equiv \sin\theta_{ij}$, θ_{ij} are the mixing angles, δ is the Dirac phase while ρ and σ are Majorana phases.
The probabilty that a neutrino ν_α is observed with flavor ν_β after having traveled a

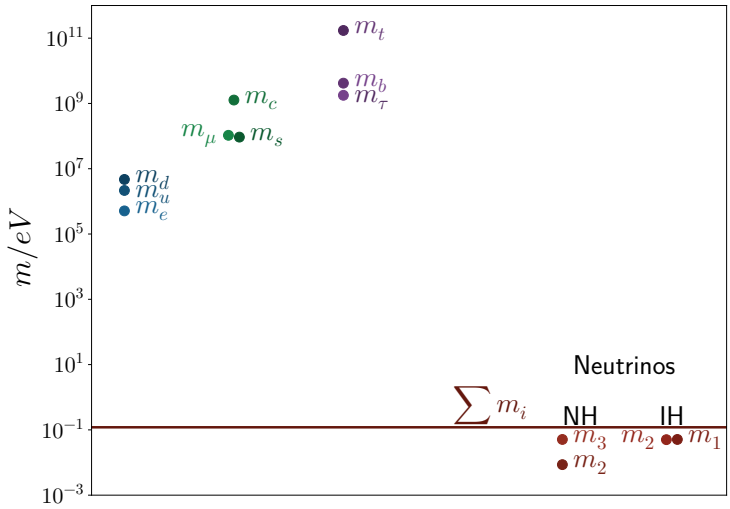

Figure 4.2: Schematical representation of the fermion mass scales in the SM, compared to the neutrino masses in the cases of NH and IH, respectively, with the lightest neutrino mass set to zero, and the upper limit on the sum of the neutrino masses by Planck [18] (see (4.2.8)).

distance L is given by

$$P_{\alpha\to\beta} = |\,\langle\nu_\beta|\nu_\alpha(t)\rangle\,|^2 = U_{\alpha i}U^*_{\beta i}U_{\alpha j}U^*_{\beta j}e^{-i\frac{\Delta m^2_{ij}L}{2E}}\,, \tag{4.2.3}$$

where we defined the mass-squared difference

$$\Delta m^2_{ij} \equiv m^2_i - m^2_j \tag{4.2.4}$$

and used $E_{i,j} \approx E + \frac{m^2_{i,j}}{2E}$. From (4.2.3), it is apparent that neutrino oscillations can only occur if neutrinos are massive. Moreover, it is striking that the transition probabilty depends only on the mass-squared differences Δm^2_{ij} and not on the absolute neutrino mass scale. Neutrino oscillation measurements can therefore only probe the mass squared differences Δm^2_{21} and $|\Delta m^2_{32}|$. As the sign of Δm^2_{32} is unkown, the neutrino mass spectrum can either follow a *normal hierarchy* (NH) or an *inverse hierarchy* (IH),

$$\text{normal hierarchy:} \qquad m_3 \gg m_2 > m_1\,, \tag{4.2.5}$$

$$\text{inverse hierarchy:} \qquad m_2 > m_1 \gg m_3\,. \tag{4.2.6}$$

Current bounds on the mass-squared differences and the mixing parameters are given in Tab. 4.1. Further constraints on the neutrino masses are provided by the KATRIN experiment which measures the endpoint of the tritium beta decay kinematic spectrum. It places a model-independent upper bound on the effective electron neutrino mass [127],

$$m^{\text{eff}}_{\nu_e} \equiv \sqrt{\sum_i m^2_i |U_{ei}|^2} \lesssim 0.8\,\text{eV}\,, 90\,\%\text{CL}\,. \tag{4.2.7}$$

Table 4.1: Neutrino oscillation data at 1σ [126] for NH (left) with $\Delta m^2_{3\ell} = \Delta m^2_{31}$ and IH (right) with $\Delta m^2_{3\ell} = \Delta m^2_{32}$.

Parameter	Value (NH)	Value (IH)
$\sin^2\theta_{12}$	$0.307^{+0.012}_{-0.011}$	$0.308^{+0.012}_{-0.011}$
$\sin^2\theta_{23}$	$0.561^{+0.012}_{-0.015}$	$0.561^{+0.012}_{-0.015}$
$\sin^2\theta_{13}$	$0.02195^{+0.00054}_{-0.00058}$	$0.02224^{+0.00056}_{-0.00057}$
$\delta/^\circ$	177^{+19}_{-20}	285^{+25}_{-28}
$\frac{\Delta m^2_{21}}{10^{-5}\,\mathrm{eV}^2}$	7.49 ± 0.19	7.49 ± 0.19
$\frac{\Delta m^2_{3\ell}}{10^{-3}\,\mathrm{eV}^2}$	$2.534^{+0.025}_{-0.023}$	$-2.510^{+0.024}_{-0.025}$

Observations based on the cosmological Standard Model place an additional upper limit on the neutrino mass. The currently strongest bound comes from the Planck collaboration [18] with[3]

$$\sum m_\nu \lesssim 0.12\,\mathrm{eV}\,. \tag{4.2.8}$$

In contrast to bounds placed by e.g. KATRIN, this bound is not model-independent and depends on the framework of the Standard Model of cosmology.
In the following, we will review the *Seesaw mechanism* which is an elegant framework that manages to account for the existence of the neutrino masses and their smallness with a minimal extension of the SM.

4.2.1 Seesaw Mechanism

Compared to the other fermions, neutrinos have a special role in the SM since they carry no charge that is conserved under the SM gauge group. This allows neutrinos to be their own antiparticles, i.e. *Majorana* particles, in contrast to the charged SM fermions which are *Dirac particles* (see App. B for details). A clear indication that neutrinos are of the Majorana type would be the observation of *neutrinoless double beta decay* ($0\nu\beta\beta$). Although it is searched for by several experiments, the half-lifes of $0\nu\beta\beta$ significantly exceed the age of the Universe, e.g. $T_{0\nu\beta\beta} > 1.8 \times 10^{26}\,\mathrm{yr}$ for $0\nu\beta\beta$ of ^{76}Ge [128]. To date, it has not been observed, leaving the nature of neutrinos ambigous. Nevertheless, neutrinos being Majorana fermions would have several significant implications both for the SM and for cosmology.
A popular mechanism that allows for the generation of naturally light neutrinos, the *Seesaw mechanism*, is build on the hypothetical Majorana nature of neutrinos. It is

[3] As briefly touched upon in Sec. 3.5, neutrinos decouple when they are still relativistic at around 1 MeV. Nowadays, they are non-relativistic and consequently, their energy density is given by $\rho_\nu = m_\nu n_\nu$. Since the neutrino temperature is related to the photon temperature, the former can be precisely determined from CMB data. In order to avoid overclosing the Universe, the total neutrino energy density has to be smaller than the critical energy density, or $\Omega_\nu < \Omega \approx 1$, yielding the bound $\sum m_\nu \lesssim 93.12\,\mathrm{eV}h^2\Omega_\nu$.

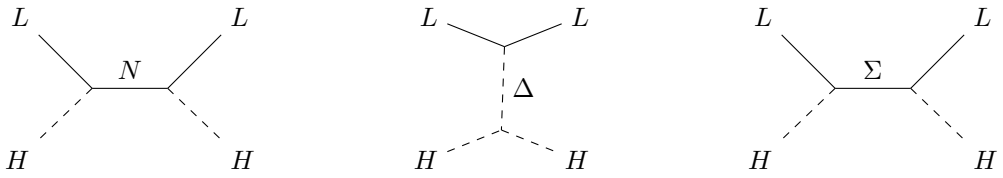

Figure 4.3: Feynman diagrams corresponding to the type I (left), type II (middle) and type III (right) Seesaw mechanisms.

related to the dimension-5 Weinberg operator [129],

$$\mathcal{L}_{\text{eff}} = \frac{c^{d=5}}{\Lambda}\left(\overline{L^C}\tilde{H}^*\right)\left(\tilde{H}^\dagger L\right) + \text{h.c.}\,, \tag{4.2.9}$$

which violates lepton number by two units. Here, Λ is the scale of new physics. After EWSB, the operator induces a Majorana mass term,

$$\mathcal{L}_{\text{eff}} = \frac{c^{d=5}v^2}{2}\left(\overline{(\nu_{\mathtt{L}})^C} + \nu_{\mathtt{L}}\right)\left(\overline{\nu_{\mathtt{L}}} + \nu_{\mathtt{L}}^C\right) \equiv \frac{c^{d=5}v^2}{2}\overline{\nu}\nu\,, \tag{4.2.10}$$

which generates naturally small neutrino masses $m_\nu \sim \Lambda^{-1}$ if Λ is large. On tree level, there exist three basic ways to generate this operator, shown in Fig. 4.3, and its realizations correspond to the type I [23], type II [130–134] and type III [135] Seesaw mechanism, respectively. In the following, we provide brief reviews these mechanisms, based on Refs. [136–141].

4.2.1.1 Type I Seesaw

In the type I Seesaw mechanism, the SM is extended by $n \geq 2$ RH SM singlet neutrinos $N_{\mathtt{R}}$. For simplicity, we assume that $n = 3$, although two RH neutrinos are already sufficient to explain neutrino masses. The relevant terms for the neutrino sector in the Lagrangian are therefore given by

$$\mathcal{L}^N_{yuk} = -\overline{L_i}Y^\nu_{ij}\tilde{H}N_{\mathtt{R}_j} - \frac{1}{2}M^{ij}_{\mathtt{R}}\overline{(N_{\mathtt{R}_i})^C}N_{\mathtt{R}_j} + \text{h.c.}\,, \tag{4.2.11}$$

$$\mathcal{L}^N_{kin} = i\overline{L}\not{D}L + i\overline{N_{\mathtt{R}}}\not{\partial}N_{\mathtt{R}}\,, \tag{4.2.12}$$

where Y^ν_{ij} is a non-diagonal 3×3 Yukawa matrix while $M^{ij}_{\mathtt{R}}$ is the mass matrix for the RH neutrinos. It is convenient to choose the basis where $M^{ij}_{\mathtt{R}}$ is both real and diagonal, allowing us to write

$$\mathcal{L}^N_{yuk} = -\overline{L_i}Y^\nu_{ij}\tilde{H}N_j - \frac{1}{2}M^i_{\mathtt{R}}\overline{(N_i)^C}N_i + \text{h.c.}\,, \tag{4.2.13}$$

$$\mathcal{L}^N_{kin} = i\overline{L}\not{D}L + \frac{i}{2}\overline{N}\not{\partial}N\,, \tag{4.2.14}$$

where we defined the Majorana neutrinos as

$$N_i \equiv N_{\mathtt{R}_i} + (N_{\mathtt{R}_i})^C = (N_i)^C\,, \tag{4.2.15}$$

and C is defined in App B. After EWSB, the mixing between the LH and RH neutrinos induces a Dirac mass m_D,

$$m_D^{ij} = \frac{Y_{ij}^{\nu} v}{\sqrt{2}}\,, \tag{4.2.16}$$

and we can write the mass terms in the Lagrangian as

$$\mathcal{L}^{\nu}_{mass} = -\frac{1}{2}\begin{pmatrix}\overline{\nu_{\mathtt{L}}} & \overline{(N_{\mathtt{R}})^C}\end{pmatrix}\underbrace{\begin{pmatrix}0 & m_D\\ m_D^T & M_{\mathtt{R}}\end{pmatrix}}_{\mathcal{M}}\begin{pmatrix}(\nu_{\mathtt{L}})^C\\ N_{\mathtt{R}}\end{pmatrix} + \text{h.c.}\,. \tag{4.2.17}$$

The $(3+n)\times(3+n)$ mass matrix $\mathcal{M}$ can be diagonalized with a unitary matrix $\tilde{U}$ as

$$\tilde{\mathcal{M}} \equiv \text{diag}\,(m_1, m_2, ..., m_{3+n}) = \tilde{U}^T \mathcal{M} \tilde{U}\,. \tag{4.2.18}$$

Thus, defining

$$\begin{pmatrix}(\nu'_{\mathtt{L}})^C\\ N'_{\mathtt{R}}\end{pmatrix} = \tilde{U}^{\dagger}\begin{pmatrix}(\nu_{\mathtt{L}})^C\\ N_{\mathtt{R}}\end{pmatrix}\,, \tag{4.2.19}$$

we can rewrite the Lagrangian (4.2.17) as

$$\mathcal{L}^{\nu}_{mass} = -\frac{1}{2}\begin{pmatrix}\overline{\nu'_{\mathtt{L}}} & \overline{(N'_{\mathtt{R}})^C}\end{pmatrix}\tilde{\mathcal{M}}\begin{pmatrix}(\nu'_{\mathtt{L}})^C\\ N'_{\mathtt{R}}\end{pmatrix} - \frac{1}{2}\begin{pmatrix}\overline{(\nu'_{\mathtt{L}})^C} & \overline{N'_{\mathtt{R}}}\end{pmatrix}\tilde{\mathcal{M}}\begin{pmatrix}\nu'_{\mathtt{L}}\\ (N'_{\mathtt{R}})^C\end{pmatrix} \tag{4.2.20}$$

$$= -\frac{1}{2}\sum_{i=1}^{3}\overline{\hat{\nu}_i} m_i \hat{\nu}_i - \frac{1}{2}\sum_{i=4}^{n}\overline{\hat{N}_i} m_i \hat{N}_i\,. \tag{4.2.21}$$

Here, the physical mass eigenstates with masses m_i are the Majorana fields,

$$\hat{N}_i \equiv N'_{\mathtt{R}_i} + \left(N'_{\mathtt{R}_i}\right)^C\,, \qquad \hat{\nu}_i \equiv \nu'_{L_i} + \left(\nu'_{L_i}\right)^C\,. \tag{4.2.22}$$

Let us now return to the matrix $\mathcal{M}$. In the *Seesaw limit* $M_{\mathtt{R}} \gg m_D$, we can blockdiagonalize $\mathcal{M}$ so that

$$\hat{U}^T \mathcal{M} \hat{U} = \text{diag}\,(\hat{m}_l, \hat{m}_h)\,, \tag{4.2.23}$$

where

$$\hat{U} \approx \begin{pmatrix}1 & \frac{m_D}{M_{\mathtt{R}}}\\ -\frac{m_D^T}{M_{\mathtt{R}}^T} & 1\end{pmatrix}\,, \qquad \hat{m}_l \approx -\frac{m_D^T m_D}{M_{\mathtt{R}}}\,, \qquad \hat{m}_h \approx M_{\mathtt{R}}\,. \tag{4.2.24}$$

Thus, in the Seesaw limit, we find light neutrinos with masses suppressed by $M_{\mathtt{R}}$ and heavy neutrinos with masses of order $M_{\mathtt{R}}$. Moreover, the light and heavy states approximately decouple,

$$\begin{pmatrix}(\tilde{\nu}_{\mathtt{L}})^C\\ \tilde{N}_{\mathtt{R}}\end{pmatrix} \equiv \hat{U}^{\dagger}\begin{pmatrix}(\nu_{\mathtt{L}})^C\\ N_{\mathtt{R}}\end{pmatrix} \approx \begin{pmatrix}(\nu_{\mathtt{L}})^C - \frac{m_D}{M_{\mathtt{R}}} N_{\mathtt{R}}\\ \frac{m_D}{M_{\mathtt{R}}}(\nu_{\mathtt{L}})^C + N_{\mathtt{R}}\end{pmatrix} \approx \begin{pmatrix}(\nu_{\mathtt{L}})^C\\ N_{\mathtt{R}}\end{pmatrix}\,, \tag{4.2.25}$$

resulting in

$$\hat{N}_i \approx N_i\,, \qquad \hat{\nu}_i \approx \nu_i\,, \tag{4.2.26}$$

and

$$\mathrm{diag}\,(m_1, m_2, m_3) \approx U^T \hat{m}_l U\,, \tag{4.2.27}$$

where U is the PMNS matrix.

4.2.1.2 Type II Seesaw

In the type II Seesaw mechanism, the SM is augmented by a scalar $\mathrm{SU}(2)_\mathrm{L}$ triplet Δ [139, 141–145],

$$\Delta = \begin{pmatrix} \frac{\Delta^+}{\sqrt{2}} & \Delta^{++} \\ \Delta^0 & -\frac{\Delta}{\sqrt{2}} \end{pmatrix}, \tag{4.2.28}$$

which carries a lepton number $L' = -2$. The relevant terms in the Lagrangian coupling Δ to L and H are given by

$$\mathcal{L} \supset \mu_\Delta \tilde{H}^T i\sigma_2 \Delta - \overline{L^C} Y^\Delta i\sigma_2 \Delta L + \mathrm{h.c.}\,, \tag{4.2.29}$$

and once Δ and H acquire non-vanishing VEVs,

$$v_\Delta = \sqrt{2}\,\langle\Delta\rangle\,\frac{\mu_\Delta v_0^2}{\sqrt{2} M_\Delta^2}\,, \qquad v_0 = \sqrt{2}\,\langle H\rangle\,, \qquad v_0^2 + 2v_\Delta^2 = v^2 \approx (246\,\mathrm{GeV})^2\,, \tag{4.2.30}$$

small neutrino masses are generated,

$$m_\nu^\Delta = \sqrt{2} Y^\nu v_\Delta\,. \tag{4.2.31}$$

Both VEVs contribute to the masses of the $W^\pm$ and Z bosons and since their ratio is tightly constrained by the ρ parameter,

$$\rho \equiv \frac{m_W^2}{m_Z^2 \cos\theta} = 1 - \frac{2v_\Delta^2}{v_0^2 + 4v_\Delta^2}\,, \tag{4.2.32}$$

the VEV of the scalar triplet is bounded from above, $v_\Delta \lesssim 4.8\,\mathrm{GeV}$.

4.2.1.3 Type III Seesaw

In the type III Seesaw mechanism, the SM is extended by $n \geq 2$ $\mathrm{SU}(2)_\mathrm{L}$ triplet fermions [139, 141, 146–150],

$$\Sigma_i = \begin{pmatrix} \Sigma_i^0/\sqrt{2} & \Sigma_i^+ \\ \Sigma_i^- & -\Sigma_i^0/\sqrt{2} \end{pmatrix}, \tag{4.2.33}$$

which induce additional terms in the Lagrangian given by

$$\mathcal{L} \supset i\mathrm{Tr}\left[\overline{\Sigma} \not{D} \Sigma\right] - \overline{L} Y_\Sigma^\dagger \Sigma \tilde{H} - \frac{1}{2}\mathrm{Tr}\left[\overline{\Sigma^C} M_\Sigma \Sigma\right] + \mathrm{h.c.}\,. \tag{4.2.34}$$

After EWSB, light neutrino masses are generated via the neutral component Yukawa term,

$$m_\nu^\Sigma = -\frac{v^2}{2} Y_\Sigma^T M_\Sigma^{-1} Y_\Sigma \,. \tag{4.2.35}$$

In terms of neutrino mass generation, the type III Seesaw is very similar to the type I Seesaw. Beyond neutrino masses though, the type III seesaw entails several features that are absent in the type I seesaw. For instance, the triplet Σ has direct interactions with gauge bosons and additionally, the charged components $\Sigma^\pm$ mix with the SM leptons.

4.3 Baryon Asymmetry

To the best of out knowledge, the observable Universe consists (almost) completely of matter and no notable amounts of anti-matter exist, suggesting a baryon asymmetric Universe. As discussed in Sec. 3.5, the BAU can be inferred from two independent observations. From the BBN measurements, the baryon-to-photon ratio is [17]

$$\eta_{B'}^{BBN} = \left.\frac{n_{B'} - n_{\overline{B'}}}{n_\gamma}\right|_0 (6.04 \pm 0.12) \times 10^{-10} \,, \tag{4.3.1}$$

while CMB data [18] gives consistent limits,

$$\Omega_{B'}^{\rm CMB} h^2 = 0.0224 \pm 0.0001 \,. \tag{4.3.2}$$

In terms of a baryon asymmetry $Y_{\Delta B'}$, these limits can be expressed as[4]

$$Y_{\Delta B'}^{\rm BBN} \approx 8.580 \times 10^{-11} \,, \qquad Y_{\Delta B'}^{\rm CMB} \approx 8.718 \times 10^{-11} \,. \tag{4.3.3}$$

In principle, it is possible that this asymmetry is indeed a (fine-tuned) initial condition. Nevertheless, we have strong reason to believe that Inflation took place in the early Universe, see Sec. 3.5, which would erase any initial baryon asymmetry. This suggests that the observed BAU has to be dynamically generated throughout the evolution of the Universe *after* the hypothetical Inflation epoch. This scenario is called *baryogenesis*. In the next section, we discuss the conditions necessary for succesfull baryogenesis before reviewing how baryon number is violated in the SM in Sec. 4.3.2. In Secs. 4.3.3 and 4.3.4, we discuss how one subclass of the baryogenesis mechanism, called *leptogenesis*, is realized in the type I and III seesaw mechanisms, respectively. For more extensive reviews

[4] Here, we used

$$\left.\frac{s}{n_\gamma}\right|_0^{g_{*s}=\frac{43}{11}} \approx 7.04$$

and

$$Y_{\Delta B'}|_0 = \left.\frac{\eta n_\gamma}{s}\right|_0 \approx \left.\frac{n_{B'}}{n_\gamma}\frac{n_\gamma}{s}\right|_0 = \left.\frac{\Omega_{B'}\rho_c}{n_\gamma m_p}\frac{n_\gamma}{s}\right|_0 \approx 3.892\,36 \times 10^{-9} \Omega_{B'} h^2$$

with [153]

$$\rho_c = (1.053\,72 \pm 0.000\,24) \times 10^{-3}\, h^2\,\text{GeV} \,, \qquad n_\gamma|_0 = 410.73 \pm 0.27 \,.$$

on baryogenesis and leptogenesis, we refer the reader to [72, 154–158].

4.3.1 Sakharov Conditions

In order to dynamically generate a baryon asymmetry, three conditions need to be fulfilled, know as the *Sakharov conditions* [19]:

1. baryon number violation
2. $\mathcal{C}$ and $\mathcal{CP}$ violation
3. departure from equilibrium

Let us discussion the conditions and their status in the SM in greater detail.

Baryon Number Violation

This condition is rather intuitive. If we start from a state with a given baryon number, it will never change unless some process violates it. In the SM, processes violating baryon number B' and lepton number L' take place due to *Instanton* and *Sphaleron* transitions which violate B' and L' by three units, respectively, and hence conserve $B' - L'$. While Instanton transitions at zero temperature are exponentially suppressed with a tunneling factor $\sim \exp(-8\pi^2/g^2)$, Sphaleron transitions at high temperature, $\mathsf{T} \gtrsim 100\,\mathrm{GeV}$, are fast, resulting in the sizable violation of B' and L'. We will discuss Instantons and Sphalerons in greater detail in Sec. 4.3.2.

$\mathcal{C}$ and $\mathcal{CP}$ Violation

If $\mathcal{C}$ and $\mathcal{CP}$ are conserved, processes involving baryons and the $\mathcal{C}/\mathcal{CP}$ conjugate processes involving antibaryons proceed at exactly the same rate, resulting in a vanishing baryon asymmetry. For example, let us consider a particle $X = X_{\mathtt{L}} + X_{\mathtt{R}}$ which carries a baryon number $B'(X) = 1$ and decays to a final state Y with $B'(Y) = 0$. Thus, decays $X_{\mathtt{L,R}} \to Y$ produce one unit of baryon number while decays $\left(\overline{X}\right)_{L,R}$ destroy one unit of baryon number, resulting in a total baryon asymmetry

$$\Delta B' \sim \Gamma\left(X_{\mathtt{L}} \to Y\right) + \Gamma\left(X_{\mathtt{R}} \to Y\right) - \Gamma\left(\left(\overline{X}\right)_{\mathtt{L}} \to \overline{Y}\right) - \Gamma\left(\left(\overline{X}\right)_{\mathtt{R}} \to \overline{Y}\right) . \tag{4.3.4}$$

However, if $\mathcal{C}$ is conserved, we have

$$\mathcal{C}: \quad \Gamma\left(X_{\mathtt{L}} \to Y\right) = \Gamma\left(\left(\overline{X}\right)_{\mathtt{L}} \to \overline{Y}\right) , \quad \Gamma\left(X_{\mathtt{R}} \to Y\right) = \Gamma\left(\left(\overline{X}\right)_{\mathtt{R}} \to \overline{Y}\right) , \tag{4.3.5}$$

and $\Delta B' = 0$ while $\mathcal{CP}$ conservation implies

$$\mathcal{CP}: \quad \Gamma\left(X_{\mathtt{L}} \to Y\right) = \Gamma\left(\left(\overline{X}\right)_{\mathtt{R}} \to \overline{Y}\right) , \quad \Gamma\left(X_{\mathtt{R}} \to Y\right) = \Gamma\left(\left(\overline{X}\right)_{\mathtt{L}} \to \overline{Y}\right) , \tag{4.3.6}$$

also yielding $\Delta B' = 0$.
While $\mathcal{C}$ is violated maximally by the weak interaction, the only source of $\mathcal{CP}$ violation in the SM in the form CKM phase is many orders of magnitude too small to generate the observed baryon asymmetry.

Departure from Equilibrium

Let us now consider a species X which violates baryon number via the processes $X \to Y, \overline{X} \to \overline{Y}$. Moreover, we assume that both X and $\overline{X}$ are in kinetic equilibrium with

$$n_{X,\overline{X}} = \int \frac{d^3p}{(2\pi)^3} f^{\text{eq}}_{X,\overline{X}}\,, \qquad f^{\text{eq}}_{X,\overline{X}} = \frac{1}{e^{\frac{E_{X,\overline{X}} - \mu_{X,\overline{X}}}{\mathsf{T}}} \pm 1}\,, \tag{4.3.7}$$

where $\mu_X, \mu_{\overline{X}}$ are the chemical potentials. If X is the only species violating baryon number, the baryon asymmetry will depend only on the difference between the number densities n_X and $n_{\overline{X}}$, or equivalently the particle numbers $N_X, N_{\overline{X}}$, i.e.

$$\Delta B' \sim n_X - n_{\overline{X}} \sim a^{-3}\left(N_X - N_{\overline{X}}\right). \tag{4.3.8}$$

Thus, if we start from a state with $\Delta B' = 0$, a non-vanishing asymmetry at a later time requires that the particle numbers $N_X, N_{\overline{X}}$ are not conserved. However, if X and $\overline{X}$ are also in chemical equilibrium, non-conservation of particle number[5] implies that the corresponding chemical potentials vanish, $\mu_X = \mu_{\overline{X}} = 0$, and together with the $\mathcal{CPT}$ theorem we find

$$n_X = n_{\overline{X}} \tag{4.3.9}$$

and consequently

$$\Delta B' = 0\,. \tag{4.3.10}$$

Thus, in order to generate a non-vanishing baryon asymmetry, a departure from equilibrium is necessary. In the SM, the electroweak phase transition was long believed to be a potential source for the out-of-equilibrium condition, provided it is strictly first order. However, the experimentally confirmed value of the Higgs mass implies that the phase transition is second order and hence does not provide suitable out-of-equilibrium dynamics.

To summarize, succesfull baryogenesis requires that the SM is extended in a way that accounts for additional sources of $\mathcal{CP}$ violation and departure from equilibrium. Moreover, the existence of Sphalerons suggests that baryogenesis could also proceed through *leptogenesis*. That is, rather than introducing a new source of baryon number violation and creating the BAU directly, it is also viable that new lepton number violating interactions induce a lepton asymmetry first, which is subsequently transferred to a baryon asymmetry via Sphaleron transitions. Before we discuss leptogenesis in greater detail in Secs. 4.3.3 and 4.3.4, we provide a short overview of Instanton and Sphaleron processes in the SM and their relation to the violation of lepton- and baryon number below.

[5] which follows from the first Sakharov condition

4.3.2 Baryon Number Violation in the SM

In this Section, we give a brief overview over the relation between Instantons, anomalies and the non-conservation of baryon- and lepton number in the SM, restricting ourselves to the basic results, following Refs. [157, 159–164]. A more detailed discussion on Instantons can be found in App. E and the references therein.

4.3.2.1 Instantons

It can be shown that *Yang-Mills* (YM) theories with gauge groups SU(N) have a topologically non-trivial vacuum structure and that as a result, the true ground state of the theory, called the θ vacuum, is a superposition of different topological sectors labeled by an integer $n = 0, \pm 1, \pm 2, ...$, so that

$$|\theta\rangle = \sum_n e^{in\theta} |n\rangle \ . \tag{4.3.11}$$

Here, θ is the *vacuum angle* with $\theta \in [0, 2\pi)$ and the integer n is commonly referred to as the *winding number*. The Instanton mediates tunneling processes between vacua with different winding numbers $n \neq m$ and is associated with a topological charge ν,

$$\nu[A] = \frac{g^2}{32\pi^2} \int d^4x F_{\mu\nu}{}^a[A] \tilde{F}^a_{\mu\nu}[A] = n - m \,, \tag{4.3.12}$$

where $F_{\mu\nu}$ is the field strength corresponding to the gauge group SU(N) and A_μ is the gauge field. These tunneling processes give rise to an additional $\mathcal{C}$- and $\mathcal{CP}$-violating term in the Lagrangian of the theory,

$$\delta\mathcal{L} = \frac{g^2 \nu\theta}{32\pi^2} F_{\mu\nu}{}^a[A] \tilde{F}^a_{\mu\nu}[A] \,. \tag{4.3.13}$$

Although the term is gauge invariant and therefore a viable contribution to the Lagrangian, it can be written as a total derivative. Since variations were assumed to vanish at the boundary, it was usually discarded. It became clear only once Instanton solutions were found that the surface term does in fact not vanish, provided that tunneling between different winding sectors takes place. What is more, theories with different θ are generally not equivalent and transitions between distinct θ vacua are forbidden. Thus, this term can have physical consequences and should be considered as an additional term of the Lagrangian. In QCD, the new parameter θ is called the strong vacuum angle and gives rise to strong $\mathcal{CP}$ violation. However, experimentally, the $\mathcal{CP}$ violation is very small which is referred to as the *strong $\mathcal{CP}$ problem*[165]. In this work, we are concerned with *electroweak Instantons*. Their effects are closely related to the B' and L' anomalies in the SM, as we will shortly review in the following.

4.3.2.2 Nonconservation of Baryon and Lepton Number

The SM, discussed in Sec. 2.2, is invariant under the transformations

$$\psi \to e^{iB'\alpha_{B'}}\psi\,, \qquad \psi \to e^{iL'\alpha_{L'}}\psi\,, \tag{4.3.14}$$

where B', L' are the baryon- and lepton numbers of ψ. Consequently, the SM posesses two accidental global symmetries related to these transformations, baryon number $U(1)_{B'}$ and lepton number $U(1)_{L'}$. Although classically conserved to all orders of perturbation theory, the interplay of electroweak Instantons with chiral anomalies results in the non-perturbative violation of B' and L'. In the following, we neglect the effect of the $U(1)_Y$ gauge group of the SM since it greatly simplifies the discussion while not affecting the results. Thus, the contribution of the electroweak θ term to the Lagrangian of the SM is given by

$$\mathcal{L}_{\theta_{EW}} = \frac{g^2\theta_{EW}}{32\pi^2} W^a_{\mu\nu}\tilde{W}^{a,\mu\nu} \tag{4.3.15}$$

where $W^a_{\mu\nu}$ is given by (2.2.10). Next, we can define the charges B' and L' in terms of the currents

$$J^\mu_{B'} = \frac{1}{3}\sum_i \left[\overline{Q}_{i,a}\gamma^\mu Q_{i,a} + \overline{U}_{i,a}\gamma^\mu U_{i,a} + \overline{D}_{i,a}\gamma^\mu D_{i,a}\right]\,, \tag{4.3.16}$$

$$J^\mu_{L'} = \sum_i \left[\overline{L_i}\gamma^\mu L_i + \overline{E_i}\gamma^\mu E_i\right]\,, \tag{4.3.17}$$

where the sum is over generations and $a = 1, 2, 3$ is the color index, yielding

$$B' = \int d^3x J^0_{B'}\,, \qquad L' = \int d^3x J^0_{L'}\,. \tag{4.3.18}$$

Classically, B' and L' are conserved and therefore

$$\partial_\mu J^\mu_{B'} = \partial_\mu J^\mu_{L'} \overset{class}{=} 0\,. \tag{4.3.19}$$

On one-loop level however, the triangle anomalies of both $U(1)_{B'}$ and $U(1)_{L'}$ with respect to $\mathrm{SU}(2)_\mathtt{L}$ (see Fig. 4.4) result in [166, 167]

$$\partial_\mu J^\mu_{B'} = \frac{g^2\mathcal{A}_{B'}}{32\pi^2} W^a_{\mu\nu}\tilde{W}^{a,\mu\nu}\,, \qquad \partial_\mu J^\mu_{L'} = \frac{g^2\mathcal{A}_{L'}}{32\pi^2} W^a_{\mu\nu}\tilde{W}^{a,\mu\nu}\,, \tag{4.3.20}$$

where $\mathcal{A}_{B',L'}$ are the anomaly factors of $[\mathrm{SU}(2)_\mathtt{L}]^2 \times U(1)_{B',L'}$. For a $[\mathrm{SU}(2)_\mathtt{L}]^2 \times U(1)_q$ anomaly with a $U(1)_q$ charge q, the anomaly factor is given by

$$\mathcal{A}_q = \sum_{\mathcal{R}} \left[\sum_\mathtt{L} 2q_\mathtt{L} T_\mathtt{L}(\mathcal{R}) - \sum_\mathtt{R} 2q_\mathtt{R} T_\mathtt{R}(\mathcal{R})\right]\,, \tag{4.3.21}$$

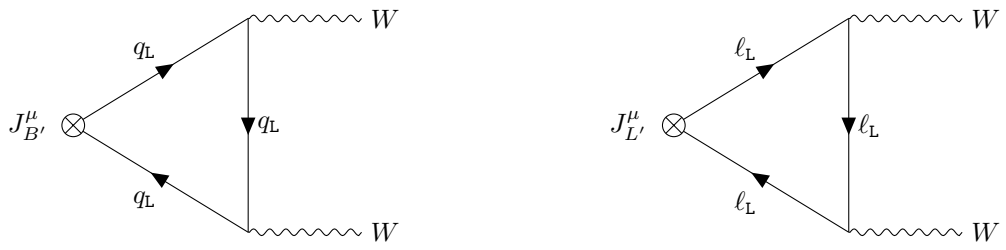

Figure 4.4: Triangle diagrams inducing the anomalous violation of B' (left) and L' (right).

where $T(\mathcal{R})$ is the index of the representation $\mathcal{R}$ under which a LH ($\mathtt{L}$) or RH ($\mathtt{R}$) field transforms. The index for singlets, doublets and triplets is given by

$$T(\mathbf{1}) = 0\,, \qquad T(\mathbf{2}) = \frac{1}{2}\,, \qquad T(\mathbf{3}) = 2\,, \tag{4.3.22}$$

respectively. In the SM, only LH particles have a non-zero index and therefore the anomaly factors $\mathcal{A}_{B',L'}$ are given by

$$\mathcal{A}_{L'} = N_{\mathtt{L}} \times L' \times 2T_{\mathtt{L}}(1) = 3 \times 1 \times 2\frac{1}{2} = 3\,, \tag{4.3.23}$$

$$\mathcal{A}_{B'} = N_{\mathtt{L}} \times C_{\mathtt{L}} \times B' \times 2T_{\mathtt{L}}(1) = 3 \times 3 \times \frac{1}{3} \times 2\frac{1}{2} = 3\,, \tag{4.3.24}$$

where $N_{\mathtt{L}} = 3$ is the number of generations of LH particles and $C_{\mathtt{L}}$ is the color multiplicity. It is striking that since $\mathcal{A}_{L'} = \mathcal{A}_{B'} = 3$, we have

$$\partial_\mu J^\mu_{B'} - \partial_\mu J^\mu_{L'} = 0\,, \tag{4.3.25}$$

implying that the combination $U(1)_{B'-L'}$ is anomaly-free.
With regard to Instantons, the anomalies have two effects. First, note that the path-integral measure $D\psi D\overline{\psi}$ is not invariant under the L' and B' transformations given in (4.3.14). Instead, it transforms as [168]

$$D\psi D\overline{\psi} \to \exp \int d^4x \frac{(\mathcal{A}_{B'}\alpha_{B'} + \mathcal{A}_{L'}\alpha_{L'})\, g^2}{32\pi^2} W^a_{\mu\nu}\tilde{W}^{a,\mu\nu} D\psi D\overline{\psi}\,, \tag{4.3.26}$$

which amounts to adding a term

$$\delta\mathcal{L} = \frac{(\mathcal{A}_{B'}\alpha_{B'} + \mathcal{A}_{L'}\alpha_{L'})\, g^2}{32\pi^2} W^a_{\mu\nu}\tilde{W}^{a,\mu\nu} \tag{4.3.27}$$

to the Lagrangian. Comparing to (4.3.15), we note that this is equivalent to a shift of the vacuum angle θ_{EW},

$$\theta_{EW} \to \theta_{EW} + \mathcal{A}_{B'}\alpha_{B'} + \mathcal{A}_{L'}\alpha_{L'}\,, \tag{4.3.28}$$

i.e. θ_{EW} can always be removed by an appropriate choice of $\alpha_{L'}$ and $\alpha_{B'}$. Thus, the electroweak vacuum angle does not have a physical effect [108, 169, 170]. Instead, t'Hooft showed that the relevance of electroweak Instantons is only revealed when vacuum-to-

vacuum transition amplitudes with different numbers of leptons and baryons in the initial and final states are considered [171]. This can be seen by taking a closer look at the divergences of the currents given in (4.3.20). By integrating over them, we find that the LHS is given by

$$\int d^4x \partial_\mu J^\mu_{B'} = B'(\infty) - B'(-\infty) \equiv \Delta B' \,, \tag{4.3.29}$$

$$\int d^4x \partial_\mu J^\mu_{L'} = L'(\infty) - L'(-\infty) \equiv \Delta L' \,, \tag{4.3.30}$$

while the RHS yields

$$\int d^4x \frac{g^2 \mathcal{A}_{B'}}{32\pi^2} W^a_{\mu\nu} \tilde{W}^{a,\mu\nu} = \mathcal{A}_{B'\nu} \,, \tag{4.3.31}$$

$$\int d^4x \frac{g^2 \mathcal{A}_{L'}}{32\pi^2} W^a_{\mu\nu} \tilde{W}^{a,\mu\nu} = \mathcal{A}_{L'\nu} \,, \tag{4.3.32}$$

where ν is the topological charge (4.3.12). We can therefore conclude that tunneling of Instantons between adjacent winding sectors, i.e. $\nu = 1$, violates B' and L' in the SM by three units,

$$\Delta B' = \Delta L' = 3 \,, \tag{4.3.33}$$

while conserving the difference, $\Delta B' - \Delta L' = 0$. Thus, a non-vanishing amplitude in the Instanton background requires that the initial and final states differ by three units of lepton and baryon number each, which corresponds to calculating an amplitude of the form

$$\Gamma_I \sim \langle 0 | \left(QQQL\right)^3 | 0 \rangle \ . \tag{4.3.34}$$

At zero temperature, the tunneling amplitude of Instantons depends only on the Instanton action S_1. It is given by

$$\Gamma_I \sim e^{-S_1} \sim e^{-\frac{8\pi^2}{g^2}} \tag{4.3.35}$$

and clearly is unobservably small. Consequently, electroweak Instantons have no measurable effect.

4.3.2.3 Sphalerons and L' to B' Conversion

While Instanton solutions correspond to tunneling processes and are therefore exponentially suppressed, transitions via thermal jumps over the barrier seperating different winding sectors are possible at non-zero temperature, see Fig. 4.5. These transitions are called *Sphaleron* processes. The temperature-dependent transition amplitude is given by

$$\Gamma_{\text{Sph}} \sim e^{-\frac{E_{\text{Sph}}}{\text{T}}} \,, \tag{4.3.36}$$

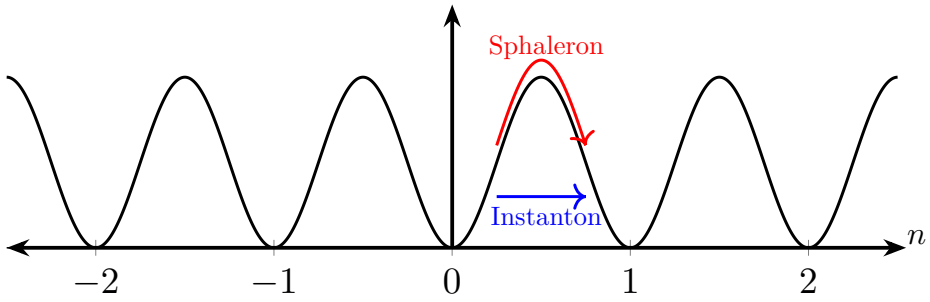

Figure 4.5: Schematical illustration of Instanton and Sphaleron transitions between different winding sectors n.

where $E_{\text{Sph}} \sim \mathcal{O}\,(\text{TeV})$ is the energy of the Sphaleron. At high temperatures in the early Universe,

$$10^2\,\text{GeV} \lesssim \mathsf{T} \lesssim 10^{12}\,\text{GeV}\,, \tag{4.3.37}$$

Sphaleron transitions are fast and induce processes of the form

$$|0\rangle \to |d_{\text{L}} d_{\text{L}} u_{\text{L}} \nu_{e,L} + s_{\text{L}} s_{\text{L}} c_{\text{L}} \nu_{\mu,L} + b_{\text{L}} b_{\text{L}} t_{\text{L}} \nu_{\tau,L}\rangle\ , \tag{4.3.38}$$

resulting in a sizable violation of B' and L'.
In the context of leptogenesis, Sphalerons are particularly interesting since they can, if in equilibrium, convert an existing $Y_{\Delta B'} - Y_{\Delta L'}$ asymmetry to a baryon asymmetry via the relation

$$Y_{\Delta B'} = C^{\text{Sph}}\,(Y_{\Delta B'} - Y_{\Delta L'})\ . \tag{4.3.39}$$

The conversion facor C^{Sph} can be calculated by analyzing relations between chemical potentials in the early Universe [72, 173–175]. For simplicity, we derive the relations at a fixed temperature with $\mathsf{T} \gg \mathsf{T}_{EWSB}$ where electroweak and Yukawa interactions are fast enough to establish chemical equilibrium. This condition can be expressed in terms of chemical potentials as [72, 155, 173, 176, 177]

$$\begin{aligned} \mu_{W^-} &= \mu_{\phi^0} + \mu_{\phi^-} = \mu_{d_{\text{L}}} - \mu_{u_{\text{L}}} = \mu_{e_{\text{L}}} - \mu_{\nu_{\text{L}}}\,, \\ \mu_{\phi^0} &= \mu_{u_{\text{R}}} - \mu_{u_{\text{L}}} = \mu_{d_{\text{L}}} - \mu_{d_{\text{R}}} = \mu_{e_{\text{L}}} - \mu_{e_{\text{R}}}\,, \end{aligned} \tag{4.3.40}$$

where we restricted ourselves to the first generation of fermions. From (4.3.38), we conclude that fast Sphaleron processes induce the additional condition

$$3\left(2\mu_{d_{\text{L}}} + \mu_{u_{\text{L}}} + \mu_{\nu_{e_{\text{L}}}}\right) = 0\,. \tag{4.3.41}$$

Before EWSB, charge $Q_{\rm EM}$ and weak isospin T_3 are conserved and we can use (3.2.19) to write

$$Y^{\rm SM}_{\Delta Q_{\rm EM}} \sim N_G N_C \left[\frac{2}{3}\left(\mu_{u_{\rm L}} + \mu_{u_{\rm R}}\right) - \frac{1}{3}\left(\mu_{d_{\rm L}} + \mu_{d_{\rm R}}\right)\right] - N_G\left(\mu_{e_{\rm L}} + \mu_{e_{\rm R}}\right) + 2\mu_{\phi^+} - 2\times 2\mu_{W^-} \tag{4.3.42}$$

$$Y^{\rm SM}_{\Delta T_3} \sim N_G N_C \times \frac{1}{2}\left(\mu_{u_{\rm L}} - \mu_{d_{\rm L}}\right) + \frac{N_G}{2}\left(\mu_{\nu_e} - \mu_{e_{\rm L}}\right) + 2\times\frac{1}{2}\left(\mu_{\phi^+} - \mu_{\phi^0}\right) - 2\times 2\mu_{W^-} \tag{4.3.43}$$

where $N_G = N_C = 3$ are for generations and color, respectively. Moreover, the asymmetries in B' and L' are related to the chemical potentials via

$$Y^{\rm SM}_{\Delta B'} \sim N_G N_C \times \frac{1}{3}\left(\mu_{u_{\rm L}} + \mu_{u_{\rm R}} + \mu_{d_{\rm L}} + \mu_{d_{\rm R}}\right)\,, \tag{4.3.44}$$

$$Y^{\rm SM}_{\Delta L'} \sim N_G\left(\mu_{e_{\rm L}} + \mu_{e_{\rm R}} + \mu_{\nu_e}\right)\,. \tag{4.3.45}$$

Putting everything together, we find that Sphalerons convert an existing $(Y_{\Delta B'} - Y_{\Delta L'})$ asymmetry into a final baryon asymmetry according to

$$Y_{\Delta B'} = \frac{28}{79}\left(Y_{\Delta B'} - Y_{\Delta L'}\right)\,. \tag{4.3.46}$$

4.3.3 Vanilla Leptogenesis

A remarkable feature of the type I Seesaw, see Sec. 4.2.1.1, is that in principle, it contains all ingredients necessary for baryogenesis via leptogenesis: Decays of the Majorana neutrinos N_i to lepton-Higgs pairs $LH, \overline{L}H^\dagger$ violate both lepton number and $\mathcal{CP}$ and if the decay rate is small enough, the decays are also out of equilibrium, hence creating a lepton asymmetry. In this section, we discuss the simplest realization of this version of leptogenesis, often called *vanilla leptogenesis* (VL), as a warm-up for the subsequent discussion of leptogenesis in the context of the Majoron model. The following discussion is based on the extensive reviews on VL that can be found in Refs. [72, 137, 154–156, 158, 178–180].

The relevant terms for leptogenesis in the Seesaw Lagrangian are given by

$$\mathcal{L} \subset -\left(Y^\nu_{\alpha i}\overline{L_\alpha}\tilde{H}N_i + \text{h.c.}\right) - \frac{1}{2}M_{N_i}\overline{N_i}N_i\,, \tag{4.3.47}$$

where $i = 1,2,3$ and $\alpha = e,\mu,\tau$. The Yukawa coupling Y^ν induces lepton number violating neutrino decays $N_i \to L_\alpha H, \overline{L_\alpha}H^\dagger$ and on tree-level, the decay rate is given by

$$\Gamma_{D_i} \equiv \Gamma(N_i \to L_\alpha H) = \Gamma(N_i \to \overline{L_\alpha}H^\dagger) = \frac{\left(Y^{\nu\dagger}Y^\nu\right)_{ii} M_{N_i}}{8\pi}\,. \tag{4.3.48}$$

Conveniently introducing the *effective neutrino mass* $\tilde{m}_i$ [180],

$$\tilde{m}_i = \frac{\left(Y^{\nu\dagger}Y^\nu\right)_{ii} v^2}{M_{N_i}}\,, \tag{4.3.49}$$

the decay rate (4.3.48) can be rewritten as

$$\Gamma_{D_i} = \frac{M_{N_i}^2 \tilde{m}_i}{8\pi v^2} \,. \tag{4.3.50}$$

4.3.3.1 $\mathcal{CP}$ Violation

Neglecting thermal effects, the $\mathcal{CP}$ violation in neutrino decays can be expressed in terms of matrix elements $\mathcal{M}\left(N_i \to L_\alpha H, \overline{L_\alpha} H^\dagger\right)$,

$$\epsilon_{i\alpha} = \frac{\left|\mathcal{M}\left(N_i \to L_\alpha H\right)\right|^2 - \left|\mathcal{M}\left(N_i \to \overline{L_\alpha} H^\dagger\right)\right|^2}{\sum_\alpha \left\{\left|\mathcal{M}\left(N_i \to L_\alpha H\right)\right|^2 + \left|\mathcal{M}\left(N_i \to \overline{L_\alpha} H^\dagger\right)\right|^2\right\}} \,. \tag{4.3.51}$$

In this form, it is immediatly apparent that the $\mathcal{CP}$ asymmetry vanishes on tree-level. Instead, it arises on one-loop level when the interference of tree-level and one-loop amplitudes as shown in Fig. 4.6 is taken into account, yielding [181]

$$\begin{aligned} \epsilon_{i\alpha} = \frac{1}{8\pi \left(Y^{\nu\dagger} Y^\nu\right)_{ii}} \sum_{j \neq i} \Bigg[& \mathrm{Im}\left[\left(Y^{\nu\dagger} Y^\nu\right)_{ji} Y^\nu_{\alpha i} Y^{\nu *}_{\alpha j}\right] f\left(\frac{M_{N_j}}{M_{N_i}}\right) \\ & + \mathrm{Im}\left[\left(Y^{\nu\dagger} Y^\nu\right)_{ij} Y^\nu_{\alpha i} Y^{\nu *}_{\alpha j}\right] \frac{M_{N_i}^2}{M_{N_i}^2 - M_{N_j}^2} \Bigg] \,, \end{aligned} \tag{4.3.52}$$

where

$$f(x) = \sqrt{x}\left[\frac{x-2}{x-1} - (1+x)\log\left(\frac{1+x}{x}\right)\right] \tag{4.3.53}$$

is a loop function. Summing over the lepton flavors α, the contributions from the second line in (4.3.52) vanish and we find

$$\epsilon_i = \sum_\alpha \epsilon_{i\alpha} = \frac{1}{8\pi \left(Y^{\nu\dagger} Y^\nu\right)_{ii}} \sum_{j \neq i} \mathrm{Im}\left[\left(Y^{\nu\dagger} Y^\nu\right)^2_{ji}\right] f\left(\frac{M_{N_j}}{M_{N_i}}\right) \,. \tag{4.3.54}$$

In this thesis, we will focus on leptogenesis in the one flavor approximation in the limit where $M_{N_1} \ll M_{N_{2,3}}$ so that (4.3.53) becomes

$$f\left(\frac{M_{N_{2,3}}}{M_{N_1}} \gg 1\right) \approx -\frac{3}{2}\sqrt{\frac{M_{N_1}}{M_{N_{2,3}}}} \,, \tag{4.3.55}$$

yielding the $\mathcal{CP}$ violation from N_1 decays as

$$\epsilon_i = -\frac{3}{16\pi \left(Y^{\nu\dagger} Y^\nu\right)_{11}} \sum_{j \neq 1} \mathrm{Im}\left[\left(Y^{\nu\dagger} Y^\nu\right)^2_{j1}\right] \frac{M_{N_1}}{M_{N_j}} \,. \tag{4.3.56}$$

An upper bound on ϵ_1 can be placed in terms of the *Davidson-Ibarra* (DI) bound [182],

$$|\varepsilon^{DI}| \leq \frac{3}{16\pi} \frac{M_N}{v^2} (m_3 - m_1) \,. \tag{4.3.57}$$

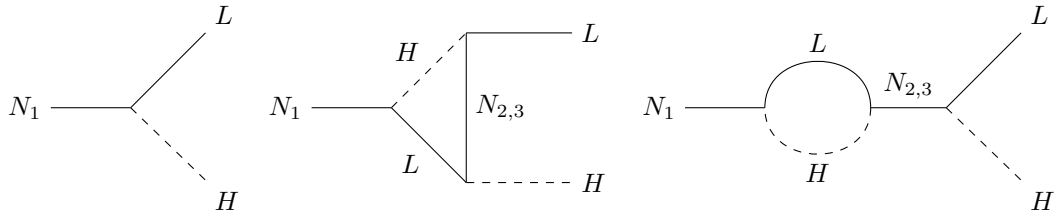

Figure 4.6: Feynman diagrams contributing to the CP violating N_1 decay.

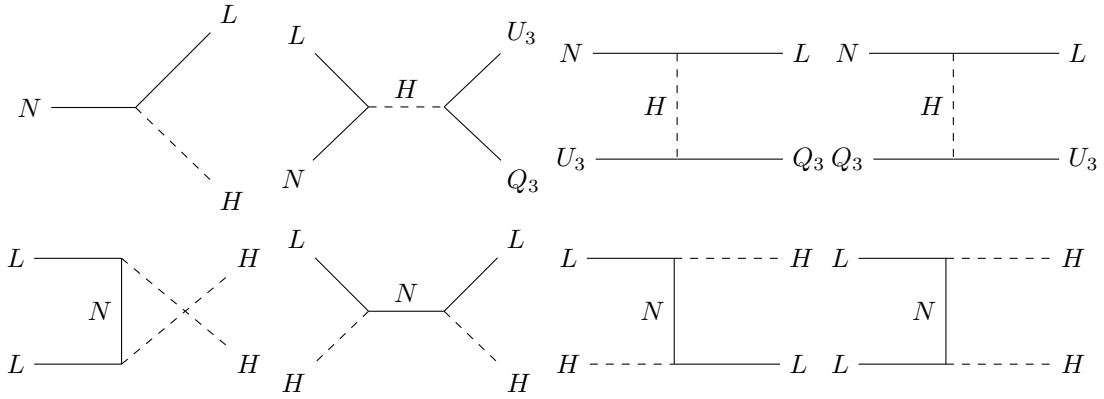

Figure 4.7: Feynman diagrams relevant for the evolution of the neutrino abundance and the lepton asymmetry in VL. The diagrams in the first row violate lepton number by one unit and change the neutrino abundance while the diagrams in the second row violate lepton number by two units and conserve the neutrino number.

If we further assume that the light neutrinos follow a NH with $m_1 \ll m_2 \ll m_3$, the DI bound (4.3.57) can be written as

$$\left|\varepsilon^{DI}\left(M_N\right)\right| \leq \frac{3}{16\pi}\frac{M_N}{v^2}\sqrt{\Delta m^2_{atm}}\,. \tag{4.3.58}$$

4.3.3.2 Boltzmann Equations

In the following, we briefly discuss the Boltzmann equations for VL. A more detailed derivation is given in App. F.2. For brevity, we will generally omit the index 1 so that $\{N, M_N, \tilde{m}, \epsilon\} \equiv \{N_1, M_{N_1}, \tilde{m}_1, \epsilon_1\}$. In our discussion, we neglect thermal effects and scattering processes involving gauge bosons. Thus, the only processes relevant for the neutrino evolution are decays and quark scatterings, see first row in Fig. 4.7. The Boltzmann equation then reads

$$s\mathcal{H}z_N\frac{\mathrm{d}Y_N}{\mathrm{d}z_N} = -\left(\delta_N - 1\right)\gamma_D - 2\gamma_Q\left(\delta_N - 1\right)\,, \tag{4.3.59}$$

In the equation above, the decay rate γ_D is given by

$$\gamma_D = n_N^{\rm eq} \frac{\mathrm{K}_1(z_N)}{\mathrm{K}_2(z_N)} \Gamma_D \,, \tag{4.3.60}$$

while the cross section for $\gamma_Q \equiv 2\gamma_{NU_3,\overline{L}Q_3} + \gamma_{NL,Q_3U_3}$ follows from (G.2.1) and (G.2.2). Concerning the Boltzmann equation for the lepton asymmetry $\Delta L'$, it is essential to include also $\Delta L' = 2$ scatterings as shown in the second row in Fig. 4.7 and substract the on-shell contribution of $LH \leftrightarrow \overline{L}H^\dagger$ scatterings, (see App. F.2), yielding

$$s\mathcal{H}z_N \frac{\mathrm{d}Y_{\Delta L'}}{\mathrm{d}z_N} = \epsilon\gamma_D \left(\delta_N - 1\right) - \delta_{\Delta L'} \left[\frac{\gamma_D}{2} + 2\gamma_{N\overline{U_3},L\overline{Q_3}} + \delta_N \gamma_{LN\leftrightarrow Q_3U_3}\right] . \tag{4.3.61}$$

However, instead of solving the Boltzmann equation for the lepton asymmetry directly, it is convenient to define an *efficiency* $\eta(z_N)$ via

$$Y_{\Delta L'}(z_N) = \epsilon Y_N^0 \eta(z_N) \,, \tag{4.3.62}$$

where $Y_N^0 \equiv Y_N(z_N \to 0)$, yielding a Boltzmann equation for the efficiency that is independent from ϵ as

$$s\mathcal{H}z_N \frac{\mathrm{d}\eta}{\mathrm{d}z_N} = \frac{1}{Y_N^0} \left(\delta_N - 1\right) \gamma_D - \frac{\eta}{Y_L^{\rm eq}} \left[\frac{\gamma_D}{2} + 2\gamma_{N\overline{U_3},L\overline{Q_3}} + \delta_N \gamma_{LN\leftrightarrow Q_3U_3}\right] . \tag{4.3.63}$$

The relevant quantity for leptogenesis is the final lepton asymmetry which we obtain after solving (4.3.84) via

$$Y_{\Delta L'}(z_N \to \infty) = \epsilon Y_N^0 \eta \,, \qquad \eta \equiv \eta(z_N \to \infty) \,, \tag{4.3.64}$$

where η is the *final efficiency* with $|\eta| \leq 1$. The thermal rates appearing in the Boltzmann equations (4.3.59) and (4.3.84) can all be expressed in terms of the single parameter $\tilde{m}$. Consequently, (4.3.59) and (4.3.84) depend only on three parameters: The initial efficiency $\eta(z_N \to 0)$, the initial neutrino abundance $Y_N(z_N \to 0)$, and $\tilde{m}$. As we are interested in *generating* a lepton asymmetry, we set $\eta(z_N \to 0) = 0$, leaving us with two free parameters, $Y_N(z_N \to 0)$ and $\tilde{m}$. Unfortunately, only model-dependent bounds on $\tilde{m}$ exits. For example, in case of a NH and provided that no cancellations occur, $m_1 \lesssim \tilde{m} \lesssim m_3 \sim 0.05\,\mathrm{eV}$ [158].

4.3.3.3 Evolution of the Efficiency

Let us now discuss the solutions of the Boltzmann equations for leptogenesis. In the following, we additionally neglect the contributions from quark scatterings so that the Boltzmann equations (4.3.59) and (4.3.84) become

$$s\mathcal{H}z_N \frac{\mathrm{d}Y_N}{\mathrm{d}z_N} = -\left(\delta_N - 1\right) \gamma_D \,, \tag{4.3.65}$$

$$s\mathcal{H}z_N \frac{\mathrm{d}\eta}{\mathrm{d}z_N} = \frac{1}{Y_N^0} \left(\delta_N - 1\right) \gamma_D - \frac{\eta}{2Y_L^{\rm eq}} \gamma_D \,. \tag{4.3.66}$$

This greatly simplifies the discussion and does not significantly affect the relevant qualitative effects. We stress however that the solutions we present in Figs. 4.8a, 4.8b and 4.10 were obtained including quark scatterings. We solve the Boltzmann equations in the range $\tilde{m} \in [0.5 \times 10^{-4}, 0.1]\,\text{eV}$ and distinguish between two initial conditions: Either the initial neutrino abundance vanishes, which we will denote by an index z,

$$Y_N(z_N \to 0) = 0 \quad \to \quad \{Y_N(z_N), \eta(z_N)\} \equiv \{Y_N^z(z_N), \eta^z(z_N)\}\,, \tag{4.3.67}$$

or the neutrinos are initially in equilibrium, which we will denote by an index t,

$$Y_N(z_N \to 0) = Y_N^{\text{eq}}(0) \quad \to \quad \{Y_N(z_N), \eta(z_N)\} \equiv \left\{Y_N^t(z_N), \eta^t(z_N)\right\}\,. \tag{4.3.68}$$

Let us first focus on the evolution of the neutrino abundance. To do so, recall from the discussion in Sec. 3.3 that the rate $\gamma_D/n_N^{\text{eq}}\mathcal{H}$ determines if neutrinos are coupled to the plasma. Thus, in Fig. 4.9 (left), we show $\gamma_D/n_N^{\text{eq}}\mathcal{H}(z_N)$ for different values of $\tilde{m}$ and note two striking features: First, γ_D/n_N^{eq} is not Boltzmann suppressed,

$$\frac{\gamma_D}{n_N^{\text{eq}}} = \frac{\mathrm{K}_1(z_N)}{\mathrm{K}_2(z_N)}\Gamma_D\,, \tag{4.3.69}$$

hence the decay rate inevitably becomes fast at some z_N and secondly, neutrinos are thermalized more efficiently the larger $\tilde{m}$ is.
With these considerations in mind, the behavior of $Y_N^t(z_N)$ as shown in Fig. 4.8a for $\tilde{m} = [5 \times 10^{-5}, 10^{-3}, 10^{-1}]\,\text{eV}$ is intuitively clear: For small $z_N < 1$, $Y_N^t(z_N)$ closely follows the equilibrium distribution $Y_N^{\text{eq}}(z_N)$ until at $z_N \sim 1$, the equilibrium distribution becomes Boltzmann suppressed. If $\tilde{m}$ is small at $z_N \sim 1$, e.g. $\tilde{m} = 5 \times 10^{-5}\,\text{eV}$ (Fig. 4.8a, panel 1), we can deduce from Fig. 4.9 (left) that the decay and scatter rates are slow, prompting the neutrino abundance $Y_N^t(z_N \gtrsim 1)$ to significantly deviate from equilibrium. Eventually, $\gamma_D/n_N^{\text{eq}}\mathcal{H}(z_N) > 0$ is reached and neutrino decays become fast, forcing $Y_N^t(z_N)$ to approach its equilibrium abundance, which therefore becomes Boltzmann suppressed. As $\tilde{m}$ increases (see e.g. Fig. 4.8a, panel 2), neutrino decays become fast already shortly after the equilibrium abundance becomes Boltzmann suppressed. Consequently, the neutrino abundance deviates from equilibrium significantly less. If $\tilde{m}$ is so large that neutrino decays are already fast at $z_N \sim 1$ when the Boltzmann suppression sets in, $Y_N^t(z_N)$ never sizably deviates from equilibrium.
For $Y_N^z(z_N)$, the situation is slightly more evolved. As long as $Y_N^z(z_N) \ll Y_N^{\text{eq}}(z_N)$ holds, we have $\delta_N^z \ll 1$ and (4.3.59) can be simplified to

$$s\mathcal{H}z_N\frac{\mathrm{d}Y_N}{\mathrm{d}z_N} = \gamma_D\,, \tag{4.3.70}$$

i.e. inverse decays populate the plasma with neutrinos. This lasts roughly until the neutrino abundance becomes equal to the equilibrium abundance at $z_N \sim z_{\text{eq}}^N$, i.e.

$$\delta_N^z(z_{\text{eq}}^N) = 1\,. \tag{4.3.71}$$

It is apparent that the neutrino production is faster for larger $\tilde{m}$ and therefore equality is reached for smaller z_N, i.e. $z_{\text{eq}}^N \sim \tilde{m}^{-1}$. For $z_N > z_{\text{eq}}^N$, the evolution of $Y_N^z(z_N)$ is similar to $Y_N^t(z_N)$: If decays are slow when both $z_N \gtrsim z_{\text{eq}}^N$ and $z_N \gtrsim 1$ hold, decays and scatterings

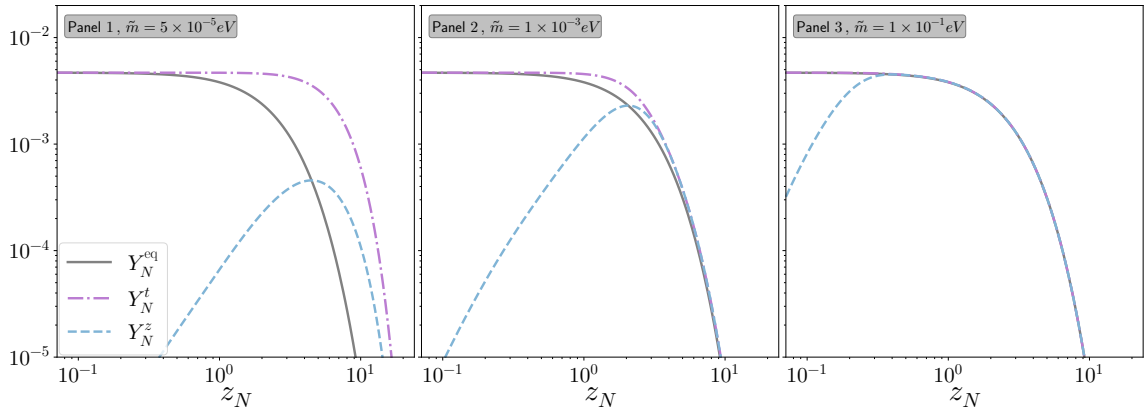

(a) Evolution of the neutrino abundance in the VL scenario for different values of $\tilde{m}$ with vanishing (dashed) or thermal (dash-dotted) initial neutrino abundances.

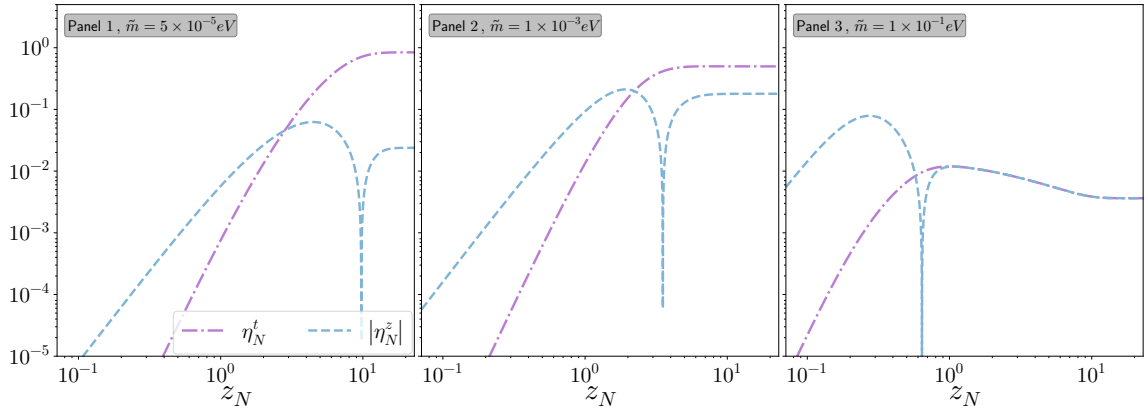

(b) Evolution of the efficiency η in the VL scenario for different values of $\tilde{m}$ with vanishing (dashed) or thermal (dash-dotted) initial neutrino abundances.

fail to establish equilibrium, resulting in $Y_N^z(z_N) > Y_N^{\rm eq}(z_N)$ (see panel 1 in Fig. 4.8a). On the other hand, if neutrino interactions are fast for $z_N \gtrsim \{z_{\rm eq}^N, 1\}$, neutrinos closely follow the equilibrium distribution (see panel 3 in Fig. 4.8a).

Next, let us discuss the evolution of the efficiency. The first term in (4.3.84) is called the *source term* as it *creates* a lepton asymmetry, while the second term proportional to η is called the *washout* (WO) term which *reduces* the efficiency. The relevant quantity that determines if washout is effective is given by $\gamma_D/n_L^{\rm eq}\mathcal{H}(z_N)$, shown in Fig. 4.9 (right). In contrast to the thermal rates normalized by $n_N^{\rm eq}$, note that $\gamma_D/n_L^{\rm eq}$ is Boltzmann suppressed and in particular, if $\tilde{m} \lesssim 10^{-3}\,\text{eV}$, it is always slower than the expansion of the Universe, $\gamma_D/n_L^{\rm eq} \lesssim \mathcal{H}$. In the following, we will therefore distinguish between the *weak washout regime* for $\tilde{m} \ll 10^{-3}\,\text{eV}$ and the *strong washout regime* for $\tilde{m} \gg 10^{-3}\,\text{eV}$.

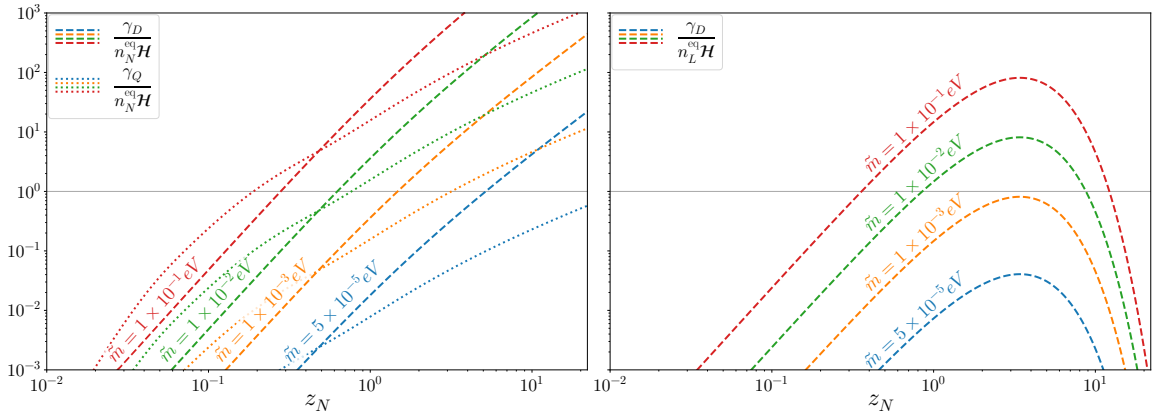

Figure 4.9: *Left:* Rates $\gamma_{D,Q}/n_N^{\rm eq}\mathcal{H}$ that govern the evolution of the neutrino abundance in VL. For $z_N \gg 1$, neutrino decays dominate the neutrino evolution. Quark scatterings are only dominant around $z_N \sim 1$ if $\tilde{m} \to 10^{-1}\,\mathrm{eV}$. *Right:* Rates $\gamma_D/n_L^{\rm eq}\mathcal{H}$ that determine when inverse decays are fast, resulting in sizable WO of the efficiency η. It is evident that WO effects are only relevant for $\tilde{m} \gtrsim 10^{-3}\,\mathrm{eV}$.

Weak Washout Regime

In the weak washout regime, the WO term is very small and neglecting it in (4.3.66) hence yields

$$s\mathcal{H}z_N\frac{\mathrm{d}\eta}{\mathrm{d}z_N} \approx \frac{1}{Y_N^0}\left(\delta_N - 1\right)\gamma_D\,. \tag{4.3.72}$$

With (4.3.65), we then find

$$\frac{\mathrm{d}\eta}{\mathrm{d}z_N} \approx -\frac{1}{Y_N^0}\frac{\mathrm{d}Y_N}{\mathrm{d}z_N}\,, \tag{4.3.73}$$

and integrating both sides yields

$$\eta(\infty) - \underbrace{\eta(0)}_{=0} = \eta = \frac{1}{Y_N^0}\left[\underbrace{-Y_N(\infty)}_{=0} + \underbrace{Y_N(0)}_{Y_N^{\rm eq}(0)}\right] = \frac{Y_N(0)}{Y_N^0}\,. \tag{4.3.74}$$

Thus, provided that WO can be neglected, the efficiency is determined by the initial neutrino abundance. However, if the initial neutrino abundance vanishes, this would imply $\eta = 0$, as is also intuitively clear: For $z_N < z_{\rm eq}^N$, we have $\delta_N - 1 < 0$, i.e. inverse decays create a *negative* efficiency until $z_N = z_{\rm eq}^N$ where

$$\eta^- \equiv \eta(z_{\rm eq}^N) < 0. \tag{4.3.75}$$

On the other hand, for $z_N > z_{\rm eq}^N$, neutrino decays produce a *positive* efficiency since $\delta_N - 1 > 0$, i.e.

$$\eta^+ \equiv \int_{z_{\rm eq}^N}^{\infty} dz_N \frac{1}{Y_N^0} \left(\delta_N - 1\right) \gamma_D > 0. \tag{4.3.76}$$

Thus, every neutrino that decays at $z_N > z_{\rm eq}^N$ contributing to η^+ was produced via an inverse decay that contributed the same amount but with opposite sign to η^-, resulting in a vanishing final asymmetry,

$$\eta = \eta^+ + \eta^- = 0\,. \tag{4.3.77}$$

In order to obtain a non-vanishing asymmetry, it is crucial to take the WO term into account. Including it slightly diminishes $|\eta^-|$, resulting in a positive final efficiency [179],

$$\eta^z \sim \left(\frac{\Gamma_D}{\mathcal{H}(M_N)}\right)^2 \sim \left(\frac{\tilde{m}}{2\times 10^{-3}\,\text{eV}}\right)^2 . \tag{4.3.78}$$

We conclude that in the weak WO regime, the efficiency in the case of a vanishing neutrino abundance increases with $\tilde{m}$, as can be seen in Fig. 4.10. On the other hand, if neutrinos are initially in equilibrium and $\tilde{m}$ sufficiently small, (4.3.74) is a reasonable approximation with

$$\lim_{\tilde{m}\to 0} \eta^t = 1\,. \tag{4.3.79}$$

However, WO processes quickly diminish η^t below its maximal value, resulting in $\eta^t \lesssim 1$ in the weak WO regime, as shown in Fig. 4.10. In Fig. 4.8b (panel 1), we show $\eta^t(z_N)$ and $|\eta^z(z_N)|$ for $\tilde{m} = 5\times 10^{-5}\,\text{eV}$, hence corresponding to the weak WO regime. Clearly, $\eta^t(z_N)$ initially increases until $Y_N(z_N)$ becomes strongly Boltzmann suppressed, resulting in $\eta^t(z_N)$ approaching η^t. As for $|\eta^z(z_N)|$, note that η^- is initially negative until it changes sign at $z_N \approx 10$ and also approaches a constant value $\eta^z \ll \eta^t$.

Strong Washout Regime

In the strong washout regime, inverse decays are fast in an interval $z_N^1 \lesssim z_N \lesssim z_N^2$, see Fig. 4.9, and in that interval, the efficiency produced by neutrino decays is efficiently washed out by inverse decays, see Fig. 4.8b (right). A fraction of the efficiency can only survive once inverse decays become Boltzmann suppressed for $z_N \gtrsim z_N^2$. Moreover, note that even if neutrinos have a vanishing initial abundance, they reach equilibrium before Boltzmann suppression sets in at $z_N \sim 1$ and consequently, the initial conditions are irrelevant in the strong WO regime. This implies that the efficiency in this regime depends only on $\tilde{m}$. Moreover, since WO is more efficient for larger $\tilde{m}$, it is evident that $\eta^{t,z}$ decrease with $\tilde{m}$, see Fig. 4.10.

Intermediate Regime

Finally, let us briefly discuss on the intermediate regime where $\tilde{m} \sim 10^{-3}\,\text{eV}$. While the transition of $\eta^t(\tilde{m})$ from the weak to the strong WO regime is only characterized by a

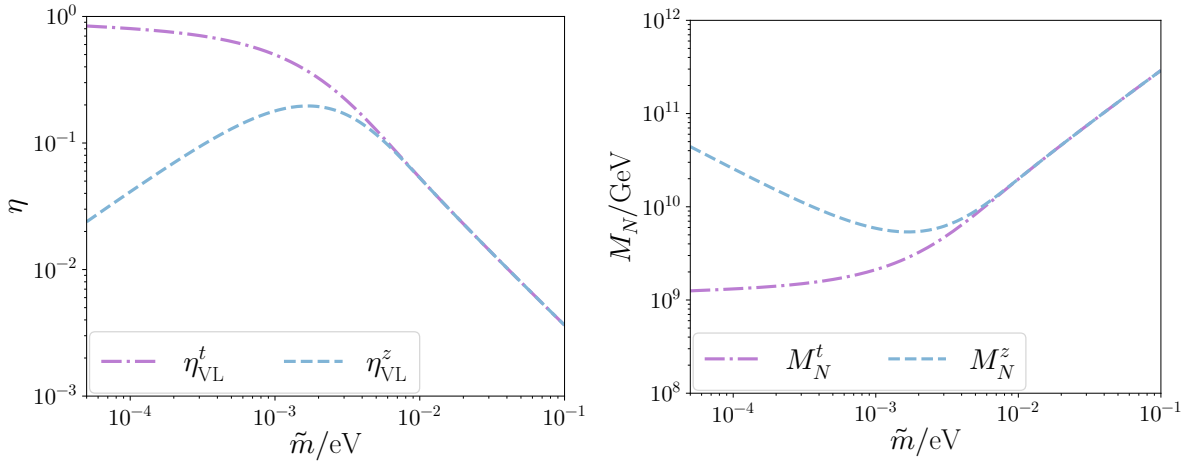

Figure 4.10: *Left:* Efficiency as a function of $\tilde{m}$ for a vanishing initial neutrino abundance ($\eta^z_{\rm VL}$) or a thermal initial neutrino abundance ($\eta^t_{\rm VL}$). In the weak WO regime, $\tilde{m} \lesssim 10^{-3}\,\mathrm{eV}$, we find that $\eta^t_{\rm VL}$ slowly decreases due to WO effects while $\eta^z_{\rm VL}$ increases due to neutrino production becoming more efficient. In the strong WO regime, $\tilde{m} \gtrsim 10^{-3}\,\mathrm{eV}$, both $\eta^t_{\rm VL}$ and $\eta^z_{\rm VL}$ decrease fast with $\tilde{m}$ and the initial neutrino abundance becomes irrelevant. *Right:* Lower limit on the neutrino mass that reproduces the observed baryon asymmetry in the VL scenario as a function of $\tilde{m}$, using the DI bound (4.3.58) and normally ordered light neutrino masses.

steeper slope, see Fig. 4.10, the behavior of $\eta^z(\tilde{m})$ changes in the intermediate regime and it peaks roughly at $\tilde{m} \sim 2 \times 10^{-3}\,\mathrm{eV}$. From the previous discussion, we know that this is due to the interplay of two related effects: In the weak washout regime, the final efficiency that survives the cancellation between η^+ and η^- arises due to washout effects in the regime $z_N \lesssim z^N_{\rm eq}$ which increase with $\tilde{m}$, thus $\eta^z \sim \tilde{m}$. As long as $\tilde{m}$ is small this has no further effect. However, as soon as $\tilde{m} \gtrsim 10^{-3}\,\mathrm{eV}$, washout effects in the $z_N \gtrsim z^N_{\rm eq}$ regime are so fast they diminish η^+, resulting in $\eta \sim \tilde{m}^{-1}$.

Before we proceed, let us shortly comment on the relevance of quark scatterings for leptogenesis. As can be seen from Fig. 4.9 (left), quark scatterings are generally only dominant compared to decays in z_N- range where $\gamma_D/n^{\rm eq}_N\mathcal{H} \lesssim 1$. This implies e.g. that including quark scatterings results in a faster population of the plasma with neutrinos if the initial neutrino abundance vanishes. Additionally, once decays and quark scatterings are fast, $\gamma_{D,Q}/n^{\rm eq}_N\mathcal{H} \gtrsim 1$, the neutrino abundance is forced to approach the equilibrium abundance slightly faster, irrespective of the initial neutrino abundance. In Fig. 4.9 (right), which is relevant for the WO regime, we do not explicitly show $\gamma_{N\overline{U_3},L\overline{Q_3}}$ and γ_{LN,Q_3U_3}, but since the only difference between Fig. 4.9 (left) and Fig. 4.9 (right) is the normalization, we can conclude that quark scatterings with regard to WO are also subdominant to decays. Thus, they slightly enhance the WO effects but do not alter the qualitative behavior significantly.

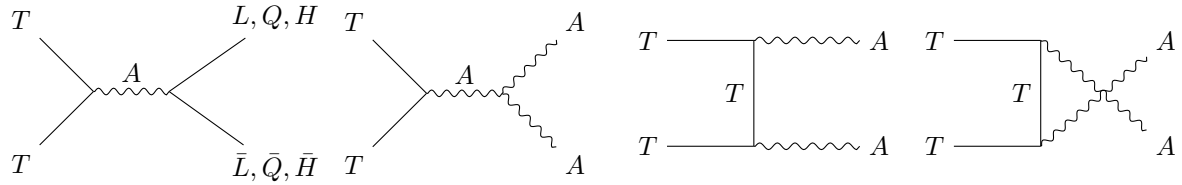

Figure 4.11: Gauge interactions of the triplet for type III leptogenesis. Here, $A = \{B, W_{1,2,3}\}$ corresponds to the gauge bosons.

4.3.3.4 Baryon Asymmetry

Combining the results from the previous sections, we can now derive a limit on the baryon asymmetry that can be generated in VL. Using the conversion rate (4.3.46) and the DI bound in the case of a normal neutrino hierarchy (4.3.58), we find

$$\left|Y^{t,z}_{\Delta B'}\right| \lesssim \frac{28}{79} Y^0_N \left|\epsilon^{DI}\left(M_N\right) \eta^{t,z}(\tilde{m})\right| \,. \tag{4.3.80}$$

Requiring that the observed value of the baryon asymmetry, given in (4.3.3), is reproduced, we can derive a lower limit on the neutrino mass M_N as a function of $\tilde{m}$,

$$M^{t,z}_N(\tilde{m}) = \frac{316 v^2 \pi}{32\sqrt{\Delta m^2_{atm}} Y^0_N} \frac{Y^{exp}_{\Delta B'}}{\eta^{t,z}} \,, \tag{4.3.81}$$

which is shown in Fig. 4.10 (right). However, we do stress that this bounds holds only if the light neutrino masses follow a NH and if $M_N \ll M_{N_{2,3}}$. If two of the heavy neutrinos are almost degenerate in mass instead, $M_{N_1} \lesssim M_{N_2}$, the $\mathcal{CP}$ asymmetry given in (4.3.52) is resonantly enhanced, resulting in [183, 184]

$$\epsilon^{\text{res}} \approx \frac{1}{2} \frac{\text{Im}\left[\left(Y^\dagger Y\right)^2_{12}\right]}{\left(Y^\dagger Y\right)_{11}\left(Y^\dagger Y\right)_{22}} \,, \tag{4.3.82}$$

which can be of order one. This scenario is referred to as *resonant leptogenesis* and leads to different Boltzmann equations since the evolutions of both N_1 and N_2 need to be taken into account. Moreover, we neglected flavor effects in the discussion above. They are generally relevant since processes that are induced by different charged lepton Yukawa couplings become fast at different temperatures due to the different sizes of these Yukawas. This clearly affects the flavor composition and therefore a dedicated analysis of leptogenesis should incorporate these effects in the Boltzmann equations and $\mathcal{CP}$ violation.

4.3.4 Type III Leptogenesis

Besides leptogenesis in a type I Seesaw scenario, another interesting scenario is leptogenesis in the framework of the type III Seesaw mechanism [148, 187, 188]. The major qualitative difference between both scenarios is that the triplet interacts via gauge scatterings, see Fig. 4.11 , which gives rise to an additional term in the Boltzmann equation

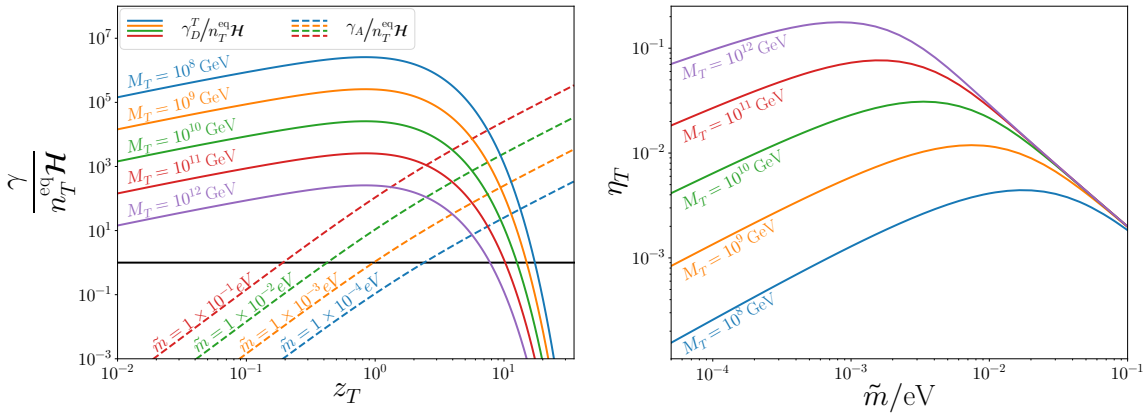

Figure 4.12: *Left:* Rate $\gamma_{D,A}^T/n_T^{\rm eq}\mathcal{H}$, relevant for the evolution of the triplet abundance Y_T. At small z_N, gauge scatterings $\gamma_A^T/n_T^{\rm eq}\mathcal{H}$ are fast, forcing Y_N^T into equilibrium and rendering the initial triplet abundances irrelevant. *Right:* Efficiency η_T as a function of $\tilde{m}$ for different triplet masses M_T. For small $\tilde{m}$, the efficiency is suppressed due to fast gauge scatterings while for large $\tilde{m}$, the efficiency is diminished via WO processes.

for the triplet abundance,

$$s\mathcal{H}z_T\frac{\mathrm{d}Y_T}{\mathrm{d}z_N} = -\gamma_D^T\left(\delta_T - 1\right) - 2\gamma_A\left(\delta_T^2 - 1\right) . \tag{4.3.83}$$

The thermal rate γ_A accounts for the gauge interactions[6] of the triplet while the decay rate γ_D^T contains an additional factor of three compared to the type I scenario due to the three components of the triplet. The Boltzmann equation for the efficiency remains unchanged and is given by

$$s\mathcal{H}z_N\frac{\mathrm{d}\eta_T}{\mathrm{d}z_N} = \frac{1}{Y_N^0}\left(\delta_T - 1\right)\gamma_D^T - \frac{\eta_T}{Y_L^{\rm eq}}\left[\frac{\gamma_D^T}{2} + 2\gamma_{N\overline{U_3},L\overline{Q_3}} + \delta_T\gamma_{LN\leftrightarrow Q_3U_3}\right] . \tag{4.3.84}$$

In contrast to the decay rate γ_D, the scattering rate γ_A is already fast at small z_N, see Fig. 4.12 (left), and efficiently thermalizes the triplet. Naively, one would expect that this renders type III leptogenesis ineffective. However, note that γ_A is doubly Boltzmann suppressed and therefore drops faster than the (inverse) decay rates. Thus, provided that M_T is large and $\tilde{m}$ is small, a sizable efficiency can be created in a short interval where gauge scatterings become slow and decays are not yet fast, see Fig. 4.12 (right). Moreover, in contrast to type I leptogenesis, the fast gauge scatterings render the final efficiency independent from the initial abundance of the triplet. Finally, note that the $\mathcal{CP}$ violation ϵ_T arises from similar diagrams as in Fig. 4.6. It is a factor of three smaller which is however cancelled by an additional factor of three for the efficiency due to the three triplet components.

[6]The corresponding cross section is given in App. G.2.2.

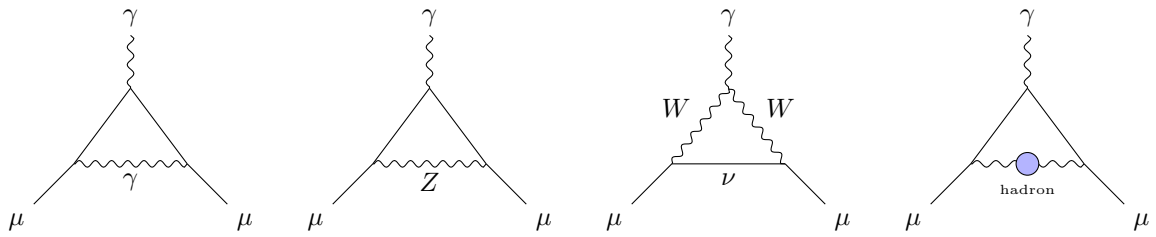

Figure 4.13: Representative Feynman diagrams of SM contributions to a_μ.

4.4 Muon Anomalous Magnetic Moment

The magnetic moment of a lepton ℓ is given by

$$\vec{\mu}_\ell = g_\ell \frac{e_\ell Q_\ell}{2m_\ell} \vec{S}\,, \tag{4.4.1}$$

where the coupling g_ℓ is the *g factor* and $\vec{S} = \vec{\sigma}/2$ is the spin. While the non-relativistic limit of the Dirac equation predicts $g_\ell = 2$, quantum corrections of the photon coupling to the lepton ℓ induce corrections to g_ℓ,

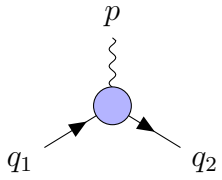

$$= (-ie_\ell)\,\bar{u}(q_2)\left[\gamma^\mu F_E\left(p^2\right) + i\tfrac{\sigma^{\mu\nu}p_\nu}{2m_\ell} F_M\left(p^2\right)\right] u(q_1)\,, \tag{4.4.2}$$

where the F_i are form factors and $\sigma^{\mu\nu} = \frac{i}{2}\left[\gamma^\mu, \gamma^\nu\right]$, see e.g. [73, 189–191]. At tree level, we have $F_E(0) = 1$ and $F_M(0) = 0$ and hence $g_\ell = 2$. At one-loop level, a non-zero contribution to g_ℓ arises,

$$F_M(0) = \frac{1}{2}\left(g_\ell - 2\right) = a_\ell\,, \tag{4.4.3}$$

which is called the *AMM*. It corresponds to an effective interaction term

$$\mathcal{L}_{\text{eff}}^{a_\ell} = -\frac{e_\ell a_\ell}{4m_\ell} \bar{\ell}\sigma^{\mu\nu}\ell F_{\mu\nu}\,. \tag{4.4.4}$$

By decomposing ℓ into its LH and RH parts,

$$\mathcal{L}_{\text{eff}}^{a_\ell} = -\frac{e_\ell a_\ell}{4m_\ell}\left(\overline{\ell_{\mathtt{L}}}\sigma^{\mu\nu}\ell_{\mathtt{R}} + \overline{\ell_{\mathtt{R}}}\sigma^{\mu\nu}\ell_{\mathtt{L}}\right) F_{\mu\nu}\,, \tag{4.4.5}$$

it is apparent that a_ℓ connects LH and RH fields and therefore, non-zero contributions to a_ℓ require chirality flips.

In the SM, the contributions to the AMM of the muon, a_μ, can be conveniently divided into QED, electroweak and hadronic contributions, see Fig. 4.13,

$$a_\mu^{\text{SM}} = a_\mu^{QED} + a_\mu^{EW} + a_\mu^{HAD}\,, \tag{4.4.6}$$

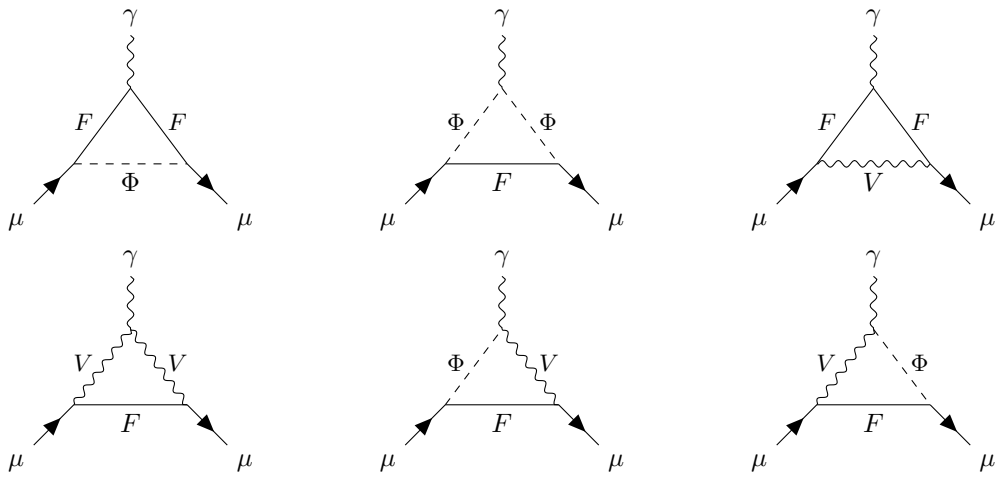

Figure 4.14: Generic contributions to a_μ where F is a fermion, Φ a scalar and V a boson.

with the main uncertainty coming from the hadronic contributions, yielding the SM prediction [45–64, 192]

$$a_\mu^{\rm SM} = (116\,591\,810 \pm 22) \times 10^{-11}\,. \tag{4.4.7}$$

The most stringent experimental bounds to date are provided by the Fermilab Muon $g-2$ experiment [44],

$$a_\mu^{\rm FNAL} = (116\,592\,055 \pm 24) \times 10^{-11} \tag{4.4.8}$$

at 0.20 ppm, which improved upon the previous bound from BNL [43],

$$a_\mu^{\rm BNL} = \left(116\,592\,089 \pm 54^{stat} \pm 33^{syst}\right) \times 10^{-11}\,, \tag{4.4.9}$$

leading to a combined world average of [44]

$$a_\mu^{\rm exp} = (116\,592\,059 \pm 22) \times 10^{-11}\,. \tag{4.4.10}$$

This indicates a 5.0σ discrepancy and has lead to significant efforts to build models that give rise to new contributions to the magnetic moment of the muon.[7]

In Fig. 4.14, we show generic one-loop diagrams that contribute to a_μ, arising due to different fields running in the loop. The size of the individual contributions significantly depends on the coupling structure of the model. In order to illustrate this, let us consider

[7]For completeness, note that shortly after submission of this thesis, a new result for the measurement of the AMM of the muon has been announced, $a_\mu^{\rm FNAL,new} = (1\,165\,920\,710 \pm 162) \times 10^{-12}$, yielding a new experiment world average of $a_\mu^{\rm exp,new} = (116\,592\,071.5 \pm 14.5) \times 10^{-11}$ [193]. Moreover, there has been significant development regarding the theory predictions of the AMM of the muon [194]. Lattice QCD calculations of the hadronic vacuum polarization contribution to the AMM of the muon have reached a remarkable precision, yielding the new SM prediction $a_\mu^{\rm SM,new} = (116\,592\,033 \pm 62) \times 10^{-11}$, which is in good agreement with experiment. Thus, based on lattice calculations, there is no longer a discrepancy between the predicted and observed values of the AMM of the muon. In contrast, data-driven methods face unresolved inconsistencies which prevent a reliable combination of the results. Thus, future measurements and improved calculations are essential in order to resolve these tensions. Note that in this work we use the theory prediction and experimental result quoted in the main text, hence operating under the assumption that there is tension between the theoretically predicted and the measured value of the AMM of the muon.

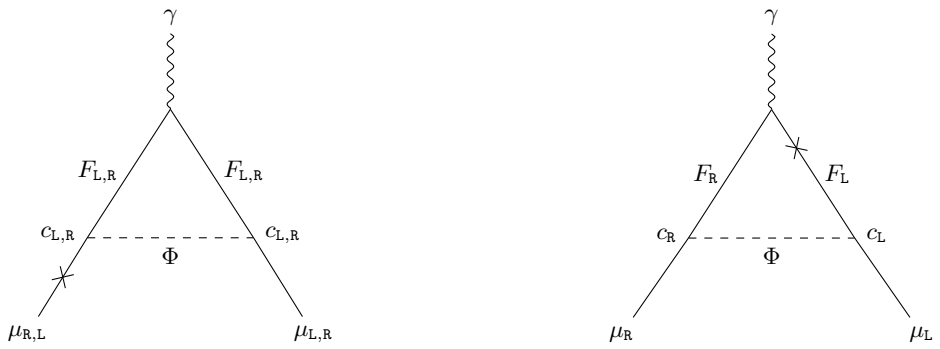

Figure 4.15: Loop diagrams that contribute to a_μ with a fermion F and a scalar ϕ propagating in the loop. The left diagram flips the chirality at the external muon line while the right diagram flips the chirality in the loop, leading to chiral enhancement.

a generic model with one additional scalar Φ and an additional fermion F with masses M_Φ and M_F, respectively, which couple to the muon via [195–197]

$$\mathcal{L} = \bar{F}(c_{\mathtt{L}} P_L + c_{\mathtt{R}} P_R)\mu\Phi + \text{h.c.}\,. \tag{4.4.11}$$

In the limit $m_\mu \ll M_F, M_\Phi$, the corresponding one-loop contribution to a_μ reads

$$a_\mu^{FFS}(c_{\mathtt{L}}, c_{\mathtt{R}}, M_F, M_\Phi) = \underbrace{\frac{m_\mu^2}{32\pi^2 M_\Phi^2}(c_{\mathtt{L}}^2 + c_{\mathtt{R}}^2) I_1\left(\frac{M_F^2}{M_\Phi^2}\right)}_{\equiv a_{\mu,1}^{FFS}} + \underbrace{\frac{m_\mu M_F}{16\pi^2 M_\Phi^2} c_{\mathtt{L}} c_{\mathtt{R}} I_2\left(\frac{M_F^2}{M_\Phi^2}\right)}_{\equiv a_{\mu,2}^{FFS}}, \tag{4.4.12}$$

where the loop functions $I_{1,2}$ are given by

$$I_1(t) = \frac{t^3 - 6t^2 + 3t + 6t\ln t + 2}{3(t-1)^4}\,, \qquad I_2(t) = \frac{t^2 - 4t + 2\ln t + 3}{(t-1)^3}\,. \tag{4.4.13}$$

The contribution $a_{\mu,1}^{FFS}$ in (4.4.12) corresponds to a chirality flip at the external muon line, see Fig. 4.15, and does not require an additional source of chiral symmetry breaking beyond the SM muon Yukawa. Moreover, a contribution to a_μ requires only $c_{\mathtt{L}}$ *or* $c_{\mathtt{R}}$ to be non-zero. On the other hand, $a_{\mu,2}^{FFS}$ flips the chirality in the loop, see Fig. 4.15, and hence provides a new source of chiral symmetry breaking. Clearly, it requires that *both* $c_{\mathtt{L}}$ and $c_{\mathtt{R}}$ are non-zero. It is illuminating to consider the limit $M_F \to \infty$ in which $a_{\mu,1,2}^{FFS}$ become

$$a_{\mu,1}^{FFS}\big|_{\frac{M_F^2}{M_\Phi^2}\to\infty} = \frac{(c_{\mathtt{L}}^2 + c_{\mathtt{R}}^2)}{96\pi^2}\frac{m_\mu^2}{M_F^2}\,, \qquad a_{\mu,2}^{FFS}\big|_{\frac{M_F^2}{M_\Phi^2}\to\infty} = \frac{c_{\mathtt{L}} c_{\mathtt{R}}}{16\pi^2}\frac{M_\mu}{M_F}\,, \tag{4.4.14}$$

where we used

$$I_1\left(\frac{M_F^2}{M_\Phi^2}\right)\Big|_{\frac{M_F^2}{M_\Phi^2}\to\infty} = \frac{M_\Phi^2}{3M_F^2}\,, \qquad I_2\left(\frac{M_F^2}{M_\Phi^2}\right)\Big|_{\frac{M_F^2}{M_\Phi^2}\to\infty} = \frac{M_\Phi^2}{M_F^2}\,. \tag{4.4.15}$$

The contribution $a_{\mu,2}^{FFS}$ is *chirally enhanced* since it is only suppressed by one power

of m_μ/M_F. Additionally, note that $a_{\mu,1}^{FFS}$ is always positive, provided that $c_{\mathtt{L}}$ and $c_{\mathtt{R}}$ are real, while $a_{\mu,2}^{FFS}$ can have either sign, depeding on the sign of $c_{\mathtt{L}}c_{\mathtt{R}}$. Thus, in order to close the gap to a_μ^{SM}, models with $c_{\mathtt{L}}c_{\mathtt{R}} \geq 0$ are desirable while in models without chiral enhancement, i.e. where either $c_{\mathtt{L}}$ or $c_{\mathtt{R}}$ vanishes, it is usually difficult to generate sufficiently sizable contributions to a_μ. Consequently, many BSM models that aim to explain the AMM of the muon involve new sources of chiral symmetry breaking that induce chirally enhanced contributions.

CHAPTER 5

The Majoron Model and Beyond

In the previous Chapters, we discussed how the SM fails to account for the existence of the observed neutrino masses. In light of the success of SSB with regard to the mass generation of the other SM particles, it seems intuitive to adopt a similar approach in the neutrino sector and use the concept of SSB to dynamically generate neutrino masses. Morever, we studied how the lightness of the neutrinos can be explained via the Seesaw mechanism, provided that they are Majorana particles and heavy RH neutrinos exist. Since the Seesaw mechanism breaks the anomaly free accidental global SM symmetry $U(1)_{B'-L'}$, it is therefore straightforward to envisage a scenario where $U(1)_{B'-L'}$ is *spontaneously* broken. This can be achieved by introducing a new scalar singlet which obtains a VEV at the Seesaw scale and hence breaks $U(1)_{B'-L'}$ spontaneously. Recalling the discussion in Sec. 2.1.2, this implies the existence of a massless Goldstone boson, called *Majoron* [28–30].[1] In many Majoron models, it is further assumed that the Majoron obtains a small mass, for example due to explicit $U(1)_{B'-L'}$ breaking terms, and since it interacts with the SM particles only beyond tree level, it is straigthforward to consider the Majoron as a candidate for DM [31–35, 42]. Moreover, as in the generic Seesaw mechanism, the Majoron model naturally contains the ingredients necessary for baryogenesis via leptogenesis [39–41], with the main difference that the neutrino evolution is affected by the additional interactions with the Majoron. Thus, it is evident that the Majoron model can address several shortcomings of the SM and cosmology at once while requiring only few new particles. However, in Ref. [199], it was claimed that Majoron models suffer from the appearance of DWs which would likely dominate the energy density of the Universe, contrary to observations, and hence rule out generic singlet Majoron models. In this Chapter, we outline why this claim is severely flawed and why Majoron models do not generally suffer from the appearance of DWs. Nevertheless, the proposed solutions to the stated DW problem suggested in Ref. [199] serve as a motivation to study the implications of extended Majoron models. In particular, we discuss how the conversion rate of a lepton- to a baryon asymmetry is altered in Majoron models that contain additional RH fermions.

This Chapter, which is largely based on the findings of Ref. [2], is structured as follows. In Sec. 5.1.1, we briefly review the singlet Majoron model, focussing on neutrino masses,

[1] In the literature, the symmetry which is spontaneously broken is often stated as $U(1)_{L'}$ rather than $U(1)_{B'-L'}$. While it is indeed irrelevant for most applications such as neutrino masses if $U(1)_{L'}$ or $U(1)_{B'-L'}$ is spontaneously broken, we note that the Goldstone couplings to gauge bosons arise from non-anomalous fermion loops and thus strictly speaking, the Majoron is the Goldstone boson of $U(1)_{B'-L'}$ [108, 198].

couplings to SM particles and the implications of massive Majorons. In Sec. 5.2, we review the claim that DWs arise in Majoron models and outline why this statement is flawed. In Sec. 5.3, we present several extensions of Majoron models, originally motivated to avoid the appearance of DWs, and discuss how these extensions affect the Sphaleron rate of L' to B' conversion. In Sec. 5.4, we summarize our results.

5.1 Majoron Model

5.1.1 Model Setup

In the singlet Majoron model, the SM is extended by three SM singlet RH neutrinos $N_{\mathtt{R}}$, carrying a lepton number of $L' = 1$, and a SM singlet complex scalar $\hat{\sigma}$ with a lepton number of $L' = -2$. This gives rise to new $U(1)_{L'}$ invariant terms in the Lagrangian $\mathcal{L}$, with the relevant kinetic and Yukawa terms for the lepton sector reading

$$\mathcal{L}^{L'}_{Yuk} = -\overline{L_i} Y^{\nu}_{ij} H E_j - \overline{L_i} Y^{\nu}_{ij} \tilde{H} N_{\mathtt{R}_j} - \frac{1}{2} g_{N_{ij}} \overline{N^C_{\mathtt{R}_i}} N_{\mathtt{R}_j} \hat{\sigma} + \text{h.c.}\,, \tag{5.1.1}$$

$$\mathcal{L}^{L'}_{kin} = i\overline{L} \not{\partial} L + i\overline{E} \not{\partial} E + i\overline{N_{\mathtt{R}}} \not{\partial} N_{\mathtt{R}} + \left(\partial_\mu \hat{\sigma}\right)^\dagger \left(\partial^\mu \hat{\sigma}\right)\,. \tag{5.1.2}$$

Moreover, the new scalar potential is given by

$$V(\hat{\sigma}, H) = -\mu^2_{\hat{\sigma}} |\hat{\sigma}|^2 + \lambda_\sigma |\hat{\sigma}|^4 - \mu^2_H |H|^2 + \lambda_H |H|^4 + 2\lambda_{mix} |\sigma|^2 |H^2|\,, \tag{5.1.3}$$

where

$$\lambda_{\hat{\sigma},H} > 0\,, \qquad \lambda_{mix} > -\sqrt{\lambda_\sigma \lambda_H}\,, \tag{5.1.4}$$

so that the potenial is bounded from below. At the Seesaw scale f, typically taken to be of order $\mathcal{O}\left(10^9\,\text{GeV}\right)$, the $U(1)_{L'}$ symmetry is spontaneously broken as $\hat{\sigma}$ develops its VEV f. In the linear representation, we can write

$$\hat{\sigma} = \frac{1}{\sqrt{2}} \left(f + \sigma + iJ\right)\,, \tag{5.1.5}$$

where σ is the massive, $\mathcal{CP}$ even Higgs field while J is the massless, $\mathcal{CP}$ odd Goldstone boson, the Majoron. We can then write (5.1.1) as

$$\mathcal{L}^{new}_{Yuk} = -\overline{L_i} Y^{\nu}_{ij} \tilde{H} N_j - \frac{1}{2\sqrt{2}} g_{N_{ij}} \overline{N^C_{\mathtt{R}_i}} N_{\mathtt{R}_j} f - \frac{1}{2\sqrt{2}} g_{N_{ij}} \overline{N^C_{\mathtt{R}_i}} N_{\mathtt{R}_j} \sigma - \frac{i}{2\sqrt{2}} g_{N_{ij}} \overline{N^C_{\mathtt{R}_i}} N_{\mathtt{R}_j} J + \text{h.c.}\,. \tag{5.1.6}$$

Analogously to Sec. 4.2.1.1, we can define heavy Majorana neutrinos in the basis where $g_{N_{ij}}$ is diagonal as

$$N_i = N_{\mathtt{R}_i} + \left(N_{\mathtt{R}_i}\right)^C = N^C_i\,, \tag{5.1.7}$$

with masses given by

$$M_{N_i} = \frac{g_{N_i} f}{\sqrt{2}}\,. \tag{5.1.8}$$

Thus, we can rewrite the Majorana mass term and the interactions of N with σ and J in (5.1.6) as

$$\mathcal{L}^{new}_{Yuk} = -\left(\overline{L_i} Y^{\nu}_{ij} \tilde{H} N_{\mathtt{R}_j} + \text{h.c.}\right) - \frac{1}{2} M_{N_i} \overline{N_i} N_i - \frac{1}{2\sqrt{2}} g_{N_i} \overline{N_i} N_i \sigma - \frac{i}{2\sqrt{2}} J \overline{N} \gamma_5 N \,. \quad (5.1.9)$$

Next, EWSB takes place once the Higgs doublet H develops its VEV v,

$$H = \frac{1}{\sqrt{2}} \begin{pmatrix} \phi^+ \\ v + h + i\phi_4 \end{pmatrix} . \quad (5.1.10)$$

In contrast to the SM though, h is not the physical mass eigenstate of the SM Higgs since it mixes with σ according to

$$\begin{pmatrix} h \\ \sigma \end{pmatrix} = \begin{pmatrix} \cos\theta & -\sin\theta \\ \sin\theta & \cos\theta \end{pmatrix} \begin{pmatrix} \tilde{h} \\ \tilde{\sigma} \end{pmatrix} , \quad (5.1.11)$$

where the mixing angle is given by

$$\theta = \frac{1}{2} \arctan\left(\frac{v}{f} \frac{\lambda_{mix}}{\lambda_\sigma - \lambda_H \frac{v^2}{f^2}} \right) . \quad (5.1.12)$$

In the following, we assume that the mixing between h and σ is small, i.e. $\cos\theta \approx 1$, so that we can approximately identify them with the correspnding mass eigenstates,

$$h \approx \tilde{h} \,, \qquad \sigma \approx \tilde{\sigma} \,, \quad (5.1.13)$$

and $v = v_{\text{SM}}$. After EWSB, we find that a Dirac mass term arises,

$$\mathcal{L}_{mass} = -\overline{\nu_{\mathtt{L}_i}} m_D^{ij} N_{\mathtt{R}_j} - M_{N_i} \overline{N^C_{\mathtt{R}_i}} N_{\mathtt{R}_i} + \text{h.c.} \,, \quad (5.1.14)$$

where m_D^{ij} is a Dirac mass with

$$m_D^{ij} = \frac{Y^{\nu}_{ij} v}{\sqrt{2}} \,. \quad (5.1.15)$$

Comparing (5.1.14) with (4.2.17), we immediatly rediscover the Seesaw mass-Lagrangian. Defining the physical Majorana mass eigenstates according to (4.2.19) and (4.2.22) as

$$n \equiv \begin{pmatrix} \hat{N} \\ \hat{\nu} \end{pmatrix} , \quad (5.1.16)$$

we can further write the neutrino couplings to J, Z and W^- as [41, 201, 202]

$$\mathcal{L}_J = -\frac{iJ}{f} \sum_{i,j=1}^{6} \overline{n_i} \left[C_{ij} \left(m_i P_{\mathtt{R}} - m_j P_{\mathtt{R}} \right) + C_{ji} \left(m_j P_{\mathtt{L}} - m_i P_{\mathtt{R}} \right) + \delta_{ij} \gamma_5 m_i \right] n_j \,, \quad (5.1.17)$$

$$\mathcal{L}_Z = \frac{g}{4\cos\theta_W} \sum_{i,j=1}^{6} \overline{n_i} \not{Z} \left[C_{ij} P_{\mathtt{L}} - C_{jiP_{\mathtt{R}}} \right] n_j \,, \quad (5.1.18)$$

$$\mathcal{L}_W = \frac{g}{\sqrt{2}} \sum_{j=1}^{6} \sum_{\alpha=1}^{3} \left(\overline{\ell_\alpha} B_{\alpha j} \not{W}^- P_{\mathtt{L}} n_j + \overline{n_j} B^*_{\alpha j} \not{W}^+ P_{\mathtt{L}} \ell_\alpha \right) , \tag{5.1.19}$$

$$\mathcal{L}_H = -\frac{h}{2 v_{\mathrm{SM}}} \sum_{i,j=1}^{6} \overline{n_i} \left[C_{ij} \left(m_i P_{\mathtt{L}} + m_j P_{\mathtt{R}} \right) + C_{ji} \left(m_j P_{\mathtt{L}} + m_i P_{\mathtt{R}} \right) \right] n_j \, , \tag{5.1.20}$$

where

$$C_{ij} = \sum_{k=1}^{3} \tilde{U}_{ki} \tilde{U}^*_{kj} \, , \qquad B_{\alpha j} = \tilde{U}^*_{\alpha j} \, , \tag{5.1.21}$$

and we assumed that the charged lepton mass matrix is diagonal. In the Seesaw limit $M_R \gg m_D$, we then find, as usual, light neutrino masses of order $-\frac{m_D^T m_D}{M_N}$ and heavy neutrino masses of order M_N. In the Casas-Ibarra parametrization [203], the Dirac masses m_D are expressed in terms of a complex orthogonal 3×3 matrix R as

$$m_D = i U \sqrt{d_l} R^T \sqrt{d_h} \, , \tag{5.1.22}$$

where U is the PMNS matrix and

$$d_l = \mathrm{diag} \left(m_1, m_2, m_3 \right) \, , \tag{5.1.23}$$

$$d_h = \mathrm{diag} \left(m_4, m_5, m_6 \right) \equiv \mathrm{diag} \left(M_{N_1}, M_{N_2}, M_{N_3} \right) \, , \tag{5.1.24}$$

are the light and heavy neutrino masses, respectively, allowing the mixing matrix $\tilde{U}$ to be reexpressed as

$$\tilde{U} \sim \begin{pmatrix} U^* & -i U^* \sqrt{d_l} R^\dagger \sqrt{d_h^{-1}} \\ -i \sqrt{d_h^{-1}} R \sqrt{d_l} & 1 \end{pmatrix} . \tag{5.1.25}$$

5.1.2 Massive Majorons

It is often assumed that the Majoron obtains a small mass m_J, for example due to explicit breaking terms in the Lagrangian or gravity effects. If $m_{1,2,3} \ll m_J \ll M_{N_{1,2,3}}$, the Majoron can decay on tree level to light neutrinos with a decay rate given by

$$\Gamma \left(J \to \nu \nu \right) \approx \frac{m_J}{16 \pi f^2} \sum_{i=1}^{3} m_i^2 \, . \tag{5.1.26}$$

Assuming that $m_J \sim \mathcal{O} \left(1 \, \mathrm{MeV} \right)$, $f \sim \mathcal{O} \left(10^9 \, \mathrm{GeV} \right)$ and taking $10^{-3} \, \mathrm{eV}^2$ as an upper limit on the sum of neutrino masses, as suggested by neutrino oscillations, we find a Majoron lifetime τ_J of order $10^{19} \, \mathrm{s}$. Comparing to the age of the Universe, $\tau_U \sim 10^{17} \, \mathrm{s}$, we note that the Majoron is sufficiently stable to be a viable DM candidate. Moreover, note that Majorons couple to neutrino mass eigenstates rather than flavor eigenstates. Thus, neutrinos produced via Majoron decay do not oscillate and the flavor ratios between source and detector are fixed, potentially leading to striking signatures in neutrino detectors [201].

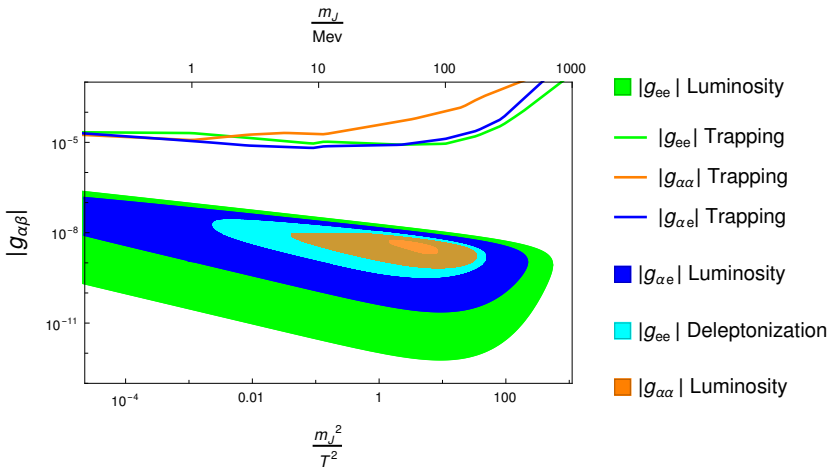

Figure 5.1: Constraints on the Majoron-neutrino coupling from SN data. The colored regions are excluded, for simplicity assuming that only one coupling constant is non-zero with $\alpha = \mu, \tau$ and T is the core temperature. The regions above the lines lead to Majoron trapping in the SN core. Figure taken from Ref. [32].

Bounds on the coupling of a massive Majoron to neutrinos can be derived e.g. from *supernova* (SN) data [32, 204] and neutrinoless double beta decay with Majoron emission [32, 205], which we will shortly review in the following.

5.1.2.1 Supernova Constraints

Although the mechanism behind the core collapse during a SN is not yet fully understood, it is generally believed that the energy released during the explosion is carried away by neutrinos. To date, the only observed SN is SN1987A [206–210] with a measured neutrino signal that is compatible with the prediction that the cooling proceeds via neutrino emission. In the context of the Majoron model, inverse Majoron decays $\nu\nu \to J$ that take place in the SN core can severely diminish the neutrino signal, hence placing bounds on the Majoron-neutrino coupling. This is commonly called the *luminosity constraint*. However, it should be taken into account that Majorons can also decay back to neutrinos in the core or become trapped via neutrino-Majoron scattering, which would prevent the neutrino signal from being altered. Thus, the luminosity constraint excludes a region in the parameter space and is not an upper limit on the neutrino-Majoron coupling. Moreover, the bounce shock that triggers the explosion depends crucially on the abundance of leptons that is trapped in the SN core during the infall stage. If inverse Majoron decays $\nu_e\nu_\alpha \to J$ with $\alpha = e, \mu, \tau$ are fast, the deleptonization of the core could prevent a succesfull explosion. This is called the *deleptonization constraint*. In Fig. 5.1, we show the SN constraints as a function of the Majoron-neutrino couplings.

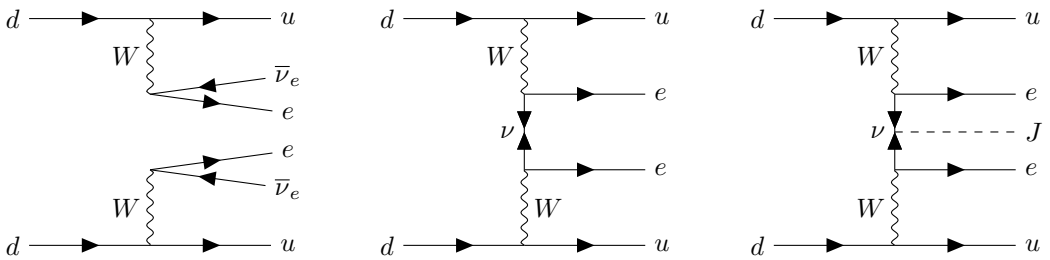

Figure 5.2: From left to right: Feynman diagrams for double beta decay ($2\nu\beta\beta$), neutrinoless double beta decay ($0\nu\beta\beta$) and neutrinoless double beta decay with Majoron emission ($0\nu\beta\beta J$).

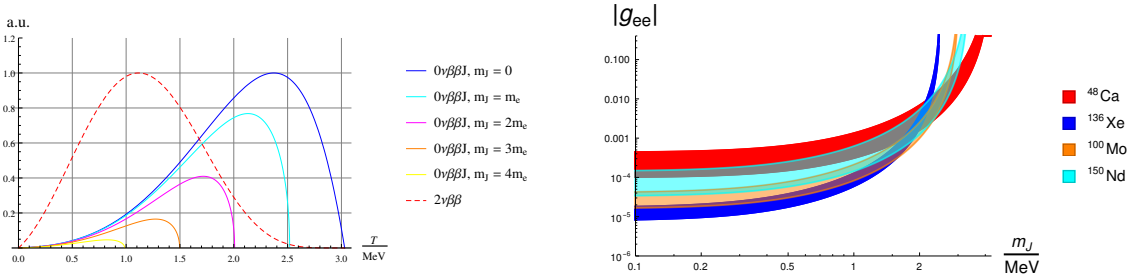

Figure 5.3: *Left:* Normalized spectrum of ^{100}Mo with $Q = 3.03\,\text{MeV}$ [211] for $2\nu\beta\beta$ and $0\nu\beta\beta J$ for different values of m_J. *Right:* Bounds on the g_{ee} from $0\nu\beta\beta J$ for different nuclei. The regions above the bands are excluded while the width of the band corresponds to the uncertainties of $g_{ee}(m_J = 0)$ placed by the collaborations. Figures taken from Ref. [32].

5.1.2.2 Neutrinoless Double Beta Decay with Majoron Emission

As briefly discussed in Sec. 4.2, the observation of $0\nu\beta\beta$ would be a smoking gun, establishing neutrinos as Majorana particles. In the Majoron model, an additional decay channel where a Majoron is emitted exists, $0\nu\beta\beta J$, see Fig. 5.2, provided that the Q-value of the nucleus exceeds the Majoron mass. The overlap of the spectrum of $0\nu\beta\beta J$ with the irreducible background of double beta decay with neutrino emission, $2\nu\beta\beta$, increases with the Majoron mass m_J, see Fig. 5.3 (left). Based on the non-observation of $0\nu\beta\beta$, upper bounds on the effective electron neutrino-Majoron coupling g_{ee} can be derived, see Fig. 5.3 (right), depending on the nucleus that decays.

In principle, one could also envisage a scenario where instead of being emitted during the decay of the nucleus, a Majoron is captured. This scenario is motivated on the basis of the Majoron being DM with the earth moving through the DM halo, which would yield a clear signal with peaks in the spectrum at the Majoron mass. In the following, we will give a rough estimate on the viability of this scenario. The Majoron capture rate is given

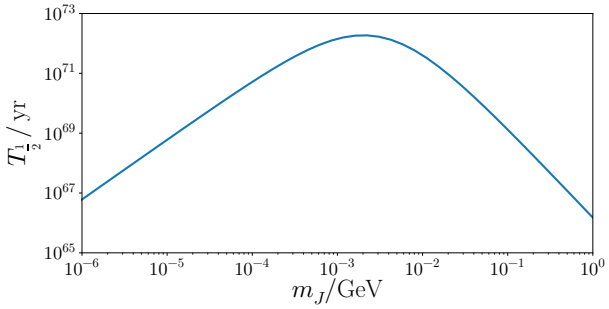

Figure 5.4: Half life of Majoron capture on Germanium with $A_{Ge} = 76$, $Z_{Ge} = 34$ and $M_{mol,Ge} = 75.919\,\mathrm{g\,mol^{-1}}$.

by

$$\Gamma_J = \sigma^J \rho_J N_{nuc} v\,, \tag{5.1.27}$$

where σ^J is the cross section of Majoron capture, $\rho_J = \rho_{\mathrm{DM}} = 0.3\,\mathrm{GeV}$ is the Majoron density, $N_{nuc} = m_{detector} M^{-1}_{mol,nuc}$ is the number of nuclei in a sample of mass $m_{detector}$ and $v = 220\,\mathrm{km\,s^{-1}}$ is the velocity. The cross section σ_J depends on the nuclear matrix element M_{0J} and is given by

$$\sigma_J = \frac{1}{2m_J v} G^J\left(Q + m_J, Z\right) \left|M_{0J}\right|^2 \left|g_{ee}(m_J)\right|^2\,, \tag{5.1.28}$$

where [212]

$$\begin{aligned} G_J = \frac{G_F^4 g_A^4}{128\pi^7 R^2 m_e^2} \int_{m_e}^{E_i+m_J-E_f-m_e} d\epsilon_1 F(Z,\epsilon_1) p_1 \epsilon_1 \int_{m_e}^{E_i+m_J-E_f-\epsilon_1} d\epsilon_2 F(Z,\epsilon_2) p_2 \epsilon_2 \\ \times \delta\left(E_i + m_J - E_f - \epsilon_1 - \epsilon_2\right) \end{aligned} \tag{5.1.29}$$

is the phase space, $R \approx 1.2 A^{\frac{1}{3}}$ is the nuclear radius and $g_A \sim 1.26$ is an effective coupling constant. Moreover, F is the Primakoff-Rosen approximation of the Fermi function,

$$F(Z,\epsilon_i) = \frac{\epsilon_i}{p_i} \frac{2\pi\alpha Z}{1 - \exp\left(-2\pi\alpha Z\right)}\,. \tag{5.1.30}$$

Determining the nuclear matrix element is highly non-trivial. However, in order to obtain a rough limit on the experimental viability of Majoron capture, we take the matrix element M_{0J} to be of order 1 and further assume $g_{ee} = 10^{-5}$. With a hypothetical ^{76}Ge detector with a mass $m_{detector} = 10^3\,\mathrm{kg}$ and $Q = 2.04\,\mathrm{MeV}$ [213], we determine the half life $T_{1/2} = \ln 2/\Gamma_J$ as a function of m_J, shown in Fig. 5.4. We find that for a Majoron mass of order MeV, the half life is of order $10^{72}\,\mathrm{yr}$. Thus, although it is an interesting possibility to consider, it does not seem feasbile to detect capture of Majoron DM .

5.2 Domain Walls in Majoron Models

Let us begin the discussion of DWs in Majoron models by briefly reviewing the argument presented in Ref. [199]. Electroweak Instanton processes break the accidental global $U(1)_{L'}$ symmetry of the SM to a Z_3 symmetry while SSB at the Seesaw scale breaks $U(1)_{L'}$ to a Z_2 symmetry. The authors of [199] argue that this mismatch results in the appearance of DWs with an energy density $\rho_{\mathrm{DW}} \sim 3f^2 m_W/2t$, where f is the VEV which breaks $U(1)_{L'}$ spontaneously. This energy density would exceed the radiation energy ρ_R unless $f_{\mathrm{DW}} \lesssim 10^{10}\,\mathrm{GeV}$. Since no observational evidence for the existence of DWs with a sizable energy density exists, the authors of [199] conclude that unless $f \ll f_{\mathrm{DW}}$, the singlet Majoron model is ruled out. As a solution, they propose to change the anomaly factor $\mathcal{A}_{L'}$ since its value determines the residual symmetry from Instanton transitions (see Sec. 4.3.2). Thus, if $\mathcal{A}_{L'}$ can be changed so that $|\mathcal{A}_{L'}| = 1, 2$, the mismatch between Z_2 and $Z_{\mathcal{A}_{L'}}$ is absent and allegedly no DWs appear. This can be easily achieved by extending the Majoron model by additional RH leptons with non-trivial $\mathrm{SU}(2)_{\mathtt{L}}$ charges. In the following, we will outline why the proposed solution to the DW problem is incorrect and that irrespective of the value of $\mathcal{A}_{L'}$, DWs in the Instanton background are absent in the singlet Majoron model.

For the following discussion, it is convenient to use the polar representation of the complex scalar $\hat{\sigma}$,

$$\hat{\sigma} = \frac{1}{\sqrt{2}} \left(f + \sigma(x)\right) e^{\frac{iJ(x)}{f}} , \tag{5.2.1}$$

instead of the linear representation used in the previous section.[2] Inserting (5.2.1) into the relevant terms of the Lagrangian given in (5.1.1) and (5.1.2) and additionally rotating the lepton fields as

$$(N_{\mathtt{R}_i}, L, E) \to e^{-\frac{iJ(x)}{2f}} \left(N_{\mathtt{R}_i}, L, E\right) , \tag{5.2.2}$$

we find

$$\mathcal{L}^{L'}_{Yuk} \supset -\overline{L_i} Y^{\nu}_{ij} H E_j - \overline{L_i} Y^{\nu}_{ij} \tilde{H} N_{\mathtt{R}_j} - \frac{1}{2\sqrt{2}} g_{N_{ij}} \left(f + \sigma\right) \overline{N^C_{\mathtt{R}_i}} N_{\mathtt{R}_j} + \mathrm{h.c.} , \tag{5.2.3}$$

$$\mathcal{L}^{L'}_{kin} \supset \frac{\partial_\mu J}{2f} \left(\overline{L_{\mathtt{R}}} \gamma^\mu L_{\mathtt{R}} + \overline{E} \gamma^\mu E + \overline{N_{\mathtt{R}}} \gamma^\mu N_{\mathtt{R}}\right) + \frac{1}{2} \left[\left(\partial_\mu \sigma\right) \left(\partial^\mu \sigma\right) + \left(1 + \frac{\sigma}{f}\right)^2 \left(\partial_\mu J\right) \left(\partial^\mu J\right) \right] , \tag{5.2.4}$$

while the potential transforms trivially. Moreover, the Jacobian from the path integral measure induces the term[3,4]

$$\delta\mathcal{L}^{Jac} = -\mathcal{A}_{L'} \frac{g^2}{32\pi^2} \frac{J}{f} W^a_{\mu\nu} \tilde{W}^{a,\mu\nu} , \tag{5.2.5}$$

[2] Note that even though we use the same notation for the fields σ and J, they do not correspond to the fields in the linear representation (5.1.5).

[3] As in Sec. 4.3.2, we neglect the effects of $U(1)_Y$.

[4] It has been shown in Ref. [198] that Majoron couplings to the electroweak gauge bosons indeed arise on one-loop level.

while the electroweak θ term is given by

$$\mathcal{L}^{\theta_{EW}} = \frac{g^2}{32\pi^2}\theta_{EW} W^a_{\mu\nu}\tilde{W}^{a,\mu\nu} \,. \tag{5.2.6}$$

Thus, we have an additional term in the Lagrangian,

$$\mathcal{L}_I = \left(\theta_{EW} - \mathcal{A}_{L'}\frac{J}{f}\right)\frac{g^2}{32\pi^2} W^a_{\mu\nu}\tilde{W}^{a,\mu\nu} \,, \tag{5.2.7}$$

which we will call the Instanton term. First considering only the terms in (5.2.3) and (5.2.4), we find that the Majoron disappears from (5.2.3) and has only derivative couplings in (5.2.4). Thus, as discussed in Sec. 2.1.2, the Lagrangian (5.2.4) is invariant under constant shifts of J. In contrast to Sec. 2.1.2 though, we also need to take the transformation properties of $N_{\mathtt{R}}$ in (5.2.3) into account which reveals that the $U(1)_{L'}$ is no longer manifest in terms of continous shifts of J and instead broken to a Z_2,

$$J \to J - 2\pi k f \,, \qquad (N_{\mathtt{R}_i}, L, E) \to e^{ik\pi}\,(N_{\mathtt{R}_i}, L, E) \;, \quad k = 0, 1 \,. \tag{5.2.8}$$

However, for simplicity, let us first assme that $g_N = 0$ so that the last term in (5.2.3) disappears. In this case, the shift symmetry in (5.2.3) and (5.2.4) under $J \to J - 2fc$ as a remnant of the spontaneously broken $U(1)_{L'}$ is manifest, where c is an arbitrary constant. Thus, we can remove θ_{EW} from (5.2.7) by performing the shift $J \to J + f\theta_{EW}/\mathcal{A}_{L'}$, while the interplay between Instantons and anomalies generates an effective potential,[5]

$$V(J) \sim 1 - \cos\left(\mathcal{A}_{L'}\frac{J}{f}\right) \,. \tag{5.2.9}$$

In this form, it is apparent that the $U(1)_{L'}$ symmetry is broken by Instantons to a discrete $Z_{\mathcal{A}_{L'}}$ and that $\mathcal{A}_{L'}$ degenerate vacua exist. Thus, the Lagrangian of the model is no longer invariant under continous shifts of J but only under discrete shifts,

$$J \to J - \frac{2\pi f n}{\mathcal{A}_{L'}} \,, \qquad n = 0, ..., \mathcal{A}_{L'} - 1 \,. \tag{5.2.10}$$

Comparing this to the discussion in Sec. 3.4.2, the conclusion would indeed be that DWs appear. Note that in contrast to the claims in Ref. [199], we reached this conslusion without the $Z_3 \neq Z_2$ argument.

Next, let us discuss what happens in the case of $g_N \neq 0$. The classical Lagrangian, see (5.2.3) and (5.2.4), is invariant under the transformations given in (5.2.8) while the term induced by Instanton transitions and anomalies is invariant under (5.2.10). As in the SM, we have $\mathcal{A}_{L'} = 3$ in generic Majoron models and consequently, there exists no transformation under which the full Lagrangian is invariant, i.e. we have $n = k = 0$ and the symmetry is completely broken. This implies two things. First, we can no longer remove θ_{EW} from the Lagrangian (5.2.7) which would imply that θ_{EW} is a physical $\mathcal{C}$ and $\mathcal{CP}$ violating parameter. Second, since the Lagrangian is no longer invariant under shifts

[5] Note that this is basically the mechanism which is used to removed the strong vacuum angle θ_{QCD} in Axion models.

of the Majoron, there exitsts only one ground state,

$$V(J) \sim 1 - \cos\left(\theta_{EW} - 3\frac{J}{f}\right) , \tag{5.2.11}$$

which implies that no DWs appear. Thus, in contrast to the claim in Ref. [199], the mismatch $Z_3 \neq Z_2$ does *prevent* the appearance of DWs in Majoron models. In fact, the solutions to the DW problem proposed in Ref. [199] tend to have the contrary effect. If e.g. the anomaly factor $\mathcal{A}_{L'}$ is changed so that $\mathcal{A}_{L'} = 2$, it is easy to conclude from the previous discussion that in this case, the potential $V(J)$ remains invariant under shifts $J \to J - \pi f n$ with $n = 0, 1$, i.e. two degenerate minima exist and DWs appear.
That the mismatch of Z_3 and Z_2 does not results in the appearance of DWs can be made transparent using another simple argument. DWs appear when a discrete symmetry is *spontaneously* broken but since Z_2 is not a subgroup of Z_3, it is impossible to break Z_3 spontaneously to Z_2.
The arguments above seem to imply that in Majoron models, either θ_{EW} is a physical parameter (if $\mathcal{A}_{L'} = 3$), or DWs appear (if e.g. $\mathcal{A}_{L'} = 2$). However, actually neither is the case. In order to see this, note that we neglected the invariance of the Lagrangian under baryon number rotations,

$$\psi \to e^{iB'\alpha_{B'}}\psi \, . \tag{5.2.12}$$

Taking this into account, we can write (5.2.7) as

$$\mathcal{L}_I^{B'} = \left(\theta_{EW} - \mathcal{A}_{L'}\frac{J}{f} + \alpha_{B'}\mathcal{A}_{B'}\right)\frac{g^2}{32\pi^2}W^a_{\mu\nu}\tilde{W}^{a,\mu\nu} = \mathcal{L}_I + \alpha_{B'}\mathcal{A}_{B'}\frac{g^2}{32\pi^2}W^a_{\mu\nu}\tilde{W}^{a,\mu\nu} \, , \tag{5.2.13}$$

and find that it is always possible to remove $\mathcal{L}_I$ with an appropriate choice of $\alpha_{B'}$, no matter what the value of $\mathcal{A}_{L'}$ is [102, 108, 169, 170, 198, 214, 215].
Finally, let us comment on the estimate given in Ref. [199] regarding the energy density of DWs in generic Majoron models. For the sake of the argument, let us assume that a Majoron potential in the Instanton background of the form (5.2.9) with $n > 1$ degenerate vacua indeed exists and cannot be rotated away. In this case, electroweak Instantons are not only responsible for the appearance of DWs but also induce a Majoron mass m_J^I. Similarly to Axion models, see Sec. 3.4.2, the surface energy density is proportional to the Majoron mass,

$$\sigma_{DW,J} \sim m_J^I f^2 \, , \tag{5.2.14}$$

yielding a lower limit on the DW energy density according to (3.4.18),

$$\rho_{DW,J} \sim m_J^I f^2 \mathcal{H} \, . \tag{5.2.15}$$

If we demand that the DW energy density $\rho_{DW,J}$ does not exceed the radiation energy density ρ_R at temperatures $\mathsf{T} \gtrsim 200\,\mathrm{MeV}$, we find an upper limit on the VEV f in terms

of the Majoron mass in the Instanton background, m_J^I, according to

$$f(m_J^I) \lesssim \left.\frac{1}{\sqrt{8\pi t(\mathsf{T}) G m_J^I}}\right|_{\mathsf{T}\sim 200\,\mathrm{GeV}} \sim 5.7\times 10^{10}\,\mathrm{GeV}^{3/2}\frac{1}{\sqrt{m_J^I}}\,, \tag{5.2.16}$$

where we used the relation

$$t(\mathsf{T}) = \left(\frac{90}{32\pi^3 G g_*}\right)^{\frac{1}{2}}\frac{1}{\mathsf{T}^2} \tag{5.2.17}$$

which holds in the radiation dominated epoch. Calculating the Majoron mass m_J^I is highly non-trivial and requires a dedicated analysis of the potential (5.2.9). In Axion models, the Axion mass in the Instanton background is usually very small, $m_{\mathtt{a}} \ll 1\,\mathrm{eV}$, and we assume that it is reasonble to invoke a similar bound for the Majoron mass. Taking a rather conservative value, $m_J^I \sim 1\,\mathrm{eV}$, the upper limit on f becomes

$$f \lesssim 1.8\times 10^{15}\,\mathrm{GeV}\,, \tag{5.2.18}$$

which is significantly larger than the "common" Seesaw scale $f \sim \mathcal{O}\,(10^9\,\mathrm{GeV})$. Thus, we conclude that DWs would only dominate the energy density of the Universe if the Seesaw scale is unusually high or the approximation of one DW per horizon grossly underestimates the number of DWs.

In Ref. [199], the energy densitiy is estimated using the W mass instead of the Majoron mass, i.e. $\rho \sim m_W f^2 \mathcal{H}$, presumably falsly assuming that the thickness of the DWs corresponds to the thickness of the barrier seperating the n-vacua through which Instantons tunnel. This yields a much more stringent bound on the VEV, $f \lesssim 8.6\times 10^{10}\,\mathrm{GeV}$, which would indeed be alarmingly close to the Seesaw scale. Nevertheless, this bound is way too restrictive due to using the mass of the W boson rather than the Majoron mass, which we reasonably expect to be significantly smaller.

To summarize, we find that the arguments made in Ref. [199] claiming the appearance of DWs in Majoron models are several flawed in several aspects and that in fact, generic singlet Majoron models do not suffer from the DW problem as long as $U(1)_{B'}$ is not broken on the Lagrangian level.[6]

5.3 Extended Majoron Models

In the following, we discuss several extensions of the singlet Majoron model that change the anomaly factor $\mathcal{A}_{L'}$ so that $|\mathcal{A}_{L'}| = 1, 2$. Although the main motivation behind these extensions was preventing of the appearance of DWs according to Ref. [199], these models have features that are interesting in the context of the Sphaleron rate and leptogenesis, as will be discussed in the following.

In principle, there exists an endless number of models that change the anomaly factor so that $|\mathcal{A}_{L'}| = 1, 2$. From the definition of $\mathcal{A}_q$ in (4.3.21), it is apparent that this change

[6] Moreover, it has recently been shown in Ref. [216] that even if $U(1)_{B'}$ is also broken on the Lagrangian level, the resulting domain walls do not necessarily dominate the energy density of the Universe.

can be easily achieved by including additional RH particles with non-zero lepton number and non-trivial $\mathrm{SU}(2)_\mathtt{L}$ quantum numbers. For simplicity, we restrict ourselves to N_T RH triplets,

$$T_{\mathtt{R}_i} = \begin{pmatrix} T^0_{\mathtt{R}_i}/\sqrt{2} & T^+_{\mathtt{R}_i} \\ T^-_{\mathtt{R}_i} & -T^0_{\mathtt{R}_i}/\sqrt{2} \end{pmatrix} \sim (1,3,0)_1\,, \tag{5.3.1}$$

and N_ξ doublets,

$$\xi_{\mathtt{R}_i} = \begin{pmatrix} \xi^0_{\mathtt{R}_i} \\ \xi^-_{\mathtt{R}_i} \end{pmatrix} \sim (1,2,-\frac{1}{2})_1\,, \tag{5.3.2}$$

carrying one unit of lepton number each. Note that in addition to each RH doublet $\xi_{\mathtt{R}_i}$, we include one additional LH field $\xi_{\mathtt{L}_i}$,

$$\xi_{\mathtt{L}_i} = \begin{pmatrix} \xi^0_{\mathtt{L}_i} \\ \xi^-_{\mathtt{L}_i} \end{pmatrix} \sim (1,2,-\frac{1}{2})_0\,, \tag{5.3.3}$$

with vanishing lepton number in order to cancel gauge anomalies. In order to avoid the appearance of Landau poles due to the running of the $\mathrm{SU}(2)_\mathtt{L}$ and $U(1)_Y$ gauge couplings, we further assume that the doublets acquire a mass at a higher mass scale.
Including these fields, the relevant terms in the $U(1)_{L'}$ invariant Lagrangian are now given by

$$\begin{aligned} \mathcal{L}^{L'}_{Yuk} &= -\overline{L_i} Y^\nu_{ij} H E_j - \overline{L_i} Y^\nu_{ij} \tilde{H} N_{\mathtt{R}_j} - \overline{L_i} Y^{ij}_T T_{\mathtt{R}_j} \tilde{H} - \frac{1}{2} g_{N_{ij}} \overline{N^C_{\mathtt{R}_i}} N_{\mathtt{R}_j} \hat{\sigma} \\ &\quad - \frac{1}{2} g_{T_{ij}} \mathrm{Tr}\left[\overline{T^C_{\mathtt{R}_i}} T_{\mathtt{R}_j} \hat{\sigma}\right] + \text{h.c.}\,, \end{aligned} \tag{5.3.4}$$

$$\begin{aligned} \mathcal{L}^{L'}_{kin} &= i\overline{L_\mathtt{R}} \not{D} L_\mathtt{R} + i\overline{E} \not{D} E + i\overline{N_\mathtt{R}} \not{\partial} N_\mathtt{R} + i\overline{\xi_{\mathtt{R}_i}} \not{D} \xi_{\mathtt{R}_i} + i\overline{\xi_{\mathtt{L}_i}} \not{D} \xi_{\mathtt{L}_i} + i\mathrm{Tr}\left[\overline{T}_{\mathtt{R}_i} \not{D} T_{\mathtt{R}_i}\right] \\ &\quad + (\partial_\mu \hat{\sigma})^\dagger (\partial^\mu \hat{\sigma})\,, \end{aligned} \tag{5.3.5}$$

and we stress that the Yukawa coupling Y_T induces an additional channel for lepton number violation alongside Y^ν. Moreover, we assume that bare mass terms with the leptons in the models involving the new RH doublets are absent.
This field content results in six different models that lead to $|\mathcal{A}_{L'}| = 1, 2$: Either the model is extended by one triplet only, i.e. $N_T = 1$ and $N_\xi = 0$, or by $N_\xi = 1, 2, 4, 5$ doublets and no triplets, or by one doublet and one triplet, $N_T = N_\xi = 1$. The anomaly factors corresponding to these cases are given by

$$\begin{aligned} &\mathcal{A}_{L'}(N_T = 1, N_\xi = 0) = -1\,, \qquad \mathcal{A}_{L'}(N_T = 0, N_\xi = 1) = 2\,, \\ &\mathcal{A}_{L'}(N_T = 0, N_\xi = 2) = 1\,, \qquad \mathcal{A}_{L'}(N_T = 0, N_\xi = 4) = -1\,, \\ &\mathcal{A}_{L'}(N_T = 0, N_\xi = 5) = -2\,, \qquad \mathcal{A}_{L'}(N_T = 1, N_\xi = 1) = -2\,. \end{aligned} \tag{5.3.6}$$

Note that $N_\xi = 3$ would result in $\mathcal{A}_{L'} = 0$ and is therefore undesireable in the context of leptogenesis. Moreover, with regard to leptogenesis, changing the anomaly factor has the effect that since $|\mathcal{A}_{L'}| \neq 3 = \mathcal{A}_{B'}$, Sphaleron transitions no longer conserve $Y_{\Delta B'} - Y_{\Delta L'}$. The conserved combination depends on N_T and N_ξ and will from now on be refered to as $Y^{N_T,N_\xi}_{\Delta(B',L')}$. A further consequence is that the conversion factor from the $Y^{N_T,N_\xi}_{\Delta(B',L')}$ asymmetry

to the baryon asymmetry $Y_{\Delta B'}$ changes. Thus, in the extended Majoron models, (4.3.39) becomes

$$Y_{\Delta B'} = C_{\mathrm{Sph}}^{N_T,N_\xi} \times Y_{\Delta(B',L')}^{N_T,N_\xi} \,. \tag{5.3.7}$$

The conserved combinations $Y_{\Delta(B',L')}^{N_T,N_\xi}$ can be directly deduced from (5.3.6) and are given in Tab. 5.1. On the other hand, determining the conversion factor $C_{\mathrm{Sph}}^{N_T,N_\xi}$ is more evolved. If we assume that the only lepton number violating interactions are induced by Y_ν and Y_T, it is apparent that a lepton asymmetry can only be created after SSB at the Seesaw scale. Using (5.1.5), we therefore write the Yukawa terms (5.3.4) as

$$\begin{aligned}\mathcal{L}_{Yuk} = &\left(-\overline{L_i} Y_{ij}^\nu \tilde{H} N_j - \overline{L} Y_{ij}^T T \tilde{H} + \text{h.c.}\right) - \frac{1}{2} M_N \overline{N} N - \frac{1}{2\sqrt{2}} g_N \overline{N} N \sigma \\ &- \frac{1}{2\sqrt{2}} g_N \overline{N} \gamma_5 N J - \frac{1}{2} M_T \mathrm{Tr}\left[\overline{T} T\right] - \frac{1}{2\sqrt{2}} g_T \mathrm{Tr}\left[\overline{T} T \sigma\right] - \frac{1}{2\sqrt{2}} g_T \mathrm{Tr}\left[\overline{T} \gamma_5 T J\right] \,,\end{aligned} \tag{5.3.8}$$

while the interactions with gauge bosons from (5.3.5) are given by

$$\begin{aligned}\mathcal{L}_{gauge}^T &= \frac{i}{2} \mathrm{Tr}\left[\overline{T} \not{D} T\right] = \frac{g}{2}\left(\overline{T^0} \not{W}^+ T^- + \overline{T^0} \not{W}^- T^+\right) + e \overline{T^+} \not{A} T^+ + \frac{g}{c_W}(1 - s_W^2) \overline{T^+} \not{Z} T^+ \,, \\ \mathcal{L}_{gauge}^{\xi_{\mathrm{R,L}}} &= \frac{g}{\sqrt{2}}\left(\overline{\xi_{\mathrm{R,L}}^0} \not{W}^+ \xi_{\mathrm{R,L}}^- + \overline{\xi_{\mathrm{R,L}}^-} \not{W}^- \xi_{\mathrm{R,L}}^0\right) + \frac{e}{2} \overline{\xi_{\mathrm{R,L}}^-} \not{A} \xi_{\mathrm{R,L}}^- \\ &\quad + \frac{g}{c_W}\left[\frac{1}{2} \overline{\xi_{\mathrm{R,L}}^0} \not{Z} \xi_{\mathrm{R,L}}^0 - (\frac{1}{2} + s_W^2) \overline{\xi_{\mathrm{R,L}}^-} \not{Z} \xi_{\mathrm{R,L}}^-\right] \,,\end{aligned} \tag{5.3.9}$$

where we neglected generation indices. Moreover, we defined

$$T \equiv \begin{pmatrix} T^0/\sqrt{2} & T^+ \\ T^- & -T^0/\sqrt{2} \end{pmatrix} = T_{\mathtt{R}} + (T_{\mathtt{R}})^c = T^C \,, \tag{5.3.10}$$

with $M_T = g_T f/\sqrt{2}$ so that $T^0 = T_{\mathtt{R}}^0 + (T_{\mathtt{R}}^0)^c$ is a Majorana fermion while the charged components are combined into a Dirac spinor as

$$T^+ = T_{\mathtt{R}}^+ + (T_{\mathtt{R}}^-)^C = (T^-)^C \,. \tag{5.3.11}$$

Analogously to Sec. 4.3.2.3, we can now use relations between the chemical potentials of the particles to determine $C_{\mathrm{Sph}}^{N_T,N_\xi}$. While a precise calculation of $C_{\mathrm{Sph}}^{N_T,N_\xi}$ requires detailed knowledge of the interaction rates between the particles in different temperature ranges so that $C_{\mathrm{Sph}}^{N_T,N_\xi}$ is a function of temperature, we adopt the commonly used simplified approach to calculate the conversion rate under specific assumptions. That is, in addition to all SM electroweak and Yukawa interactions being fast (see Sec. 4.3.2.3), we also assume that the gauge interactions of T and $\xi_{\mathrm{R,L}}$ are in equilibrium so that

$$\mu_{W^-} = \mu_{T^-} - \mu_{T^0} = \mu_{\xi_{\mathtt{R}}^-} - \mu_{\xi_{\mathtt{R}}^0} = \mu_{\xi_{\mathtt{L}}^-} - \mu_{\xi_{\mathtt{L}}^0} \,, \tag{5.3.12}$$

and

$$\mu_{T^+} = \mu_{\overline{T^-}} = -\mu_{T^-} \,, \qquad \mu_{\xi^{0,-}_{\mathrm{R,L}}} = -\mu_{\overline{\xi^{0,-}_{\mathrm{R,L}}}} \,. \tag{5.3.13}$$

Moreover, fast (inverse) decays $\sigma, J \leftrightarrow T^0 T^0$ result in

$$\mu_{T^0} = \mu_\sigma = \mu_J = 0 \,. \tag{5.3.14}$$

In addition, fast Sphaleron transitions induce another relation between the chemical potentials. In the SM with $A_{L'} = 3$, the relation is given by (4.3.41). However, since $A_{L'} \neq 3$, we need to formulate model dependent relations that reflect that fast Sphaleron transitions violate lepton number by $\mathcal{A}_{L'}$ units, see Tab. 5.1. Moreover, before EWSB, conservation of T^3 and Q implies (see (4.3.42) and (4.3.43))

$$Y_{\Delta T^3} \sim Y^{\mathrm{SM}}_{\Delta T^3} + \frac{N_\xi}{2}\left(\xi^0_{\mathtt{R}} - \xi^-_{\mathtt{R}}\right) + \frac{N_\xi}{2}\left(\xi^0_{\mathtt{L}} - \xi^-_{\mathtt{L}}\right) - 2N_T \mu_{T^-} \,, \tag{5.3.15}$$

$$Y_{\Delta Q_{\mathrm{EM}}} \sim Y^{\mathrm{SM}}_{\Delta Q_{\mathrm{EM}}} - N_\xi \mu_{\xi^-_{\mathtt{R}}} - N_\xi \mu_{\xi^-_{\mathtt{L}}} - 2N_T \mu_{T^-} \,, \tag{5.3.16}$$

while the baryon and lepton asymmetries can be expressed as

$$Y_{\Delta B'} \sim Y^{\mathrm{SM}}_{\Delta B'} \sim N_G N_C \times \frac{1}{3}\left(\mu_{u_{\mathtt{L}}} + \mu_{u_{\mathtt{R}}} + \mu_{d_{\mathtt{L}}} + \mu_{d_{\mathtt{R}}}\right) \,, \tag{5.3.17}$$

$$Y_{\Delta L'} \sim N_G\left(\mu_{e_{\mathtt{L}}} + \mu_{e_{\mathtt{R}}} + \mu_{\nu_e}\right) + N_\xi\left(\mu_{\xi^0_{\mathtt{R}}} + \mu_{\xi^-_{\mathtt{R}}}\right) \,, \tag{5.3.18}$$

respectively. Combining everything, we obtain model dependent conversion factors $C^{N_T,N_\xi}_{\mathrm{Sph}}$ which can be found in Tab. 5.1. Note that including the doublets $\xi_{\mathtt{R}}$ adds more parameters than conditions and consequently, $C^{N_\xi \neq 0}_{\mathrm{Sph}}$ still depens on the chemical potentials.
To summarize, we find that extensions of Majoron models with RH $\mathrm{SU}(2)_{\mathtt{L}}$ fermions carrying lepton number change the anomaly factor $\mathcal{A}_{L'}$ as well as the conversion factor between the L' and B' asymmetries. In particular, note that the lepton asymmetries in $Y_\Delta\,(B', L')$ receive a factor of three compared to the SM, i.e. if we assume that no initial baryon asymmetry exists, we have

$$\left|Y^{N_T,N_\xi\neq 0}_{\Delta B'}\right| = 3\left|C^{N_T,N_\xi\neq 0}_{\mathrm{Sph}} Y_{L'}\right| \,, \qquad \left|Y^{N_T,N_\xi=0}_{\Delta B'}\right| = \frac{29}{78}\left|Y_{L'}\right| \,, \tag{5.3.19}$$

which seems to suggest that a given lepton asymmetry can produce a larger baryon asymmetry if $N_T, N_\xi \neq 0$. Nevertheless, if we e.g. consider the triplet model, we find numerically,

$$\left|Y^{N_T=1}_{\Delta B'}\right| \approx 0.35443\left|Y_{L'}\right| \,, \qquad \left|Y^{N_T,N_\xi=0}_{\Delta B'}\right| \approx 0.335788\left|Y_{L'}\right| \,, \tag{5.3.20}$$

and the smaller conversion factor in the triplet model diminishes the conversion rate, rendering it only slightly larger than the value in VL.[7] Thus, the question of whether leptogenesis in the Majoron model extended by the triplet T is viable essentially depends on the lepton asymmetry that can be generated by L' violating decays and scatterings

[7] However, we stress that we used simplifying assumptions when calculating the conversion factors $C^{N_T,N_\xi\neq 0}_{\mathrm{Sph}}$ and depending on the masses and couplings of T and ξ, the conversion factor may drastically change.

Table 5.1: Overview of the combinations of $Y_{\Delta(B',L')}$ that are conserved by Sphaleron transitions in the models with different numbers of triplets T and doublets ξ, alongside the relations induced between the chemical potentials if Sphaleron transitions are in equilibrium and the corresponding conversion factor C^{Sph}. Note that the value for C^{Sph} is only valid if the relations given in (4.3.40), (5.3.12), (5.3.13) and (5.3.14) hold.

N_T	N_ξ	$Y_{\Delta(B',L')}$	Sphaleron	C_{Sph}
0	0	$Y_{\Delta B'} - Y_{\Delta L'}$	$2\mu_{d_L} + \mu_{u_L} + \mu_{\nu_{e_L}} = 0$	$\frac{28}{79}$
1	0	$Y_{\Delta B'} + 3Y_{\Delta L'}$	$\mu_{d_\mathrm{L}} + 8\mu_{d_\mathrm{R}} + 11\mu_{e_\mathrm{R}} - 6\mu_{e_\mathrm{L}} - 6\mu_{\nu_\mathrm{L}} = 0$	$\frac{76}{679}$
0	1	$2Y_{\Delta B'} - 3Y_{\Delta L'}$	$\mu_{d_\mathrm{L}} + 8\mu_{d_\mathrm{R}} + 8\mu_{e_\mathrm{R}} - 3\mu_{e_\mathrm{L}} - 6\mu_{\nu_\mathrm{L}} = 0$	$-\frac{4(-22\mu_{\nu_L}+\mu_{\xi^0_\mathrm{R}}+\mu_{\xi^0_\mathrm{L}})}{1166\mu_{\nu_L}+229\mu_{\xi^0_\mathrm{R}}-35\mu_{\xi^0_\mathrm{L}}}$
0	2	$Y_{\Delta B'} - 3Y_{\Delta L'}$	$\mu_{d_\mathrm{L}} + 8\mu_{d_\mathrm{R}} + 9\mu_{e_\mathrm{R}} - 4\mu_{e_\mathrm{L}} - 6\mu_{\nu_\mathrm{L}} = 0$	$\frac{4(\mu_{\nu_L}-2(\mu_{\xi^0_\mathrm{R}}+\mu_{\xi^0_\mathrm{L}}))}{535\mu_{\nu_L}+241\mu_{\xi^0_\mathrm{R}}-35\mu_{\xi^0_\mathrm{L}}}$
0	4	$Y_{\Delta B'} + 3Y_{\Delta L'}$	$\mu_{d_\mathrm{L}} + 8\mu_{d_\mathrm{R}} + 11\mu_{e_\mathrm{R}} - 6\mu_{e_\mathrm{L}} - 6\mu_{\nu_\mathrm{L}} = 0$	$\frac{76\mu_{\nu_L}+32(\mu_{\xi^0_\mathrm{R}}+\mu_{\xi^0_\mathrm{L}})}{679\mu_{\nu_L}+578\mu_{\xi^0_\mathrm{R}}-22\mu_{\xi^0_\mathrm{L}}}$
0	5	$2Y_{\Delta B'} + 3Y_{\Delta L'}$	$\mu_{d_\mathrm{L}} + 8\mu_{d_\mathrm{R}} + 12\mu_{e_\mathrm{R}} - 7\mu_{e_\mathrm{L}} - 6\mu_{\nu_\mathrm{L}} = 0$	$\frac{4(58\mu_{\nu_L}+25(\mu_{\xi^0_\mathrm{R}}+\mu_{\xi^0_\mathrm{L}}))}{1742\mu_{\nu_L}+65(25\mu_{\xi^0_\mathrm{R}}+\mu_{\xi^0_\mathrm{L}})}$
1	1	$2Y_{\Delta B'} + 3Y_{\Delta L'}$	$\mu_{d_\mathrm{L}} + 8\mu_{d_\mathrm{R}} + 12\mu_{e_\mathrm{R}} - 7\mu_{e_\mathrm{L}} - 6\mu_{\nu_\mathrm{L}} = 0$	$\frac{4(58\mu_{\nu_L}+5(\mu_{\xi^0_\mathrm{R}}+\mu_{\xi^0_\mathrm{L}}))}{13(134\mu_{\nu_L}+25\mu_{\xi^0_\mathrm{R}}+\mu_{\xi^0_\mathrm{L}})}$

and requires a detailed analysis of the dynamical of the model.

5.4 Summary

In this chapter, we have reviewed the singlet Majoron model and discussed possible extensions thereof by right-handed $\mathrm{SU}(2)_\mathrm{L}$ particles. The Majoron is the Goldstone boson of the spontaneously broken global $U(1)_{B'-L'}$ of the SM model which we have assumed to obtain a small mass by some unspecified mechanism. We have outlined why the generic singlet Majoron model does not suffer from the domain wall problem, in contrast to the claims in Ref. [199]. This renders the proposed solution to extend the Majoron model with additional right-handed $\mathrm{SU}(2)_\mathrm{L}$ particles futile with regard to domain walls. Nevertheless, we have shown that introducing additional right-handed $\mathrm{SU}(2)_\mathrm{L}$ particles does have interesting effects as it changes the anomaly factor of the $[\mathrm{SU}(2)_\mathrm{L}]^2 \times U(1)_{L'}$ anomaly of the SM and hence also the conversion rate with which Sphaleron processes transfer a lepton asymmetry to a baryon asymmetry.

CHAPTER 6

Leptogenesis in the Majoron + Triplet Model

In the previous Chapter, we have introduced the Majoron model as a compelling solution to the neutrino mass problem in the SM and discussed possible extensions by RH fermions. These extensions change the anomaly factor of the $[\mathrm{SU}(2)_\mathrm{L}]^2 \times U(1)_{L'}$ anomaly and consequently also the conversion rate with which Sphalerons convert a lepton asymmetry to a baryon asymmetry. Moreover, as we will analyze in this Chapter, the additional particles change the dynamics of leptogensis due to their interactions with particles in the plasma and hence affect the lepton asymmetry that can be generated in such models. For simplicity, we will focus on leptogenesis in one particular extension of the Majoron model, the *Majoron+Triplet model* (MTM), where an additional RH $\mathrm{SU}(2)_\mathrm{L}$ triplet fermion is introduced.[1] This Chapter is based on the findings of Ref. [3].

In order to reduce the complexity of the MTM, we make two adjustments compared to the model introduced in Sec. 5.3. First, we assume that λ_{mix} is sufficiently small so that the scalar mixing term $\sim |\hat{\sigma}|^2|H|^2$ in (5.1.3) can be neglected and $\hat{\sigma}$ and H decouple, yielding the σ-dependent scalar potential after SSB at the Seesaw scale as

$$V_\sigma = \frac{m_\sigma^2}{2}\sigma^2 + k_\sigma J^2\sigma + k_\sigma\sigma^3 + \lambda_\sigma J^2\sigma^2 + \frac{\lambda_\sigma}{4}J^4 + \frac{\lambda_\sigma}{4}\sigma^4 + \text{const}\,. \tag{6.0.1}$$

Here, we have

$$f = \frac{\mu_\sigma}{\sqrt{\lambda_\sigma}}\,, \qquad k_\sigma = \lambda_\sigma f\,, \qquad m_\sigma = \sqrt{\lambda_\sigma} f\,, \tag{6.0.2}$$

where m_σ is the mass of σ. Moreover, we introduce an additional Z_2 symmetry under which T_R is odd while all other particles are even. Consequently, the Yukawa term (5.3.8)

[1] We chose to focus on the MTM rather than one of the models containing additional doublets, as discussed in the previous Chapter, for several reasons. First, the conversion factor is independent from chemical potentials, and hence the qualitative discussion significantly more simple. Second, the models containing doublets may suffer from Landau poles, further complicating the doublet models. Third, the MTM entails several features not only from type I Seesaw, but also type III Seesaw. Fourth, although not part of the following discussion, the generic MTM introduces additional sources of lepton number violation which we expect to have interesting phenomenological effects.

becomes after SSB

$$\mathcal{L}_{Yuk} = \left(-\overline{L_i} Y^{\nu}_{ij} \tilde{H} N_j + \text{h.c.}\right) - \frac{1}{2} M_N \overline{N} N - \frac{1}{2\sqrt{2}} g_N \overline{N} N \sigma \\ - \frac{1}{2\sqrt{2}} g_N \overline{N} \gamma_5 N J - \frac{1}{2} M_T \text{Tr}\left[\overline{T} T\right] - \frac{1}{2\sqrt{2}} g_T \text{Tr}\left[\overline{T} T \sigma\right] - \frac{1}{2\sqrt{2}} g_T \text{Tr}\left[\overline{T} \gamma_5 T J\right] , \tag{6.0.3}$$

i.e. the Yukawa coupling between T, H and L is absent and no mixing between the triplet and the charged SM leptons occurs. Note that the only source of lepton number violation in (6.0.3) is the neutrino Yukawa coupling Y^{ν}.
Compared to VL, see Sec. 4.3.3, we can anticipate that the dynamics of leptogenesis in the MTM are altered due to the presence of new interactions between the additional particles. Although no new source of lepton number violation exists, leaving the form of the Boltzmann equation for the efficiency unchanged, several of the new interactions affect the neutrino abundance which enters the Boltzmann equation for the efficiency (see Fig. 6.1). The corresponding scattering rates can be combined into a summed scattering rate γ_S as

$$\gamma_S \equiv \gamma_{NN,TT} + \gamma_{NN,JJ} + \gamma_{NN,\sigma\sigma} + \gamma_{NN,\sigma J} + \text{Br}_{\sigma,NN} \gamma_{\sigma,NN} , \tag{6.0.4}$$

where $\text{Br}_{\sigma,NN} \equiv \frac{\Gamma_{\sigma\to NN}}{\sum_{i=N,T,J} \Gamma_{\sigma\to ii}}$ is the branching ratio of $\sigma \to NN$. If the scattering rate γ_S is fast,

$$\gamma_S > n_N^{\text{eq}} \mathcal{H} , \tag{6.0.5}$$

we expect that the neutrino population is kept close to equilibrium and consequently, a lepton asymmetry can only be generated once γ_S becomes slow compared to the Hubble parameter. This closely resembles the dynamics in the type III leptogenesis discussed in Sec. 4.3.4. The main difference between both scenarios is that the fermion that generates the lepton asymmetry in type III leptogenesis is thermalized via gauge interactions while in the MTM, the neutrinos are thermalized via interactions with T, σ and J, which are induced by the free parameters g_N, g_T and λ_σ. Consequently, we can analyze how different values of these couplings affect the leptogenesis mechanism. One drawback of leptogenesis in the MTM is that the neutrino evolution is governed by the same couplings that determine the evolution of T, σ and J, see Fig. 6.2. which suggests that a more careful treatment of their respective abundances is necessary. More precisely, it appears reasonable to solve not only the Boltzmann equations for the neutrino abundance and the efficiency but also for T, σ and J, i.e. we need to solve five Boltzmann equations instead of two. Nevertheless, as we will explore in detail later, it is also convenient to discuss a simplified scenario where we indeed only solve the Boltzmann equations for the neutrino abundance and the efficiency while assuming that T, σ and J are in equilibrium. Our aim is to obtain an understanding of the effects that these parameters have on the leptogenesis mechanism. Therefore, we study several different combinations of parameters which we anticipate to yield valuable insights and for the most part consider the MTM as a toy model rather than a fully developed model. Nevertheless, as we will see, straightforward

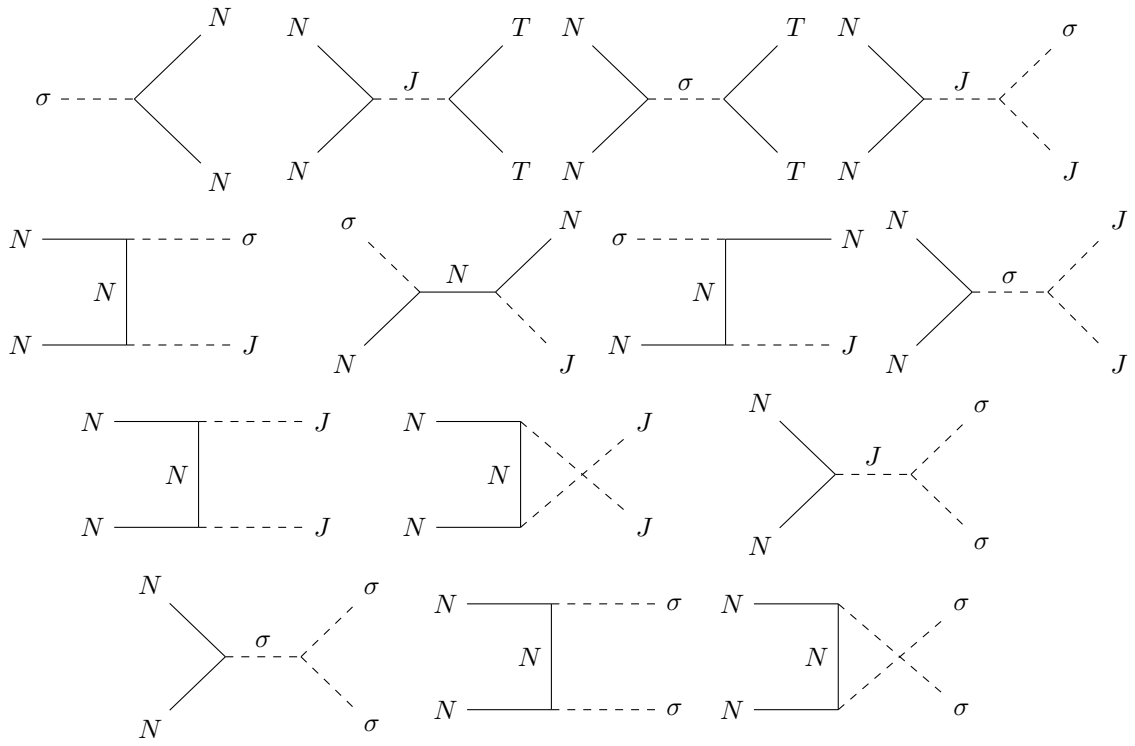

Figure 6.1: Feynman diagrams for interactions that change the neutrino abundance in the MTM, in addition to the VL diagrams given in Fig. 4.7.

constraints on the model arise from DM considerations.
This Chapter is structured as follows. In Sec. 6.1, we present the Boltzmann equations for leptogenesis in the MTM while in Sec. 6.2, we state the parameters we used to solve them. We present an overview of the results in Sec. 6.3.1 before providing detailed discussions of leptogenesis for different paramters in Secs. 6.3.2 to 6.3.5. In Sec. 6.4, we explore the implications on the model with regard to DM while in Sec. 6.5, we discuss limits on the baryon asymmetry that can be generated in the MTM. Finally, in Sec. 6.6, we provide a summary of the results presented in this Chapter.

6.1 Boltzmann Equations

In this section, we only present the Boltzmann equations that govern leptogenesis in the MTM while their detailed derivation is given in App. F.3. Defining

$$\delta_{sub} = \delta_\sigma - \delta_J^2 \mathrm{Br}_{\sigma,JJ} - \delta_N^2 \mathrm{Br}_{\sigma,NN} - \delta_T^2 \mathrm{Br}_{\sigma,TT} \,, \tag{6.1.1}$$

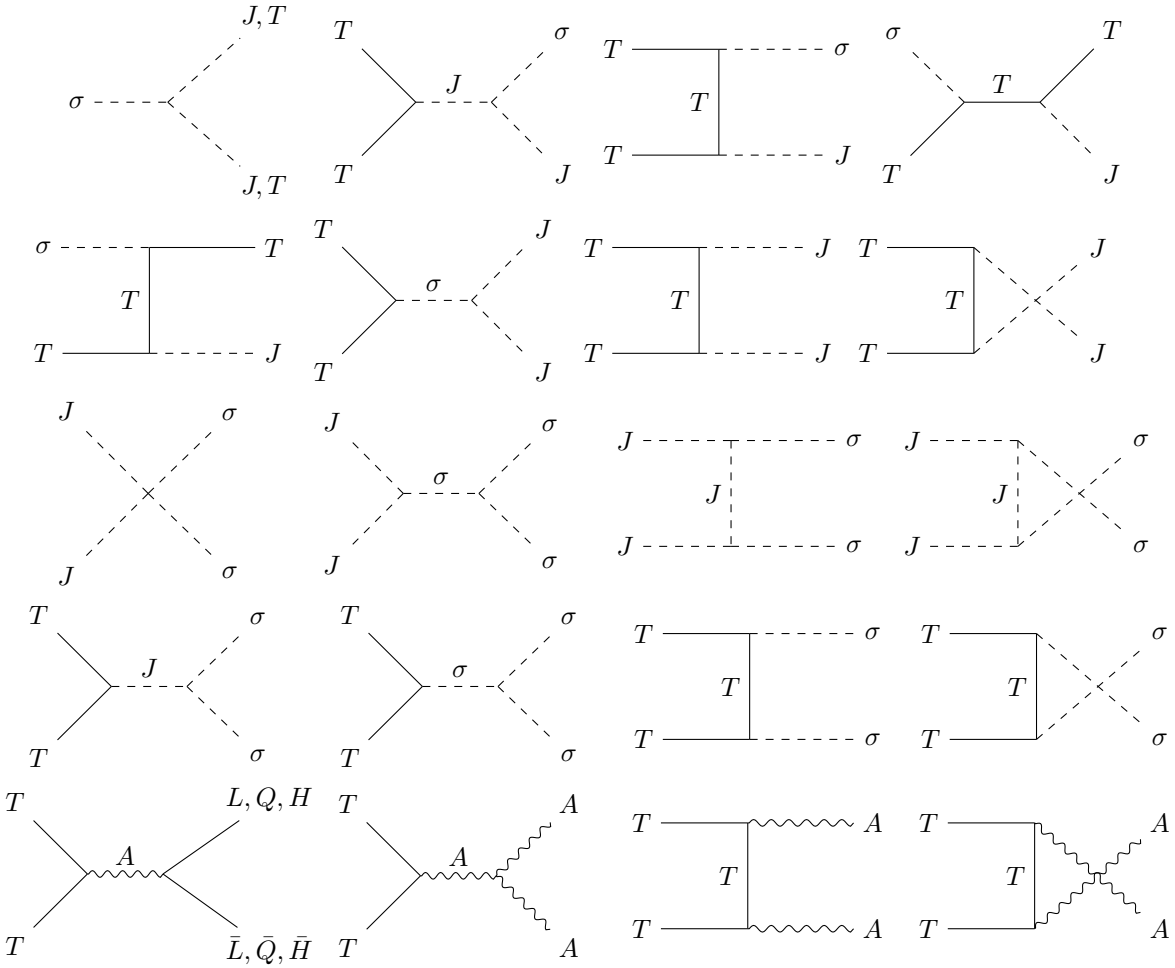

Figure 6.2: Feynman diagrams for interactions that change the abundances of T, σ and J in the MTM. Here, $A = \{B, W_{1,2,3}\}$ corresponds to the gauge bosons.

$$\begin{aligned}\rho \equiv & \left(1-\delta_J^2\right)\left(\gamma_{NNJJ} - \mathrm{Br}_{\sigma,JJ}\gamma_{\sigma,NN}\right) + \left(1-\delta_T^2\right)\left(\gamma_{NNTT} - \mathrm{Br}_{\sigma,TT}\gamma_{\sigma,NN}\right) \\ & + \left(1-\delta_\sigma^2\right)\gamma_{NN\sigma\sigma} + \left(1-\delta_\sigma\delta_J\right)\gamma_{NN\sigma J} + \left(1-\delta_\sigma\right)\gamma_{\sigma,NN} \\ = & \left(1-\delta_J^2\right)\gamma_{NNJJ} + \left(1-\delta_T^2\right)\gamma_{NNTT} + \left(1-\delta_\sigma^2\right)\gamma_{NN\sigma\sigma} + \left(1-\delta_\sigma\delta_J\right)\gamma_{NN\sigma J} \\ & + \left[\left(1-\delta_\sigma\right) - \left(1-\delta_J^2\right)\mathrm{Br}_{\sigma,JJ} - \left(1-\delta_T^2\right)\mathrm{Br}_{\sigma,TT}\right]\gamma_{\sigma,NN}\,,\end{aligned} \tag{6.1.2}$$

and writing the Boltzmann equation for the triplet as the sum of its components, $Y_T = Y_T^0 + Y_T^+ + Y_T^-$, the full set of coupled Boltzmann equations for N, T, σ and J is

given by

$$\begin{aligned} s\mathcal{H}z_N\frac{\mathrm{d}Y_N}{\mathrm{d}z_N} =& -(\delta_N-1)\gamma_D - 2(\delta_N-1)\gamma_Q - 2\left(\delta_N^2-\delta_T^2\right)\gamma_{NNTT} \\ & - 2\left(\delta_N^2-\delta_J^2\right)\gamma_{NNJJ} - 2\left(\delta_N^2-\delta_\sigma^2\right)\gamma_{NN\sigma\sigma} - 2\left(\delta_N^2-\delta_J\delta_\sigma\right)\gamma_{NN\sigma J} \\ & + 2\delta_{sub}\gamma_{\sigma,NN} \\ \equiv& s\mathcal{H}z_N\frac{\mathrm{d}Y_N^{\mathrm{VL}}}{\mathrm{d}z_N} - 2(\delta_N^2-1)\gamma_S - 2\rho\,, \end{aligned} \tag{6.1.3}$$

$$s\mathcal{H}z_N\frac{\mathrm{d}Y_N^{\mathrm{VL}}}{\mathrm{d}z_N} \equiv -(\delta_N-1)\gamma_D - 2(\delta_N-1)\gamma_Q\,, \tag{6.1.4}$$

where $\frac{\mathrm{d}Y_N^{\mathrm{VL}}}{\mathrm{d}z_N}$ is the Boltzmann equation for the neutrino abundance in the VL scenario and

$$\begin{aligned} s\mathcal{H}z_N\frac{\mathrm{d}Y_T}{\mathrm{d}z_N} =& -2\left(\delta_T^2-\delta_N^2\right)\gamma_{TTNN} - 2\left(\delta_T^2-\delta_J^2\right)\gamma_{TTJJ} - 2\left(\delta_T^2-\delta_\sigma^2\right)\gamma_{TT\sigma\sigma} \\ & - 2\left(\delta_T^2-\delta_\sigma\delta_J\right)\gamma_{TT\sigma J} - 2\left(\delta_T^2-1\right)\gamma_{T,gauge} + 2\delta_{sub}\gamma_{\sigma,TT}\,, \end{aligned} \tag{6.1.5}$$

$$\begin{aligned} s\mathcal{H}z_N\frac{\mathrm{d}Y_\sigma}{\mathrm{d}z_N} =& -2\left(\delta_\sigma^2-\delta_N^2\right)\gamma_{\sigma\sigma NN} - 2\left(\delta_\sigma^2-\delta_T^2\right)\gamma_{\sigma\sigma TT} - 2\left(\delta_\sigma^2-\delta_J^2\right)\gamma_{\sigma\sigma JJ} \\ & - \left(\delta_\sigma\delta_J-\delta_T^2\right)\gamma_{\sigma JTT} - \left(\delta_\sigma\delta_J-\delta_N^2\right)\gamma_{\sigma JNN} - (\delta_N\delta_\sigma-\delta_N\delta_J)\gamma_{N\sigma NJ} \\ & - (\delta_T\delta_\sigma-\delta_T\delta_J)\gamma_{T\sigma TJ} - \left(\delta_\sigma-\delta_N^2\right)\gamma_{\sigma,NN} - \left(\delta_\sigma-\delta_T^2\right)\gamma_{\sigma,TT} \\ & - \left(\delta_\sigma-\delta_J^2\right)\gamma_{\sigma,JJ}\,, \end{aligned} \tag{6.1.6}$$

$$\begin{aligned} s\mathcal{H}z_N\frac{\mathrm{d}Y_J}{\mathrm{d}z_N} =& -2\left(\delta_J^2-\delta_N^2\right)\gamma_{JJNN} - 2\left(\delta_J^2-\delta_\sigma^2\right)\gamma_{JJ\sigma\sigma} - 2\left(\delta_J^2-\delta_T^2\right)\gamma_{JJTT} \\ & - \left(\delta_J\delta_\sigma-\delta_N^2\right)\gamma_{J\sigma NN} - \left(\delta_J\delta_\sigma-\delta_T^2\right)\gamma_{J\sigma TT} - (\delta_J\delta_N-\delta_\sigma\delta_N)\gamma_{JN\sigma N} \\ & - (\delta_J\delta_T-\delta_\sigma\delta_T)\gamma_{JT\sigma T} + 2\delta_{sub}\gamma_{\sigma,JJ}\,. \end{aligned} \tag{6.1.7}$$

Note that in the simplified scenario where σ, J and T are in equilibrium, i.e. $\delta_{T,\sigma,J}=1$, only the Boltzmann equation for the neutrino evolution is relevant and (6.1.3) reduces to

$$s\mathcal{H}z_N\frac{\mathrm{d}Y_N}{\mathrm{d}z_N} = -(\delta_N-1)\gamma_D - 2(\delta_N-1)\gamma_Q - 2\left(\delta_N^2-1\right)\gamma_S\,. \tag{6.1.8}$$

If additionally $\gamma_S\to 0$ holds, we recover the Boltzmann equation for VL, (6.1.4). Finally, the Boltzmann equation for the efficiency is the same as in VL and therefore given by (4.3.59),

$$s\mathcal{H}z_N\frac{\mathrm{d}\eta}{\mathrm{d}z_N} = \frac{1}{Y_N^0}(\delta_N-1)\gamma_D - \frac{\eta}{Y_L^{\mathrm{eq}}}\left[\frac{\gamma_D}{2} + 2\gamma_{N\overline{U_3},L\overline{Q_3}} + \delta_N\gamma_{LN\leftrightarrow Q_3U_3}\right]\,. \tag{6.1.9}$$

6.2 Parameters

In the MTM, several new parameters appear by virtue of the new interactions. While the thermal rates that appear in VL, i.e. γ_D and γ_Q, depend only on the effective neutrino

mass $\tilde{m}$, the additional thermal rates that are relevant in the MTM are independent from $\tilde{m}$ and instead depend on the VEV f and the couplings g_N, g_T and λ_σ. Moreover, the Boltzmann equations for the particle abundances depend on the initial abundances, similarly to VL. In order to gain an understanding of the impact the respective parameters have on the evolution of the abundances, we adopt the approach to vary $\tilde{m}$ and one of the three couplings, g_N, g_T, λ_σ, while keeping the other two fixed. Since we anticipate that the value of g_N is more relevant for the dynamics of leptogenesis than the values of g_T and λ_σ, our main focus is on the effect of variations of g_N in the range $g_N \in [0.1, 1]$, and the interplay with the value of $\tilde{m}$ in the range $\tilde{m} \in [0.5 \times 10^{-4}, 0.1]\,\text{eV}$. Concerning g_T and λ_σ, we then distinguish between two cases,

$$\text{Case } A: \qquad g_N \in [0.1, 1]\,, \quad g_T = 1\,, \qquad \lambda_\sigma = 1\,, \tag{6.2.1}$$

$$\text{Case } B: \qquad g_N \in [0.1, 1]\,, \quad g_T = 10^{-7}\,, \quad \lambda_\sigma = 1\,. \tag{6.2.2}$$

Moreover, in order to discuss the effect of changes of g_T and λ_σ, we briefly consider two additional cases,

$$\text{Case } C: \qquad g_N = 1\,, \quad g_T \in \left[10^{-7}, 1\right]\,, \quad \lambda_\sigma = 1\,, \tag{6.2.3}$$

$$\text{Case } D: \qquad g_N = 1\,, \quad g_T = 10^{-7}\,, \qquad \lambda_\sigma \in \left[10^{-2}, 1\right]\,. \tag{6.2.4}$$

For the cases A and B, we also study the simplified scenario mentioned in the previous section where T, σ and J are assumed to be in equilibrium,

$$\text{Case } \hat{A}: \qquad g_N \in [0.1, 1]\,, \quad g_T = 1\,, \qquad \lambda_\sigma = 1\,, \quad \delta_{T,\sigma,J}(z_N) = 1\,\forall z_N\,, \tag{6.2.5}$$

$$\text{Case } \hat{B}: \qquad g_N \in [0.1, 1]\,, \quad g_T = 10^{-7}\,, \quad \lambda_\sigma = 1\,, \quad \delta_{T,\sigma,J}(z_N) = 1\,\forall z_N\,. \tag{6.2.6}$$

Note that the lepton asymmetry in the MTM is produced only after SSB at the Seesaw scale. We will therefore direct our focus at temperatures smaller than f and solve the Boltzmann equations for $z_N \geq z_I \equiv g_N/\sqrt{2}$. Concerning the initial abundances, we restrict ourselves to the two limiting cases: Either all particles are in equilibrium at z_I which we denote by an index t,

$$\{\hat{A}_t, \hat{B}_t\}: \qquad Y_N(z_N) = Y_N^{\text{eq}}(z_N)\,, \tag{6.2.7}$$

$$\{A_t, B_t, C_t, D_t\}: \qquad Y_{N,T,\sigma,J}(z_N) = Y_{N,T,\sigma,J}^{\text{eq}}(z_N)\,, \tag{6.2.8}$$

or all particles have a vanishing initial abundance, denoted by an index z,

$$\{A_z, B_z, C_z, D_z\}: \qquad Y_{N,T,\sigma,J}(z_N) = 0\,, \tag{6.2.9}$$

$$\{\hat{A}_z, \hat{B}_z\}: \qquad Y_N(z_N) = 0\,. \tag{6.2.10}$$

For the most part, we will fix the VEV at $f = 10^{10}\,\text{GeV}$, although a short discussion of the relevance of the value of the VEV is given in Sec. 6.5. Since the objective in the leptogenesis mechanism is to generate a lepton asymmetry, we assume that the efficiency vanishes at z_I. Moreover, as Majoron models where J obtains a small mass are highly interesting with regard to DM, we include a small but non-vanishing Majoron mass in our calculations. For concreteness, we use $m_J \sim 10^{-3}\,\text{GeV}$, although the exact numerical value is irrelevant as long as it is sufficiently small. We compare our results to VL,

Table 6.1: Parameters and initial condtions used to solve to Boltzmann equations given in Sec. 6.1. Cases $\hat{A}, \hat{B}$ correspond to the simplified scenario where $\delta_{T,\sigma,J}(z_N) = 1 \forall z_N$ while in cases A, B, C, D, the full set of Boltzmann equations for N, T, σ, J is considered. The index $t(z)$ denotes that the corresponding Boltzmann equations are solved with thermal (vanishing) initial particle abundances. Note that M_N does not have an effect on η_{VL}.

Case	g_N	g_T	λ_σ	f/GeV	$\tilde{m}$/eV	$Y_N(z_I)$	$Y_{\sigma,J,T}(z_I)$
$\hat{A}_z$	$[0.1, 1]$	1	1	10^{10}	$[5 \times 10^{-5}, 10^{-1}]$	0	
$\hat{A}_t$	$[0.1, 1]$	1	1	10^{10}	$[5 \times 10^{-5}, 10^{-1}]$	$Y_N^{\mathrm{eq}}(z_I)$	
$\hat{B}_z$	$[0.1, 1]$	10^{-7}	1	10^{10}	$[5 \times 10^{-5}, 10^{-1}]$	0	
$\hat{B}_t$	$[0.1, 1]$	10^{-7}	1	10^{10}	$[5 \times 10^{-5}, 10^{-1}]$	$Y_N^{\mathrm{eq}}(z_I)$	
A_z	$[0.1, 1]$	1	1	10^{10}	$[5 \times 10^{-5}, 10^{-1}]$	0	0
A_t	$[0.1, 1]$	1	1	10^{10}	$[5 \times 10^{-5}, 10^{-1}]$	$Y_N^{\mathrm{eq}}(z_I)$	$Y_{\sigma,J,T}^{\mathrm{eq}}(z_I)$
B_z	$[0.1, 1]$	10^{-7}	1	10^{10}	$[5 \times 10^{-5}, 10^{-1}]$	0	0
B_t	$[0.1, 1]$	10^{-7}	1	10^{10}	$[5 \times 10^{-5}, 10^{-1}]$	$Y_N^{\mathrm{eq}}(z_I)$	$Y_{\sigma,J,T}^{\mathrm{eq}}(z_I)$
C_z	1	$[10^{-7}, 1]$	1	10^{10}	$[5 \times 10^{-5}, 10^{-1}]$	0	0
C_t	1	$[10^{-7}, 1]$	1	10^{10}	$[5 \times 10^{-5}, 10^{-1}]$	$Y_N^{\mathrm{eq}}(z_I)$	$Y_{\sigma,J,T}^{\mathrm{eq}}(z_I)$
D_z	1	1	$[10^{-2}, 1]$	10^{10}	$[5 \times 10^{-5}, 10^{-1}]$	0	0
D_t	1	1	$[10^{-2}, 1]$	10^{10}	$[5 \times 10^{-5}, 10^{-1}]$	$Y_N^{\mathrm{eq}}(z_I)$	$Y_{\sigma,J,T}^{\mathrm{eq}}(z_I)$
VL_z					$[5 \times 10^{-5}, 10^{-1}]$	0	
VL_t					$[5 \times 10^{-5}, 10^{-1}]$	$Y_N^{\mathrm{eq}}(z_I)$	

discussed in Sec. 4.3.3, where the efficiency depends only on the value of $\tilde{m}$ and the initial neutrino abundance. An overview of the parameter assignments of the various cases is given in Tab. 6.1. Before we proceed with the discussion of leptogenesis, let us shortly discuss the decay channels of σ to pairs of N, σ and T, respectively, with decay rates given by

$$\Gamma_{\sigma\to NN} = \frac{g_N^2}{8\pi}\sqrt{\frac{m_\sigma^2}{4} - M_N^2}\,, \quad \Gamma_{\sigma\to TT} = \frac{3g_T^2}{8\pi}\sqrt{\frac{m_\sigma^2}{4} - M_T^2}\,, \quad \Gamma_{\sigma\to JJ} = \frac{k_\sigma^2}{16\pi m_\sigma^2}\sqrt{\frac{m_\sigma^2}{4} - m_J^2}\,. \tag{6.2.11}$$

Note that $\sigma \to NN$ and $\sigma \to TT$ are kinematically only allowed when $g_N \leq 0.7$ and $g_T \leq 0.7$, respectively, and are therefore forbidden for certain parameter ranges of the different cases, see Fig. 6.3. Moreover, note that in case D, both $\mathrm{Br}_{\sigma\to NN}$ and $\mathrm{Br}_{\sigma\to TT}$ are kinematically forbidden for all values of $\lambda_\sigma \in [0.01, 1]$.

6.3 Results for the Efficiency

6.3.1 Comparison of the Results

In this section, we give a brief overview of the results for the efficiency in the various cases introduced in the previous section before individually discussing the dynamics of

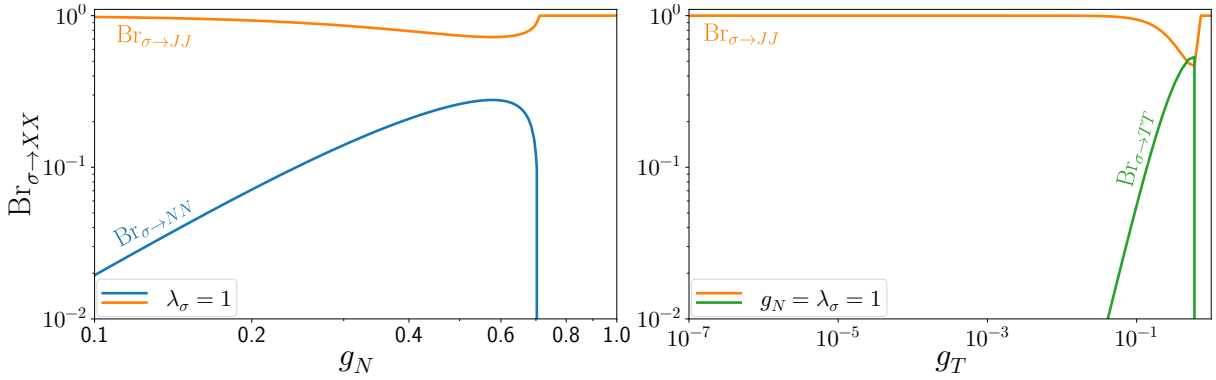

Figure 6.3: *Left:* Branching ratios of $\sigma \to NN$ and $\sigma \to JJ$ as functions of g_N, relevant for cases $A, B, \hat{A}, \hat{B}$. We stress that in cases $A, \hat{A}$ the decay $\sigma \to TT$ is kinematically forbidden while in cases $B, \hat{B}$, the branching ratio $\mathrm{Br}_{\sigma\to TT}$ is of order 10^{-13} and can therefore be neglected. We find that σ-decays to a pair of Majorons are clearly the dominant decay channel over the full g_N range. Above $g_N = 0.7$, σ-decays to a pair of neutrinos are kinematically forbidden, resulting in $\mathrm{Br}_{\sigma\to JJ} = 1$. *Right:* Branching ratios of $\sigma \to TT$ and $\sigma \to JJ$ as functions of g_T, relevant for case C. Note that $\sigma \to NN$ is kinematically forbidden. We find that $\mathrm{Br}_{\sigma\to TT}$ is only sizable compared to $\mathrm{Br}_{\sigma\to JJ}$ around $g_T \lesssim 0.7$. For $g_T > 0.7$, it is kinematically forbidden.

leptogenesis in greater detail. We calculate the relevant thermal rates using (G.1.1) and (G.1.7), using the cross sections given in App. G.2. Note that the thermal rates depend only on g_T if T appears in either the initial or final state. Afterwards, we numerically solve the Boltzmann equations given in (6.1.4)-(6.1.8) for the parameter choices given in Tab. 6.1.

First, we find that the final efficiencies only depend on the initial abundances of the particles in case B while the final efficiencies for the remaining parameter ranges are independent from the initial abundances. In these cases, we therefore omit the indices t, z so that

$$\eta_{\hat{A}} \equiv \eta_{\hat{A}}^{t,z}\,, \qquad \eta_{\hat{B}} \equiv \eta_{\hat{B}}^{t,z}\,, \qquad \eta_A \equiv \eta_A^{t,z}\,, \qquad \eta_C \equiv \eta_C^{t,z}\,, \qquad \eta_D \equiv \eta_D^{t,z}\,. \tag{6.3.1}$$

Next, let us focus on the efficiencies in the cases $\hat{A}, \hat{B}, A$ and B. The results are presented in Figs. 6.4 and 6.5 in terms of density plots of $\eta(g_N, \tilde{m})$ (left panel) while the middle and right panels show $\eta(\tilde{m})$ and $\eta(g_N)$ for exemplary values of g_N and $\tilde{m}$, respectively. It is evident that the final efficiencies in the cases $\hat{A}, \hat{B}, A$ and B_t display similar features:

- The efficiencies initially increase with $\tilde{m}$, reach a maximum at some $\tilde{m}_{\max}$, and subsequently decline.
- For $\tilde{m} \to 0.1$, the efficiencies eventually assume the same value as in the WO regime in VL and subsequently evolve in the same way. For brevity, we will refer to this as $\eta^{WO}(\tilde{m})$. There are, nevertheless, two exceptions: In case $\hat{B}$ with $g_N \sim 0.7$, we find $\eta_{\hat{B}}(\tilde{m})|_{\tilde{m}\to 0.1} < \eta^{WO}(\tilde{m})$ while in case A with $g_N \sim 1$, we have $\eta_A(\tilde{m})|_{\tilde{m}\to 0.1} > \eta^{WO}(\tilde{m})$. Otherwise, η^{WO} is independent from g_N.

- For $\tilde{m} \lesssim 10^{-2}\,\mathrm{eV}$, we find that the efficiencies in the MTM never reach the almost maximal efficiency of VL_t. Moreover, it is evident that η strongly depends on g_N in this range. In particular, η decreases with g_N until it reaches a minimum at $g_N \sim 0.7$ and increases again. Notably, this behavior is much more pronounced in cases $\hat{A}$ and $\hat{B}$.

In order to compare the final efficiencies numerically, we show $\eta_{\hat{A},\hat{B}}/\eta_{A,B}$ and $\eta_{\hat{A},A}/\eta_{\hat{B},B}$ in the upper and lower panels of Fig. 6.6, respectively. It is striking that at $g_N \sim 0.7$, we have $\eta_{\hat{A}}/\eta_A \ll 1$ and $\eta_{\hat{B}}/\eta_B \ll 1$ while for $g_N \nsim 0.7$, the differences between the respective efficiencies become much less pronounced. Moreover, we find that $\eta_{\hat{A}}/\eta_{\hat{B}}$ and η_A/η_B deviate from 1 only for $g_N \to 1$.
Next, let us discuss case B_z. Unlike the previous cases, we find that η_B^z is negative in a triangular region defined by $0.1 \leq g_N \lesssim 0.24$ and $5 \times 10^{-5}\,\mathrm{eV} \leq \tilde{m} \lesssim 2.5 \times 10^{-3}\,\mathrm{eV}$ and therefore differs from η_B^t. Thus, the intial abundances are relevant in this region. Outside of this region, η_B^z is positive and we have $\eta_B^z \sim \eta_B^t$, i.e. the initial abundances are irrelevant. This is also highlighted in Fig. 6.7 (left) where we show $|\eta_B^z|/\eta_B^t$. Consequently, we can divide the $g_N - \tilde{m}$ plane in an *initial abundance* (IA) regime where the initial abundances are relevant and an ~~IA~~ regime where the initial abundances are irrelevant, as is schematically shown in Fig. 6.7 (right), with the boundary between both regimes given by $(g_N, \tilde{m}) \equiv (g_N^{IA}, \tilde{m}^{IA})$.

Finally, in Fig. 6.8, we show the efficiencies in cases C and D in terms of density plots of $\eta(x, \tilde{m})$(left panel) while the middle and right panels show $\eta(\tilde{m})$ and $\eta(x)$ with $x = g_T, \lambda_\sigma$. It is evident that the efficiencies do not significantly depend on g_T or λ_σ and in particular, note that $\eta_C(g_T)$ becomes constant for $g_T \lesssim 10^{-3}$. This suggests that both $\eta_C(g_T \lesssim 10^{-3})$ and η_B are independent from g_T. We explicitly confirmed this by calculating $\eta_B(g_T = 0)$ which agrees with η_B. This implies that the results for the efficiency from case B are applicable not only in the MTM but instead are valid also in generic Majoron models.

To summarize, we find that the efficiencies that can be generated in the MTM are overall smaller than the efficiencies in VL unless WO is strong. Nevertheless, it is still possible to obtain a sizable final efficiency if g_N is sufficiently small. Additionally, we find that the initial abundances are rendered irrelevant apart from case B where g_N and g_T are both small. Moreover, we stress that the final efficiencies in the simplified scenario can be up to a factor of one hundred smaller than the efficiencies in cases A, B, indicating that the full set of Boltzmann equations should be considered. Finally, if g_T is sufficiently small, $g_T \lesssim 10^{-3}$, the existence of the triplet is irrelevant for the dynamics of leptogenesis in the MTM. Similarly, changing the value of λ_σ has only a negligible effect on the efficiency. In the following section, we will therefore direct our focus to the cases $\hat{A}, \hat{B}, A$ and B and discuss the evolution of the efficiency and the particle abundances in greater detail.
Note that similarly to VL, the effect of the quark scatterings on the qualitative results, which we will discuss in the following, is negligible. For simplicity, we will therefore omit the quark scatterings while disussing the overall behavior of the evolution of the particle abundances and the efficiency, unless otherwise mentioned. Nevertheless, we stress that

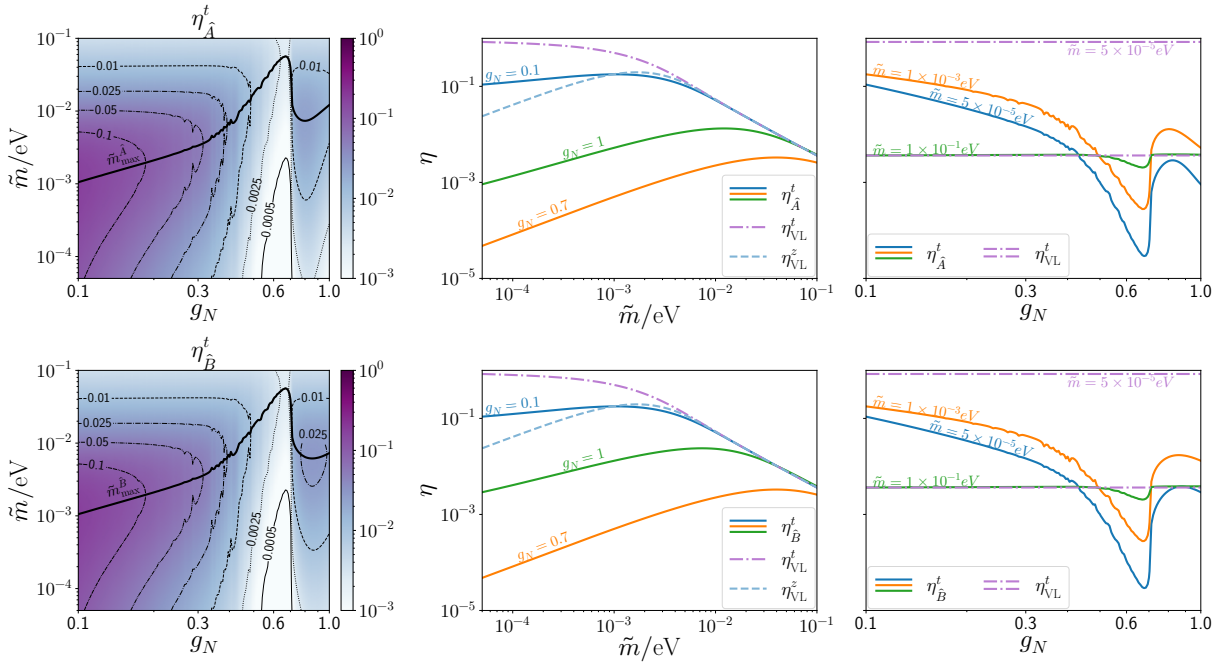

Figure 6.4: *Left:* Density plots of $\eta_{\hat{A}}$ (upper figure) and $\eta_{\hat{B}}$ (lower figure) in the $g_N - \tilde{m}$ plane. The black lines indicates at which $\tilde{m}$ the efficiency reaches its maximum. *Middle:* $\eta_{\hat{A}}$ (upper figure) and $\eta_{\hat{B}}$ (lower figure) as functions of g_N. *Right:* $\eta_{\hat{A}}$ (upper figure) and $\eta_{\hat{B}}$ (lower figure) as functions of $\tilde{m}$. See text for discussion.

we did include the quark scatterings when solving the Boltzmann equations.

6.3.2 Cases $\hat{A}, \hat{B}$

In this section, we provide a more detailed discussion of cases $\hat{A}$ and $\hat{B}$, starting with an analysis of how the thermal rate γ_S depends on g_N. Afterwards, we focus on the evolution of the neutrino abundance and the efficiency. For brevity, we refer to generic quantities in the simplified scenario with a hat and only distinguish between case $\hat{A}$ and case $\hat{B}$ when necessary.

6.3.2.1 Discussion of γ_S

The summed scattering rate γ_S, as defined in (6.0.4), receives contributions from several scattering processes and inverse σ-decays that are affected differently by changes of g_N. This is highlighted in Fig. 6.10 where we show γ_S as well as the individual thermal rates for $g_N = [0.1, 0.7, 1]$. Focussing on the total rate γ_S first, we note that γ_S is fast for small z_N, i.e.

$$\frac{\gamma_S}{n_N^{\text{eq}} \mathcal{H}}(z_N) > 1\,, \tag{6.3.2}$$

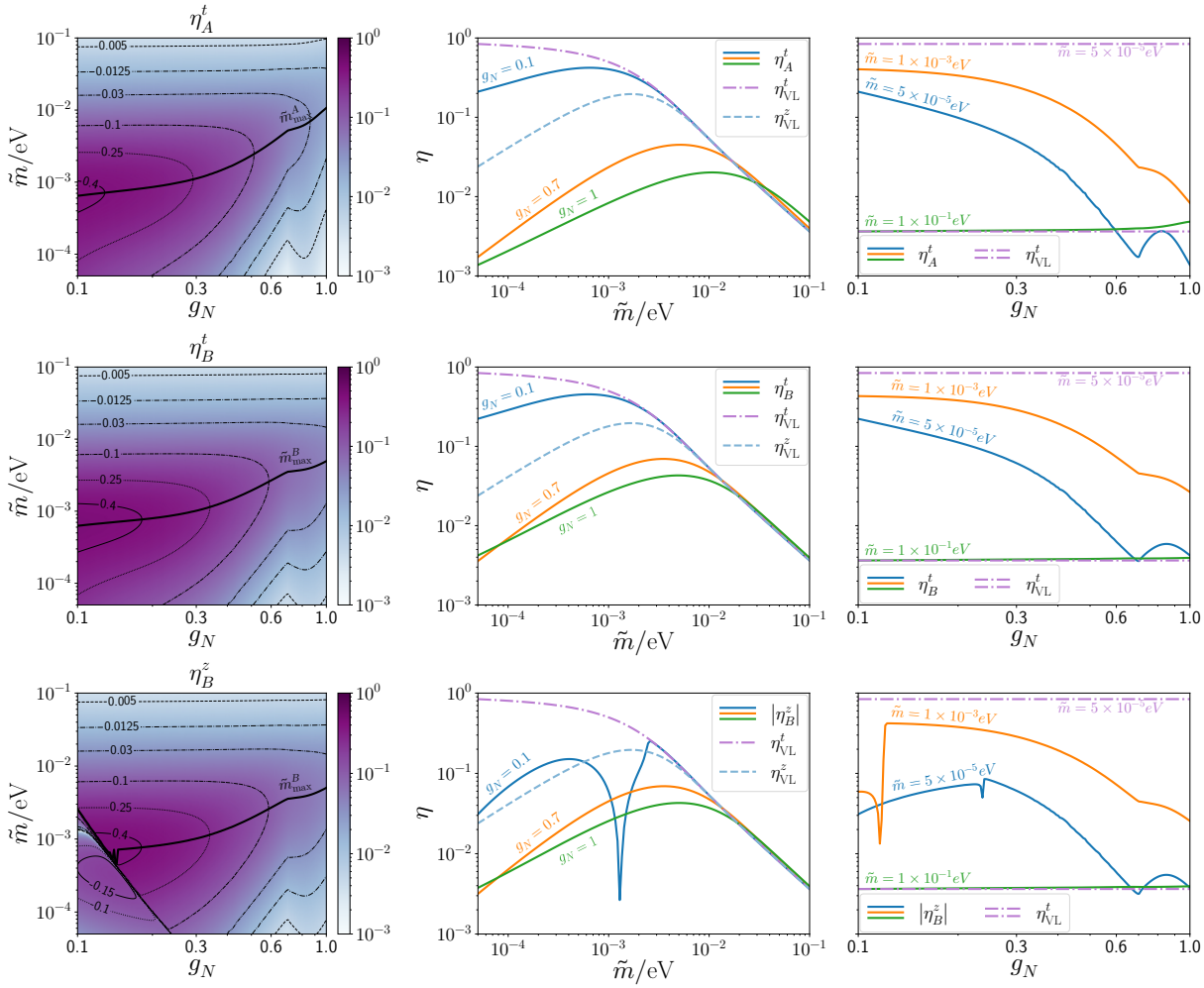

Figure 6.5: *Left:* Density plots of η_A (top row), η_B^t (middle row) and η_B^z (bottom row) in the $g_N - \tilde{m}$ plane. The black lines indicates at which $\tilde{m}$ the efficiency reaches its maximum. *Middle:* η_A (top row), η_B^t (middle row) η_B^z (bottom row) as functions of g_N. *Right:* η_A (top row), η_B^t (middle row) η_B^z (bottom row) as functions of $\tilde{m}$. See text for discussion.

before eventually becoming Boltzmann suppressed. Consequently, at $z_N = z_S^{\text{eq}}$, equality is reached in (6.3.2) so that

$$\frac{\gamma_S}{n_N^{\text{eq}} \mathcal{H}}(z_S^{\text{eq}}) = 1\,, \tag{6.3.3}$$

and hence γ_S becomes ineffective for $z_N > z_S^{\text{eq}}$. In Fig. 6.9, we show z_S^{eq} for cases $\hat{A}$ and $\hat{B}$ as functions of g_N. It is apparent that $z_S^{\text{eq},\hat{A}}$ and $z_S^{\text{eq},\hat{B}}$ are identical for $g_N \lesssim 0.7$, indicating that γ_S does not significantly depend on g_T. Moreover, we find that z_S^{eq} increases until $g_N \sim 0.7$. At $g_N \sim 0.7$, both $z_S^{\text{eq},\hat{A}}$ and $z_S^{\text{eq},\hat{B}}$ drop, eventually reach a minimum and increase again. In order to make the behavior of z_S^{eq} more transparent, let us now discuss

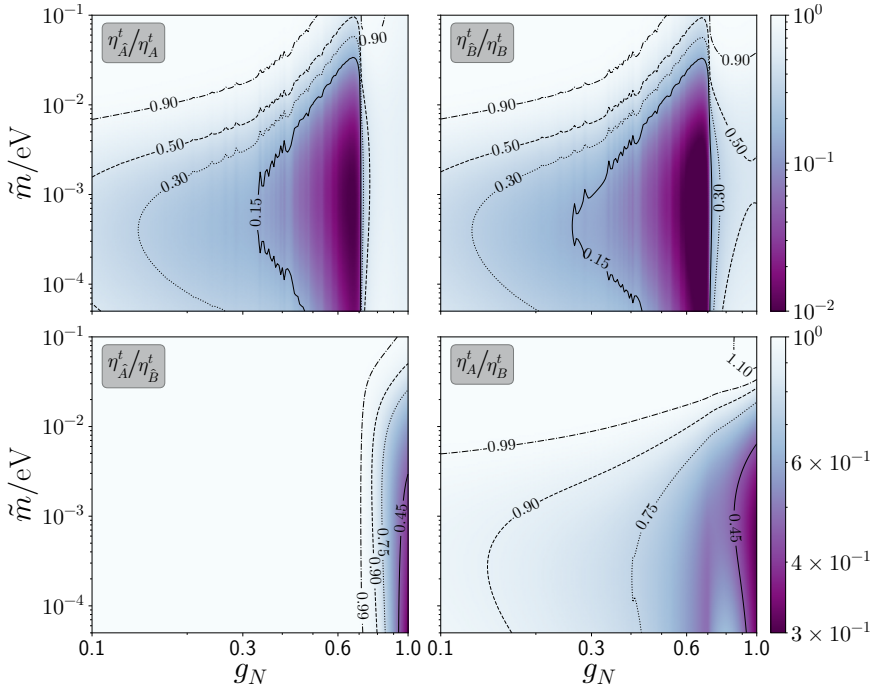

Figure 6.6: *Upper figures:* Density plots of $\eta_{\hat{A}}/\eta_A$ (left) and $\eta_{\hat{B}}/\eta^t_B$ (right) in the $g_N - \tilde{m}$ plane. *Lower figures:* Density plots of $\eta_{\hat{A}}/\eta_{\hat{B}}$ (left) and η_A/η^t_B (right) in the $g_N - \tilde{m}$ plane. See text for discussion.

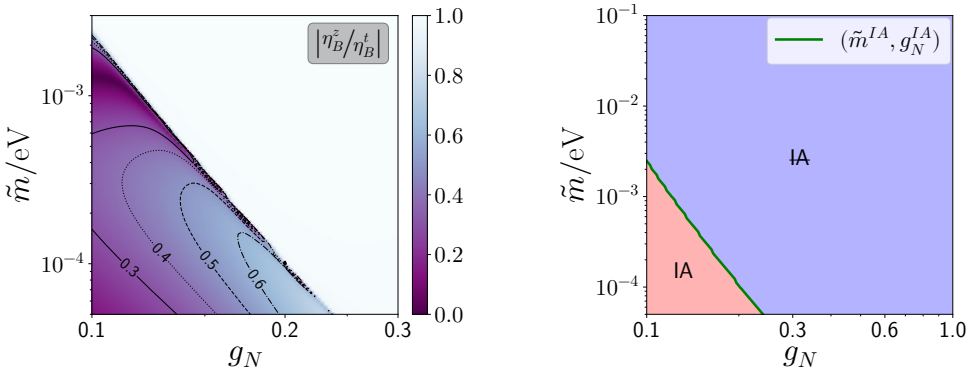

Figure 6.7: *Left:* Density plot of $|\eta^z_B/\eta^t_B|$ in the $g_N - \tilde{m}$ plane. *Right:* Schematic illustration of the IA and ~~IA~~ regimes with $(g_N^{IA}, \tilde{m}^{IA})$. See text for discussion.

the individual rates that appear in γ_S.
From Fig. 6.10, it is clear that for $g_N \leq 0.7$, γ_S is dominated by $\gamma_{\sigma,NN}$ and $\gamma_{NN,JJ}$. They are both independent of g_T and therefore identical for cases $\hat{A}$ and $\hat{B}$. As g_N increases from $g_N = 0.1$ to $g_N = 0.7$, the overall magnitude of the thermal rates increases, hence they are fast longer, i.e. $z_S^{\rm eq}$ increases. This is especially striking for $\gamma_{\sigma,NN}/n_N$ where $\Gamma_{\sigma\to NN}|_{g_N\leq 0.7} \sim g_N^3$, (see Fig. 6.3). Additionally, the Boltzmann suppresion of $\gamma_{\sigma,NN}/n_N$

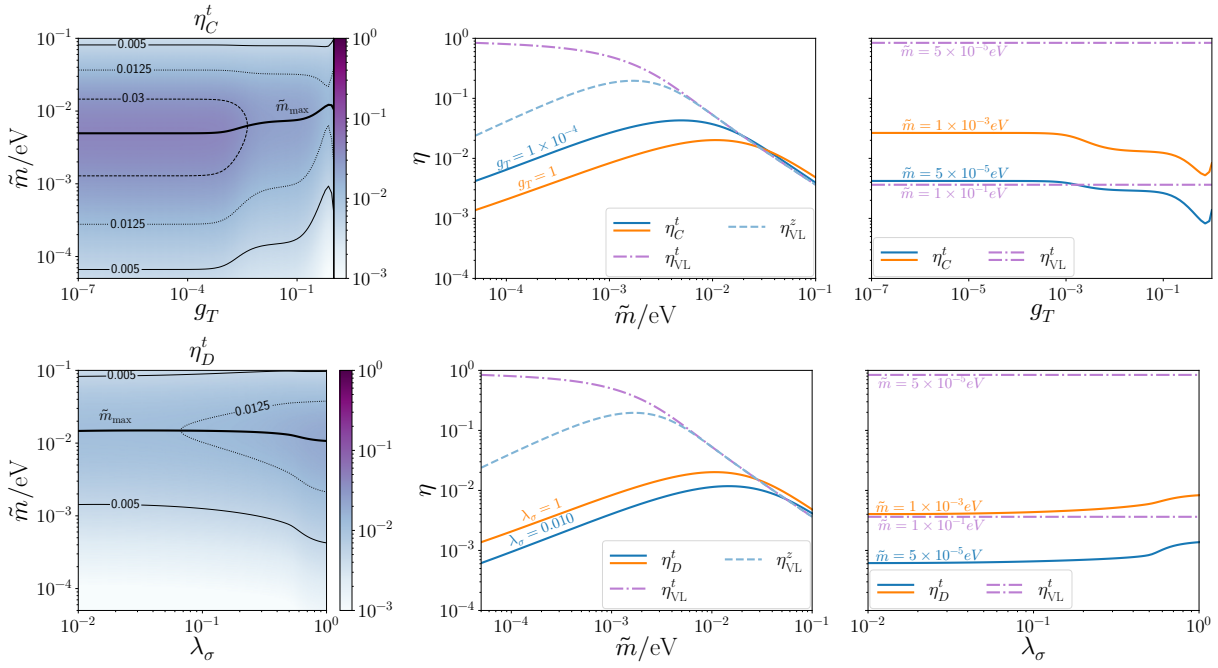

Figure 6.8: *Left:* Density plots of η_C^t (upper figure) and η_D^t (lower figure) in the $g_T - \tilde{m}$- and $\lambda_\sigma - \tilde{m}$ plane, respectively. The black lines indicates at which $\tilde{m}$ the efficiency reaches its maximum. *Middle:* η_C^t (upper figure) and η_D^t (lower figure) as functions of g_T and λ_σ, respectively. *Right:* η_C^t (upper figure) and η_D^t (lower figure) as functions of $\tilde{m}$. See text for discussion.

depends on g_N. Using

$$z_\sigma = \frac{m_\sigma}{M_N} z_N = \frac{\sqrt{2}}{g_N} z_N \,, \tag{6.3.4}$$

we find

$$\frac{\gamma_{\sigma,NN}}{n_N^{\text{eq}}} \propto \Gamma_{\sigma\to NN} \frac{n_\sigma^{\text{eq}}}{n_N^{\text{eq}}} \sim \Gamma_{\sigma\to NN} \begin{cases} \left(\frac{\sqrt{2}}{g_N}\right)^{\frac{3}{2}} \mathrm{e}^{-\frac{\sqrt{2}}{g_N} z_N} \,, & z_N < 1 \,, \\ \frac{m_\sigma}{M_N} \mathrm{e}^{-\left(\frac{\sqrt{2}}{g_N} - 1\right) z_N} \,, & z_N > 1 \,, \end{cases} . \tag{6.3.5}$$

Thus, the Boltzmann suppression of $\gamma_{\sigma,NN}/n_N$ decreases with g_N.
For $g_N > 0.7$, σ-decays to a pair of neutrinos are kinematically forbidden. Hence, in case $\hat{A}$, $\gamma_S^{\hat{A}}$ is dominated by neutrino scatterings to a pair of triplets, $NN \leftrightarrow TT$, which roughly scales as

$$\frac{\gamma_{NN,TT}}{n_N^{\text{eq}}} \sim \frac{n_T^{eq^2}}{n_N^{\text{eq}}} \sim e^{-\left(\frac{2g_T}{g_N} - 1\right) z_N} \qquad z_N > 1 \,, \tag{6.3.6}$$

and again the Boltzmann suppression decreases with g_N, translating to an increasing $z_S^{\text{eq},\hat{A}}(g_N)|_{g_N>0.7}$. In case $\hat{B}$ on the other hand, $NN \leftrightarrow TT$ scatterings are strongly sup-

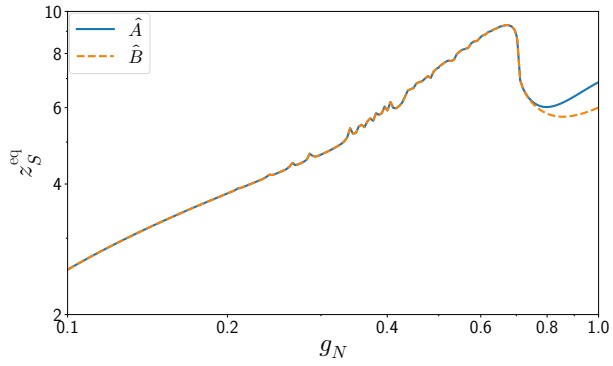

Figure 6.9: $z_S^{\rm eq}(g_N)$ as defined in (6.3.3) with the blue solid line corresponding to case $\hat{A}$ und the orange dashed line corresponding to case $\hat{B}$. For $g_N \ll 0.7$ and $g_N > 0.7$, both $z_S^{\rm eq,\hat{A}}$ and $z_S^{\rm eq,\hat{B}}$ increase with g_N as the decay rate increases with g_N, see Fig. 6.3. Additionally, the Boltzmann suppression of $\gamma_{\sigma,NN}/n_N^{\rm eq}$ decreases with g_N, see (6.3.5). Moreover, $z_S^{\rm eq}$ is determined by interactions involving only N, σ and J, i.e. independent from g_T and hence equal for cases $\hat{A}$ and $\hat{B}$. At $g_N \sim 0.7$, both $z_S^{\rm eq,\hat{A}}$ and $z_S^{\rm eq,\hat{B}}$ rapidly drop as $\gamma_{\sigma,NN}$ becomes kinematically forbidden. Consequently the overall magnitudes of $\gamma_S^{\hat{A}}$ and $\gamma_S^{\hat{B}}$ decrease (see Fig. 6.10). For $g_N > 0.7$, we have $z_S^{\rm eq,\hat{A}} > z_S^{\rm eq,\hat{B}}$, i.e. the summed scattering rate γ_S in case $\hat{B}$ decouples faster than in case $\hat{A}$. This can be traced back to the decreasing Boltzmann suppression as $g_N \to 1$ in case $\hat{A}$, see (6.3.6).

pressed by the smallness of g_T. Thus, $\gamma_S^{\hat{B}}$ is dominated by neutrinos scatterings with σ and J in the final states (which are subdominant in case $\hat{A}$), resulting in an only slightly increasing $z_S^{\rm eq,\hat{B}}(g_N)|_{g_N>0.7}$.

Neutrino Abundance

Having discussed γ_S individually, let us now compare the new scattering rates in the MTM to the rates γ_D and γ_Q that also appear in VL. This will allow us to give qualitative estimates on the neutrino evolution.

Recalling that $\gamma_{S,D,Q}/n_N^{\rm eq}\mathcal{H}$ are the relevant rates for the neutrino evolution, we show them as functions of z_N for several values of g_N and $\tilde{m}$ in Fig. 6.10 (left). For small z_N, γ_S is the dominant thermal rate while both γ_D and γ_Q are slow compared to the expansion of the Universe. However, $\gamma_S/n_N^{\rm eq}$ is Boltzmann suppressed while $\gamma_D/n_N^{\rm eq}$ and $\gamma_Q/n_N^{\rm eq}$ are not and thus eventually, γ_D becomes dominant. Quark scatterings on the other hand are always subdominant to either γ_S or γ_D. We can therefore broadly distinguish between two regimes. In the *scatter regime*, the neutrino evolution is driven by fast neutrino scatterings to T, σ and J, thereby suppressing neutrino decays. In the *decay regime*, neutrino scatterings become inefficient and consequently, the neutrino evolution is dominated by lepton number violating neutrino decays. Neglecting the quark scatterings

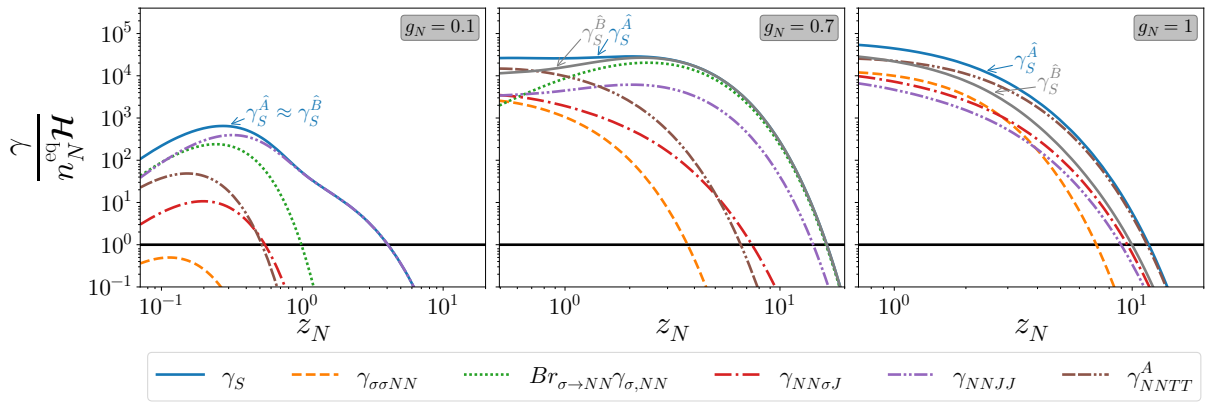

Figure 6.10: Thermal rates of scattering processes that are relevant for the neutrino evolution in the MTM with $g_N = 0.1$ (left), $g_N = 0.7$ (middle) and $g_N = 1$ (right). Note that $\gamma_{\sigma\sigma NN}, \gamma_{NN\sigma J}, \gamma_{NNJJ}$ and $\gamma_{\sigma,NN}$ are identical for cases $\hat{A}$ and $\hat{B}$. Moreover, $\gamma^{\hat{B}}_{NN,TT}$ is strongly suppressed compared to $\gamma^{A}_{NN,TT} = \gamma^{\hat{A}}_{NN,TT}$ and not shown here. For $g_N = 0.1$, the summed scattering rate γ_S is dominated by $\gamma_{NN,JJ}$ while $\gamma^{\hat{A}}_{NN,TT}$ is significantly smaller and hence $\gamma_S^{\hat{A}} \approx \gamma_S^{\hat{B}}$. As g_N increases, the overall magnitude of the thermal rates increases. Moreover, as g_N increases, the contribution of $\gamma^{\hat{A}}_{NN,TT}$ to $\gamma_S^{\hat{A}}$ grows so that eventually $\gamma_S^{\hat{A}} > \gamma_S^{\hat{B}}$. Note that for $g_N > 0.7$, $\sigma \leftrightarrow NN$ becomes kinematically forbidden and at $g_N = 1$, $\gamma_S^{\hat{A}}$ is dominated by $\gamma^{\hat{A}}_{NN,TT}$. In case $\hat{B}$, neutrino-triplet scatterings $\gamma_{NN,TT}$ are not sizable and instead, $\gamma_S^{\hat{B}}$ is dominated by scatterings involving σ. We further stress that we used z_I as the lower limit for the z_N-range presented and consequently, the respective plot range changes with g_N.

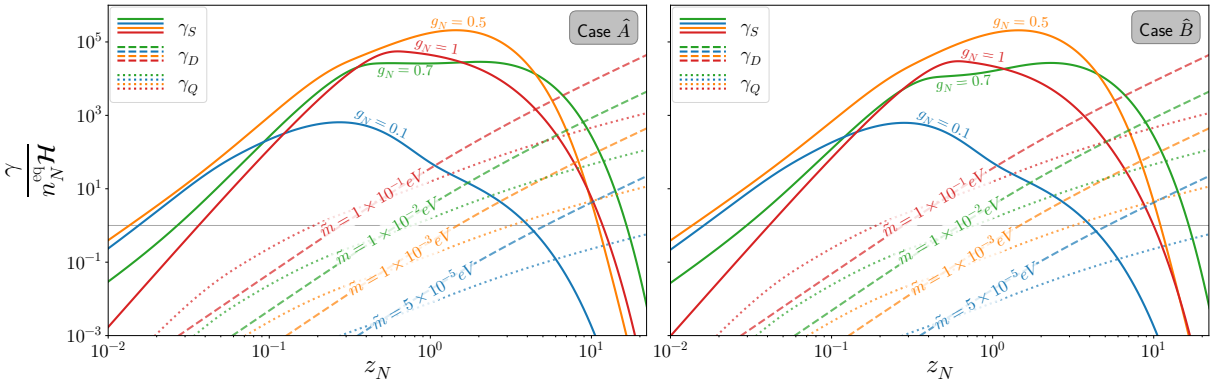

Figure 6.11: Thermal rates relevant for the evolution of Y_N (see (6.1.8)) for $g_N = [0.1, 0.5, 0.7, 1]$ and $\tilde{m} = [5\times10^{-5}, 10^{-3}, 10^{-2}, 10^{-1}]$eV for case $\hat{A}$ (left) and case $\hat{B}$ (right). For small z_N, $\gamma_S/n_N^{\rm eq}\mathcal{H}$ exceeds $\gamma_D/n_N^{\rm eq}\mathcal{H}$ until it drops due to Boltzmann suppression and subsequently, $\gamma_D/n_N^{\rm eq}\mathcal{H}$ becomes dominant. γ_Q is always subdominant to either γ_S or γ_D. Note that $\gamma_S^{\hat{A}}$ and $\gamma_S^{\hat{B}}$ are equal for $g_N < 0.7$ while for $g_N > 0.7$, we find that $\gamma_S^{\hat{B}}$ drops slightly faster.

and with a Taylor expansion of (6.1.8), we can write

$$s\mathcal{H}z_N\frac{\mathrm{d}Y_N}{\mathrm{d}z_N} = -\left(\delta_N - 1\right)\gamma_D - 4\left(\delta_N - 1\right)\gamma_S\,, \tag{6.3.7}$$

and express the neutrino evolution in the scatter and decay regime as

$$s\mathcal{H}z_N\frac{\mathrm{d}}{\mathrm{d}z_N}\hat{Y}_N \approx \begin{cases} s\mathcal{H}z_N\frac{\mathrm{d}}{\mathrm{d}z_N}\hat{Y}_N^{scatter} = -\left(\hat{\delta}_N - 1\right)4\gamma_S\,, & z_N \lesssim z_S\,, \\ s\mathcal{H}z_N\frac{\mathrm{d}}{\mathrm{d}z_N}\hat{Y}_N^{decay} = -\left(\hat{\delta}_N - 1\right)\gamma_D\,, & z_N \gtrsim z_S\,. \end{cases} \tag{6.3.8}$$

From (6.3.7), we find that the transition from the scatter to the decay regime occurs at $z_S(\tilde{m}, g_N)$ defined via

$$4\gamma_S(z_N = z_S, \tilde{m}) = \gamma_D(z_N = z_S, g_N)\,. \tag{6.3.9}$$

In Fig. 6.12 (upper panels), we show a density plot of $z_S^{\hat{A}}$ in the $g_N - \tilde{m}$ plane (left) as well as $z_S^{\hat{A}}(\tilde{m})$ (middle) and $z_S^{\hat{A}}(g_N)$ (right) for exemplary values of g_N and $\tilde{m}$, respectively. We find that z_S decreases with $\tilde{m}$, as is also apparent from Fig. 6.11: For larger $\tilde{m}$, γ_D exceeds $4\gamma_S$ at smaller z_N and hence $z_S(\tilde{m}) \sim 1/\gamma_D(\tilde{m}) \sim 1/\tilde{m}$. On the other hand, we find that $z_S(g_N)$ behaves similarly to $z_S^{\mathrm{eq}}(g_N)$. The transition from the scatter to the decay regime occurs when γ_S is Boltzmann suppressed and therefore drops rapidly, i.e. it essentially depends on when the Boltzmann suppression sets in. As discussed above, z_S^{eq} is also largely determined by the Boltzmann suppression, and therefore $z_S(g_N) \sim z_S^{\mathrm{eq}}(g_N)$. Moreover, if $\tilde{m}$ is small, z_S is shifted to slightly larger z_N compared to z_S^{eq} due to the smallness of γ_D and vice versa. Additionally, note that $z_S^{\hat{B}}$ differs from $z_S^{\hat{A}}$ only for $g_N \gtrsim 0.7$.
Next, note that $z_S > z_S^{\mathrm{eq}}$ implies that neutrino scatterings dominate the neutrino evolution while not being fast enough to keep them in equilibrium. This is highlighted in Fig. 6.13 where we show $Y_{N_{\hat{A}}}^t(z_N)$ and $Y_{N_{\mathrm{VL}}}^{t,z}$ for $g_N = 0.1$ (left) and $g_N = 1$ (right) with $\tilde{m} = 5 \times 10^{-5}\,\mathrm{eV}$. Comparing $Y_{N_{\hat{A}}}$ and $Y_{N_{\mathrm{VL}}}$, we find that for $z_N < z_S^{\mathrm{eq}}$, the neutrino abundance in the MTM closely follows the equilibrium abundance while $Y_{N_{\mathrm{VL}}}$ significantly deviates from equilibrium. However, since $z_S^{\mathrm{eq},\hat{A}} < z_S^{\hat{A}}$ for the parameters used in Fig. 6.13, the neutrino abundance at $z_S^{\hat{A}}$ exceeds the equilibrium abundance. In the decay regime with $z_N > z_S^{\hat{A}}$, we find that $Y_{N_{\hat{A}}}^t$ approaches $Y_{N_{\mathrm{VL}}^z}$, indicating that the evolution of both abundances is driven by γ_D.
Finally, γ_S is so effective at establishing equilibrium that even in the case of a vanishing initial neutrino abundance, the neutrinos reach their equilibrium abundance almost instantly, irrespective of the values of g_N and $\tilde{m}$, respectively. We will therefore not distinguish between $\hat{Y}_N^t(z_N)$ and $\hat{Y}_N^z(z_N)$ in the following.

Efficiency

Although we established above that in the case of a vanishing initial neutrino abundance, neutrinos reach equilibrium so quickly that the initial abundance is irrelevant, it is instructive to briefly discuss the evolution of the efficiency in this scenario in comparison with VL. Recall that in VL, neutrinos are produced via lepton number violating inverse

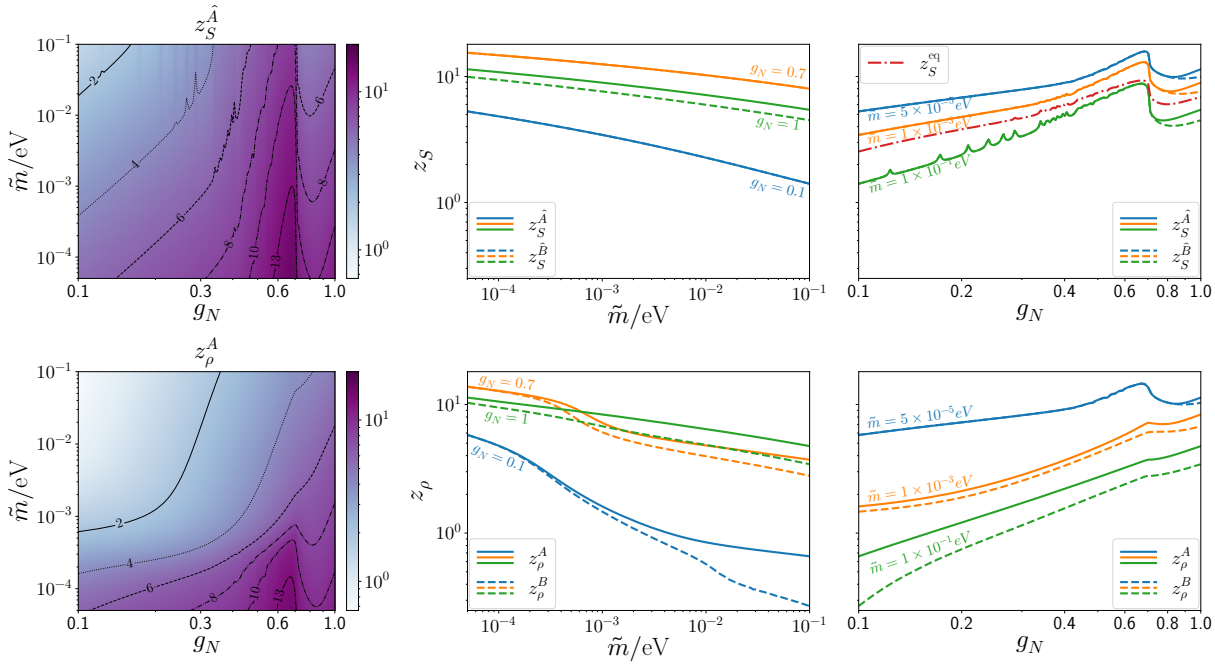

Figure 6.12: Upper figures: *Left:* Density plot of $z_S^{\hat{A}}$ in the $g_N - \tilde{m}$ plane. *Middle:* $z_S^{\hat{A}}$ (solid) and $z_S^{\hat{B}}$ (dashed) as functions of $\tilde{m}$. *Right:* $z_S^{\hat{A}}$ (solid), $z_S^{\hat{B}}$ (dashed) and $z_S^{\text{eq},\hat{A}}$(dash-dotted) as functions of g_N. Note that for $g_N \leq 0.7$, we have $z_S^{\hat{A}} \sim z_S^{\hat{B}}$. It is evident that depending on tha value of $\tilde{m}$, z_S is shifted to either slightly larger or slightly smaller values compared to z_S^{eq}, but qualitatively behaves roughly the same. **Lower figures:** *Left:* Density plot of z_ρ^A in the $g_N - \tilde{m}$ plane. *Middle:* z_ρ^A (solid) and z_ρ^B (dashed) as functions of $\tilde{m}$. *Right:* z_ρ^A (solid) and z_ρ^B (dashed) as functions of g_N.

decays and quark scatterings, giving rise to a negative efficiency η_{VL}^-, while neutrino decays create a positive efficiency η_{VL}^+ at a later stage, yielding a total positive efficiency. In the MTM on the other hand, the neutrino population is mostly generated by lepton number conserving interactions and almost instantly reaches equilibrium at $z_{\text{eq}}^N \gtrsim z_I$, prompting $d\hat{\eta}^z/dz_N$ to change sign. Hence, the negative efficiency $\hat{\eta}^-$ created in the MTM is much less sizable compared to η_{VL}^- and consequently, $\hat{\eta}^z$ changes sign and subsequently approaches $\hat{\eta}_t$ for significantly smaller z_N. This is highlighted in Fig. 6.14 where we show $\eta_{\hat{A}}^{t,z}(z_N)$ and $\eta_{\text{VL}}^{t,z}(z_N)$ for $g_N = [0.1, 0.7, 1]$ and $\tilde{m} = [5 \times 10^{-5}, 10^{-3}, 10^{-1}]$eV.[2] From Fig. 6.14, it is also apparent that the negative efficiency η^- increases with $\tilde{m}$, as is intuitively clear.[3]
In the following, we will discuss the evolution of the efficiency for different values of g_N and $\tilde{m}$ in greater detail and for simplicity, we will restrict ourselves to $\hat{\eta}^t$. In analogy to the discussion of VL, let us first focus on the regime where WO effects are small. Hence,

[2]Panels 8 and 9 in Fig. indicate that η_{VL}^z changes sign for smaller z_N compared to $\hat{\eta}^z$. We note however that the Boltzmann equations for VL are solved starting from $z_N = 0$ while the Boltzmann equations in the MTM are solved starting from $z_N = z_I > 0$. Thus, when discussing how fast $\hat{\eta}^z$ and η_{VL}^z change sign, it should be kept in mind that in the latter case, the leptogenesis era starts significantly earlier.

[3]In Fig. 6.14, we only show $\eta_{\hat{A}}$. From the discussion of the neutrino evolution in the previous section, it should be clear that the same reasoning applies for $\eta_{\hat{B}}$.

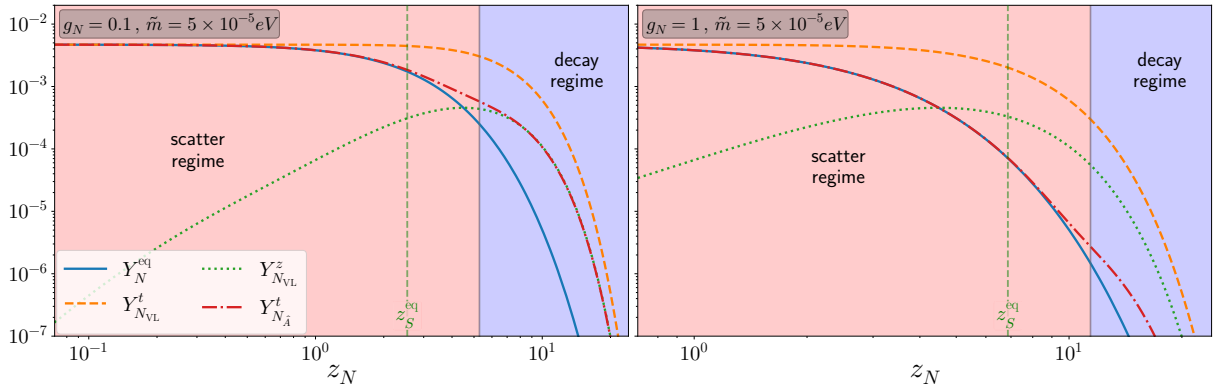

Figure 6.13: Evolution of $Y^t_{N_{\hat{A}}}(z_N)$ and $Y^{t,z}_{N_{\rm VL}}(z_N)$ compared to $Y^{\rm eq}_N(z_N)$, with $g_N = 0.1$ (left) and $g_N = 1$ (right). The red region denotes the scatter regime where the neutrino evolution in the MTM is dominated by scattering processes, while the blue region denotes the decay regime where (inverse) neutrino decays are dominant. The vertical line corresponds to $z_S^{\rm eq}$ where the scattering processes decouple. Note that the lower limits of the z_N-range are given by z_I and hence depend on g_N.

the Boltzmann equation for the efficiency can be written as

$$s\mathcal{H}z_N \frac{\mathrm{d}}{\mathrm{d}z_N}\hat{\eta} = \frac{1}{Y_N^0}\left(\hat{\delta}_N - 1\right)\gamma_D \,. \tag{6.3.10}$$

In the scatter and decay regimes introduced in (6.3.8), we can then write (6.3.10) as

$$\frac{\mathrm{d}}{\mathrm{d}z_N}\hat{\eta} \approx \begin{cases} -\frac{1}{Y_N^0}\frac{\gamma_D}{4\gamma_S}\frac{\mathrm{d}}{\mathrm{d}z_N}\hat{Y}_N \,, & z_N \lesssim z_S \,, \\ -\frac{1}{Y_N^0}\frac{\mathrm{d}}{\mathrm{d}z_N}\hat{Y}_N \,, & z_N \gtrsim z_S \,, \end{cases} \tag{6.3.11}$$

yielding the final efficiency as

$$\hat{\eta}(z_N \to \infty) = \frac{1}{Y_N^0}\left(\hat{Y}_N(z_S) - \int_{z_I}^{z_S} \mathrm{d}z' \frac{\gamma_D}{4\gamma_S}\frac{\mathrm{d}}{\mathrm{d}z_N}\hat{Y}_N\right) . \tag{6.3.12}$$

In the scatter regime, neutrinos scatter rather than decay and consequently, the efficiency is suppressed by $4\gamma_S$. In the decay regime, neutrino scatterings become irrelevant and the suppression disappears, leaving neutrinos to freely decay. Thus, the efficiency is mainly determined by the neutrino abundance at z_S and consequently, the larger z_S, the larger the Boltzmann suppression at $\hat{Y}_N(z_S)$ and the smaller number of neutrinos that can create an efficiency via lepton number violating decays. Consequently, in light of the discussion in the previous section, we can deduce that $\hat{\eta}(\tilde{m}) \sim 1/z_S(\tilde{m}) \sim \tilde{m}$ and $\hat{\eta}(g_N) \sim 1/z_S(g_N) \sim 1/z_S^{\rm eq}$, which is also apparent when comparing Fig. 6.4 and Fig. 6.12. This is especially striking at $g_N \sim 0.7$, where the suppression is maximal and hence the efficiency minimal.

For larger $\tilde{m}$, WO effects eventually become relevant and need to be taken into account, see Fig. 4.9. Let us assume that WO effects are in equilibrium in a range $z_N^1 \lesssim z_N \lesssim z_N^2$. In VL, the efficiency is then diminished by WO processes for $z_N \gtrsim z_N^1$ and hence decreases

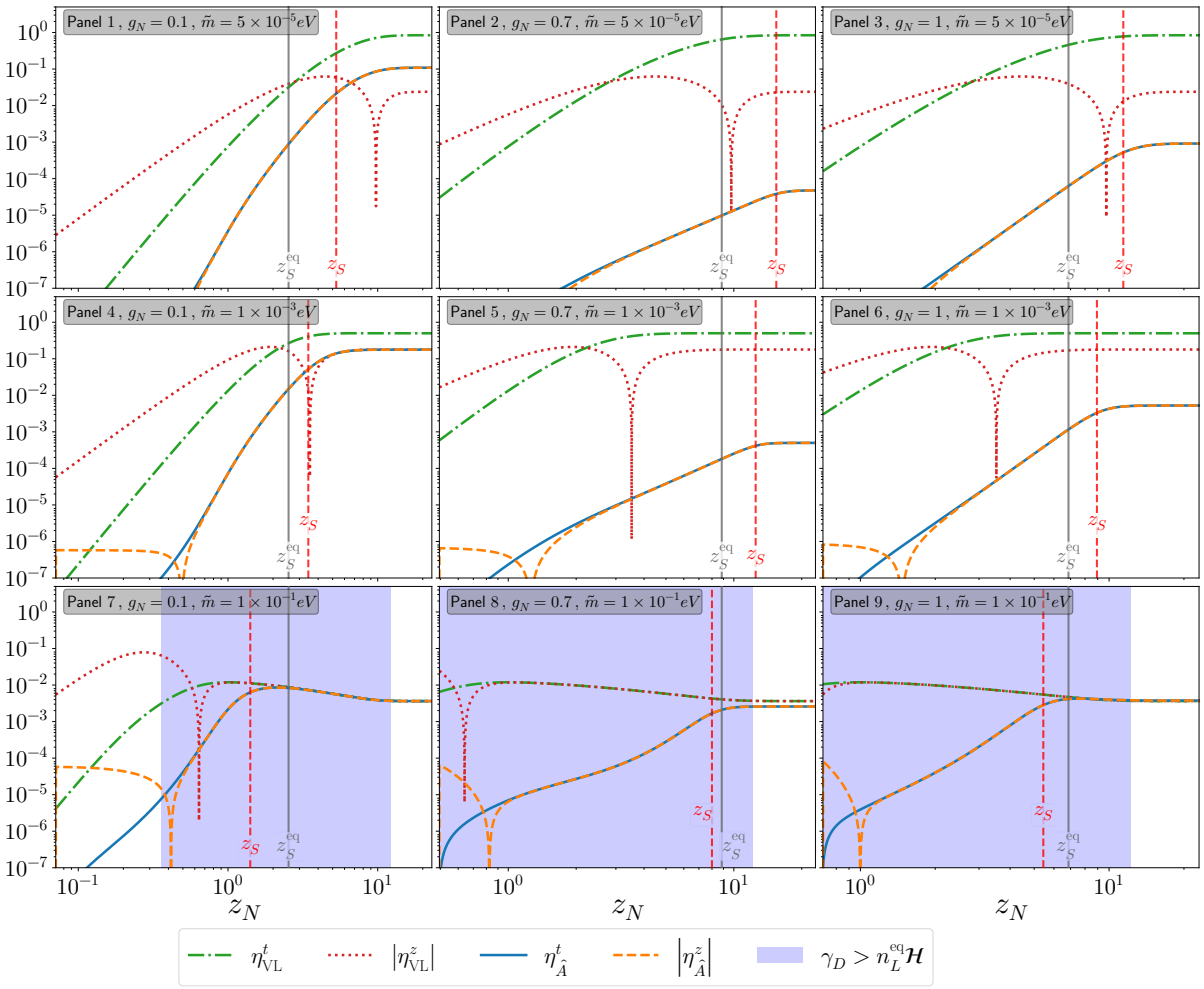

Figure 6.14: Evolution of the efficiencies $\eta^{t,z}_{\mathrm{VL}}$ and $\eta^{t,z}_{\hat{A}}$ for $g_N = [0.1, 0.7, 1]$ and $\tilde{m} = [5 \times 10^{-5}, 10^{-3}, 10^{-1}]$eV. The blue region in panels 7–9 indicates where inverse neutrino decays are in equilibrium, the solid vertical line denotes z_S^{eq} and the dashed vertical line denotes z_S. Note that the lower limits of the z_N-range are given by z_I and hence depend on g_N. As the efficiency in VL does not depend on g_N, η^t_{VL} and η^z_{VL} are the same in each column. Note that in panels 1–7, the initially negative efficiency $\eta^z_{\hat{A}}(z_N)$ changes sign significantly faster than $\eta^z_{\mathrm{VL}}(z_N)$ due to a larger number of neutrinos in the MTM being created via lepton number conserving interactions with σ, J and T. Comparing $\eta^t_{\hat{A}}$ and η^t_{VL}, the suppression of $\eta^t_{\hat{A}}$ while $z_N < z_S$ holds is evident. In particular, even if inverse decays are in equilibrium (panels 7–9), they are not very effective at diminishing $\eta^t_{\hat{A}}$ until the suppression is lifted at z_S and $\eta^t_{\hat{A}}$ becomes sizable.

with $\tilde{m}$. In contrast, the situation in the MTM is more evolved. The WO term is proportional to the efficiency, and hence efficient WO requires not only that inverse decays are fast but also that a sufficiently sizable efficiency already exists. Since the main portion of the efficiency in the MTM is created around z_S, we can roughly estimate that WO effects are only relevant for $z_N \gtrsim \mathrm{Max}\,[z_N^1, z_S]$. This tends to reduce the z_N-range where WO has sizable effects on the efficiency, see panels 7-9 in Fig. 6.14. Consequently, we can determine a rough estimate on the minimal value $\tilde{m} =: \tilde{m}_S$ where WO effects become relevant for a given g_N as

$$\frac{\gamma_D}{n_L^{\mathrm{eq}}\mathcal{H}}(\tilde{m}_S, z_S) = 1\,. \tag{6.3.13}$$

Thus, for $\tilde{m} < \tilde{m}_S$, WO effects are irrelevant, $\hat{\eta} \sim \tilde{m}$ (*"~~WO~~ regime"*), and the evolution of the efficiency is determined by neutrino scatterings while for $\tilde{m} > \tilde{m}_S$, WO results in $\hat{\eta} \sim 1/\tilde{m}$ (*"WO regime"*) and leptogenesis proceeds similarly to VL.[4] We therefore expect that $\hat{\eta}(\tilde{m})$ reaches a maximum around $\tilde{m} \gtrsim \tilde{m}_S$.[5] In Fig. 6.15, we compare $\tilde{m}_S(g_N)$ to the value where the maximum is actually reached, which we will denote by $\hat{\tilde{m}}_{\mathrm{max}}(g_N)$, and find indeed $\hat{\tilde{m}}_{\mathrm{max}} \gtrsim \tilde{m}_S \sim z_S$. Therefore, the suppression caused by the scattering processes greatly reduces the efficiency, which in turn severely limits the $\tilde{m}$ range where WO processes influence the efficiency compared to VL. In particular, the maximal suppression around $g_N \sim 0.7$ results in $\hat{\eta} < \eta^{WO}$ and WO processes are ineffective even for $\tilde{m} \to 0.1\,\mathrm{eV}$.

To summarize, we find that the scattering processes induced by the new interactions in the MTM render the model similar to type III leptogenesis in the sense that the scattering processes rapidly thermalize the neutrinos, resulting in a final efficiency that is independent from the initial neutrino abundance. Moreover, over a significant part of the parameter space, fast scattering processes prevent neutrinos from decaying, resulting in a sizable suppression of the efficiency. Once WO processes take over, the evolution of the efficiency is similar to VL.

6.3.3 Case A

Having discussed the dynamics of leptogenesis in the simplified scenario of the MTM, we will now proceed to discuss the more evolved scenarios when T, σ and J can have non-equilibrium abundances. This has a major impact on the evolution of the neutrino abundance. In the simplified scenario and in VL, the neutrino abundance is compared to the equilibrium abundance, i.e. how much δ_N deviates from one. However, as is clear from the structure of the Boltzmann equations in (6.1.3), (6.1.5), (6.1.6) and (6.1.7), we now need to compare δ_N to $\delta_{T,\sigma,J}$. More precisely, if for instance $\delta_T > \delta_N$, the neutrino abundance is enhanced by $TT \leftrightarrow NN$ scatterings while $\delta_T < \delta_N$ implies that the neutrino abundance is diminished. Since we are now dealing with four coupled Boltzmann

[4] This discussion is similar to the discussions of type III leptogenesis in Ref. [148, 187].

[5] We expect that that maximum is reached for $\tilde{m} \gtrsim \tilde{m}_S$ rather than $\tilde{m} \sim \tilde{m}_S$ since $\gamma_D/n_L^{\mathrm{eq}}\mathcal{H}(\tilde{m}_S, z_N)$ is Boltzmann suppressed around z_S and thus effective WO, i.e. $\gamma_D/n_L^{\mathrm{eq}}\mathcal{H}(\tilde{m}, z_N > z_S) > 1$ requires $\tilde{m} \gtrsim \tilde{m}_S$.

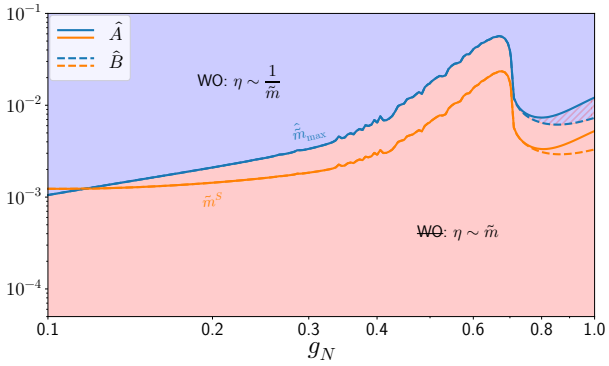

Figure 6.15: Comparison of $\tilde{m}_S$ and $\hat{\tilde{m}}_{\max}$ for case $\hat{A}$ (solid) and case $\hat{B}$ (dashed). In the red region, the final efficiency is governed by scattering processes and thus $\eta_{\hat{A},\hat{B}} \sim \tilde{m}$. In the blue region, the final efficiency is independent from the effects of scattering processes and dictated by WO processes, analogously to the strong WO regime in VL and thus $\eta_{\hat{A},\hat{B}} \sim 1/\tilde{m}$. The hatched region corresponds to the WO regime in case $\hat{A}$ and to the ~~WO~~ regime in case $\hat{B}$. Moreover, it is apparent that $\tilde{m}_S$ and $\hat{\tilde{m}}_{\max}$ essentially depend on the final efficiency, and hence also on z_S, and therefore $\tilde{m}_S, \hat{\tilde{m}}_{\max} \sim z_S \sim z_S^{\text{eq}}$.

equations that determine the evolution of the particle abundances, it is evident that the details are highly non-trivial and a qualitative discussion as in the simplified scenario is not feasible. Instead, we will focus our following discussion on some fundamental features.

6.3.3.1 Thermal Rates

The Boltzmann equations given in (6.1.3), (6.1.5), (6.1.6) and (6.1.7) depend on several thermal rates. In order to keep the discussion simple, we restrict ourselves to the ones that have significant effects on the evolution of the particle abundances. These rates are shown in Fig. 6.16, normalized to the respective equilibrium number density. If we consider e.g. the thermal rates that govern the evolution of T, we find that the dominant processes are the gauge scatterings $TT \leftrightarrow AA$ with

$$\frac{\gamma^A_{TT,AA}}{n_T^{\text{eq}}} \sim \left(\frac{g_N}{z_N}\right)^{\frac{3}{2}} \exp^{-\frac{z_N}{g_N}} . \tag{6.3.14}$$

Thus, the Boltzmann suppresion of $\gamma^A_{TT,AA}/n_T^{\text{eq}}$ depends on g_N and we can anticipate that the triplet freezes out at $z_N^{T,fo} = z_T^{fo} g_N \sim 10 g_N$.
The evolution of J is governed by (inverse) decays, $\sigma \leftrightarrow JJ$, and scatterings, $NN \leftrightarrow JJ$, which are also subject to g_N-dependent Boltzmann suppression,

$$\frac{\gamma_{\sigma,JJ}}{n_J^{\text{eq}}} \sim \frac{n_\sigma^{\text{eq}}}{n_J^{\text{eq}}} \sim \left(\frac{m_\sigma z_N}{M_N}\right)^{\frac{3}{2}} \exp^{-\frac{\sqrt{2}}{g_N} z_N} , \tag{6.3.15}$$

$$\frac{\gamma_{NNJJ}}{n_J^{\rm eq}} \sim \frac{n_N^{\rm eq2}}{n_J^{\rm eq}} \sim \begin{cases} \left(\frac{M_N}{z_N}\right)^3 , & z_N < 1 , \\ M_N^3 \exp^{-2z_N} , & z_N > 1 . \end{cases} \tag{6.3.16}$$

The evolution of σ is governed by (inverse) σ-decays, either a pair of Majorons or neutrinos, which are not Boltzmann suppressed,

$$\frac{\gamma_{\sigma,JJ}}{n_\sigma^{\rm eq}} = \frac{{\rm K}_1(z_N)}{{\rm K}_2(z_N)}\Gamma_{\sigma\to JJ} , \qquad \frac{\gamma_{\sigma,NN}}{n_\sigma^{\rm eq}} = \frac{{\rm K}_1(z_N)}{{\rm K}_2(z_N)}\Gamma_{\sigma\to NN} . \tag{6.3.17}$$

Finally, the thermal rates that govern the neutrino evolution have already been discussed in the previous section.

Abundances

Similarly to the previously discussed scenario, we find that N, T, σ and J almost immediatly reach thermal equilibrium at $z_N \sim z_I$ if the initial abundances vanish. We will therefore omit the t, z indices for Y_{N,T,σ,J_A} in the following. Moreover, in light of our discussion of the simplified scenario, we attempt to approach the neutrino evolution in a similar manner to (6.3.8). That is, we distinguish between a scatter regime where we anticipate that the neutrino evolution is governed by neutrino scatterings involving T, σ and J, and a decay regime where lepton number violating decays are presumably dominant[6] so that

$$s\mathcal{H}z_N \frac{\rm d}{{\rm d}z_N} Y_{N_A} \approx s\mathcal{H}z_N \begin{cases} \frac{\rm d}{{\rm d}z_N} Y_{N_A}^{scatter} = -2(\delta_{N_A}^2 - 1)\gamma_S - 2\rho_A , & z_N < z_\rho^A , \\ \frac{\rm d}{{\rm d}z_N} Y_{N_A}^{decay} = -(\delta_{N_A} - 1)\gamma_D , & z_N > z_\rho^A , \end{cases} \tag{6.3.18}$$

where the transition from the scatter to the decay regime occurs at z_ρ^A. Concerning the scatter regime, it is evident that the first term proportional to γ_S diminishes the neutrino abundance. Even though the sign of ρ_A is not trivial, see (6.1.2), we note that $-\rho_A$ is always positive and if it is sufficiently sizable, we can conclude that the ρ_A-term enhances the neutrino abundance. Overall, we find for the most part that $\left[(\delta_{N_A}^2 - 1)\gamma_S\right](z_N) > |\rho_A(z_N)|$ holds and hence the neutrino abundance decreases with z_N. In the decay regime, it is evident that the Boltzmann equation that governs in the neutrino evolution is the same as in the simplified scenario. Consequently, we expect that the only difference between the neutrino evolution in cases $\hat{A}$ and A is due to the neutrino abundances present at $z_S^{\hat{A}}$ and z_ρ^A, respectively.

In Fig. 6.12 (lower panels), we show density plots of $z_\rho^A(\tilde{m}, g_N)$ (left), $z_\rho^A(\tilde{m})$ (middle) and $z_\rho^A(g_N)$ (right) for $g_N = [0.1, 0.7, 1]$ and $\tilde{m} = [5 \times 10^{-5}, 10^{-3}, 10^{-1}]$eV, respectively. Moreover, since the relevant quantity that governs the evolution of the efficiency is the deviation of the neutrino abundance from equilibrium Δ_N defined as

$$\Delta_i \equiv \delta_i - 1 , \tag{6.3.19}$$

[6] Note that we again neglect quark scatterings throughout the discussion.

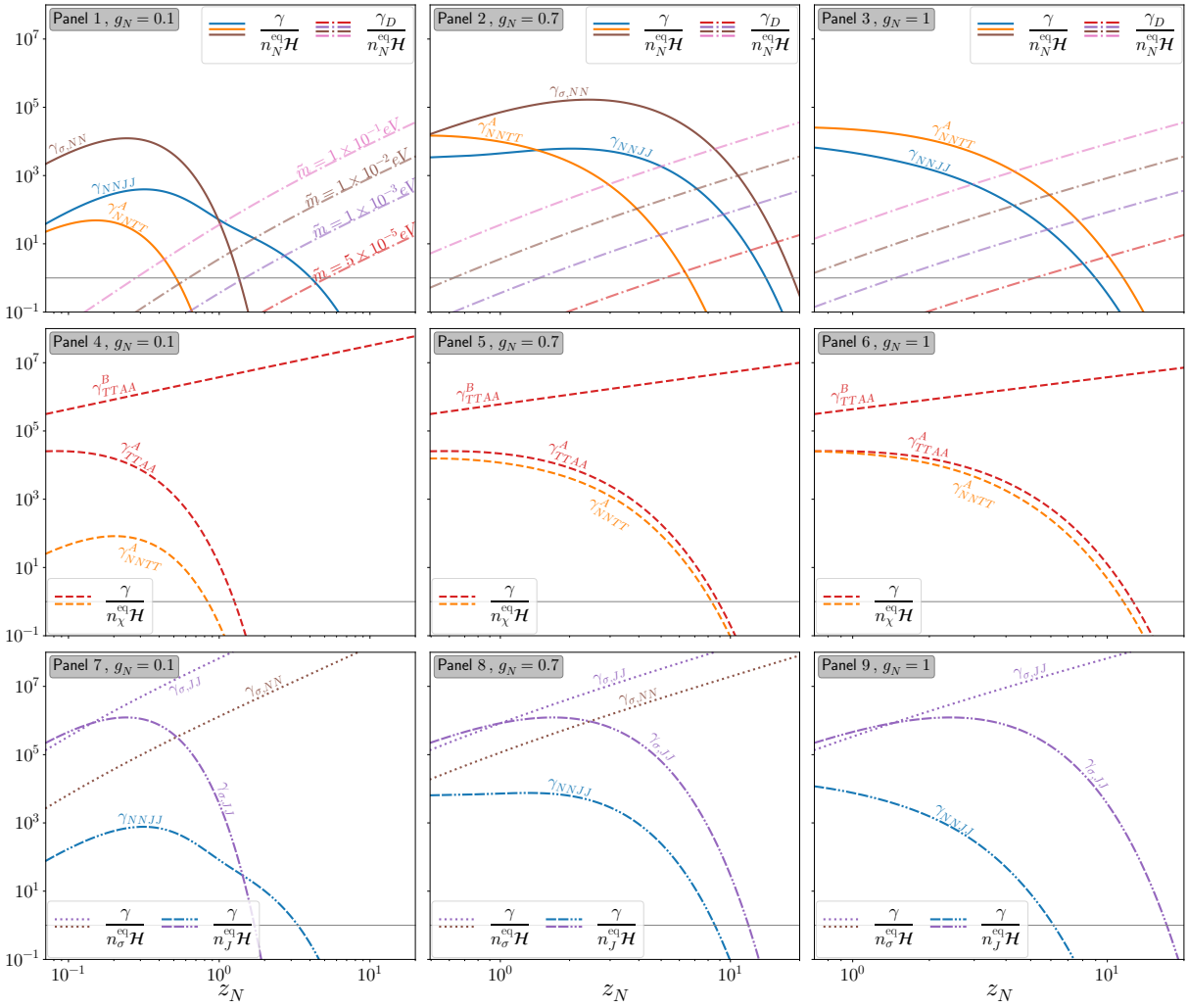

Figure 6.16: Thermal rates relevant for the evolution of N (panels 1–3), T (panels 4–6), σ (panels 7–9) and J (panels 7–9) for $g_N = 0.1$ (left), $g_N = 0.7$ (middle) and $g_N = 1$ (right). The thermal rates without T in the initial or final state are indentical for cases A and B. Note that the lower limits of the z_N-range are given by z_I and hence depend on g_N. See text for details.

it is convenient to disucss the evolution of $\Delta_{N_{A,\hat{A}}}(z_N)$, as shown in Fig. 6.17, rather than $dY_{N_{A,\hat{A}}}/dz_N(z_N)$.

In the scatter regime, the thermal rates that govern the neutrino evolution are independent from $\tilde{m}$ and hence $\Delta_{N_A}(z_N)|_{z_N<z_\rho^A}$ and $\Delta_{N_{\hat{A}}}(z_N)|_{z_N<z_S^{\hat{A}}}$ do not depend on $\tilde{m}$, as is also evident from Fig. 6.17. The effects of g_N on the evolution of the neutrino abundance in the scatter regime are highly non-trivial. From panels 1 and 2 in Fig. 6.17 we can infer that $\Delta_{N_A}(z_N)|_{z_N<z_\rho^A} \gg \Delta_{N_{\hat{A}}}(z_N)|_{z_N<z_S^{\hat{A}}}$, i.e. the neutrino abundance in the simplified scenario deviates significantly less from equilibrium compared to case A. This can

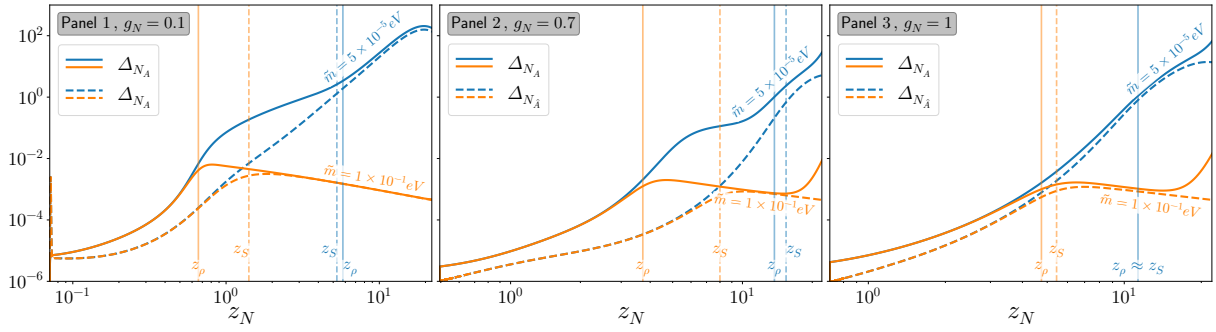

Figure 6.17: Evolution of Δ_{N_A} (solid lines) and $\Delta_{N_{\hat{A}}}$ (dashed lines) for $\tilde{m} = [5 \times 10^{-5}, 10^{-1}]$eV and $g_N = 0.1$ (panel 1), $g_N = 0.7$ (panel 2), $g_N = 1$ (panel 3). The vertical solid lines indicate z_ρ^A while the vertical dashed lines denote $z_S^{\hat{A}}$. Note that the lower limits of the z_N-range are given by z_I and hence depend on g_N. In the scatter regimes, i.e. $z_N < z_\rho^A$ and $z_N < z_S$ for case A and $\hat{A}$, respectively, the neutrino evolution is determined by scatterings involving T, σ and J and consequently, $\Delta_{N_A}(z_N)|_{z_N < z_\rho^A}$ and $\Delta_{N_{\hat{A}}}(z_N)|_{z_N < z_S^{\hat{A}}}$ are independent from $\tilde{m}$. We find that for $z_N \ll \{z_\rho^A, z_S\}$, the neutrino abundance in case A deviates from equilibrium notably stronger than in case $\hat{A}$. In the decay regime, $z_N > \{z_\rho^A, z_S\}$, and for $g_N = 0.1$ (panel 1), the neutrino evolution is entirely driven by inverse neutrino decays and apart from the different conditions at $z_N = z_\rho^A$ and $z_N = z_S$, respectively, independent from the scattering processes. Thus, we find that in the decay regime $\Delta_{N_A}(z_N)$ approaches $\Delta_{N_{\hat{A}}}(z_N)$. For $g_N \geq 0.7$ (panels 2 and 3) on the other hand, $\Delta_{N_A}(z_N)$ initially approaches $\Delta_{N_{\hat{A}}}(z_N)$ in the decay regime but eventually increases again when T freezes out and enhances the neutrino abundance.

be explained by considering the Boltzmann equations given in (6.1.3) and (6.1.8). In the simplified scenario, neutrinos interact by definition only with particles that are in perfect equilibrium, i.e. the term

$$\hat{A}: \quad \left(\delta_{N_{\hat{A}}} - 1\right) \gamma_S \tag{6.3.20}$$

always forces neutrinos into equilibrium, provided that γ_S is fast. On the other hand, if T, σ and J can deviate from equilibrium, the individual terms are e.g. of the form

$$A: \quad \left(\delta_N^2 - \delta_X^2\right) \gamma_{NN,XX} \,. \tag{6.3.21}$$

Thus, if a process $\gamma_{NN,XX}$ is fast, the abundances strive towards $\delta_N \sim \delta_X$ and not towards $\delta_N \to 1$. Moreover, the only particle that *directly* interacts with a species that we assume to be in perfect equilibrium is T via the gauge scatterings $TT \leftrightarrow AA$. Since the gauge scatterings are fast, we indeed have $\delta_T \to 1$. If N, σ and J *would* have very fast interactions with T, this *would* also result in $\delta_T \sim \delta_{N,\sigma,J} \sim 1$. However, the only fast interaction involving T is $NN \leftrightarrow TT$, which is not as fast at changing the neutrino abundance for as $\sigma \leftrightarrow NN$ and $NN \leftrightarrow JJ$ (at least for $g_N \leq 0.7$), see Fig. 6.16. In other words, the neutrino abundance strives towards the same abundance as the particles it dominantly interacts with, and given that σ and J are not perfectly in equilibrium either, this clearly implies $\Delta_{N_A}(z_N)|_{z_N < z_\rho^A} \gg \Delta_{N_{\hat{A}}}(z_N)|_{z_N < z_S^{\hat{A}}}$ for $g_N \leq 0.7$. Moreover, recall that the evo-

lution of σ is governed by interactions that are *not* Boltzmann suppressed, while the corresponding interactions that determine the evolution of N and J *are* Boltzmann suppressed. Thus, if $\tilde{m}$ and g_N are so small that neutrinos are not thermalized via $N \leftrightarrow LH$ when the Boltzmann suppression sets in, fast σ-decays produce an overabundance of N and J, i.e. $\delta_{N_A} > 1$, for $z_N < z_\rho^A$, see e.g. Fig. 6.18.
In contrast, for $g_N > 0.7$, neutrino interactions with T are sufficiently fast, forcing neutrinos more efficiently into equilibrium and hence $\Delta_{N_A}(z_N)|_{z_N<z_\rho^A} \gtrsim \Delta_{N_{\hat{A}}}(z_N)|_{z_N<z_S^{\hat{A}}}$. Moreover, $\sigma \leftrightarrow NN$ is kinematically forbidden and $\gamma_{\sigma,JJ}/n_J^{\mathrm{eq}}\mathcal{H}$ is fast up to large z_N, hence σ decays do not create notable overabundances of N or J.
Next, let us consider the transition from the scatter to the decay regime. From (6.3.18), it is evident that *when* the transition from the scatter to the decay regime takes place in case A depends strongly on the abundances of N, σ, J and T. This is in contrast to case $\hat{A}$, where we could predict z_S based on the thermal rates alone. From Fig. 6.12, we find that overall, z_ρ^A behaves similarly to z_S as $\tilde{m}$ and g_N change, i.e. z_ρ^A decreases with $\tilde{m}$ and increases with g_N. Yet, we find two striking qualitative differences. First, z_ρ^A drops faster with $\tilde{m}$ compared to z_S and secondly, the peak at $g_N \sim 0.7$ present in z_S washes out in z_ρ^A once $\tilde{m} \gtrsim 10^{-3}\,\mathrm{eV}$. In order to roughly quantify this effect, recall that the transition from the scatter to the decay regime in case A occurs at

$$\left|\frac{\mathrm{d}}{\mathrm{d}z_N} Y_{N_A}^{scatter}(z_N = z_\rho^A)\right| = \left|\frac{\mathrm{d}}{\mathrm{d}z_N} Y_{N_A}^{decay}(z_N = z_\rho^A)\right| . \tag{6.3.22}$$

If neutrinos are close to equilibrium at z_ρ^A, we can use

$$\delta_{N_A} = 1 + \epsilon\,, \qquad \epsilon \ll 1\,, \tag{6.3.23}$$

and rewrite (6.3.22) as

$$\gamma_D \approx 4\gamma_S + \frac{2\rho_A}{\epsilon}\,. \tag{6.3.24}$$

Thus, we can interpret $2\rho_A/\epsilon$ as a modification of the summed scattering rate γ_S which arises due to $\delta_{T,\sigma,J} \neq 1$. Since $2\rho_A/\epsilon < 0$, we conclude that the transition from the scatter to the decay regime roughly takes place at

$$\gamma_D \lesssim 4\gamma_S\,, \tag{6.3.25}$$

and hence $z_\rho^A \lesssim z_S$. To put it differently, $\delta_{T,\sigma,J} \neq 1$ in case A effectively slows down the scattering rates involving N, σ, J and T and therefore allows lepton number violating neutrino decays to take over for smaller z_N.
Let us now discuss the decay regime. For $g_N < 0.7$ we find, as expected, that $\Delta_{N_A} \to \Delta_{N_{\hat{A}}}$ for $z_N \gg z_\rho^A, z_S^{\hat{A}}$, i.e. the neutrino evolution both in cases A and $\hat{A}$ is determined by γ_D while the scattering processes are irrelevant. For $g_N \geq 0.7$ on the other hand, Δ_{N_A} starts to deviate from $\Delta_{N_{\hat{A}}}$ for $z_N \to 20$. This behavior is especially prominent for $\tilde{m} = 10^{-1}\,\mathrm{eV}$ and can be traced back to effects from the evolution of T. At $z_N \sim 10 g_N$, T begins to freeze out, resulting in $\delta_{T_A} > \delta_{N_A}$, hence enhancing the neutrino abundance. Thus, although neutrino decays dominate the neutrino evolution, scattering processes involving

T are not completely negligible.

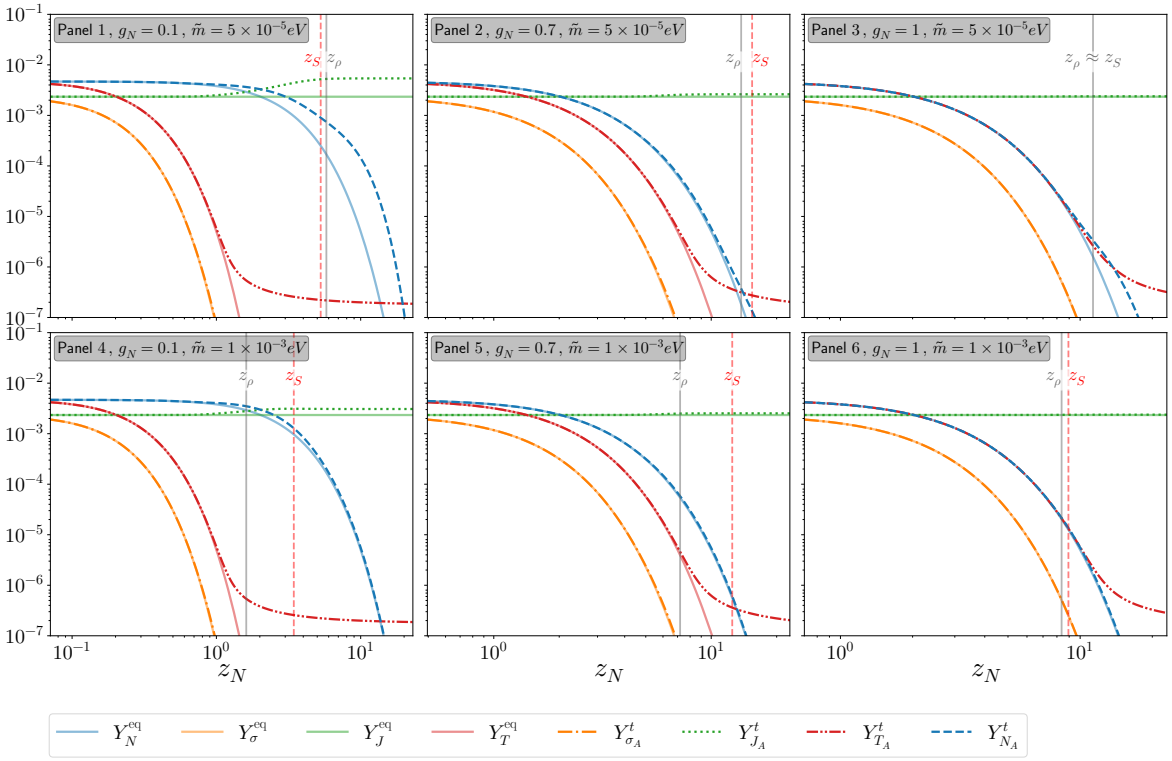

Figure 6.18: Evolution of the abundances of N, σ, T and J for $g_N = [0.1, 0.7, 1]$ and $\tilde{m} = [5 \times 10^{-5}, 10^{-2}]$eV. In the right figure, we have $g_N = g_T$ and therefore $Y_N^{\text{eq}} = Y_T^{\text{eq}}$. Note that the lower limits of the z_N-range are given by z_I and hence depend on g_N. For small z_N, scattering proccesses and (inverse) σ-decays keep N, T, σ and J close to equilibrium. At $z_T = z_N/g_N \sim 10$, the gauge interactions of T decouple and consequently, T begins to freeze out, independently from $\tilde{m}$. On the other hand, σ never sizably deviates from equilibrium, irrespective of g_N and $\tilde{m}$. In contrast, the evolutions of N and J are severely affected by the values of g_N and $\tilde{m}$. If g_N and $\tilde{m}$ are small, see for example panel 1, their abundances overshoot the equilibrium abundances. Moreover, while the neutrino abundance drops due to lepton number violating neutrino decays, the Majoron abundance freezes out once the interactions with N and σ decouple. For larger g_N and $\tilde{m}$, see e.g. panel 6, neither the neutrino- nor the Majoron abundance significantly deviates from equilibrium.

Efficiency

In Fig. 6.20, we show $\eta_{A,\hat{A},VL}(z_N)$ for $g_N = [0.1, 0.7, 1]$ and $\tilde{m} = [5 \times 10^{-5}, 10^{-2}]$eV. If the initial abundances of $Y_{N,T,\sigma,J}$ vanish, we find analogously to the simplified scenario that neutrinos are mainly produced via scattering processes involving T, σ and J while only a fraction of neutrinos stems from lepton number violating inverse decays and quark scatterings. In comparison with the simplified scenario though, the portion of neutrinos produced from lepton number violating interactions is slightly larger since T, σ and J

initially vanish as well. Hence, the for $z_N \gtrsim z_I$, the efficiency $\eta_A^z(z_N)$ is negative and changes sign slightly later than $\eta_{\hat{A}}^z(z_N)$, but sill faster than η_{VL}^z. For simplicity, we therefore restrict the following discussion to η_A^t.

To begin, let us first consider the regime where $\tilde{m}$ is sufficiently small to render WO effects insignificant. Hence, we can write the Boltzmann equations for the efficiency in the scatter and decay regime, respectively, as

$$\frac{\mathrm{d}}{\mathrm{d}z_N}\eta_A = \frac{1}{s\mathcal{H}z_N}(\delta_{N_A}-1)\gamma_D\frac{1}{Y_N^0} \approx \begin{cases} -\frac{1}{Y_N^0}\frac{\gamma_D}{4\gamma_S}\left(\frac{\mathrm{d}}{\mathrm{d}z_N}Y_{N_A}+\frac{2\rho_A}{s\mathcal{H}z_N}\right), & z_N < z_\rho^A\,, \\ -\frac{1}{Y_N^0}\frac{\mathrm{d}}{\mathrm{d}z_N}Y_{N_A}\,, & z_N > z_\rho^A\,, \end{cases} \tag{6.3.26}$$

yielding the final efficiency as

$$\eta_A(\infty) = \eta_A(z_\rho^A) + \frac{1}{Y_N^0}Y_{N_A}(z_\rho^A)\,. \tag{6.3.27}$$

From (6.3.26), it is apparent that the same suppresion factor, $\gamma_D/4\gamma_S$, as in the simplified scenario reappears. However, as discussed previously, neutrinos deviate more from equilibrium than in the simplified scenario, i.e.

$$\left|\frac{dY_{N_A}}{dz_N}+\frac{2\rho_A}{s\mathcal{H}z_N}\right| \gg \left|\frac{dY_{N_{\hat{A}}}}{dz_N}\right|\,, \tag{6.3.28}$$

which counteracts the suppression. Consequently, $\eta_A(z_N)$ can become comparably sizable already in the scatter regime, unlike the efficiency in the simplified scenario which is created mainly around $z_S^{\hat{A}}$. This is prominent in Fig. 6.20 (panels 1–3) where we find $\eta_A\left(z_\rho^A\right) \gg \eta_{\hat{A}}\left(z_S^{\hat{A}}\right)$ with $z_\rho^A \sim z_S^{\hat{A}}$. Recalling that we had $z_\rho^A \lesssim z_S^{\hat{A}}$ for the most part of the parameter space, we note that the efficiency η_A is additionally enhanced compared to $\eta_{\hat{A}}$ due to $Y_{N_A}\left(z_\rho^A\right) > Y_{N_{\hat{A}}}\left(z_\rho^A\right)$. In other words, in the simplified scenario, fewer neutrinos that are capable of lepton number violating decays exist at $z_S^{\hat{A}}$ than to z_ρ^A. Nevertheless, note that even though the suppression of the efficiency in the scatter regime is less pronounced in case A compared to the simplified scenario $\hat{A}$, the largest portion of the efficiency $\eta_A(z_N)$ is produced when the transition to the scatter regime takes place around z_ρ^A.

Considering the final efficiencies, see Fig. 6.5, we find that apart from the quantitative differences, η_A behaves similarly to $\eta_{\hat{A}}$ and increases with $\tilde{m}$ until a maximum is reached at $\tilde{m}_{\mathrm{max}}^A$. Afterwards, WO effects become relevant and hence $\eta_A(\tilde{m}) \sim 1/\tilde{m}$. Moreover, since the efficiency η_A is most effectively created around z_ρ^A, we find $\eta_A \sim 1/z_\rho^A$. Note that even though η_A is less suppressed in the scatter regime than $\eta_{\hat{A}}$, we find similarly to the simplified scenario that the suppression is sufficient to render WO effects irrelevant until the decay regime is reached at z_ρ^A, see Fig. 6.19 (panels 7-9), and thus $\tilde{m}_{\mathrm{max}}^A \sim z_\rho^A$, see Fig. 6.19.

Before we proceed, let us shortly discuss the efficiency in the limiting case where $g_N \to 1$ and $\tilde{m} \to 10^{-1}\,\mathrm{eV}$. As discussed in Sec. 6.3.1, the final efficiency η_A slightly exceeds the efficiency η^{WO} that is usually obtained when WO effects are strong. This can be traced back to two effects. The suppression of $\eta_A(z_N)$ in the scatter regime is maximal

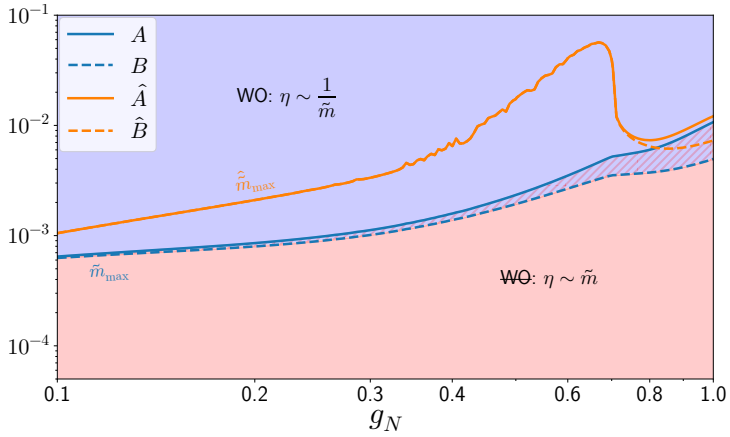

Figure 6.19: Comparison of $\tilde{m}_{\max}$ and $\hat{\tilde{m}}_{\max}$ for cases $\hat{A}, A$ (solid) and $\hat{B}, B$ (dashed). The red shading indicates the region where the final efficiency in cases A, B is determined by scattering processes and neutrino decays and hence proportional to $\tilde{m}$. The final efficiency in the blue region is determined by WO processes, resulting in $\eta_{A,B} \sim 1/\tilde{m}$. The hatched region corresponds to the WO regime in case A and to the ~~WO~~ regime in case B. While the strong suppression of the efficiency in the simplified scenario results in a peak around $g_N \sim 0.7$ in $\hat{\tilde{m}}_{\max}$, we can easily see that due to the weaker suppression in cases A, B, this peak is absent in $\tilde{m}^{A,B}_{\max}$. Nevertheless, similarly to $\hat{\tilde{m}}_{\max} \sim z_S$, we find $\tilde{m}_{\max} \sim z_\rho$ which indicates that even though the suppression of the efficiencies in cases A, B is weaker compared to the simplified scenario, the efficiency is still mainly created around z_ρ and hence WO is only effective for $z_N > z^A_\rho$. Next, note that the absence of interactions with T in case B renders the scattering processes less efficient at thermalizing the neutrinos compared to case A, resulting in $\tilde{m}^B_{\max} < \tilde{m}^A_{\max}$.

for $g_N \sim 1$ and WO is only effective for $\tilde{m} \gtrsim 10^{-2}\,\text{eV}$, see Fig. 6.19, and even in the limit $\tilde{m} \to 10^{-1}\,\text{eV}$, WO effects actually diminish the efficiency only for $z_N \gtrsim 6$ (see Fig. 6.20, panel 9). However, at $z_N \sim 10$, T starts to freeze out and as discussed previously, this slightly enhances the neutrino abundance and therefore counteracts WO effects. Thus, even when WO effects are strong, the evolution of the efficiency is not entirely driven by VL interactions.

To summarize this discussion, we find that the efficiency in case A is enhanced compared to case $\hat{A}$ where $\delta_{T,\sigma,J} = 1$. Accounting for $\delta_{T,\sigma,J} \neq 1$ has the effect that neutrinos can deviate more from equilibrium, enhancing the efficiency in the scatter regime. Additionally, the transition from the scatter to the decay regime tends to occur at smaller z_N compared to the simplified scenario, and hence before the neutrino abundance is diminished due to Boltzmann suppression.

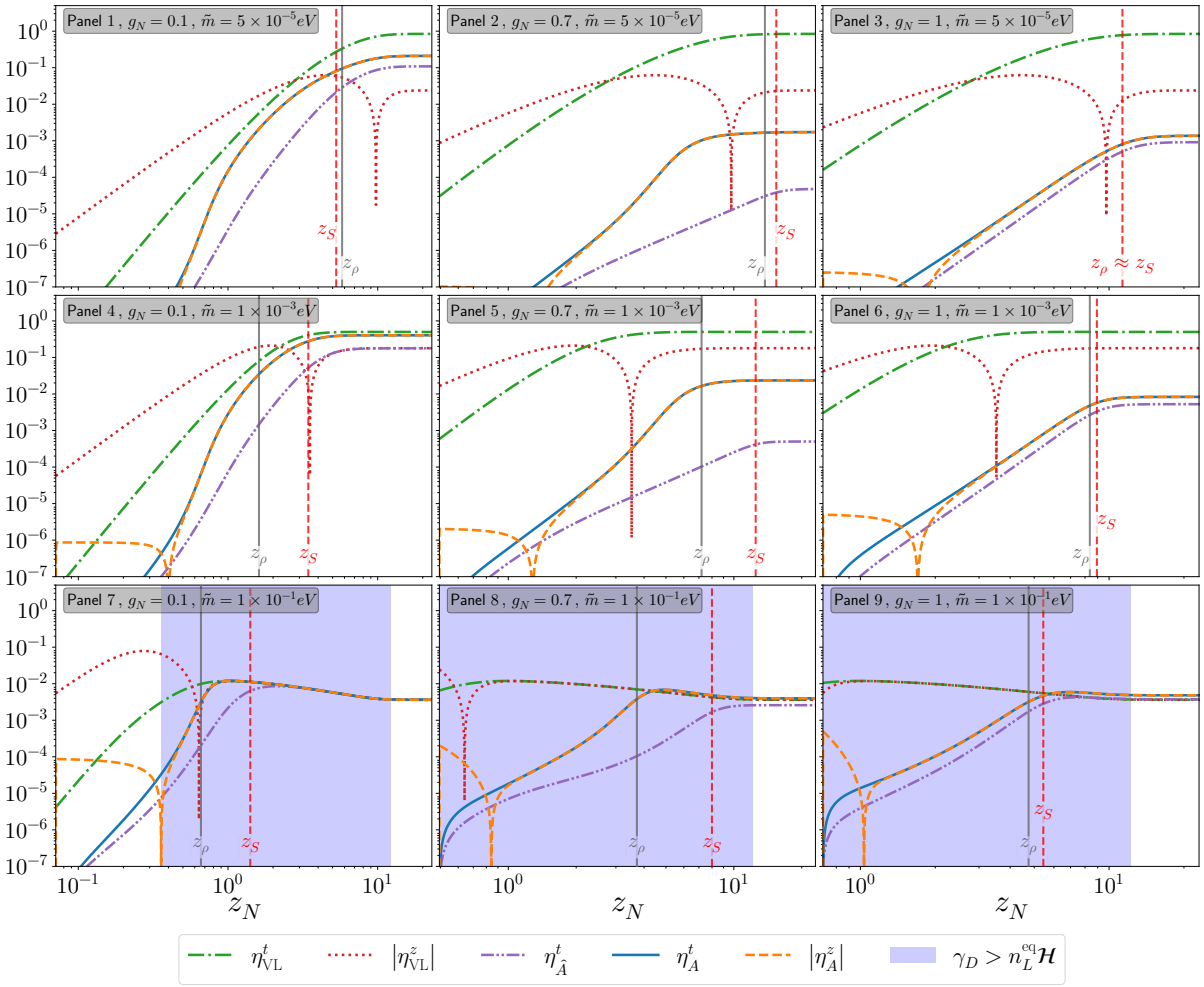

Figure 6.20: Efficiencies $\eta_A^{t,z}$, $\eta_{\hat{A}}^t$ and $\eta_{\rm VL}^{t,z}$ as functions of z_N. The blue region indicates where inverse decays are in equilibrium, the solid vertical line denotes z_ρ and the dashed vertical line denotes z_S. Note that the lower limits of the z_N-range are given by z_I and hence depend on g_N. As the efficiency in VL does not depend on g_N, $\eta_{\rm VL}^t$ and $\eta_{\rm VL}^z$ are the same in each column. It is evident that the efficiency η_A^t is less suppressed in the scatter regime compared to the efficiency in the simplified scenatio $\eta_{\hat{A}}^t$. Moreover, in panels 7–9, it is apparent that WO processes diminish η_A notably only once the transition to the scatter regime takes place, i.e. once $z_N \gtrsim z_\rho^A$. Considering η_A^z, the neutrino production occurs mainly via lepton number violating inverse decays and quark scatterings, in contrast to e.g. case $\hat{A}$.

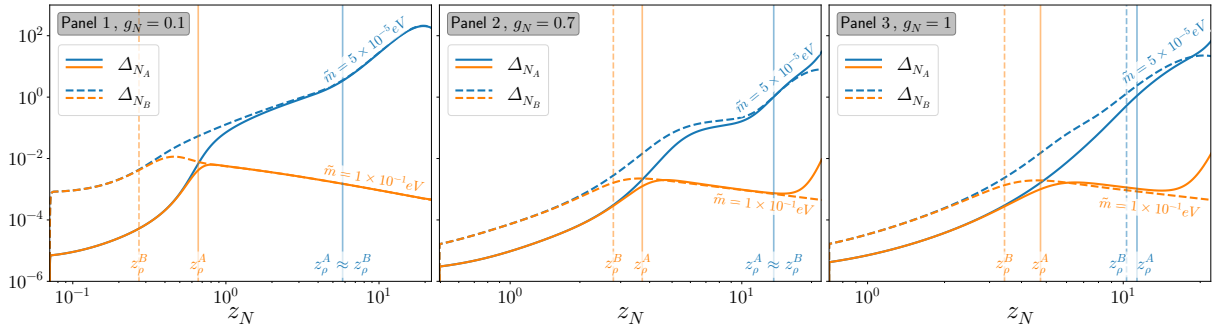

Figure 6.21: Evolution of Δ_{N_A} (solid lines) and Δ_{N_B} (dashed lines) for different values of $\tilde{m} = [5 \times 10^{-5}, 10^{-1}]$eV and $g_N = 0.1$ (panel 1), $g_N = 0.7$ (panel 2), $g_N = 1$ (panel 3). The vertical solid lines indicate z_ρ^A while the vertical dashed lines belong to z_ρ^B. Note that the lower limits of the z_N-range are given by z_I and hence depend on g_N. Due to the absence of interactions with T in case B, the neutrino abundance in the scatter regime deviates more from the equilibrium abundance compared to case A where $NN \leftrightarrow TT$ scatterings are fast.

6.3.4 Case B

6.3.4.1 Thermal Rates

In Fig. 6.16, we show the most relevant thermal rates for the evolution of the abundances of N, σ, T and J. In contrast to case A, the gauge interactions of T are fast throughout the whole leptogenesis era and in particular, T does not freeze out and remains in equilibrium. Moreover, the thermal rate $\gamma^B_{NN,TT}$ is negligibly small while the remaining thermal rates are independent from g_T and thus identical to case A. Hence, we can conclude that the evolutions of N, σ and J are decoupled from the evolution of T.

6.3.4.2 Discussion of case B_t

With the results from the previous section in mind, the discussion of leptogenesis in case B_t is straightforward. It is evident that the main difference between case A and case B_t is the absence of sizable interactions of N, σ, J with the thermalized triplet in the latter case. Thus, as can also be seen in Fig. 6.21, the neutrino abundance in case B_t in the scatter regime deviates more from equilibrium than in case A. Moreover, the overall magnitude of neutrino scatterings is smaller in case B_t, translating to $z_\rho^B \lesssim z_\rho^A$. It is then clear that η_B^t should slightly exceed η_A, in agreement with Fig. 6.6. Note that in contrast to case A, T does not begin to freeze out around $z_N \sim 10$, and hence the enhancement of the efficiency for $g_N \geq 0.7$ and $z_N \to 20$ is absent in case B. Finally, since $\eta_B^t(z_N) \gtrsim \eta_A^t(z_N)$, WO effects become relevant for smaller $\tilde{m}$ compared to case A, hence $\tilde{m}^B_{\max} < \tilde{m}^A_{\max}$, see Fig. 6.19.

6.3.4.3 Discussion of case B_z

Abundances

Recall that in the previously discussed scenarios, the initial abundances of N, T, σ and J are irrelevant as fast scatterings almost immediatly thermalize them, even if the initial abundances vanish. In case B_z, the situation is different. The triplet T has fast gauge interactions and is therefore always near equilibrium, $\delta_T \sim 1$. However, N, σ and J do not have sizable interactions with T and consequently, triplet scatterings do not populate the plasma with N, σ and J, in contrast to case A. Instead, the Boltzmann equation for the neutrino evolution at $z_N \sim z_I$ is the same as in VL, see the discussion in Sec. 4.3.3.3, i.e.

$$s\mathcal{H}z_N \frac{\mathrm{d}}{\mathrm{d}z_N} Y^z_{N_{B,VL}} \approx \gamma_D \,, \qquad \delta^z_{N_B} \ll 1 \,, \tag{6.3.29}$$

and inverse decays populate the plasma with neutrinos. These neutrinos have fast interactions with σ and J, i.e. once a non-vanishing neutrino abundance exists, neutrino scatterings populate the plasma with σ and J and the Boltzmann equation in case B_z now becomes

$$s\mathcal{H}z_N \frac{\mathrm{d}}{\mathrm{d}z_N} Y^z_{N_B} \approx \gamma_D + \kappa \,, \qquad \delta^z_{N_B} \ll 1 \,. \tag{6.3.30}$$

Here, we defined

$$\kappa \equiv -2(\overline{\delta_N}^2 - \overline{\delta_J}^2)\gamma_{NNJJ} - 2(\overline{\delta_N}^2 - \overline{\delta_\sigma}^2)\gamma_{NN\sigma\sigma} - 2(\overline{\delta_N}^2 - \overline{\delta_J\delta_\sigma})\gamma_{NN\sigma J} + 2\overline{\delta_{sub}}\gamma_{\sigma,NN} \,, \tag{6.3.31}$$

with $\overline{\delta_i} \equiv \delta^z_{i_B}$. The sign of κ is crucial for the neutrino evolution. Initially, when $\delta_\sigma \sim \delta_J \sim 0$, κ is clearly negative and hence diminishes the neutrino abundance. If κ stays negative, this implies that it takes the neutrinos longer to reach an equilibrium abundance compared to VL. On the other hand, if κ changes sign at some point, the plasma is populated with neutrinos via σ- and J-scatterings, hence neutrinos reach equilibrium faster. In order to make this more transparent, let us first define that a species i reaches its equilibrium abundance at z^i_{eq}, i.e. when

$$Y^z_{i_B}(z^i_{\mathrm{eq}}) = Y^{\mathrm{eq}}_i(z^i_{\mathrm{eq}}) \tag{6.3.32}$$

with

$$Y^z_{i_B}(z_N) \begin{cases} < Y^{\mathrm{eq}}_i(z_N) \,, & z_N < z^i_{\mathrm{eq}} \,, \\ > Y^{\mathrm{eq}}_i(z_N) \,, & z_N > z^i_{\mathrm{eq}} \,, \end{cases} \tag{6.3.33}$$

holds. Moreover, let us define $(g^{IA}_N, \tilde{m}^{IA})$ so that

$$z^N_{\mathrm{eq}}(\tilde{m}^{IA}, g^{IA}_N) = 1 \,, \tag{6.3.34}$$

with

$$z^N_{\mathrm{eq}}(\tilde{m} < \tilde{m}^{IA}, g_N < g^{IA}_N) > 1 \,, \tag{6.3.35}$$

$$z_{\rm eq}^{N}(\tilde{m} > \tilde{m}^{IA}, g_N > g_N^{IA}) < 1\,. \tag{6.3.36}$$

In Fig. 6.22, we show $z_{\rm eq}^{(N,\sigma,J)}$ in terms of density plots in the $g_N - \tilde{m}$ plane where the white line corresponds to $\tilde{m}^{IA}(g_N)$. In the green region, the respective particle reaches equilibrium faster than $z_N = 1$. This is sufficiently fast in the context of leptogenesis to consider it as instant. The grey regions indicate that the respective particle has not reached equilibrium until $z_N = 10$.[7] It is evident that $\tilde{m}^{IA}(g_N)$ not only separates the parameter space into two region where neutrinos reach either equilibrium slowly or fast but that the same separation holds for the thermalization of σ and J. Recalling Fig. 6.7, is is also clear that the region where the particles do not reach equilibrium until $z_N = 1$ coincides with the IA region.

Let us now discuss how different values of $\tilde{m}$ and g_N affect the dynamics with which the plasma is populated with N, σ and J in greater detail. For convenience, we show $z_{\rm eq}^{N}(g_N)$ and $z_{\rm eq}^{N}(\tilde{m})$ in Fig. 6.23 for $g_N = [0.1, 0.2, 0.24]$ and $\tilde{m} = [5\times10^{-5}, 5\times10^{-4}, 2.5\times10^{-3}]$eV, respectively, while in Fig. 6.24, we show $Y^{z}_{(N,\sigma,J)_B}(z_N)$. First, let us focus on $g_N = 0.1$ and $\tilde{m} = 5\times10^{-5}\,$eV. From Fig. 6.24 (panel 1), it is evident that the plasma is populated with neutrinos very slowly, owing to the smallness of γ_D. Consequently, the scatterings in κ populate the plasma with σ and J slowly as well, hence diminishing the neutrino abundance. Clearly, it takes neutrinos longer to reach equilibrium than in to VL, i.e. $z_{\rm eq}^{N} > z_{\rm eq}^{\rm VL}$, and additionally, the scattering processes in κ become Boltzmann suppressed before σ and J reach their respective neutrino abundances. As $\tilde{m}$ increases, inverse decays become more efficient at populating the plasma with neutrinos and consequently, the abundances of σ and J that are produced by neutrino scatterings before κ becomes Boltzmann suppressed increase as well (see e.g. panel 4 with $\tilde{m} = 5\times10^{-4}\,$eV in Fig. 6.24). Thus, it still takes neutrinos longer to reach equilibrium than in VL. Compared to $z_{\rm eq}^{N}(\tilde{m} = 5\times10^{-5}\,{\rm eV})$ though, note that neutrinos reach equilibrium faster, hence $z_{\rm eq}^{N} \sim 1/\tilde{m}$. This lasts until $\tilde{m} \sim \tilde{m}^{IA} \sim 2.5\times10^{-3}\,$eV (panel 7 in Fig. 6.24), where the plasma is populated with neutrinos sufficiently fast so that sizable abundances of σ and J arise before Boltzmann suppression sets in. This prompts κ to change sign and hence σ and J scatterings enhance the neutrino abundance. As is apparent from Fig. 6.23, this results in a rapid drop of $z_{\rm eq}^{N}(\tilde{m})$ around $\tilde{m}^{IA}$ while $z_{\rm eq}^{\rm VL}(\tilde{m})$ continues to drop steadily. Moreover, note that for $\tilde{m} \gtrsim \tilde{m}^{IA}$, $z_{\rm eq}^{N}$ continues to appraoch z_I.

On the other hand, as g_N changes while $\tilde{m} < \tilde{m}^{IA}$, neutrinos scatter away to populate the plasma with σ and J more efficiently, but not yet fast enough to reach sizable σ and J abundances, hence it takes neutrinos longer to reach equilibrium and $z_{\rm eq}^{N} \sim g_N$, see Fig. 6.23. In comparison, $z_{\rm eq}^{\rm VL}$ does not depend on g_N and thus $z_{\rm eq}^{N} < z_{\rm eq}^{\rm VL}$. Eventually, at $g_N \sim g_N^{IA}$, neutrino scatterings are so fast at producing σ and J populations that κ changes sign. Thus, $z_{\rm eq}^{N}$ drops rapidly at $g_N \sim g_N^{IA}$ and neutrinos reach equilibrium faster than in VL.

Thus, we find that the dynamics with which the plasma is populated with N, σ and J

[7] We use this cut-off for visual purposes and stress that the exact numerical value is irrelevant. Note that since Boltzmann suppression effects are strong around $z_N \sim 10$, it is reasonable to assume that the evolutions of σ and J do not significantly affect the neutrino evolution if $z_N > 10$.

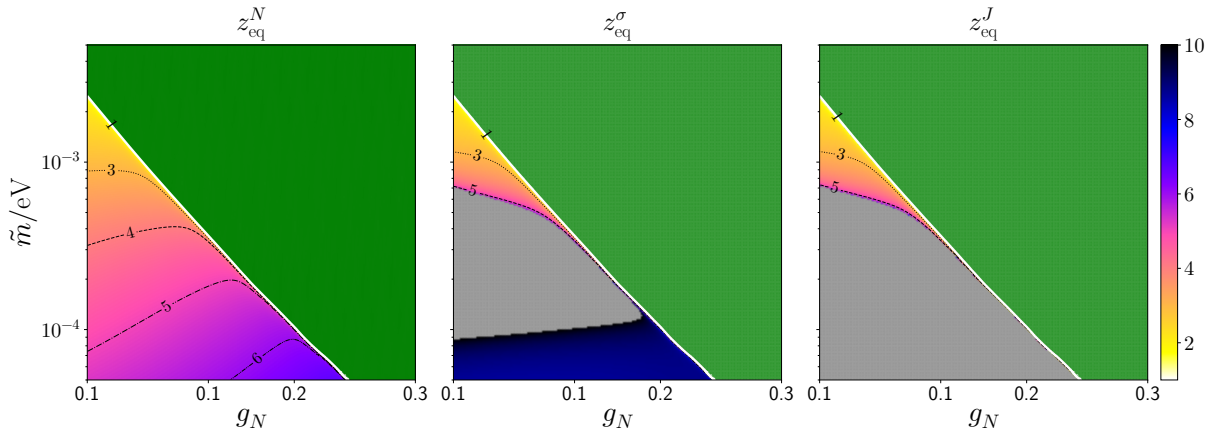

Figure 6.22: Density plots of $z_{\rm eq}^{(N,\sigma,J)}$ in the $g_N - \tilde{m}$ plane. The green regions indicate where thermalization proceeds rapidly so that $z_{\rm eq}^i \ll 1$. In the grey region, the respective particle is not thermalized until $z_N = 10$. The white lines indicate $z_{\rm eq}^i = 1$. Note that we show only a subset of the full $g_N - \tilde{m}$ plane. See text for details.

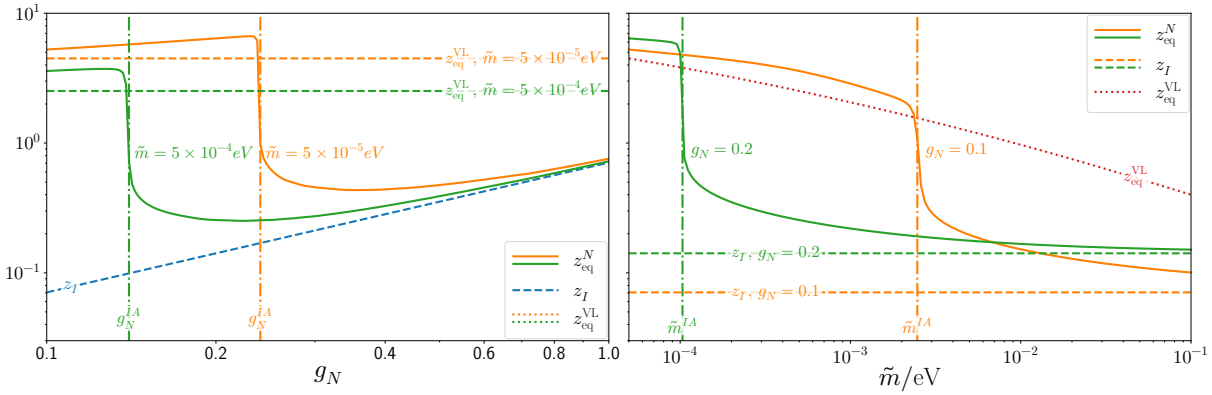

Figure 6.23: *Left:* $z_{\rm eq}^N$ as a function of g_N for $\tilde{m} = [5\times10^{-5}, 5\times10^{-4}]$eV, compared to $z_{\rm eq}^{\rm VL}$ and z_I. *Right:* $z_{\rm eq}^N$ as a function of $\tilde{m}$ for $g_N = [0.1, 0.2]$, compared to $z_{\rm eq}^{\rm VL}$ and z_I. We note that $z_{\rm eq}^{\rm VL}$ (z_I) is constant in the left (right) panel as it does not depend on g_N ($\tilde{m}$). The dash-dotted line denotes g_N^{IA} (left) and $\tilde{m}^{IA}$ (right), respectively. See text for details.

is very sensitive to the interplay between g_N and $\tilde{m}$. If $(g_N, \tilde{m}) < (g_N^{IA}, \tilde{m}^{IA})$, the scatterings involving σ and J slowly diminish the neutrino abundance. On the other hand, if $(g_N, \tilde{m}) > (g_N^{IA}, \tilde{m}^{IA})$, sizable populations of σ and J arise that in turn enhance the neutrino abundance.

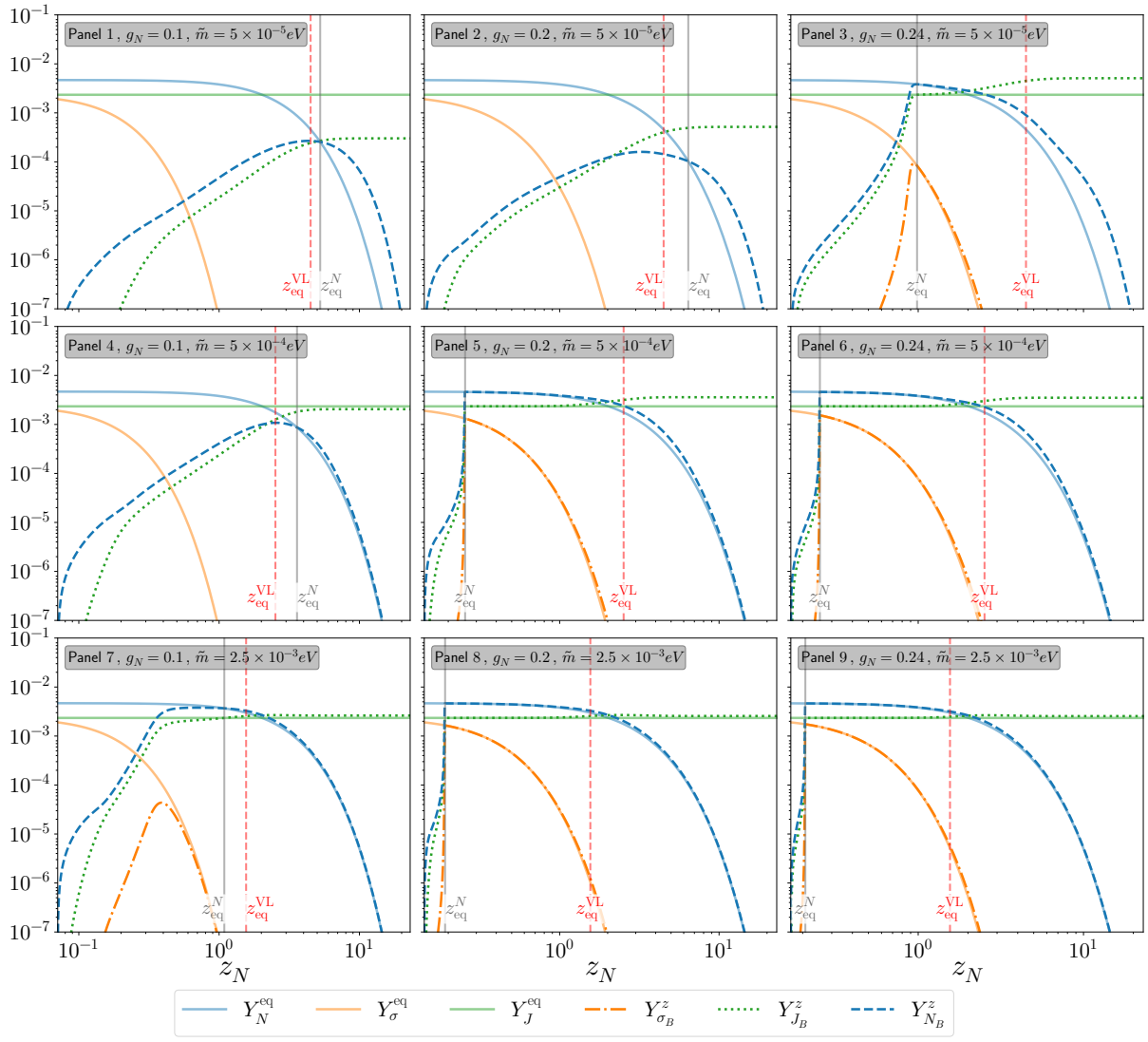

Figure 6.24: Evolution of $Y_{N,\sigma,J}(z_N)$, compared to the respective equilibrium abundances, for $g_N = [0.1, 0.2, 0.24]$ and $\tilde{m} = [5 \times 10^{-5}, 5 \times 10^{-4}, 2.5 \times 10^{-3}]$eV. The vertical solid line indicates $z_{\rm eq}^N$ while the vertical dashed line indicates $z_{\rm eq}^{\rm VL}$. We do not show Y_T as it is always close to equilibrium. Note that in panels 1, 2 and 4, Y_σ does not appear since no sizable abundances of σ are produced. The Majoron never reaches equilibrium and hence freezes in once the interactions with N and σ decouple. Comparing e.g. panels 1 and 2, it becomes apparent how slightly increasing g_N slows the neutrino thermalization down due to an enhanced scattering rate of neutrinos to Majorons. In panel 3, g_N is sufficiently sizable to render the interactions between N, σ and J strong enough to briefly thermalize them before these interactions decouple. Similarly, increasing $\tilde{m}$ enhances the neutrino production and therefore indirectly also enhances the production of σ and J, thus thermalizing them faster (see panels 2, 4 and 8).

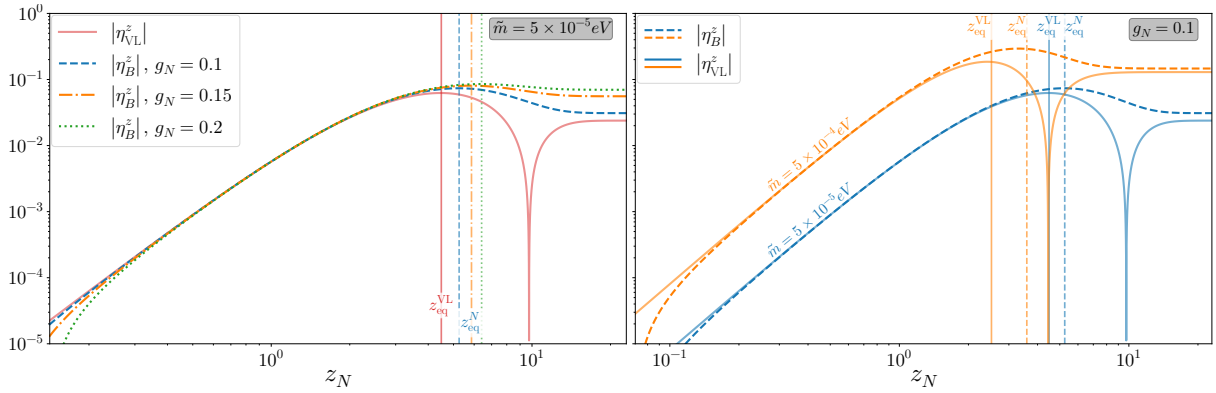

Figure 6.25: *Left:* Evolution of $|\eta^z_B|$ for $g_N = [0.1, 0.15, 0.2]$ (dashed, dash-dotted, dotted) and $\tilde{m} = 5 \times 10^{-5}$ eV, compared to $|\eta^z_{\rm VL}|$ (solid). For $z_I \ll z_N \ll \{z^N_{\rm eq}, z^{\rm VL}_{\rm eq}\}$, the evolution of the efficiency is dominated by (inverse) neutrino decays and therefore independent of g_N. The efficiencies $|\eta^z_B|(z_N)$ and $|\eta^z_{\rm VL}|(z_N)$ increase with z_N until they peak at $z^N_{\rm eq}$ and $z^{\rm VL}_{\rm eq}$, respectively. In VL, $\eta^z_{\rm VL}(z_N)$ eventually changes sign while $\eta^z_B(z_N)$ stays negative. As $z^N_{\rm eq}$ increases with g_N, we have $\eta^z_B(z^N_{\rm eq})|_{g_N=0.1} < \eta^z_B(z^N_{\rm eq})|_{g_N=0.15} < \eta^z_B(z^N_{\rm eq})|_{g_N=0.2}$. *Right:* Evolution of $|\eta^z_B|$ (solid) for $g_N = 0.1$ and $\tilde{m} = [5 \times 10^{-5}, 5 \times 10^{-4}]$eV, compared to $|\eta^z_{\rm VL}|$ (dashed). For $z_N \ll \{z^N_{\rm eq}, z^{\rm VL}_{\rm eq}\}$, the evolution of the efficiency is determined by $\gamma_D \sim \tilde{m}$, i.e. a larger $\tilde{m}$ enhances the negative part of η^z_B and $\eta^z_{\rm VL}$ produced in $z_N \ll z^N_{\rm eq}$ and $z_N \ll z^{\rm VL}_{\rm eq}$, respectively. As neutrinos are thermalized faster, $z^N_{\rm eq}$ and $z^{\rm VL}_{\rm eq}$ decrease with $\tilde{m}$.

Efficiency

From the discussion in Sec. 4.3.3.3, recall that in the scenario of an initially vanishing neutrino abundance, the final efficiency $\eta^z_{\rm VL}$ can be divided into a negative efficiency that is produced until $z^{\rm VL}_{\rm eq}$ and a positive efficiency produced afterwards. Thus, we can anticpate that the value of $z^N_{\rm eq}$ in leptogenesis in the MTM will affect the evolution of the efficiency. In the IA regime $(g_N, \tilde{m}) > (g^{IA}_N, \tilde{m}^{IA})$, it is clear that the evolution of the efficiency is similar to case B_t and therefore, the relevant scenario to consider is $(g_N, \tilde{m}) < (g^{IA}_N, \tilde{m}^{IA})$. In this regime, $\tilde{m}$ is small, allowing us to neglect WO effects in the Boltzmann equation for the efficiency,

$$s\mathcal{H}z_N \frac{\mathrm{d}}{\mathrm{d}z_N}\eta^z_B \approx \frac{1}{Y^0_N}(\overline{\delta_N} - 1)\gamma_D \,. \tag{6.3.37}$$

As in VL, see Sec. 4.3.3.3, the inverse decays that populate the plasma with neutrinos also generate a negative efficiency,

$$s\mathcal{H}z_N \frac{\mathrm{d}}{\mathrm{d}z_N}\eta^z_B \overset{z_N \ll z^N_{\rm eq}}{\approx} -\frac{1}{Y^0_N}\gamma_D \tag{6.3.38}$$

so that

$$\eta^-_B \equiv \eta(z^N_{\rm eq}) < 0 \,. \tag{6.3.39}$$

Thus, while $z_N \ll \{z_{\rm eq}^N, z_{\rm eq}^{\rm VL}\}$, the efficiency $\eta_B^z(z_N)$ evolves in the same way as $\eta_{\rm VL}^z(z_N)$ and is independent from g_N, as is also highlighted in Fig. 6.25. Eventually, neutrinos reach equilibrium and for $z_N > z_{\rm eq}^N$, a positive efficiency is produced with

$$\eta_B^+ \equiv \int_{z_{\rm eq}^N}^{\infty} {\rm d}z_N \, \frac{1}{Y_N^0}(\overline{\delta_N} - 1)\gamma_D \frac{1}{s\mathcal{H}z_N} > 0\,. \tag{6.3.40}$$

If we further assume that for $z_N > z_{\rm eq}^N$, neutrino scatterings to σ and J are already irrelevant due to Boltzmann suppression, (inverse) decays $N \leftrightarrow LH$ are the only relevant processes and we find

$$\eta_B^+ \eqsim \frac{1}{Y_N^0} Y_{N_B}^z(z_{\rm eq}^N)\,, \tag{6.3.41}$$

and can express the final efficiency as

$$\eta_B^z(z_{\rm eq}^N(\tilde{m}, g_N), \tilde{m}, g_N) = \eta_B^+(z_{\rm eq}^N(\tilde{m}, g_N), \tilde{m}, g_N) + \eta_B^-(z_{\rm eq}^N(\tilde{m}, g_N), \tilde{m}, g_N)\,. \tag{6.3.42}$$

Moreover, recall from Fig. 6.7 that η_B^z is negative for certain parts of the parameter space which implies $|\eta^-| > \eta^+$. For the following discussion, it is convenient to define that η_B^z changes sign at $(\tilde{m} =: \tilde{m}^{\pm}, g_N =: g_N^{\pm})$, i.e.

$$\eta_B^+(\tilde{m}^{\pm}, g_N^{\pm}) = |\eta_B^-(\tilde{m}^{\pm}, g_N^{\pm})| \tag{6.3.43}$$

so that

$$\eta_B^z(\tilde{m}, g_N) < 0\,, \quad (\tilde{m}, g_N) < (\tilde{m}^{\pm}, g_N^{\pm})\,, \tag{6.3.44}$$

$$\eta_B^z(\tilde{m}, g_N) > 0\,, \quad (\tilde{m}, g_N) > (\tilde{m}^{\pm}, g_N^{\pm})\,. \tag{6.3.45}$$

In order to discuss how η_B^z depends on $z_{\rm eq}^N, \tilde{m}$ and g_N in greater detail, we show $|\eta_B^-|, \eta_B^+$ and η_B^z as functions of g_N (left) and $\tilde{m}$ (right) with $\tilde{m} = 5 \times 10^{-5}\,{\rm eV}$ and $g_N = 0.1$, respectively, in Fig 6.26. Note that in the blue regions, the initial conditions are relevant for the final efficiency, while in the red regions, the initial conditions are irrelevant for the final efficiency.

In the left panel, it is evident that $|\eta_B^z|$ changes sign at $g_N^{\pm} \sim g_N^{IA}$, hence the blue region corresponds not only to the IA regime but also to a negative final efficiency, $\eta_B^z < 0$. Moreover, from (6.3.38), it is clear that $|\eta_B^-(g_N)| \sim z_{\rm eq}^N(g_N)$ and hence $|\eta_B^-| \sim g_N$. On the other hand, the Boltzmann suppression of the neutrino abundance for $z_N > 1$ implies that

$$Y_{N_B}^z(z_{\rm eq}^N) \sim {\rm e}^{-z_{\rm eq}^N}\,, \tag{6.3.46}$$

and thus $\eta_B^+ \sim 1/z_{\rm eq}^N(g_N) \sim 1/g_N$. Thus, as g_N increases, the absolute value of the negative efficiency increases while the positive contribution decreases. Overall, this implies that η_B^z decreases with g_N or, since η_B^z is negative, $|\eta_B^z| \sim g_N$. Once $g_N \sim g_N^{IA} \sim g_N^{\pm}$ is reached, neutrinos reach equilibrium so quickly that the initial abundances are rendered irrelevant and the contribution from η_B^- becomes insignificant. Hence, η_B^z changes sign, resulting in $\eta_B^z \sim \eta_B^+ > 0$.

Concerning the right panel of Fig. 6.26, we find that $\tilde{m}^{\pm} < \tilde{m}^{IA}$, i.e. η_B^z changes sign

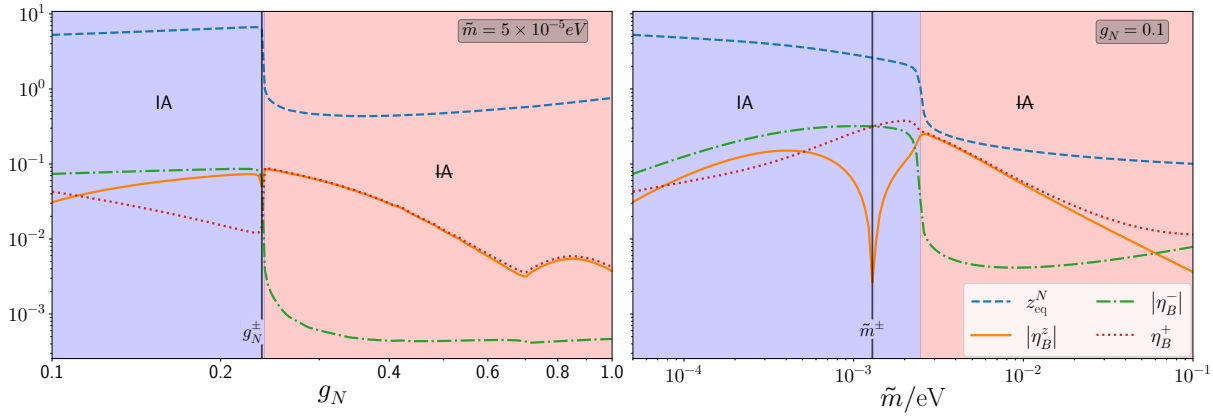

Figure 6.26: *Left:* $|\eta_B^z|$, $|\eta_B^-|$, η_B^+ and $z_{\rm eq}^N$ as functions of g_N with $\tilde{m} = 5 \times 10^{-5}\,$eV. In the blue region, the final efficiency depends on the initial abundances while in the red region, the final efficiency is independent from the initial abundances. The vertical line denotes $g_N^{\pm}$. *Right:* $|\eta_B^z|$, $|\eta_B^-|$, η_B^+ and $z_{\rm eq}^N$ as functions of $\tilde{m}$ with $g_N = 0.1$. In the blue region, the final efficiency depends on the initial abundances while in the red region, the final efficiency is independent from the initial abundances. The vertical line denotes $\tilde{m}^{\pm}$. Note that $|\eta_B^-|$ begins to increase again once $\tilde{m} \gtrsim 10^{-2}\,$eV holds. This is due to washout processes reducing the efficiency and independent from the scattering processes in the MTM.

while the initial conditions are still relevant. Moreover, from (6.3.38), it is evident that the neutrino production via inverse decays proceeds faster for larger $\tilde{m}$ and therefore $|\eta_B^-| \sim 1/z_{\rm eq}^N(\tilde{m}) \sim \tilde{m}$. This implies in turn that the Boltzmann suppression of the neutrino abundance at $z_{\rm eq}^N(\tilde{m})$ increases with $\tilde{m}$ and hence $\eta_B^+ \sim z_{\rm eq}^N(\tilde{m}) \sim 1/\tilde{m}$. Thus, both $|\eta_B^-|$ and η_B^+ increase with $\tilde{m}$. However, $\eta_B^+(\tilde{m})$ eventually increases faster and approaches $|\eta_B^-|$ before taking over. Thus, the transition from $\eta_B^z < 0$ to $\eta_B^z > 0$ is not as rapid as in the left panel of Fig. 6.26 and results in a sizable $\tilde{m}$ range around $\tilde{m}^{\pm}$ where the final efficiency almost vanishes. The final efficiency becomes only sizable once $|\eta_B^-|$ drops around $\tilde{m}^{IA}$ when neutrino thermalization becomes fast, resulting in $\eta_B^z \sim \eta_B^+ > 0$. Thus, the region around $\tilde{m}^{\pm}$ where η_B^z almost vanishes depends crucially on the difference between $\tilde{m}^{IA}$ and $\tilde{m}^{\pm}$ which in turn depends on g_N. Since η_B^+ decreases with g_N faster than $|\eta_B^-|$ increases, a slight increase of g_N compared to $g_N = 0.1$ diminishes η_B^+ compared to $|\eta_B^-|$ and hence moves $\tilde{m}^{\pm}$ closer to $\tilde{m}^{IA}$. Note that the gap closes roughly at $g_N \sim 0.15$ so that $\tilde{m}^{\pm}(0.15 \gtrsim g_N^{IA}) \approx \tilde{m}^{IA}(0.15 \gtrsim g_N^{IA})$.

To summarize, we find that the interactions of neutrinos with σ and J can either significantly slow down how fast neutrinos reach equilibrium or enhance it, depending on the values of $\tilde{m}$ and g_N. If $z_{\rm eq}^N$ is comparably large, the amount of neutrinos that can produce a positive efficiency for $z_N \gtrsim z_{\rm eq}^N$ is severely diminished, so that either the final efficiency remains negative or is even approximately cancelled. Thus, the final efficiency in the parameter space where both $\tilde{m}$ and g_N are small depends significantly on the initial abundances and the interplay between N, σ and J.

6.3.5 Cases C, D

From the comparison of cases A and B, it is easy to understand of the behavior of the efficiency in case C where $g_N = \lambda_\sigma = 1$ and $g_T \in [10^{-7}, 1]$. As g_T decreases, the magnitude of the thermal rate $\gamma_{NN,TT}$ decreases as well, and hence the neutrino abundance deviates more from equilibrium. Thus, as can be seen in Fig. 6.8, the efficiency η_C initially increases with g_T. However, at $g_T \lesssim 10^{-3}$, $\gamma_{NN,TT}$ becomes ineffective, prompting the evolution of T to decouple from the evolutions of N, σ and J and hence $\eta_C\,(g_T \lesssim 10^{-3})$ becomes constant. Moreover, note that since $g_N = 1$, the efficiency is strongly suppressed compared to VL unless $\tilde{m} \to 0.1$.
In case D, we vary λ_σ in the range $[10^{-2}, 1]$ and find that η_D slightly decreases with λ_σ. However, since most of the thermal rates appearing in the Boltzmann equations for leptogenesis depend non-trivially on λ_σ, it is not feasible to make qualitative statements on the λ_σ-dependence of the efficiency η_D.

6.4 Dark Matter

In the previous section, we have exclusively focussed on the implications different values of the parameters g_N, g_T, λ_σ and $\tilde{m}$ have on the evolution of the particle abundances and the efficiency. However, in the discussions of cases A and B, we saw that the interactions that govern the evolutions of J and T eventually decouple. Consequently, their abundances either freeze in or -out, and it is therefore reasonable to discuss the implications of the models with regard to DM .

6.4.1 Majoron

As discussed in Sec. 5.1.1, the Majoron can be a valid DM candidate in the generic singlet Majoron model, provided that it acquires a suitable mass and decays to light neutrinos are sufficiently slow. In this work, we do not specify a mechanism that generates the required Majoron mass m_J and merely focus on the implications of Majoron DM in the context of the MTM, assuming that the decay width to neutrinos is sufficiently small to render the Majoron stable on cosmological time scales.
In the leptogenesis era, the Majoron interacts via scatterings and (inverse) decays with N, σ and T. These interactions eventually become Boltzmann suppressed and decouple around $z_N^d \sim 10$, yielding a constant Majoron abundance $Y_J(z_N^d)$ that depends on the values of $g_N, \tilde{m}$ and g_T as well as on the initial abundances. In case A and B_t, the Majoron freezes out with an abundance $Y_J(z_N^d) \geq Y_J^{\mathrm{eq}}(z_N^d)$, see Fig. 6.18, while in case B_z with $(\tilde{m}, g_N) \lesssim (\tilde{m}^{IA}, g_N^{IA})$, the Majoron does not necessarily reach equilibrium and thus freezes in with $Y_J(z_N^d) \leq Y_J^{\mathrm{eq}}(z_N^d)$, see Fig. 6.24. Using (4.1.7) and (4.1.4) and demanding $\Omega_J(m_J^{\mathrm{DM}}) \overset{!}{=} \Omega_{\mathrm{DM}}$, we can determine the Majoron mass that is necessary in order to obtain DM that only consists of Majorons. Note that this implies an upper limit on the Majoron mass: A smaller Majoron mass than m_J^{DM} would merely indicate that

contributions to the DM relic density from other species are necessary, while $m_J > m_J^{\rm DM}$ would overproduce DM . In Fig. 6.27, we show density plots of $m_J^{\rm DM}$ in the $g_N - \tilde{m}$ plane for case B_t (left) and case B_z (middle). We stress that the constraints from case A and B_t result in almost identical constraints hence we present only the results for case B_t. It is apparent that the Majoron contribution to the DM relic density places tight constraints on the Majoron mass. In case B_t, the Majoron has to be lighter than $\sim \mathcal{O}\,(10^2\,\text{eV})$ while in the IA region in case B_z, the limit is slightly weaker with $m_J \lesssim \mathcal{O}\,(10^3\,\text{eV})$. However, such a light Majoron would constitute hot DM and therefore be problematic in the context of structure formation. Thus, the Majoron in the MTM is not a good DM candidate.[8] Moreover, in order for the model to remain valid and unless the mechanism that generates the Majoron mass affects the production of the relic Majoron density, the Majoron either needs to be *significantly* lighter than $m_J^{\rm DM}$ so that the contribution to DM becomes insignificant, or Majoron decays to neutrinos need to be sufficiently fast so that no Majoron relic density survives.

6.4.2 Triplet

As discussed above, the triplet dominantly interacts *with* and is thermalized *by* gauge interactions, while the interactions with N, σ and J are subdominant or even irrelevant, depending on the size of g_T. This implies that the triplet freezes out once gauge interactions decouple at $z_T \sim 10$ and the abundance becomes constant. In order to determine the relic density of T, we therefore solve a simplified Boltzmann equation for the evolution of the triplet abundance, only including gauge scatterings,

$$s\mathcal{H}z_N \frac{\mathrm{d}Y_T}{\mathrm{d}z_N} = -2\left(\delta_T^2 - 1\right)\gamma_{T,gauge}\,. \tag{6.4.1}$$

For $g_T \ll 1$, this is an excellent approximation since the triplet decouples at $z_N = g_N g_T^{-1} z_T \sim g_N g_T^{-1} 10$ and therefore long after the interactions with N, σ and J have decoupled. We solve (6.4.1) for g_T in the range $10^{-7} \leq g_T \leq 1$ and determine the relic density Ω_T using (4.1.7) and $Y_T(z_T \to \infty)$. In Fig. 6.27 (right panel), we show $\Omega_T(g_T)$, restricted to the range $10^{-7} \leq g_T \leq 10^{-5}$. It is apparent that $\Omega_T(g_T)$ scales linearly and already exceeds the DM relic density $\Omega_{\rm DM}$ for $g_T \gtrsim 2.9\times10^{-7}$ or equivalently $M_T \gtrsim 2\,\text{TeV}$. Moreover, the collaborations Atlas [217] and CMS [218] place lower bounds on the triplet mass in the context of the type III Seesaw,

$$M_T^{Atlas} \approx 910\,\text{GeV}\,, \qquad M_T^{CMS} \approx 840\,\text{GeV}\,, \tag{6.4.2}$$

corresponding to

$$g_T^{Atlas} \approx 1.19 \times 10^{-7}\,, \qquad g_T^{CMS} \approx 1.29 \times 10^{-7}\,. \tag{6.4.3}$$

Recalling that the efficiency in the MTM is independent from g_T for $g_T \lesssim 10^{-3}$, see Fig. 6.8, this implies that case B is tightly constrained but viable while case A is excluded.

[8] In principle, the Majoron could still be a good DM if it is not in kinetic equilibrium when the relic density freezes out. However, since the Boltzmann equations in Sec. 6.24 and the associated results are only valid under the assumption that kinetic equilibrium holds and therefore we will not entertain this possibility further.

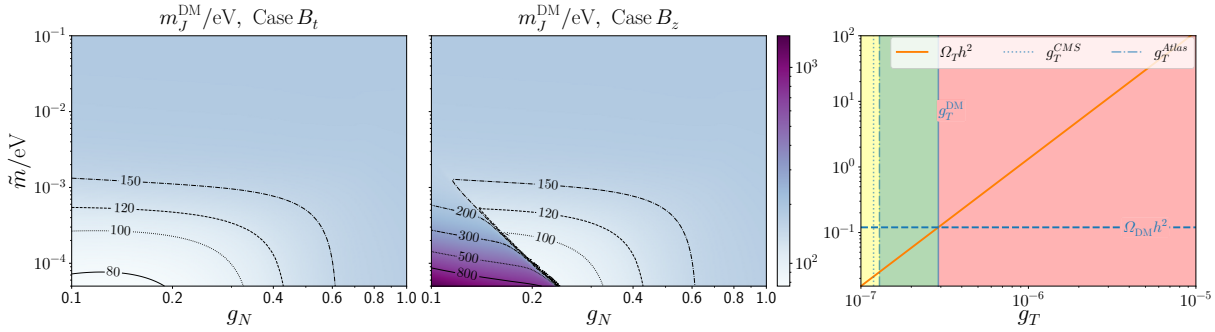

Figure 6.27: *Left, middle:* Upper limits on the Majoron mass that do not overproduce DM for case B_t (left) and B_z (middle) in the $g_N - \tilde{m}$ plane. Note that these constraints are only valid if Majoron decays to light neutrinos are sufficiently slow. *Right:* Triplet relic density $\Omega_T h^2$ as a function of g_T, compared to the DM relic density $\Omega_{\rm DM} h^2$. In the green region, the triplet relic density does not exceed the DM relic density and is in agreement with bounds from Atlas and CMS placed on the triplet mass. In the red region, DM is overproduced while in the yellow region, bounds from Atlas are violated.

We stress that the relic density of the triplet arises since we assumed that the mixing term with the SM lepton and Higgs doublet is absent. If this term were present, the triplet could decay to a lepton-Higgs pair and the DM constraints would be lifted. However, introducing this term would also significantly alter the dynamics of leptogenesis and the evolution of the particle abundances and would require solving a different set of Boltzmann equations. Although this scenario appears highly interesting, it is beyond the scope of this work.

6.5 Baryon Asymmetry

As discussed in Sec. 5.3, the conversion rate of an exisiting asymmetry in $Y_{\Delta(\Delta B', \Delta L')}$ to a baryon asymmetry changes in the MTM compared to VL since Sphaleron transitions conserve $\Delta B' + 3\Delta L'$ rather than $\Delta B' - \Delta L'$. With case A being ruled out by DM constraints, let us restrict the following discussion to case B. With $g_T \sim 10^{-7}$, it is reasonable to assume that the triplet is in equilibrium when Sphaleron processes are active. If the SM Yukawa and gauge interactions are in equilibrium as well, the relation between $Y_{(\Delta B' + 3\Delta L')}$ and $Y_{\Delta B'}$ derived in Sec. 5.3 applies,

$$Y_{\Delta B'} = \frac{76}{679} Y_{(\Delta B' + 3\Delta L')} \,. \tag{6.5.1}$$

Moreover, recall that the equivalent relation in VL is given by

$$Y_{\Delta B'} = \frac{28}{79} Y_{(\Delta B' - \Delta L')} \tag{6.5.2}$$

and if no other sources of baryon number violation are present we find

$$|Y_{\Delta B'}| = \begin{cases} 3 \times \frac{76}{679} Y^B_{\Delta L'} & \approx 0.35443 |Y^B_{\Delta L'}|\,, \\ \frac{28}{79} Y^{\rm VL}_{\Delta L'} & \approx 0.335788 |Y^{\rm VL}_{\Delta L'}|\,, \end{cases} \tag{6.5.3}$$

i.e. the baryon asymmetry that can be generated from a given lepton asymmetry in the MTM is numerically almost identical to VL. Using (4.3.64) and (6.5.1), we can determine the amount of $\mathcal{CP}$ violation that is necessary to reproduce the experimentally observed baryon asymmetry $Y^{exp}_{\Delta B'}$, see (4.3.3), as

$$\varepsilon(\tilde{m}, g_N) = \frac{679}{76 \times 3} \frac{Y^{exp}_{\Delta B'}}{Y^0_N \eta(\tilde{m}, g_N)}\,. \tag{6.5.4}$$

If no additional sources of $\mathcal{CP}$ violation other than neutrino decays are present, the heavy neutrinos are strongly hierarchical, $M_{N_{2,3}}/M_{N_1} \to \infty$, and the light neutrinos follow a NH, the DI bound on the $\mathcal{CP}$ violation, $|\varepsilon| \leq |\varepsilon^{DI}|$, given in (4.3.57), applies. In Fig. 6.28, we show density plots of ε in the $g_N - \tilde{m}$ plane (left), $\varepsilon(\tilde{m})$ (middle) and $\varepsilon(g_N)$ (right) for $g_N = [0.1, 0.7, 1]$ and $\tilde{m} = [5 \times 10^{-5}, 10^{-3}, 10^{-1}]$eV, respectively. Additionally, we show the DI bound, $\varepsilon^{DI}(\tilde{m})$ and $\varepsilon^{DI}(g_N)$. It is evident that the $\mathcal{CP}$ violation that is required to reproduce the experimentally observed baryon asymmetry in the MTM is at least about one order of magnitude larger than the maximal $\mathcal{CP}$ violation that can be obtained according to the DI bound. Moreover, note that the efficiency in VL does not depend on the neutrino mass M_N and therefore, it is (at least in principle) possible to fulfill the DI bound for a given efficiency by simply increasing M_N. In the MTM, this does not work since the efficiency depends on g_N. Even worse, we have $\varepsilon \sim 1/\eta_B \sim g_N$ as well as $\varepsilon^{DI} \sim g_N$, i.e. if we increase g_N to enhance the DI bound, the required $\mathcal{CP}$ vioalation increases as well. This does, however, not imply that leptogenesis in the MTM is not feasible. The DI bound is only valid in the limit $M_{N_{2,3}}/M_{N_1} \to \infty$ and a weaker hierarchy can resonantly enhance the efficiency beyond the DI bound [183]. Depending on the size of g_N, a weak hierarchy is in fact difficult to avoid since the masses $M_{N_{2,3}}$ arise due to the same VEV as M_{N_1} and perturbativity of $g_{N_{2,3}}$ prevents them from becoming arbitrarily large. Moreover, we have neglected flavor effects in the Boltzmann equations. It has been shown in Ref. [148] that flavor effects in type III leptogenesis enhance the efficiency in the regime where WO effects are dominant. We expect that a similar enhancement appears in the WO regime of the MTM. In the ~~WO~~ regime on the other hand, leptogenesis is driven by flavor independent scattering processes and consequently, only negligible flavor effects are expected. Additionally, note that although commonly used in the literature, the constant conversion rate from the lepton to the baryon asymmetry via Sphaleron processes is a gross oversimplification and precise results would require to determine a conversion rate that not only depends on the flavors which are equilibrium at a given epoch but also takes the temperature dependence of Sphaleron transitions into account [172].
Lastly, recall that we have obtained the results for the fixed VEV $f = 10^{10}\,\text{GeV}$. Before we conclude, let us therefore briefly explore the impact the value of the VEV has onr the efficiency. For simplicity, we determine $\eta_B(f)$ at $g_N = 0.1$ and $\tilde{m} = 10^{-3}\,\text{eV}$ in the range $10^6\,\text{GeV} \leq f \leq 10^{12}\,\text{GeV}$, as shown in Fig. 6.29. For comparison, we also translate the

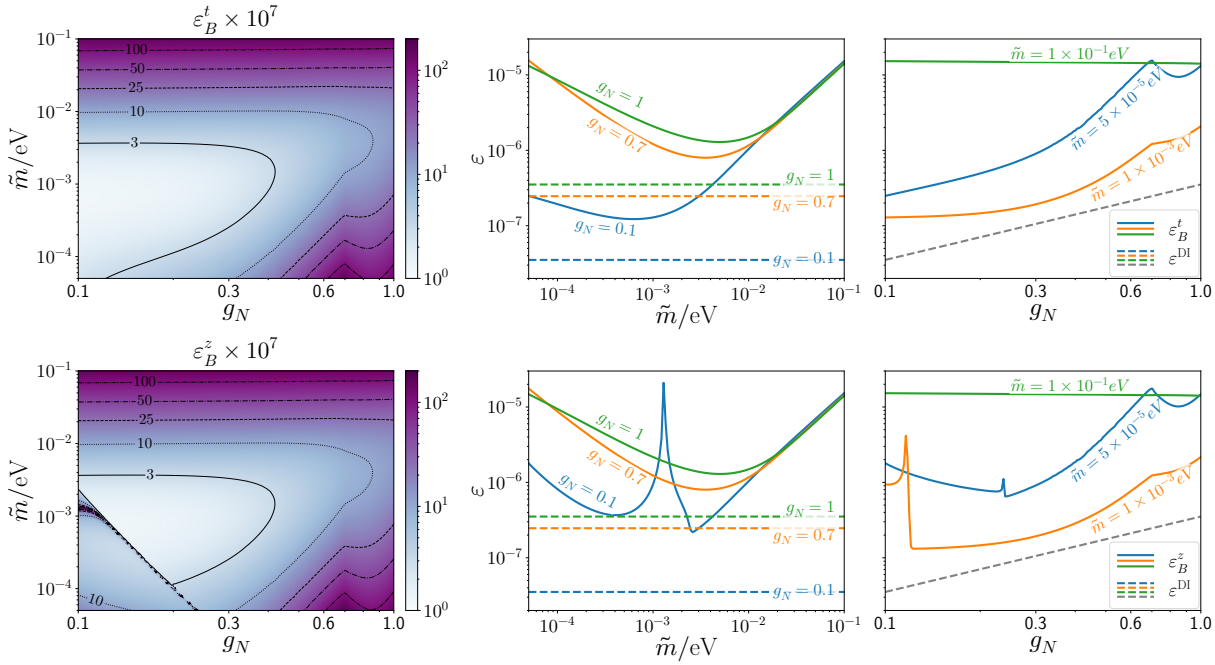

Figure 6.28: *Left:* Density plots of the CP violation $|\varepsilon_B^t|$ (top) and $|\varepsilon_B^z|$ (bottom), required to explain the experimentally observed baryon asymmetry in case B in the MTM. *Middle:* $|\varepsilon_B^t|$ (top) and $|\varepsilon_B^z|$ (bottom) as functions of $\tilde{m}$ (solid lines) for $g_N = [0.1, 0.7, 1]$. The dashed lines corresponds to ε^{DI}. *Right:* $|\varepsilon_B^t|$ (top) and $|\varepsilon_B^z|$ (bottom) as functions of g_N (solid lines) for $\tilde{m} = [5 \times 10^{-5}, 10^{-3}, 10^{-1}]$eV. The dashed line corresponds to ε^{DI}.

DI bound into a lower bound on the efficiency required to produce experimental data,

$$\eta^{DI}(M_N(f)) \equiv \frac{679}{3 \times 76} \frac{Y_B^{exp}}{Y_N^0 \varepsilon^{DI}(M_N(f))} \sim \frac{1}{f} \,. \tag{6.5.5}$$

We find that the efficiency increases with the VEV and closes the gap between η_B and η^{DI}. Thus, if the DI bound is valid, the MTM could still reproduce the observed baryon asymmetry provided that the VEV is sufficiently large.

6.6 Summary

In this Chapter, we have studied the leptogenesis mechanism in the Majoron+Triplet model in great detail. In order to reduce the complexity of the model, we have neglected the mixing between the SM Higgs doublet and the new singlet scalar. Moreover, we have invoked a Z_2 symmetry in order to avoid the appearance of a Yukawa term that mixes the triplet and the SM leptons. Although this term is highly interesting as it induces an additional channel for lepton number violation, including it is beyond the scope of this work.

We have derived the Boltzmann equations for leptogenesis and considered two different

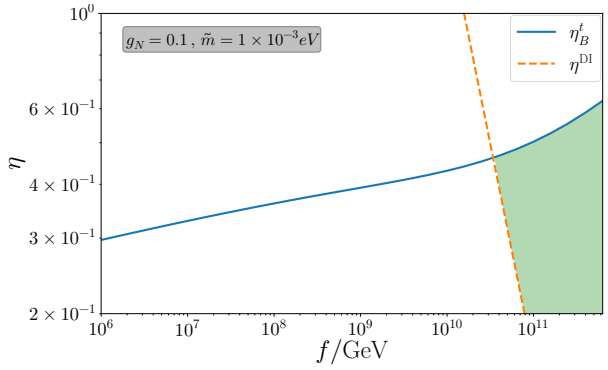

Figure 6.29: Efficiency η_B^t for $g_N = 0.1$ and $\tilde{m} = 10^{-3}\,\mathrm{eV}$ as a function of the VEV f, compared to η^{DI} as defined in (6.5.5). In the green region, η_B^t is sizable enough to reproduce the experimentally observed baryon asymmetry with a CP violation ε that fulfills the DI bound.

scenarios: In the simplified scenario, we have assumed that neutrinos can deviate from equilibrium while the remaining new particles are in equilibrium, leaving us to solve two Boltzmann equations, one for the neutrino abundance and one for the efficiency that parametrizes the out-of-equilibrium conditions relevant for leptogenesis. Afterwards, we have considered scenarios where all additional particles can deviate from equilibrium, in total resulting in five coupled Boltzmann equations. We have solved the Boltzmann equations for various different assignments of the model parameters in order to determine the final efficiency. Notably, we find that the results for the final efficiency are up to two orders of magnitude larger if the full set of Boltzmann equations is solved rather than only the Boltzmann equations for the neutrino abundance and the efficiency. Moreover, we find that in the limit where the triplet-Majoron coupling is small, the results for the efficiency are independent from the model parameter associated with the triplet and hence are also valid in the generic singlet Majoron model. Thus, we conclude that the common approach to assume that the new scalars appearing in the Majoron model follow their equilibrium abundances [39] can drastically underestimate the final efficiency.

We find that the final efficiency significantly depends on the Majoron-neutrino coupling g_N and the effective neutrino mass $\tilde{m}$. The coupling g_N drives the lepton number conserving scatterings between the neutrinos and the new particles which prevent neutrinos from creating a lepton asymmetry via decays, thereby suppressing the final efficiency. On the other hand, for large effective neutrino masses, i.e. $\tilde{m} \to 0.1\,\mathrm{eV}$, leptogenesis essentially proceeds analogously to the standard type I Seesaw scenario and the new scattering processes are rendered irrelevant. Moreover, we find that for most of the parameter assignments we have considered, the final efficiency is independent from the initial particle abundances, either due to fast inverse neutrino decays or fast scatterings between neutrinos and the new particles.

The new scatterings also serve to create relic abundances of the Majoron and the triplet which can be used to constrain the paramters of the model. For the parameter sets we have considered, the Majoron is no longer a valid DM candidate since the masses that are

in agreement with DM being cold yield a Majoron relic density that exceeds the DM relic density. Concerning the triplet, we find that a small triplet mass, or equivalently a small Majoron-triplet coupling, is required to avoid overproduction of DM, placing constraints on the parameters we have considered in our analysis.
We also have studied the $\mathcal{CP}$ violation that is necessary to reproduce the observed baryon asymmetry and find that it exceeds the Davidson-Ibarra bound on the $\mathcal{CP}$ violation unless the vacuum expectation value f that breaks lepton number is sufficiently large, $f \gtrsim 10^{11}\,\mathrm{GeV}$. However, this bound can easily be evaded by taking resonance effects into account. Moreover, we have performed our analysis in the one-flavor approximation. Taking flavor effects into account can significantly enhance the efficiency in the high-$\tilde{m}$ limit, while we expect that the efficiency is not significantly altered in the region of the parameter space where scatterings between the new particles are dominant [148].

CHAPTER 7

Muon Anomalous Magnetic Moment from Vectorlike Leptons in a 2HDM + S Model

In Sec. 4.4, we discussed that the AMM of the muon provides a striking hint at the need for BSM physics. In particular, models that introduce new sources of chirality flips in the muon sector are of importance due to the chiral enhancement of the one-loop contribution. Although new contributions to a_μ can already arise in one-field extensions of the SM, most models extend the SM by at least two fields, one being a fermion and the other being either a scalar or a vector boson. Since many GUT models predict new fermions, it seems natural to explore if they can induce the desired contribution to the muon AMM. In particular, E_6 unification and trinification models, see App. D, contain a conjugate pair of $\mathrm{SU}(2)_\mathrm{L}$ doublets that describe a VLL. In principle, sizable contributions to a_μ can already arise in a model that contains only one additional scalar singlet besides the VLL [219]. However, the most simple realization of this model is excluded due to the large mixing angles required in the scalar sector. Instead, we consider a model that contains one additional Higgs doublet mixing with the SM Higgs and the BSM scalar singlet.

As we will discuss in the following, including both the VLL and two new scalars in the model has interesting phenomenological implications due to the mixing it induces in the extended muon- and scalar sectors. Although one can envisage several distinct implementations of such a model, we pick a specific model that yields chirally enhanced contributions to the AMM of the muon.

This Chapter is based on [1] and structured as follows. In Sec. 7.1, we present the field content of the model and the relevant terms of the Lagrangian. In Sec. 7.2, we study the mass spectrum and vacuum structure of the scalar sector where several features discussed in Sec. 2.3 reappear. In Sec. 7.3, we focus on the mixing in the muon sector and discuss how the one-loop contributions to the AMM of the muon arise. In Sec. 7.4, we study constraints on the model parameters from Higgs decays and discuss potential new sources of *lepton flavor violation* (LFV) as well as present current collider limits. In Sec. 7.5, we present data sets that are compatible with the aforementioned constraints and simultaneously explain the AMM of the muon before we summarize our results in Sec. 7.6.

7.1 Model Overview

We consider a model with a scalar sector that consists of two Higgs doublets $H_{1,2}$ with VEVs $v_{1,2}$ and a scalar singlet S with VEV v_S,

$$H_{1,2} = \begin{pmatrix} h_{1,2}^+ \\ \frac{1}{\sqrt{2}}(v_{1,2} + h_{1,2} + i\rho_{1,2}) \end{pmatrix} , \quad S = \frac{1}{\sqrt{2}}\left(v_S + S'\right) , \tag{7.1.1}$$

while the lepton sector is extended by two muon-type $\mathrm{SU}(2)_\mathrm{L}$ doublets $L_{M,M'}$,

$$L_M = \begin{pmatrix} \nu_M \\ M \end{pmatrix}_L , \qquad L'_M = \begin{pmatrix} \nu_M \\ M \end{pmatrix}_R . \tag{7.1.2}$$

In order to generate a non-vanishing contribution to the muon AMM, the new fields need to couple to the SM muons on tree level. Moreover, we aim to construct a scalar sector that does not induce FCNCs, as discussed in Sec. 2.3 . In order to achieve this, we impose a Z_4 symmetry with charge assignments as given in Tab. 7.1, yielding the scalar potential

$$\begin{aligned} V =& -\mu_1^2|H_1|^2 - \mu_2^2|H_2|^2 - \mu_S^2 S^2 + \lambda_1|H_1|^4 + \lambda_2|H_2|^4 + \lambda_S S^4 \\ &+ 2\lambda_3|H_1|^2|H_2|^2 + 2\lambda_4(H_1^\dagger H_2)(H_2^\dagger H_1) + \lambda_5\left[(H_1^\dagger H_2)^2 + (H_2^\dagger H_1)^2\right] \\ &+ 2\eta_1|H_1|^2 S^2 + 2\eta_2|H_2|^2 S^2 , \end{aligned} \tag{7.1.3}$$

and the muonic Lagrangian

$$\mathcal{L} = -g\overline{L_\mu}H_1\mu_R - y\overline{L_M}H_2\mu_R - y'\overline{L_\mu}L'_M S - m_M\overline{L_M}L'_M + \text{h.c.} , \tag{7.1.4}$$

where $L_\mu = \begin{pmatrix} \nu_\mu & \mu \end{pmatrix}_L^T$ is the $\mathrm{SU}(2)_\mathrm{L}$ muon doublet and μ_R is the corresponding $\mathrm{SU}(2)_\mathrm{L}$ singlet. Note that in contrast to the SM fermions, the VLLs can have bare mass terms and thus do not rely on SSB to become massive.

Let us briefly motivate the charge assignments given in Tab. 7.1. First, we aim to construct a model that does not induce FCNCs as is common in generic 2HDMs. As discussed in Sec. 2.3, it is in principle sufficient to impose a Z_2 symmetry, rather than a Z_4, under which H_1 and H_2 have opposite charges. In this case, odd powers of S would appear in the scalar potential which are forbidden under Z_4. Thus, imposing a Z_4 symmetry rather than a Z_2 significantly simplifies the scalar sector. Next, note that the coupling structure of the Yukawa sector severely depends on the charge assignments under Z_4. Although contributions to the AMM of the muon already arise if either y or y' are non-zero, we have chosen the charge assignments so that both terms are non-zero.[1] For simplicity, we also set $\eta_1 = 0$ so that the mixing between the two doublets and the singlet arises only via η_2.

[1] As we will see later, if the alignment limit in the scalar sector is exact and the mixing in the muon sector vanishes, chirally enhanced contributions arise only if both y and y' are nonzero.

	H_1	H_2	L_μ	μ_R	L_M	L'_M	S
$(\mathrm{SU}(3)_C, \mathrm{SU}(2)_L)_{U(1)_Y}$	$(1,2)_{1/2}$	$(1,2)_{1/2}$	$(1,2)_{-1/2}$	$(1,1)_{-1}$	$(1,2)_{-1/2}$	$(1,2)_{-1/2}$	$(1,1)_0$
Z_4	1	-1	$-i$	$-i$	$+i$	$+i$	-1

Table 7.1: Field content and charge assignments relevant for the discussed model.

7.2 Scalar Sector

7.2.1 Mass Spectrum and Alignment Limit

The scalar sector of the model exhibits several similarities to the 2HDM discussed in Sec. 2.3, albeit being more complex due to the additional scalar singlet. With

$$\tan\beta = \frac{v_2}{v_1}\,, \qquad v_{SM}^2 = v_1^1 + v_2^2\,, \tag{7.2.1}$$

we note that the mass eigenstates and masses of the charged and $\mathcal{CP}$ odd fields $H^\pm, A$ are still given by (2.3.7) and (2.3.8), respectively. The mass matrix for the $\mathcal{CP}$ even scalars h_1, h_2, S' on the other hand is given by

$$M^2 = \begin{pmatrix} M^2_{h_1h_1} & M^2_{h_1h_2} & M^2_{h_1S} \\ M^2_{h_1h_2} & M^2_{h_2h_2} & M^2_{h_2S} \\ M^2_{h_1S} & M^2_{h_2S} & M^2_{SS}, \end{pmatrix}\,, \tag{7.2.2}$$

where the matrix elements are given by

$$M^2_{h_1h_1} = \frac{2\lambda_1\left(v^2\tilde{\eta}_2 + \kappa\right)}{\sigma}\,, \tag{7.2.3}$$

$$M^2_{h_1h_2} = 2\lambda_{345}\sqrt{\frac{v^2\tilde{\eta}_2 + \kappa}{\sigma}}\sqrt{\frac{\lambda_{345}v^2\lambda_S - \kappa}{\sigma}}\,, \tag{7.2.4}$$

$$M^2_{h_1S} = 0\,, \tag{7.2.5}$$

$$M^2_{h_2h_2} = -\frac{2\lambda_2\left(\kappa - \lambda_{345}v^2\lambda_S\right)}{\sigma}\,, \tag{7.2.6}$$

$$M^2_{h_2S} = 2\eta_2\sqrt{\frac{\lambda_{345}v^2\lambda_S - \kappa}{\sigma}}\sqrt{\frac{\delta_{345}\eta_2 - \Lambda_2\mu_S^2}{\sigma}}\,, \tag{7.2.7}$$

$$M^2_{SS} = -\frac{2\lambda_S\left(\Lambda_2\mu_S^2 + \eta_2\left(\lambda_{345}v^2 - \mu_2^2\right)\right)}{\sigma}\,, \tag{7.2.8}$$

and we introduced the shorthand notations

$$\begin{aligned} \lambda_{345} &= \lambda_3 + \lambda_4 + \lambda_5\,, & \Lambda_i &= \lambda_i - \lambda_{345}\,, & \sigma &= \eta_2^2 - \Lambda_2\lambda_S\,, \\ \kappa &= \lambda_S\mu_2^2 - \eta_2\mu_S^2\,, & \delta_i &= \mu_2^2 - \lambda_i v^2\,, & \tilde{\eta}_2 &= \eta_2^2 - \lambda_2\lambda_S\,. \end{aligned} \tag{7.2.9}$$

As usual, we find the mass eigenstates h^0, H^0, S^0 via

$$\begin{pmatrix} h^0 \\ H^0 \\ S^0 \end{pmatrix} = U \begin{pmatrix} h_1 \\ h_2 \\ S' \end{pmatrix} , \qquad M^2_{diag} := \mathrm{diag}(m^2_{h^0}, m^2_{H^0}, m^2_{S^0}) = U^T M^2 U , \tag{7.2.10}$$

where

$$U = \begin{pmatrix} c_{12}c_{13} & s_{12}c_{13} & s_{13} \\ -s_{12}c_{23} - c_{12}s_{23}s_{13} & c_{12}c_{23} - s_{12}s_{23}s_{13} & s_{23}c_{13} \\ s_{12}s_{23} - c_{12}c_{23}s_{13} & -c_{12}s_{23} - s_{12}c_{23}s_{13} & c_{23}c_{12} \end{pmatrix} \equiv \begin{pmatrix} U_{11} & U_{12} & U_{13} \\ U_{21} & U_{22} & U_{23} \\ U_{31} & U_{32} & U_{33} \end{pmatrix} , \tag{7.2.11}$$

with $c_{ij} = \cos\theta_{ij}$, $s_{ij} = \sin\theta_{ij}$. By rotating to the Higgs basis,

$$\begin{pmatrix} h^0_{SM} \\ \hat{H} \\ \hat{S} \end{pmatrix} = U_\beta U^T \begin{pmatrix} h^0 \\ H^0 \\ S^0 \end{pmatrix} \quad U_\beta = \begin{pmatrix} \cos\beta & \sin\beta & 0 \\ -\sin\beta & \cos\beta & 0 \\ 0 & 0 & 1 \end{pmatrix} , \tag{7.2.12}$$

we obtain a relation between $\hat{h}$ and the mass eigenstates h^0, H^0, S^0,

$$h^0_{SM} = \cos\theta_{13}\cos(\beta - \theta_{12})h^0 - \cos\theta_{13}\sin(\beta - \theta_{12})H^0 + \sin\theta_{13}S^0 , \tag{7.2.13}$$

and hence can impose an alignment limit where either h^0 or H^0 are aligned with the SM Higgs h^0_{SM}. We will restrict ourselves to the scenario where

$$\theta_{13} \approx 2\pi n , \qquad \theta_{12} \approx \beta + 2\pi n , \qquad n = 0, 1, 2, ... , \tag{7.2.14}$$

so that h^0 is aligned with the SM Higgs, i.e. $m^0_h \approx 125\,\mathrm{GeV}$. Note that compared to the 2HDM, the additional mixing with the scalar singlet induces an additional condition for the alignment limit.
Finally, the scalar kinetic term,

$$\mathcal{L}^{scalar}_{kin} = (D_\mu H_1)^\dagger (D^\mu H_1) + (D_\mu H_2)^\dagger (D^\mu H_2) + \frac{1}{2}(\partial_\mu S)(\partial^\mu S) , \tag{7.2.15}$$

induces couplings of the scalars to the gauge bosons. In the mass basis, we have

$$\mathcal{L}^{scalar}_{VV} \sim \left(g_{h^0VV} h^0 + g_{H^0VV} H^0 + G_{S^0VV} \right) \tag{7.2.16}$$

where

$$g_{h^0VV} \sim c_{13}\cos(\beta - \theta_{12}) , \tag{7.2.17}$$

$$g_{H^0VV} \sim c_{23}\sin(\beta - \theta_{12}) - s_{23}s_{13}\cos(\beta - \theta_{12}) , \tag{7.2.18}$$

$$g_{S^0VV} \sim s_{23}\sin(\theta_{12} - \beta) - c_{23}s_{13}\cos(\theta_{12} - \beta) , \tag{7.2.19}$$

and $VV = WW, ZZ$. In this form, it is evident that h^0 has SM-like couplings to the gauge bosons in the alignment limit (7.2.14).

7.2.2 Vacuum Stability

As in the generic 2HDM, vacuum stability requires that the potential (7.1.3) is bounded from below. The couplings of the singlet scalar S modify the conditions given in (2.3.27)

which now read [86]

$$\begin{aligned} \lambda_{1,2,S} > 0\,, \quad \sqrt{\lambda_S\lambda_1} + \eta_1 > 0\,, \\ \sqrt{\lambda_S\lambda_2} + \eta_2 > 0\,, \quad \sqrt{\lambda_S\lambda_1} + \lambda_{345} > 0\,, \quad \sqrt{\frac{\lambda_1}{\lambda_2}}\eta_2 + \eta_1 \geq 0\,, \end{aligned} \tag{7.2.20}$$

if $\lambda_4 \geq |\lambda_5|$ and

$$\begin{aligned} \lambda_{1,2,S} > 0\,, \quad \sqrt{\lambda_S\lambda_1} + \eta_1 \geq 0\,, \quad \sqrt{\lambda_S\lambda_2} + \eta_2 > 0\,, \quad \sqrt{\lambda_S\lambda_2} - \eta_2 \geq 0\,, \\ -\eta_2\sqrt{\frac{\lambda_1}{\lambda_2}} - \eta_1 \geq 0\,, \quad \lambda_S\lambda_{345} - \eta_1\eta_2 + \sqrt{(\eta_1^2 - \lambda_S\lambda_1)\eta_2^2 - \lambda_S\lambda_2)} \geq 0\,, \end{aligned} \tag{7.2.21}$$

if $\lambda_4 < |\lambda_5|$.
Moreover, we consider only "normal", i.e. charge and $\mathcal{CP}$ conserving, vacua,

$$\langle H_{1,2}\rangle = \begin{pmatrix} 0 \\ \frac{1}{\sqrt{2}}v_{1,2} \end{pmatrix}\,, \quad \langle S\rangle = \frac{1}{\sqrt{2}}v_S\,, \tag{7.2.22}$$

and minimizing (7.1.3),

$$\frac{\partial V}{\partial\phi}\Big|_{\phi=\langle\phi\rangle} = 0\,, \quad \phi = \{h_1, h_2, S\}\,, \tag{7.2.23}$$

we find 8 distinct extrema with energies $\mathcal{E}_i\,, i \in [1,8]$. They are given in Tab. 7.2 where we used the abbreviations

$$\Lambda_{12} = \lambda_1\lambda_2 - \lambda_{345}^2\,, \tag{7.2.24}$$

$$\epsilon = \lambda_{345}\mu_2^2 - \lambda_1\lambda_2 v^2\,, \tag{7.2.25}$$

$$\begin{aligned} \alpha = \mu_S^2 + \eta_2^2\big(2\lambda_S\big(\mu_2^4\big(\lambda_{345}^2 + \Lambda_{12}\big) + \Lambda_{12}v^4\big(\lambda_{345}^2 + \Lambda_{12}\big) \\ -\mu_2^2\big(\delta_{345}\lambda_{345}^2 + \lambda_1 v^2\left(\lambda_{345}\left(\lambda_{345} + \Lambda_2\right) + \Lambda_{12}\right)\big)\big) - \lambda_2\Lambda_1^2\mu_S^4\big)\,, \end{aligned} \tag{7.2.26}$$

$$\begin{aligned} \beta = -2\delta_1\eta_2^3\mu_S^2 + \lambda_S\left(\lambda_S\left(2\delta_{345}\lambda_{345}\mu_2^2 - \delta_2^2\lambda_1 + \lambda_2\left(\lambda_{345}^2v^4 - \mu_2^4\right)\right) - \Lambda_2^2\mu_S^4\right) \\ + 2\eta_2\lambda_S\mu_S^2\left(\delta_2\lambda_1 - 2\lambda_{345}\mu_2^2 + \lambda_2\mu_2^2 + \lambda_{345}^2v^2\right) + \eta_2^2\left(\left(\lambda_2 - \lambda_1\right)\mu_S^4\right. \\ \left.+\lambda_S\left(\mu_2^4 + v^4\left(\lambda_{345}^2 + 2\Lambda_{12}\right) - 2\lambda_1\mu_2^2v^2\right)\right) - \eta_2^4\lambda_1 v^4\,. \end{aligned} \tag{7.2.27}$$

In this work, we focus on the scenario where all scalars develop a VEV, $v_{1,2,S} \neq 0$, and hence demand that $\mathcal{E}_4 < \mathcal{E}_{1,2,3,5,6,7,8}$ so that $\mathcal{E}_4$ is the stable ground state.

i	v_1^2	v_2^2	v_S^2	$\mathcal{E}_i$
1	0	$-\frac{\kappa}{\tilde{\eta}_2}$	$\frac{\eta_2\mu_2^2-\lambda_2\mu_S^2}{\tilde{\eta}_2}$	$\frac{-2\eta_2\mu_2^2\mu_S^2+\mu_2^4\lambda_S+\lambda_2\mu_S^4}{4\eta_2^2-4\lambda_2\lambda_S}$
2	0	$\frac{\mu_2^2}{\lambda_2}$	0	$-\frac{\mu_2^4}{4\lambda_2}$
3	$\frac{\delta_2\lambda_S-\frac{\eta_2(\lambda_2\Lambda_1\mu_S^2+\eta_2\epsilon)}{\Lambda_{12}}}{\sigma}$	$\frac{\delta_{345}(\eta_2^2\lambda_1-\Lambda_{12}\lambda_S)+\eta_2\lambda_{345}\Lambda_1\mu_S^2}{\Lambda_{12}\sigma}$	0	$\frac{\alpha}{4\Lambda_{12}\sigma^2}$
4	$\frac{v^2\tilde{\eta}_2+\kappa}{\sigma}$	$\frac{\lambda_{345}v^2\lambda_S-\kappa}{\sigma}$	$\frac{\delta_{345}\eta_2-\Lambda_2\mu_S^2}{\sigma}$	$\frac{\beta}{4\sigma^2}$
5	0	0	$\frac{\mu_S^2}{\lambda_S}$	$-\frac{\mu_S^4}{4\lambda_S}$
6	$\frac{v^2(\lambda_1\tilde{\eta}_2+\lambda_{345}^2\lambda_S)+\kappa\Lambda_1}{\lambda_1\sigma}$	0	$\frac{\mu_S^2}{\lambda_S}$	$-\frac{\lambda_S(v^2(\lambda_1\tilde{\eta}_2+\lambda_{345}^2\lambda_S)+\kappa\Lambda_1)^2+\lambda_1\sigma^2\mu_S^4}{4\lambda_1\sigma^2\lambda_S}$
7	$\frac{v^2(\lambda_1\tilde{\eta}_2+\lambda_{345}^2\lambda_S)+\kappa\Lambda_1}{\lambda_1\sigma}$	0	0	$-\frac{(v^2(\lambda_1\tilde{\eta}_2+\lambda_{345}^2\lambda_S)+\kappa\Lambda_1)^2}{4\lambda_1\sigma^2}$
8	0	0	0	0

Table 7.2: Extrema energies $\mathcal{E}_i$ and the corresponding VEVs for the potential (7.1.3) in the case $\eta_1 = 0$.

7.3 Muon Sector

The Lagrangian (7.1.4) induces mixing between the muon-type leptons, yielding a non-diagonal muon mass matrix given by

$$\mathcal{L}_{mass} \propto \begin{pmatrix}\overline{(\mu_R)^C} & \overline{(\mu_L)} & \overline{(M_R)^C} & \overline{(M_L)}\end{pmatrix} \underbrace{\begin{pmatrix} 0 & gv_1 & 0 & yv_2 \\ gv_1 & 0 & y'v_S & 0 \\ 0 & y'v_S & 0 & m_M \\ yv_2 & 0 & m_M & 0 \end{pmatrix}}_{=:K} \begin{pmatrix} \mu_R \\ (\mu_L)^C \\ M_R \\ (M_L)^C \end{pmatrix} . \quad (7.3.1)$$

Defining the 2×2 matrices

$$\tilde{m}_\mu \equiv \begin{pmatrix} 0 & gv_1 \\ gv_1 & 0 \end{pmatrix} , \quad \tilde{m}_{mix} \equiv \begin{pmatrix} 0 & yv_2 \\ y' & v_S \end{pmatrix} , \quad \tilde{m}_M \equiv \begin{pmatrix} 0 & m_M \\ m_M & 0 \end{pmatrix} , \quad (7.3.2)$$

where

$$\tilde{m}_\mu \sim m_\mu \mathbb{1}_{2\times2} , \quad \tilde{m}_M \sim m_M \mathbb{1}_{2\times2} , \quad \tilde{m}_{mix} \sim \sqrt{yy'v_2v_S}\mathbb{1}_{2\times2} , \quad (7.3.3)$$

we can write the mass matrix K in terms of 2×2 blocks,

$$K := \begin{pmatrix} \tilde{m}_\mu & \tilde{m}_{mix} \\ \tilde{m}_{mix}^T & \tilde{m}_M \end{pmatrix} . \quad (7.3.4)$$

Blockdiagonalization of K in the limit $\tilde{m}_M \gg \tilde{m}_{mix}$ then yields the mass eigenstates and masses,[2]

$$\begin{pmatrix} \hat{\mu} \\ \hat{M} \end{pmatrix} = V^T \begin{pmatrix} \mu^f \\ M^f \end{pmatrix} , \qquad K_1 \sim \tilde{m}_\mu , \qquad K_2 \sim \tilde{m}_M , \quad (7.3.5)$$

[2]We assume that the mass matrix of the charged leptons in the SM is diagonal.

where V is an orthogonal mixing matrix that diagonalizes K,

$$\text{diag}\,(K_1, K_2) = V^T K V\,, \qquad V := \begin{pmatrix} V_{\mu\mu} & -V_{\mu M} \\ V_{\mu M} & V_{MM} \end{pmatrix} = \begin{pmatrix} \cos\alpha & -\sin\alpha \\ \sin\alpha & \cos\alpha \end{pmatrix}\,, \tag{7.3.6}$$

and

$$\mu^f \equiv \begin{pmatrix} \mu_R \\ (\mu_L)^C \end{pmatrix}\,, \qquad M^f \equiv \begin{pmatrix} M_R \\ (M_L)^C \end{pmatrix}\,. \tag{7.3.7}$$

Thus, the mixing angle α is given by

$$\tan\alpha \approx -\frac{m_{mix}^T}{m_M} \approx -\frac{m_\mu}{m_{mix}}\,. \tag{7.3.8}$$

and

$$m_{mix}^T m_{mix} \approx m_\mu m_M \approx y v_2 y' v_S\,. \tag{7.3.9}$$

Taking both the mixing in the scalar as well as in the muon sector into account, the couplings of the scalars h^0, H^0, S^0 to the muon-type mass eigenstates read

$$\begin{aligned} \mathcal{L} =& - h^0 g_{h^0}^{\mu\mu} \overline{\hat{\mu}_{\mathtt{L}}} \hat{\mu}_{\mathtt{R}} - h^0 g_{h^0}^{MM} \overline{\hat{M}_{\mathtt{L}}} \hat{M}_{\mathtt{R}} - h^0 g_{h^0 \mathtt{L}} \overline{\hat{\mu}_{\mathtt{L}}} M_{\mathtt{R}} - h^0 g_{h^0 \mathtt{R}} \overline{\hat{M}_{\mathtt{L}}} \hat{\mu}_{\mathtt{R}} \\ & - H^0 g_{H^0}^{\mu\mu} \overline{\hat{\mu}_{\mathtt{L}}} \hat{\mu}_{\mathtt{R}} - H^0 g_{H^0}^{MM} \overline{\hat{M}_{\mathtt{L}}} \hat{M}_{\mathtt{R}} - H^0 g_{H^0 \mathtt{L}} \overline{\hat{\mu}_{\mathtt{L}}} M_{\mathtt{R}} - H^0 g_{H^0 \mathtt{R}} \overline{\hat{M}_{\mathtt{L}}} \hat{\mu}_{\mathtt{R}} \\ & - S^0 g_{S^0}^{\mu\mu} \overline{\hat{\mu}_{\mathtt{L}}} \hat{\mu}_{\mathtt{R}} - S^0 g_{S^0}^{MM} \overline{\hat{M}_{\mathtt{L}}} \hat{M}_{\mathtt{R}} - S^0 g_{S^0 \mathtt{L}}^{\mu M} \overline{\hat{\mu}_{\mathtt{L}}} M_{\mathtt{R}} - S^0 g_{S^0 \mathtt{R}}^{\mu M} \overline{\hat{M}_{\mathtt{L}}} \hat{\mu}_{\mathtt{R}}\,, \end{aligned} \tag{7.3.10}$$

where we denoted the mass eigenstates with a hat and the couplings are given in App. H.

7.3.1 Muon Anamolous Magnetic Moment

The model induces contributions to the AMM of the muon where M and one of the new scalars, h^0, H^0, S^0, run in the loop, see Fig. 7.1 , yielding the total BSM contribution

$$\begin{aligned} a_\mu^{BSM} =& a_\mu^{FFS}(g_{h^0,\mathtt{L}}, g_{h^0,\mathtt{R}}, m_M, m_{h^0}) + a_\mu^{FFS}(g_{H^0,\mathtt{L}}, g_{H^0,\mathtt{R}}, m_M, m_{H^0}) \\ & + a_\mu^{FFS}(g_{S^0,\mathtt{L}}, g_{S^0,\mathtt{R}}, m_M, m_{S^0})\,, \end{aligned} \tag{7.3.11}$$

where a_μ^{FFS} is given by (4.4.12). It is evident that each individual term depends non-trivially on the mixing parameters in the scalar and muon sector, respectively, and on the values of the couplings y, y'. Thus, for simplicity, it is instructive to consider the exact alignment limit, $\beta = \theta_{12}$, and assume that the mixing in the muon sector vanishes, $V_{\mu\mu} = 1, V_{\mu M} = 0$. In this case, the relevant couplings read

$$g_{h^0,\mathtt{L}}^{\mu M} = y' s_{12} s_{23}\,, \qquad g_{h^0,\mathtt{R}}^{\mu M} = -y s_{12} c_{23}\,, \tag{7.3.12}$$

$$g_{H^0,\mathtt{L}}^{\mu M} = -y' c_{12} s_{23}\,, \qquad g_{H^0,\mathtt{R}}^{\mu M} = y c_{12} c_{23}\,, \tag{7.3.13}$$

$$g_{S^0,\mathtt{L}}^{\mu M} = y' c_{23} c_{12}\,, \qquad g_{S^0,\mathtt{R}}^{\mu M} = y s_{23}\,, \tag{7.3.14}$$

and we find that the chirally enhanced contributions to a_μ are present for all three loop diagrams unless $s_{23} = 0$ or $c_{23} = 0$. Nevertheless, note that slight deviations from

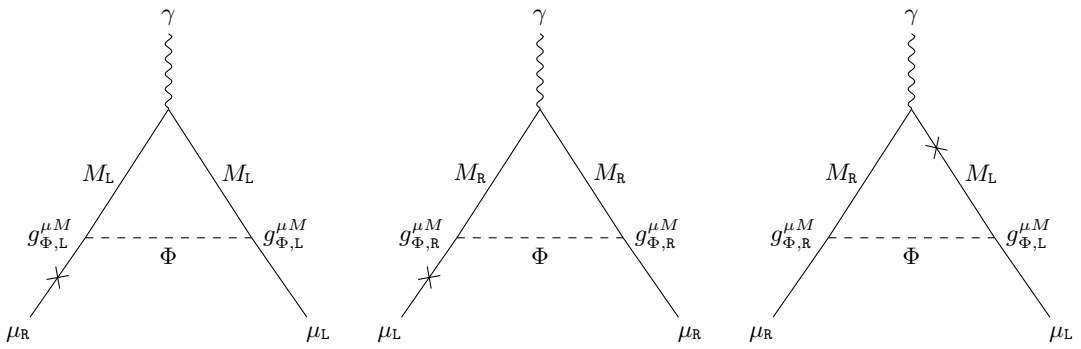

Figure 7.1: Feynman diagrams contributing to a_μ in the model with the new muon type charged fermions with $\Phi = \{h^0, H^0, S^0\}$.

$\beta = \theta_{12}, V_{\mu\mu} = 1, V_{\mu M} = 0$ can result in delicate cancellations between the terms that contribute to the couplings, see App. H, and may result in significantly different coupling structures.

7.4 Constraints

7.4.1 Higgs Decays

In this section, we discuss how the branching ratios of Higgs decays are altered due to the mixing in the scalar and muon sectors, respectively, compared to the SM branching ratios. For convenience, we define

$$\Delta\Gamma\left(h^0 \to ab\right) := \frac{\Gamma\left(h^0 \to ab\right)^M}{\Gamma\left(h^0 \to ab\right)^{SM}} \,. \tag{7.4.1}$$

7.4.1.1 Leptonic Higgs Decays

In the SM, the tree level decay rate of h^0 to a pair of muons is given by

$$\Gamma(h^0 \to \mu\mu)^{SM} \sim \frac{m_\mu}{v_{\mathrm{SM}}} \,, \tag{7.4.2}$$

while in the model discussed here, the decay rate follows from

$$\mathcal{L} = g^{\mu\mu}_{h^0} h^0 \overline{\hat{\mu}} \hat{\mu} \,, \tag{7.4.3}$$

where $g^{\mu\mu}_{h^0}$ is given in App H. Thus, we have $\Gamma(h^0 \to \mu\mu)^M \sim g^{\mu\mu}_{h^0}$ and

$$\Delta\Gamma(h^0 \to \mu\mu) := \frac{\Gamma(h^0 \to \mu\mu)^M}{\Gamma(h^0 \to \mu\mu)^{SM}} = \left| \frac{v_{\mathrm{SM}}}{m_\mu} g^{\mu\mu}_{h^0} \right|^2 \,. \tag{7.4.4}$$

Recent results from CMS [225] on Higgs to muon decays at 99.7% CL are given by

$$\frac{(\sigma\mathcal{B}(h^0 \to \mu\mu))_{obs}}{(\sigma\mathcal{B}(h^0 \to \mu\mu))_{SM}} = 1.19^{+1.28}_{-1.24}\,. \tag{7.4.5}$$

7.4.1.2 $h^0 \to \gamma\gamma$

The dominant SM contribution to Higgs diphoton decays comes from one-loop diagrams with either top-quarks or W-bosons propagating in the loop, see Fig. 7.2, corresponding to a SM decay rate

$$\Gamma(h^0 \to \gamma\gamma)_{SM} \propto \left|\frac{2}{v}A_1(\tau_W) + \frac{2}{v}N_C Q_t^2 A_{1/2}(\tau_t)\right|^2\,, \tag{7.4.6}$$

where A_1 and $A_{1/2}$ are loop functions, given in App. I, $N_C = 3$ is the color multiplicity, $Q_t = 2/3$ is the top quark charge and $\tau_i := 4m_i^2/m_h^2$. The decay rate in our model is altered due to the modified h^0 couplings to W bosons,

$$\mathcal{L} \sim g_{h^0WW} h^0 W_\mu^+ W^{-\mu}\,, \tag{7.4.7}$$

where g_{h^0WW} is given in (7.2.17). The previously discussed constraints on the tree-level leptonic Higgs decays imply that $g_{h^0\mu\mu}$ can not significantly deviate from the tree-level Yukawa couplings, thus the contribution from muons running in the loop is strongly suppressed compared to the top quark loop, similarly to the SM. On the other hand, the new muon type fermions M have Yukawa couplings to h^0 on tree level,

$$\mathcal{L} = g_{h^0}^{MM}\overline{M}Mh^0\,, \tag{7.4.8}$$

where $g_{h^0}^{MM}$ is given H in. This term induces an additional one-loop contribution and modifies the decay rate,

$$\Gamma(h^0 \to \gamma\gamma)_M \propto \left|\frac{2}{v}g_{h^0WW}A_1(\tau_W) + \frac{2}{v_1}N_C Q_t^2 A_{1/2}(\tau_t) + \frac{2g_{h^0}^{MM}}{m_M}Q_M^2 A_{1/2}(\tau_M)\right|^2\,. \tag{7.4.9}$$

Stringent constraints on Higgs diphoton decays are provided by CMS [226] where

$$\frac{(\sigma\mathcal{B}(h^0 \to \gamma\gamma))_{obs}}{(\sigma\mathcal{B}(h^0 \to \gamma\gamma))_{SM}} = 1.12^{+0.27}_{-0.27} \tag{7.4.10}$$

at 99.7% CL.

7.4.1.3 $h^0 \to \gamma Z$

Similarly to the diphoton decay, the Higgs boson can also decay to a photon and a Z boson. The leading SM contribution is again induced by top-quarks and W-bosons running in the loop, resulting in a decay width given by

$$\Gamma(h^0 \to \gamma Z)_{SM} = \left|\frac{2}{v}\cot\vartheta_W A_1(\tau_W,\lambda_W) + \frac{2}{v}\frac{2N_C Q_t}{\sin\vartheta_W\cos\vartheta_W}(T_3^{(t)} - 2Q_t\sin\vartheta_W^2)A_{1/2}(\tau_t,\lambda_t)\right|^2\,. \tag{7.4.11}$$

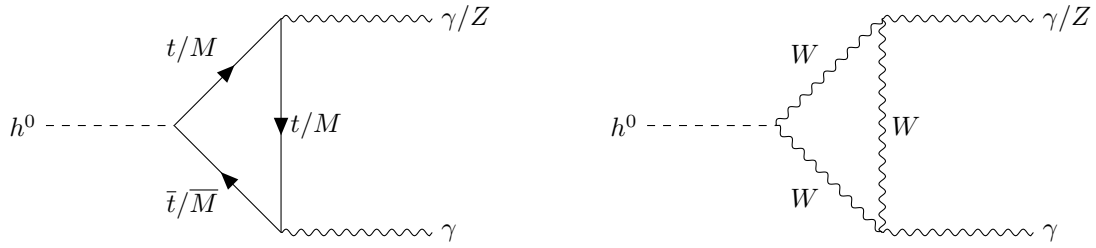

Figure 7.2: Feynman diagrams for $h^0 \to \gamma\gamma(Z)$ at 1-loop order.

Process	Limit	Reference	Process	Limit	Reference
$\mu \to e\gamma$	4.2×10^{-13}	[228]	$\mu\text{Au} \to e\text{Au}$	7.0×10^{-13}	[229]
$\tau \to e\gamma$	3.3×10^{-8}	[230]	$\mu\text{Ti} \to e\text{Ti}$	6.1×10^{-13}	[231]
$\tau \to \mu\gamma$	4.4×10^{-8}	[230]			
$\mu \to 3e$	1.0×10^{-12}	[232]			
$\tau \to 3e$	2.7×10^{-8}	[233]			
$\tau \to 3\mu$	2.1×10^{-8}	[233]			

Table 7.3: Overview of current limits on LFV decays (left) and capture rates (right). A more extensive list of LFV violating processes can be found in Ref. [153].

The contributions in the model considered here arise from the same terms in the Lagrangian as in the case of diphoton decays, see (7.4.7) and (7.4.8). Hence, the modified decay rate is given by

$$\begin{aligned}\Gamma(h^0 \to \gamma Z)_M = \Big| & \frac{2}{v} \cot\vartheta_W g_{h^0WW} A_1(\tau_W, \lambda_W) \\ & + \frac{2}{v_1} \frac{2N_C Q_t}{\sin\vartheta_W \cos\vartheta_W} (T_3^{(t)} - 2Q_t \sin\vartheta_W^2) A_{1/2}(\tau_t, \lambda_t) \\ & + \frac{2g_{h^0}^{MM}}{m_M} \frac{2Q_M}{\sin\vartheta_W \cos\vartheta_W} (2T_3^{(M)} - 2Q_M \sin\vartheta_W^2) A_{1/2}(\tau_M, \lambda_M) \Big|^2 . \end{aligned} \tag{7.4.12}$$

Stringent constraints on the $h^0 \to \gamma Z$ come from CMS [227],

$$\frac{(\sigma(pp \to h^0)\mathcal{B}(h^0 \to \gamma Z))_{obs}}{(\sigma(pp \to h^0)\mathcal{B}(h^0 \to \gamma Z))_{SM}} = 2.4^{+2.7}_{-2.7} , \tag{7.4.13}$$

at 99.7% CL.

7.4.2 Lepton Flavor Violation

In this section, we explore the possibility that the model involving the new muon type leptons induces new contributes to LFV violating processes, such as charged LFV decays $\ell \to \ell'\gamma$, charged three body decays $\ell \to \ell_1\bar{\ell}_2\ell_3$ and $\mu \to e$ conversion via nuclei, with current experimental bounds summarized in Tab. 7.3. Non-zero contributions to LFV arise due to mixing between neutrino mass- and flavor eigenstates and therefore strongly

depend on the BSM mechanism that accounts for the observed neutrino masses. In the following, we restrict ourselves to a qualitative discussion of LFV, assuming that some unspecified mechanism generates the neutrino masses. However, note that depending on the details underlying the neutrino mass generation, the conclusions may not be valid. We further assume that lepton flavor violating processes arise only due to neutrino mixing,

$$|\nu_\alpha\rangle = \sum_k U_{\alpha k} \, |\nu_k\rangle \ , \tag{7.4.14}$$

where in the SM extended by neutrino masses (νSM), U is the 3×3 PMNS matrix and $\alpha = e, \mu, \tau,\ k = 1, 2, 3$ while in the model with an extended muon sector, U is a 5×5 mixing matrix and $\alpha = e, \mu, \tau, M^L, M^R,\ k = 1, 2, 3, 4, 5$.
Let us begin with the discussion of radiative lepton decays, see Fig. 7.3. Note that there is no additional contribution from a loop similar to Fig. 7.1 since e and τ do not mix with M. For simplicity, we restrict the following discussion to $\mu \to e\gamma$. The branching ratio can be expressed in terms of elements of the mixing matrices U and V as [23, 234, 235]

$$\mathrm{Br}(\mu \to e\gamma) \propto |G_{\mu e}|^2 \, , \qquad G_{\mu e} = \sum_i \sum_\beta^{\mu, M} U_{ei} U^*_{\beta i} V_{\mu\beta} G_\gamma(x_i) \, , \tag{7.4.15}$$

where $x_i = m_i^2/m_W^2$, m_i are the neutrino masses and $G_\gamma(x_i)$ is a loop function,

$$G_\gamma(x_i) = -\frac{x(2x^2 + 5x - 1)}{4(1-x)^3} - \frac{3x^3}{2(1-x)^4} \ln x \, . \tag{7.4.16}$$

In the νSM, the sum over β in (7.4.15) is redundant and in the limit $m_i^2/m_W^2 \to 0$, we find that $\mathrm{Br}(\mu \to e\gamma)_{\nu\mathrm{SM}}$ is strongly suppressed via the GIM mechanism,

$$\mathrm{Br}(\mu \to e\gamma)_{\nu\mathrm{SM}} \propto \left| \sum_{i=2}^{3} \frac{U_{ei} U^*_{\mu i} \Delta m^2_{i1}}{m_W^2} \right| \sim 10^{-54} \, , \tag{7.4.17}$$

where $\Delta m^2_{i1} \equiv m_i^2 - m_1^2$ are the mass squared differences of the neutrino masses and we used

$$G_\gamma(x) \approx \begin{cases} \frac{x}{4} \, , & x \ll 1 \, , \\ \frac{1}{2} \, , & x \gg 1 \, . \end{cases} \tag{7.4.18}$$

On the other hand, the extended muon sector renders the analysis of the branching ratio significantly more evolved, since it now also depends on $m_{4,5}$ and V,

$$G^M_{\mu e} = \sum_{i=2}^{3} \frac{\Delta m^2_{i1}}{4m_W^2} U_{ei} \left(V_{\mu\mu} U^*_{\mu i} + V_{\mu M} U^*_{Mi} \right) + \underbrace{\sum_{i=4}^{5} U_{ei} \left[G(x_i) - \frac{m_1^2}{4m_W^2} \right] \left(V_{\mu\mu} U^*_{\mu i} + V_{\mu M} U^*_{Mi} \right)}_{\equiv G^{4,5}_{\mu e}} \, . \tag{7.4.19}$$

The first term in (7.4.19) is dominated by the GIM suppression and as in the SM, it is of order $\mathcal{O}(\Delta m^2_{i1}/m_W^2)$ and hence does not give a sizable new contribution to $\mathrm{Br}(\mu \to e\gamma)$.

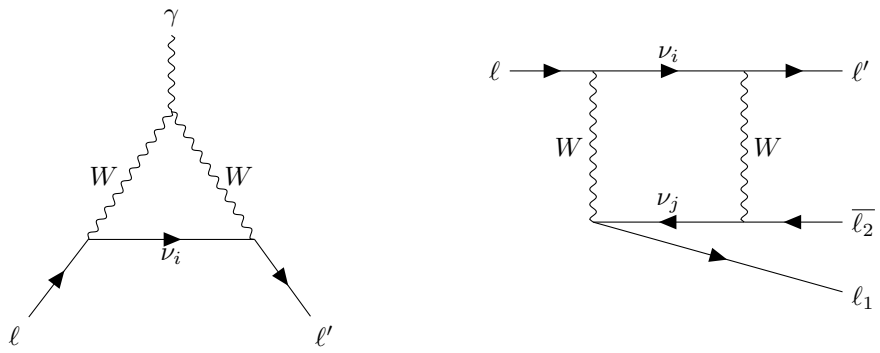

Figure 7.3: *Left:* Feynman diagram for $\ell \to \gamma\ell'$ at 1-loop-order where ℓ, ℓ' are charged SM leptons with one of them being a muon and ν_i is a neutrino in its mass eigenstate. *Right:* Exemplary contribution to charged LFV three body decays $\ell \to \ell'\ell_1\overline{\ell_2}$.

The second term depends on the mass scale of $m_{4,5}$. If the new neutrinos are light, hence $m_{4,5}^2/m_W^2 \to 0$, we find

$$G_{\mu e}^{4,5} \sim \sum_{i=4}^{5} U_{ei} \frac{\Delta m_{i1}^2}{4m_W^2} \left(V_{\mu\mu}U_{\mu i}^* + V_{\mu M}U_{Mi}^*\right) . \tag{7.4.20}$$

Thus, irrespective of the values of the mixing matrix elements, the GIM mechanism suppresses the decay rate, similarly to the SM. In contrast, if the neutrinos are heavy, $m_{4,5}^2/m_W^2 \to \infty$, we have

$$G_{\mu e}^{4,5} \sim \sum_{i=4}^{5} U_{ei} \left[\frac{1}{2} - \frac{m_1^2}{4m_W^2}\right] \left(V_{\mu\mu}U_{\mu i}^* + V_{\mu M}U_{Mi}^*\right) \sim \frac{1}{2}\sum_{i=4}^{5} U_{ei} \left(V_{\mu\mu}U_{\mu i}^* + V_{\mu M}U_{Mi}^*\right) \tag{7.4.21}$$

and the GIM mechanism is unoperative. Nevertheless, the rate of LFV still depends on the mixing between the SM sector and the new muon type neutrinos which we expect to be very small. Thus, even if the masses of the new neutrinos are large, we anticipate that the small mixing between the neutrino sectors renders radiative LFV decays negligibly small, similarly to LFV in the type I Seesaw mechanism (see e.g. [235, 236]).

Besides radiative decays, it is also possible that LFV occurs due to $\mu \to e$ conversion in nuclei. As can be seen in Fig. 7.4, $\mu \to e$ conversion does not require that a real photon is radiated, hence more diagrams contribute to the conversion rate compared to radiative decays. Moreover, the conversion rate also depends significantly on the nucleus involved and its atomic mass and number, A and Z, overall rendering the theoretical description of $\mu \to e$ conversion significantly more evolved. While a detailed discussion is beyond the scope of this work, we note that the $\mu \to e$ rate depends on the same combinations of the mixing matrices U and V as radiative decays. Thus, we draw the same conclusion that the anticipated small mixing between both neutrinos sectors severely suppresses new contributions to the conversion rate.

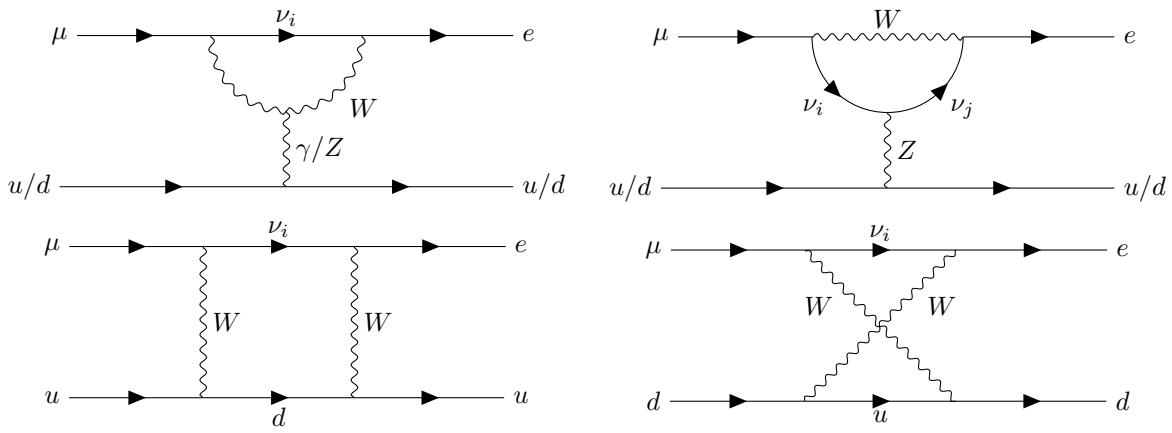

Figure 7.4: Feynman diagrams for the $\mu \to e$ conversion where ν_i is a neutrino in its mass eigenstate.

Finally, let us briefly consider the case of three-body decays $\ell \to \ell_1 \bar{\ell}_2 \ell_3$. In Fig. 7.3 (right), we show a representative feynman diagram that contributes to the amplitude. Nevertheless, we stress that various other diagrams can appear as well, see Ref. [235] for details, and hence the amplitude is highly non-trivial. As a naive guess, we expect that each vertex involving a muon adds a factor $V_{\mu\beta}$ while each vertex involving a neutrino yields a factor $U_{\alpha i}$ and as in the previously discussed processes, the rate depends on the sum over products of elements of U and V and we assume that similar arguments regarding the suppression via the mixing between both neutrino sectors hold. However, we stress that this analysis is highly superficial and more precise statements would require a detailed study of the neutrino sector.

7.4.3 Collider Signals

At *pp* colliders, several channels for VLL production exist. For example, VLLs can be produced via exchange of electroweak gauge bosons and decay to $W\nu$, see Fig. 7.5. More detailed studies of collider signatures can be found e.g. in Ref. [237]. So far, collider searches are focused on the search for VLLs that couple to the τ lepton [238–241], with the most stringent bounds provided by CMS excluding tauphillic VLLs up to masses of 1040 GeV[242]. While VLLs coupling to electrons and muons, respectively, have not yet been probed, CMS used results from LHC Run-2 to project the sensitivity to the HL-LHC for models including VLLs that couple to electrons and muons [243]. With a total integrated luminosity of $3000\,\text{fb}^{-1}$ at $\sqrt{s} = 14\,\text{TeV}$, they expect to exclude vectorlike doublets that couple to muons at 95 % CL up to a mass of 1630 GeV. The only directly applicable bounds for the model discussed here are searches for additional heavy leptons at LEP which place a significantly weaker lower limit on the mass at around 100 GeV [244]. Thus, future dedicated searches at colliders are necessary to provide stringent constraints on the muonphillic VLLs considered in the model discussed in this work.

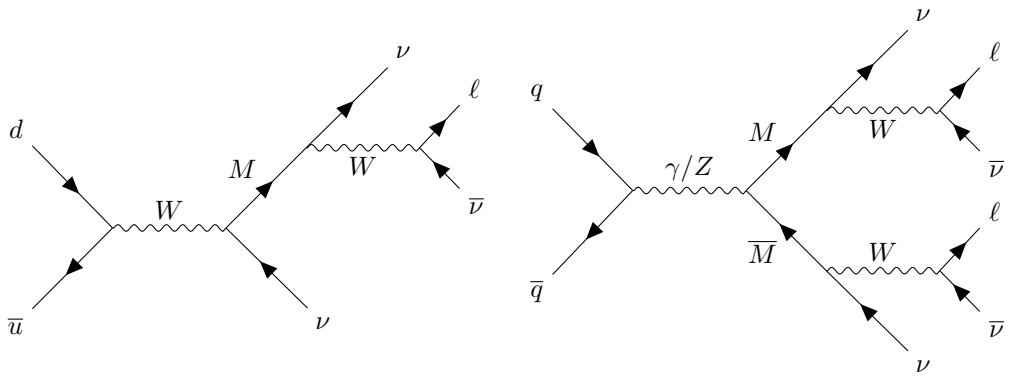

Figure 7.5: Examples of signal channel feynman diagrams with $\ell + E_{miss}$ (left) and $2\ell + E_{miss}$ (right) signatures.

7.5 Results

In the previous sections, we discussed various constraints on the model containing VLLs and BSM scalars. In order to explore if parameter sets exist that are compatible with these constraints while also yielding a suitable contribution to the AMM of the muon, we have performed random scans over the free parameters of the model. Before we present our results, let us briefly outline the procedure used to find valid parameter sets.
In the scalar sector, bounds on the couplings arise from vacuum stability, see (7.2.20) and (7.2.21) and Tab. 7.2 with $\mathcal{E}_4 < \mathcal{E}_{1,2,3,5,6,7,7}$. In order to find viable sets of couplings, we perform random scans over the ranges

$$0 \leq \lambda_{1,2,S} \leq 1\,, \quad -1 \leq \lambda_{3,4,5} \leq 1\,, \quad -1 \leq \eta_2 \leq 1\,, \quad \eta_1 = 0\,. \tag{7.5.1}$$

These couplings are used to determine the scalar mass spectrum, see Sec. 7.2, where we impose the additional bounds

$$\frac{v_{\rm SM}^2}{1+50^2} \leq v_1^2 \leq \frac{v_{\rm SM}^2}{2}\,, \qquad 0.9 \leq \cos\theta_{13} \leq 1\,, \tag{7.5.2}$$

$$0 \leq \mu_S \leq 100\,\text{GeV}\,, \qquad \cos\beta - 0.1 \leq \cos\theta_{12} \leq \cos\beta + 0.1\,, \tag{7.5.3}$$

and explicitly verify that the resulting scalar masses are positive. In Fig. 7.6, we show scatter plots of the identified parameter sets in the scalar sector consistent with the aforementioned constraints. It is apparent that a wide range of parameters yield viable scalar sectors. Notably, we find that smaller values of $\tan\beta \lesssim 20$ and $v_S \lesssim 300\,\text{GeV}$ are favored, although outliers exist where $20 \lesssim \tan\beta \lesssim 50$ and $300 \lesssim v_S \lesssim 1400\,\text{GeV}$.

Next, we use these parameters to determine a muon sector that is consistent with the constraints discussed in Sec. 7.4[3] while simultaneously reproducing the observed value of the muon AMM. That is, we scan for values of the vectorlike fermion mass m_M and

[3]Note that for $\Delta\Gamma\left(h^0 \to \mu\mu\right)$ and $\Delta\Gamma\left(h^0 \to \gamma Z\right)$ we impose $\Delta\Gamma\left(h^0 \to \gamma Z, \mu\mu\right) = 0$ as a lower bound.

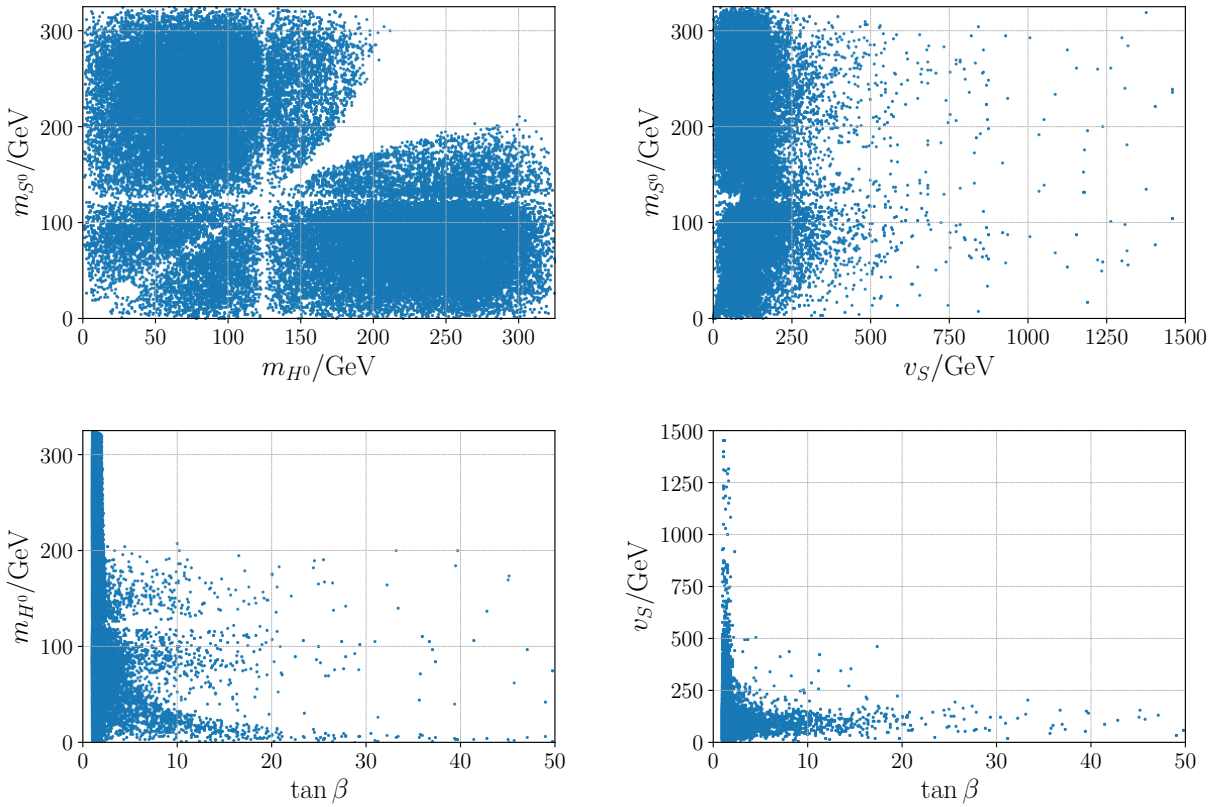

Figure 7.6: Data sets allowed by the constraints from Sec. 7.4 with an alignment limit according to (7.5.3).

couplings y, y' in the range

$$100\,\text{GeV} \leq m_M \leq 10\,000\,\text{GeV}\,, \qquad -3 \lesssim y, y' \lesssim 3\,, \tag{7.5.4}$$

that are in agreement with (4.4.10) while also being compatible with the experimental constraints from Higgs decays discussed in Sec. 7.4.1.1-7.4.1.3. In Fig. 7.7, we show a_μ^{model} and $\Delta\Gamma\,(h^0 \to \mu\mu, \gamma\gamma, \gamma Z)$ for 9 exemplary chosen data sets as functions of the VLL mass m_M that agree with all bounds over a non-vanishing range of m_M[4] We stress that the respective constraints depend not only on m_M but are also on the specific combination of parameters from Sec. 7.4 that enter equations (7.4.4), (7.4.9) and (7.4.12), respectively. Nevertheless, we conclude that the model discussed here can give contributions to the AMM of the muon that are compatible with constraints from Higgs decays. Finally, if future searches for VLLs coupling to muons at CMS [243] exclude VLL masses up to $m_M \sim 1.6\,\text{TeV}$, the viable parameter space of the model would be restricted as e.g. set 4 in Fig. 7.7 would be excluded.

[4]The corresponding data sets are given in Tab. J.1.

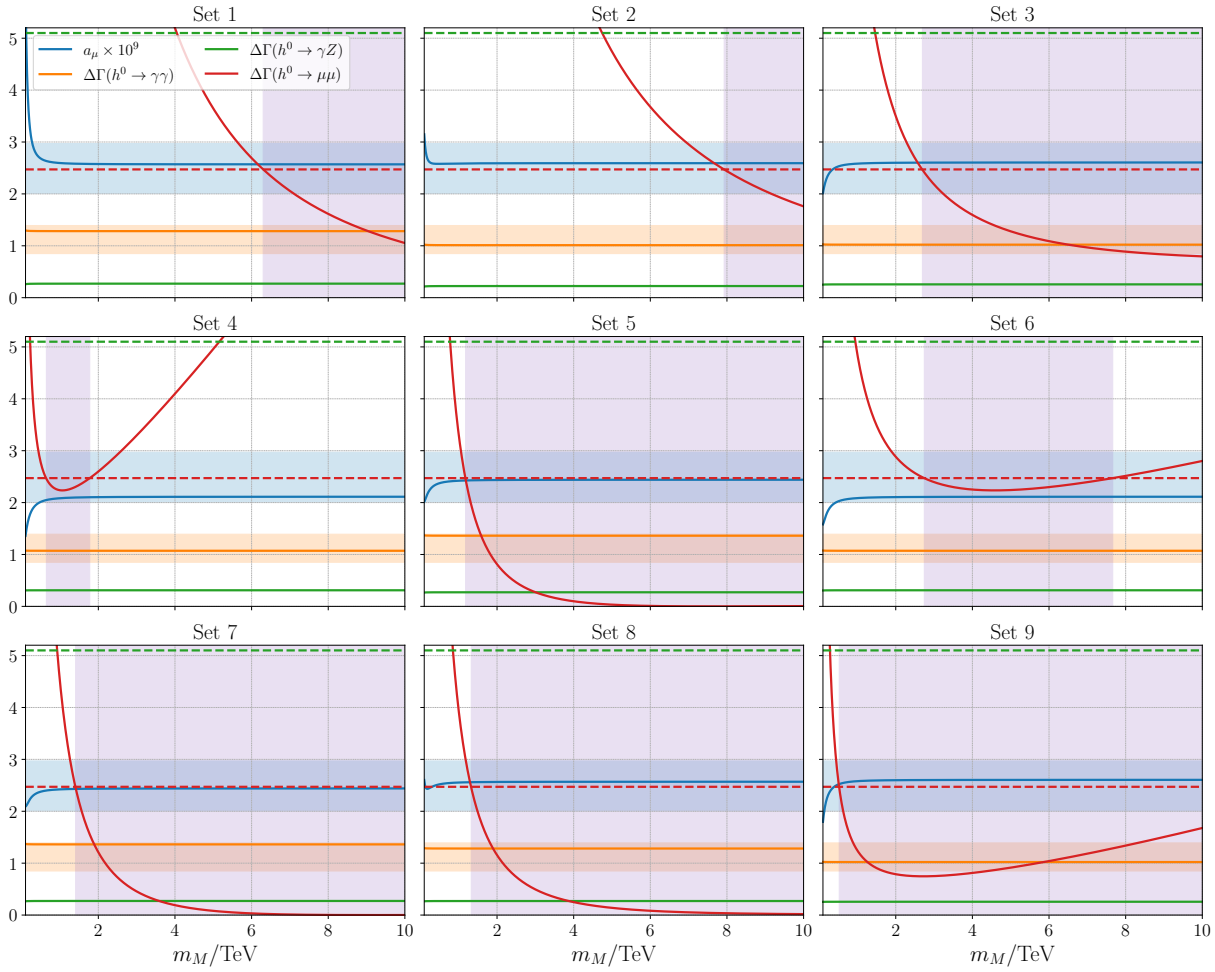

Figure 7.7: Muon AMM a_μ as a function of the vectorlike lepton mass m_M for nine exemplary data sets, see Tab. J.1. In the purple region, a_μ is in agreement with (4.4.10) and constraints from Higgs decays are met. The blue region corresponds to the uncertainty of $\Delta a_\mu = a_\mu^{exp} - a_\mu^{SM}$. The orange region corresponds to the limits on $h^0 \to \gamma\gamma$. The red (green) dashed line indicates the upper limit on $h^0 \to \gamma Z(h^0 \to \mu\mu)$.

7.6 Summary

In this Chapter, we have considered an extension of the SM by a scalar singlet, an additional Higgs doublet and a VLL coupling to muons with a mass of order $\mathcal{O}(1 - 10\,\text{TeV})$ as an explanation of discrepancy between the observed and the predicted values of the AMM of the muon. We have derived constraints on the scalar sector in a setup that yields chirally enhanced contributions to the AMM of the muon, taking constraints from vacuum stability and the alignment limit into account. The couplings of the BSM scalars and VLLs induce mixing in both the scalar and the muon sector of the model and hence invoke bounds on the model parameters from Higgs decays. We find that the contribution to the

AMM of the muon and the modification of the Higgs decay rates depend significantly on the free parameters of the model. Overall, various parameter sets are in agreement with experimental constraints. More stringent constraints on the model could be supplied by future searches for VLLs. Lastly, the model does not induce sizable contributions to LFV processes.

CHAPTER 8

Conclusion

In this thesis, we have discussed evidence for the existence of new physics on the basis of the SM of particle physics and cosmology. To do so, we have focussed on two different SM extensions: Majorons and vector-like leptons.

The Majoron is the Goldstone boson which arises when the global $U(1)_{B'-L'}$ of the SM is spontaneously broken. In Chapter 5, we have reviewed the generic Singlet Majoron model and outlined the relevance of massive Majorons as a DM candidate. Despite its success, the Majoron model has been subject to criticism as the symmetry breaking mechanism associated with the Majoron has been considered to be a potential origin of domain walls, similarly to Axion models. As cosmic domain walls are usually highly problematic in the context of cosmology, their existence would essentially rule out the simplest realizations of the Majoron model. However, as we have outlined in this thesis, Majoron models do not suffer from the appearance of domain walls and therefore remain highly relevant as an explanation of the origin of neutrino masses.
Moreover, we have discussed the implications of extensions of the Majoron model by RH fermions. Originally motivated as a solution to the disputed domain wall problem, these extensions remain interesing due to the impact of the new particles on the way leptogenesis proceeds in these models. Besides changing the anomaly factor of the $[\mathrm{SU}(2)_\mathrm{L}] \times U(1)L'$ anomaly of the SM, and therefore also the conversion rate with which Sphaleron processes transfer a lepton asymmetry into a baryon asymmetry, the additional particles also affect the dynamics that create the lepton asymmetry. In Chapter 6, we have focussed on the extension of the Majoron model by a RH $\mathrm{SU}(2)_\mathrm{L}$ triplet fermion and explored if the model can provide suitable conditions for succesfull leptogenesis. For simplicity, we have focussed on a model where the triplet does not couple directly to the lepton- and scalar sectors of the SM, hence restricting the source of lepton number violation to the neutrino Yukawa coupling. Despite participating in various scattering processes with the new particles, we find that the efficiency with which neutrino interactions violate lepton number is still sizable and, depending on the parameters of the model, can reproduce the observed BAU. Notably, this result does also apply to the generic singlet Majoron model and not only to the extension including the triplet. Moreover, we find that it is essential to include the out-of-equilibrium dynamics of *all* BSM particles of the model when solving the Boltzmann equations that govern leptogenesis, rather than taking only the out-of-equilibrium dynamics of the heavy neutrinos into account. The commonly employed latter approach drastically

underestimates the efficiency and results in a lepton asymmetry that is up to a factor of one hundred smaller compared to the more detailed treatment of the out-of-equilibrium dynamics. Finally, we have deduced constraints on the parameters of the model from the relic abundances of both the Majoron and the triplet. We find that the Majoron is ruled out as a DM candidate as it would either overproduce DM or constitute hot DM, rather than the cold DM required for structure formation. In order to evade this bound, the Majoron has to be *significantly* lighter than 100 eV. The relic density of the triplet is dictated by its mass, and hence its coupling to the new singlet scalar. If the triplet is sufficiently light, $M_T \sim 1\,\text{TeV}$, we find that triplet DM - that is also in agreement with bounds on the triplet mass from Atlas and CMS - is viable.
We conclude that leptogenesis in (extended) Majoron models is a feasible scenario. Given that we focussed on the necessity of a careful treatment of the out-of-equilibrium dynamics of the BSM sector, future works that include other intricate effects neglected here are in order. For example, the impact of flavor in the Boltzmann equations or the resonant enhancement of the $\mathcal{CP}$ violation appear worthwhile to examine, just as the possibility of lepton number violating triplet decays.

In Chapter 7, we have discussed a model that aims to address the discrepancy between the observed and the predicted values of the anomalous magnetic moment of the muon, inspired by vector-like leptons appearing in grand unified theories based on the breaking of E_6. We have explored an extension of the SM that contains vector-like leptons coupling to muons alongside a new singlet scalar and a second Higgs doublet. This induces mixing both in the scalar sector as well as in the extended muon sector and has a rich phenomenology. We have deduced constraints on the paramters of the model based on the stability of the scalar potential and the alignment limit, similar to two-Higgs doublet models, as well as bounds from Higgs decays. Moreover, we have briefly investigated the prospect of lepton flavor violation arising in the model, finding no clear indication for new contributions that significantly exceed the lepton flavor violation in the SM. We have performed random scans over the parameters of the model and find that the model can easily fulfill the considered bounds while providing a desirable contribution to the anomalous magnetic moment of the muon. For future works, dedicated searches for vector-like leptons coupling to muons at the LHC could serve to derive more stringent constraints on the parameter space.

APPENDIX A

Notation and Conventions

Unless otherwise mentioned, we work in natural units,

$$\hbar = c = k_B = 1\,, \tag{A.0.1}$$

so that

$$[\text{length}] = [\text{time}] = [\text{mass}]^{-1} = [\text{temperature}]^{-1} = [\text{energy}]^{-1}\,. \tag{A.0.2}$$

In these units, the Planck mass, -length and -time only depend on the gravitational constant G,

$$\mathrm{M_{Pl}} = \frac{1}{\sqrt{G}}\,, \mathrm{l_{Pl}} = \mathrm{t_{Pl}} = \sqrt{G}\,. \tag{A.0.3}$$

The metric tensor is given by

$$\eta_{\mu\nu} = \eta^{\mu\nu} = \mathrm{diag}\,(1,-1,-1,-1) \tag{A.0.4}$$

with

$$\eta_{\mu\nu}\eta^{\mu\nu} = 4\,. \tag{A.0.5}$$

The contra- and covariant coordinates are given by

$$x^\mu = (t,x,y,z) = (t,\vec{x})\;, \qquad x_\mu = (t,-x,-y,-z) = (t,-\vec{x})\;, \tag{A.0.6}$$

while the corresponding derivatives read

$$\partial_\mu = \frac{\partial}{\partial x^\mu} = \left(\frac{\partial}{\partial t}, \vec{\nabla}\right)\,, \qquad \partial^\mu = \frac{\partial}{\partial x_\mu} = \left(\frac{\partial}{\partial t}, -\vec{\nabla}\right)\,. \tag{A.0.7}$$

The Christoffel symbols in terms of a metric $g_{\mu\nu}$ are given by

$$\Gamma^\rho_{\nu\mu} = \frac{1}{2} g^{\rho\eta}\left(\partial_\nu g_{\mu\eta} + \partial_\mu g_{\nu\eta} - \partial_\eta g_{\nu\mu}\right)\,, \tag{A.0.8}$$

while the Ricci tensor $R_{\mu\nu}$ and the Ricci scalar R are defined as

$$R_{\mu\nu} = \partial_\alpha \Gamma^\alpha_{\mu\nu} - \partial_\nu \Gamma^\alpha_{\alpha\mu} + \Gamma^\alpha_{\alpha\beta}\Gamma^\beta_{\mu\nu} - \Gamma^\alpha_{\mu\beta}\Gamma^\beta_{\alpha\nu} \tag{A.0.9}$$

$$R = g^{\mu\nu} R_{\mu\nu}\,. \tag{A.0.10}$$

Moreover, the covariant derivative reads

$$\Delta_\nu V^{\mu\lambda} = \partial_\nu V^{\mu\lambda} + \Gamma^\mu_{\nu\rho} V^{\rho\lambda} + \Gamma^\lambda_{\nu\rho} V^{\mu\rho}\,. \tag{A.0.11}$$

The Pauli matrices are given by

$$\sigma^1 = \begin{pmatrix} 0 & 1 \\ 1 & 0 \end{pmatrix}, \quad \sigma^2 = \begin{pmatrix} 0 & -i \\ i & 0 \end{pmatrix}, \quad \sigma^3 = \begin{pmatrix} 1 & 0 \\ 0 & -1 \end{pmatrix} \tag{A.0.12}$$

and satisfy the identities

$$[\sigma_i, \sigma_j] = 2i\epsilon^{ijk}\sigma_k\,, \quad \{\sigma_i, \sigma_j\} = 2\delta_{ij}\,, \quad \mathrm{Tr}\,[\sigma_i\sigma_j] = 2\delta_{ij}\,, \tag{A.0.13}$$

where ϵ^{ijk} is the totally antisymmetrik tensor with $\epsilon^{123} = 1$, while $[\,,\,]$ and $\{\,,\,\}$ are the commutator and anti-commutator, respectively. Moreover, the linear combinations $\sigma^{\pm}$ are defined as

$$\sigma^+ = \frac{1}{2}\left(\sigma^1 + i\sigma^2\right), \qquad \sigma^- = \frac{1}{2}\left(\sigma^1 - i\sigma^2\right). \tag{A.0.14}$$

The gamma matrices γ^μ, $\mu = 0, 1, 2, 3$ satisfy the Clifford-Algebra,

$$\{\gamma^\mu, \gamma^\nu\} = 2\eta^{\mu\nu}\mathbb{1}_4\,, \tag{A.0.15}$$

while the fifth gamma matrix γ^5 is defined as

$$\gamma^5 = i\gamma^0\gamma^1\gamma^2\gamma^3\,. \tag{A.0.16}$$

Useful identities that follow from the Clifford-Algebra are

$$\gamma^0\gamma^\mu\gamma^0 = (\gamma^\mu)^\dagger \tag{A.0.17}$$

$$\gamma^5 = \left(\gamma^5\right)^\dagger \tag{A.0.18}$$

$$\left(\gamma^5\right)^2 = \mathbb{1}_4 \tag{A.0.19}$$

$$\{\gamma^5, \gamma^\mu\} = 0\,. \tag{A.0.20}$$

The chiral projection operators are defined as

$$P_{\mathtt{R}} = \frac{1}{2}(1 + \gamma^5)\,, \quad P_{\mathtt{L}} = \frac{1}{2}(1 - \gamma^5)\,, \tag{A.0.21}$$

and satisfy

$$P_{\mathtt{R}} + P_{\mathtt{L}} = 1\,, \quad P_{\mathtt{R}}^2 = P_{\mathtt{R}}\,, \quad P_{\mathtt{L}}^2 = P_{\mathtt{L}}\,. \tag{A.0.22}$$

APPENDIX B

Dirac and Majorana Fermions

In this section, we briefly review the properties of Dirac- and Majorana fermions, following [246]. Massive fermion fields can be either *Dirac* or *Majorana* fields. Majorana fermions are their own antiparticles, hence they need to fulfill the reality condition

$$\psi^C = \psi\,, \tag{B.0.1}$$

where ψ^C is the antiparticle,

$$\psi^C \equiv C\overline{\psi}^T \tag{B.0.2}$$

and C has the properties

$$C^\dagger = C^T = C^{-1} = -C\,, \qquad C\gamma_\mu C^{-1} = -\gamma_\mu^T\,. \tag{B.0.3}$$

In the Dirac representation of the gamma matrices, C can be expressed as

$$C = i\gamma^2\gamma^0\,. \tag{B.0.4}$$

Both Dirac and Majorana fermions can be expressed in terms of two-component, massless Weyl fields. Weyl fields are either LH or RH, i.e. a LH Weyl field χ satisfies

$$P_{\mathtt{L}}\chi = \chi\,, \qquad P_{\mathtt{R}}\chi = 0\,. \tag{B.0.5}$$

Using (B.0.2), we find the antiparticle

$$\chi^C = (P_{\mathtt{L}}\chi)^C = P_{\mathtt{R}}\chi^C\,, \tag{B.0.6}$$

i.e. χ^C is RH.[1] It is now easy to see that we can define a Majorana field ψ_M with a single Weyl field χ as

$$\psi_M = \chi + \chi^C = (\psi_M)^C\,. \tag{B.0.9}$$

Recalling that mass terms in the SM couple LH and RH fields, it is evident that arranging the fields in this way enables us to write down a non-vanishing Majorana mass term,

$$\overline{\psi_M}\psi_M = \overline{\chi}\chi^C + \overline{(\chi^C)}\chi\,. \tag{B.0.10}$$

[1] Note that C should not be confused with the operation of charge conjugation $\mathcal{C}$ given by

$$\mathcal{C}\psi\mathcal{C}^{-1} = \alpha_C\psi\,, \tag{B.0.7}$$

where α_C is a phase. While C brings a LH particle to a RH antiparticle, $\mathcal{C}$ acts on a chiral field according to

$$\mathcal{C}\psi_L\mathcal{C}^{-1} = \alpha_C\left(\psi^C\right)_L\,, \tag{B.0.8}$$

i.e. it does not affect chirality.

On the other hand, massive Dirac fermions ψ_D require two independent Weyl fields χ_1, χ_2 which have opposite handness, i.e.

$$\psi_D = \chi_1 + \chi_2 = P_{\mathtt{L}}\chi_1 + P_{\mathtt{R}}\chi_2\,, \tag{B.0.11}$$

which yields the mass term

$$\overline{\psi_D}\psi_D = \overline{\chi_1}\chi_2 + \overline{\chi_2}\chi_1\,. \tag{B.0.12}$$

From the definition (B.0.1), it is apparent that Majorana fermions can not carry charges. Consequently, the charged fermions in the SM are Dirac fields. Neutrinos on the other hand do not carry conserved charges and can therefore be Majorana fields.

APPENDIX C

Numerical Values

Table C.1: Numerical values for the SM parameters used in this thesis [153] where $\alpha \equiv \frac{e^2}{4\pi}$ is the fine structure constant, $G_F \equiv \frac{\sqrt{2}g}{8m_W^2}$ is the Fermi coupling constant and $\alpha_s \equiv \frac{g_s^2}{4\pi}$.

Parameter	Value
m_e	$(0.510\,998\,950\,00 \pm 0.000\,000\,000\,15)$ MeV
m_μ	$(105.658\,375\,5 \pm 0.000\,002\,3)$ MeV
m_τ	(1776.93 ± 0.09) MeV
m_u	(2.16 ± 0.07) MeV
m_d	(4.70 ± 0.07) MeV
m_c	(1.2730 ± 0.0046) MeV
m_s	(93.5 ± 0.8) MeV
m_t	(172.57 ± 0.29) GeV
m_b	(4.183 ± 0.007) GeV
m_h	(125.20 ± 0.11) GeV
α	$(7.297\,352\,569\,3 \pm 0.000\,000\,001\,1) \times 10^{-3}$
G_F	$(1.166\,378\,8 \pm 0.000\,000\,6) \times 10^{-5}\,\text{GeV}^{-2}$
α_s	0.1180 ± 0.0009
$\sin\theta'_{12}$	$0.225\,01 \pm 0.000\,68$
$\sin\theta'_{13}$	$0.003\,732^{+0.000090}_{-0.000085}$
$\sin\theta'_{23}$	$0.041\,83^{+0.00079}_{-0.00069}$
δ'	1.147 ± 0.026
$\sin^2\theta_W$	$0.231\,29 \pm 0.000\,04$
m_W	(80.3692 ± 0.0133) GeV
m_Z	(91.1880 ± 0.0020) GeV

APPENDIX D

Grand Unified Theories

We know that despite its success in e.g. the prediction of the Higgs mass, the SM is not complete. Moreover, given that the electromagnetic and the weak force are unified at high energies to the electroweak force, it does not seem too far fetched to assume that at even higher energies, all three SM gauge interactions are unified into a larger gauge group G. Such a theory is called a *grand unified theory* (GUT). At this point, the task is mainly a group theoretic one: Find a gauge group G that can be broken to G_{SM}. Popular examples of larger groups that have G_{SM} as a subgroup are SU(5), $SO(10)$ and E_6[153, 247]. For example, SU(5) is the smallest group that has G_{SM} as a subgroup. It has 24 generators and hence contains 12 new gauge bosons. The SM fermions transform under the $\overline{\mathbf{5}}$ or $\mathbf{10}$ representations of SU(5) and branch according to [27]

$$\overline{\mathbf{5}} = \underbrace{(\mathbf{1},\mathbf{2})_{-\frac{1}{2}}}_{L} + \underbrace{(\overline{\mathbf{3}},\mathbf{1})_{\frac{1}{3}}}_{(d_{\text{R}})^C}, \qquad \mathbf{10} = \underbrace{(\mathbf{1},\mathbf{1})_{1}}_{(e_{\text{R}})^C} + \underbrace{(\mathbf{3},\mathbf{2})_{\frac{1}{6}}}_{Q} + \underbrace{(\mathbf{3},\overline{\mathbf{3}})_{-\frac{2}{3}}}_{(u_{\text{R}})^C}, \tag{D.0.1}$$

where we used the notation $(\text{SU}(3)_X, \text{SU}(2)_{\text{L}})_{U(1)_Y}$. In $SO(10)$ models with a breaking pattern

$$SO(10) \to \text{SU}(5) \times U(1)_X\,, \tag{D.0.2}$$

the SM fermions can be accomodated in a single $\mathbf{16}$ dimensional representation which branches as

$$\mathbf{16} = \mathbf{10} + \overline{\mathbf{5}} + \mathbf{1} = \underbrace{(\mathbf{1},\mathbf{2}) + (\overline{\mathbf{3}},\mathbf{1}) + (\mathbf{1},\mathbf{1}) + (\mathbf{3},\mathbf{2}) + (\mathbf{3},\overline{\mathbf{3}})}_{\text{SM fermions}} + (\mathbf{1},\mathbf{1})\,, \tag{D.0.3}$$

where we have omitted the $U(1)_X$ charges for readability. As in SU(5), the SM fermions transform under either $\overline{\mathbf{5}}$ or $\mathbf{10}$ while an additional singlet fermion which transforms as $(\mathbf{1},\mathbf{1})$ is predicted. Next, E_6 has several maximal subgroups that can break to G_{SM}. One possible breaking pattern is $E_6 \to SO(10) \times U(1)$ [248–250] where the fundamental representation $\mathbf{27}$ branches as

$$\mathbf{27} = \mathbf{16} + \mathbf{1}_1 + \mathbf{10}_{-2} + \mathbf{1}_4\,. \tag{D.0.4}$$

Again neglecting the $U(1)$ parts for brevity, the full $E_6 \to SO(10) \to \text{SU}(5) \to G_{\text{SM}}$ branching rule is given by

$$\mathbf{27} = \mathbf{16} + \mathbf{10} + \mathbf{1} = (\mathbf{10} + \overline{\mathbf{5}} + \mathbf{1}) + (\mathbf{5} + \overline{\mathbf{5}}) + \mathbf{1} \tag{D.0.5}$$

$$= \underbrace{(\mathbf{1},\mathbf{2}) + (\overline{\mathbf{3}},\mathbf{1}) + (\mathbf{1},\mathbf{1}) + (\mathbf{3},\mathbf{2}) + (\mathbf{3},\overline{\mathbf{3}})}_{\text{SM fermions}} + (\mathbf{1},\mathbf{1}) + (\mathbf{1},\overline{\mathbf{2}}) + (\mathbf{1},\mathbf{2}) \\ + (\mathbf{3},\mathbf{1}) + (\overline{\mathbf{3}},\mathbf{1}) + (\mathbf{1},\mathbf{1})\,. \tag{D.0.6}$$

Another breaking pattern of E_6 is $E_6 \to \mathrm{SU}(3)_C \times \mathrm{SU}(3)_{\mathtt{L}} \times \mathrm{SU}(3)_{\mathtt{R}} \to G_{\mathrm{SM}}$ which is often called *trinification* [251–267]. It has a branching rule

$$\mathbf{27} = (\mathbf{3},\mathbf{3},\mathbf{1}) + (\overline{\mathbf{3}},\mathbf{1},\overline{\mathbf{3}}) + (\mathbf{1},\overline{\mathbf{3}},\mathbf{3}) \tag{D.0.7}$$

$$= \underbrace{(\mathbf{1},\mathbf{2}) + (\overline{\mathbf{3}},\mathbf{1}) + (\mathbf{1},\mathbf{1}) + (\mathbf{3},\mathbf{2}) + (\mathbf{3},\overline{\mathbf{3}})}_{\text{SM fermions}} + (\mathbf{1},\mathbf{1}) + (\mathbf{1},\overline{\mathbf{2}}) + (\mathbf{1},\mathbf{2}) \\ + (\mathbf{3},\mathbf{1}) + (\overline{\mathbf{3}},\mathbf{1}) + (\mathbf{1},\mathbf{1})\,, \tag{D.0.8}$$

where we again omitted $U(1)$ indices for brevity. Thus, besides the SM fermions, we find that in E_6 GUTs, two additional singlets and a conjugate pair of $\mathrm{SU}(2)_{\mathtt{L}}$ doublets and triplets, respectively, appear.

APPENDIX E

Instantons

In a nutshell, YM theories have a non-trivial vacuum structure and Instantons are the *classical solutions to the euclidian equations of motion with finite action* that tunnel between the different degenerate zero-energy states. Despite being very precise, this statement often raises more questions than it answers. In order to make sense of this statement, we will divide the matter into several steps. In order to set the notation in euclidian spacetime and motivate why it is indeed interesting to search for classical solutions in euclidian spacetime, we discuss a simple example from quantum mechanics, the double well potential. Next, since the degenerate vacua between which Instantons tunnel are classified by a topological invariant, the winding number, we will provide a brief introduction to homotopy theory. With this machinery at hand, we are finally be able to discuss the vacuum structure of YM theories and Instantons as tunneling solutions. Last but not least, we discuss the phenomenolgical relevance of Instantons and their relation to the chiral anomaliy. For details, we refer the reader to the standard literature on Instantons in Refs. [96, 161, 163]. More recent reviews are e.g. presented in Refs. [75, 164, 268–270]

E.1 Instantons in Quantum Mechanics

Let us consider the Lagrangian of a particle with unit mass in a potential $V(x)$,

$$\mathcal{L} = \frac{1}{2}\left(\frac{dx}{dt}\right)^2 - V(x)\,. \tag{E.1.1}$$

In the path integral formalism, the amplitude of a transition from x_i at the intial time $-\frac{t_0}{2}$ to x_f at final time $\frac{t_0}{2}$ is given by[1]

$$Z(x_f, x_i) = \langle x_f |\, e^{-\frac{iHt_0}{\hbar}}\, |x_i\rangle = \mathcal{N}\int D[x] e^{i\frac{S[x]}{\hbar}}\,, \tag{E.1.2}$$

where S is the action,

$$S = \int_{-\frac{t_0}{2}}^{\frac{t_0}{2}} dt \mathcal{L}(x, \dot{x})\,, \tag{E.1.3}$$

[1] In this section, we will keep $\hbar$.

H is the Hamiltonian and $D[x]$ integrates over all paths with boundary conditions $x(-\frac{t_0}{2}) = x_i$, $x(\frac{t_0}{2}) = x_f$. Moreover, inserting a full set of eigenstates of the Hamiltonian,

$$H\left|n\right\rangle = E_n\left|n\right\rangle \,, \tag{E.1.4}$$

the LHS of (E.1.2) becomes a sum of oscillating exponential functions,

$$Z(x_f, x_i) = \left\langle x_f\right| e^{-\frac{iHt_0}{\hbar}}\left|x_i\right\rangle = \sum_n e^{-\frac{iE_n t_0}{\hbar}}\left\langle x_f|n\right\rangle\left\langle n|x_i\right\rangle \,. \tag{E.1.5}$$

In order to find the ground state energy, it is convenient to substitute

$$t \to -i\tau \,, \tag{E.1.6}$$

where τ is now a spatial coordinate, despite often being referred to as *imaginary time*. Thus, the substitution transforms Minkowski space into euclidian space. With this substitution, (E.1.5) becomes a sum of decreasing exponentials,

$$Z(x_f, x_i) = \left\langle x_f\right| e^{-\frac{H\tau_0}{\hbar}}\left|x_i\right\rangle = \sum_n e^{-\frac{E_n\tau_0}{\hbar}}\left\langle x_f|n\right\rangle\left\langle n|x_i\right\rangle \,, \tag{E.1.7}$$

and in the limit $\tau_0 \to \infty$, we find that the ground state dominates,

$$\lim_{\tau_0\to\infty} Z(x_f, x_i) = e^{-\frac{E_0\tau_0}{\hbar}}\left\langle x_f|0\right\rangle\left\langle 0|x_i\right\rangle \,, \tag{E.1.8}$$

and thus

$$E_0 = -\hbar \lim_{\tau\to\infty}\frac{1}{\tau_0}\ln Z(x_f, x_i)\,. \tag{E.1.9}$$

Moreover, the RHS of (E.1.2) can now be written in terms of the euclidian action,

$$S_E = \int_{-\frac{\tau_0}{2}}^{\frac{\tau_0}{2}} d\tau \mathcal{L}_E \,, \tag{E.1.10}$$

$$\mathcal{L}_E = \frac{1}{2}\left(\frac{dx}{d\tau} + V(x)\right) \,, \tag{E.1.11}$$

where $\mathcal{L}_E$ is the euclidian Lagrangian, as

$$Z(x_f, x_i) = \mathcal{N}\int D[x] e^{-\frac{S_E[x]}{\hbar}} \,. \tag{E.1.12}$$

In the semiclassical limit, $\hbar \to 0$, the matrix element (E.1.12) will be dominated by path for which the action S_E is minimal (i.e. stationary).
In order to gain a visual understanding, let us assume that the potential has the form

$$V(x) = (x^2 - x_0^2)^2 \tag{E.1.13}$$

which has two minima, at x_0 and at $-x_0$. We know of course that in this scenario, tunneling between the two zero-energy states takes place and that the true ground state

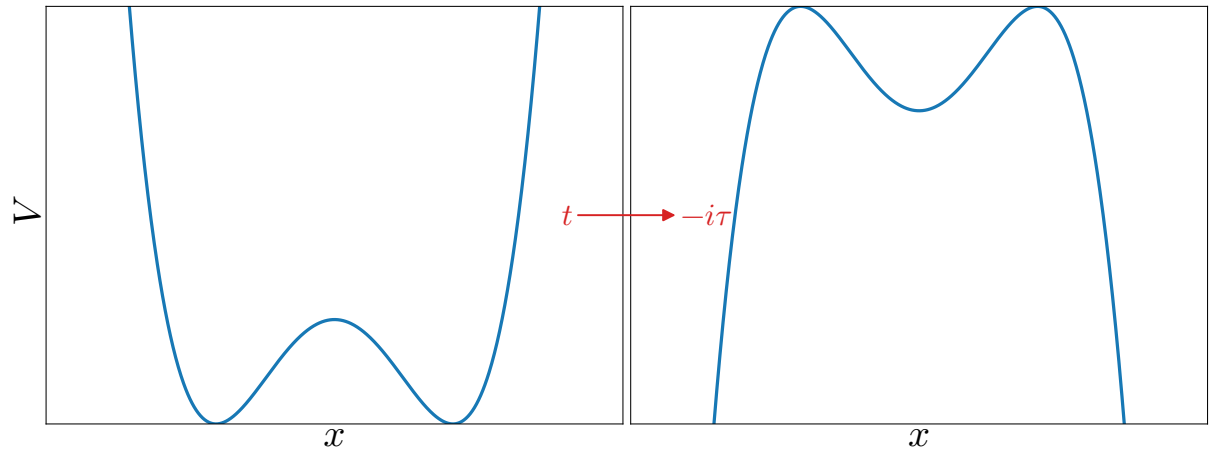

Figure E.1: The potential (E.1.13) (left) and the euclidian version (right).

is a superposition,

$$|vac\rangle = \frac{1}{\sqrt{2}}\left(|x_0\rangle + |-x_0\rangle\right) . \tag{E.1.14}$$

Instead of taking the usual path, let us know try to calculate the tunneling amplitude in the semiclassical limit, $\hbar \to 0$. It is easy to see that in Minkowski space, there are no classical path leading from $-x_0$ to x_0. However, note from $\mathcal{L}_E$ that the rotation to euclidian space corresponds to turning the potential upside down, i.e. we are now considering a particle in a potential $-V(x)$, see Fig. E.1. Clearly, there exists now a classical path from $-x_0$ to x_0, i.e. a solution to the equation of motion

$$-\frac{\delta S_E[x]}{\delta \tau} = \frac{d^2x}{d\tau^2} - \frac{dV(x)}{dx} = 0 \tag{E.1.15}$$

with the boundary conditions $x_i = -x_0, x_f = x_0$, given by

$$x_{cl}(\tau) \equiv x_0 \tanh\left(\sqrt{2}x_0\tau\right) . \tag{E.1.16}$$

By definition, the action corresponding to the solution (E.1.16) is stationary and as discussed above, in the semiclassical limit $\hbar \to 0$, it gives the dominant contribution to the path integral (E.1.12). Thus, we can approximate the tunneling amplitude as

$$Z(x_f, x_i) \approx e^{-\frac{S_E[x_{cl}]}{\hbar}} \tag{E.1.17}$$

where

$$S_E[x_{cl}] = \frac{4\sqrt{2}}{3}x_0^3 . \tag{E.1.18}$$

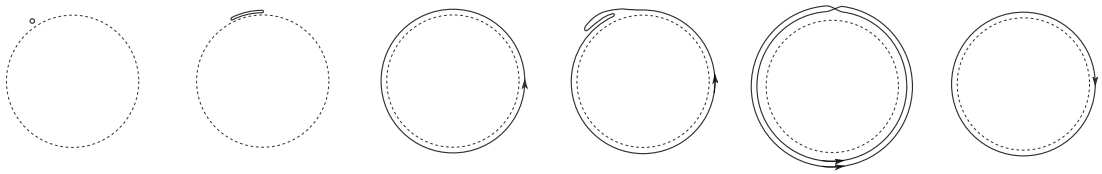

(a) $n = 0$ **(b)** $n = 0$ **(c)** $n = 1$ **(d)** $n = 1$ **(e)** $n = 2$ **(f)** $n = -1$

Figure E.2: Visualization of the winding number for mappings $S^1 \to S^1$.

E.2 Homotopy classes

In order to understand the Instanton solutions, we need some basic understanding of topology, more precisely of homotopy classes. In the following, we will give a short overview on the relevant notions without mathematical rigor.
First, consider two functions $f(x), g(x)$ that define a map from one topological space X to another topological space Y. If $f(x)$ and $g(x)$ can be continously transformed into each other, they are homotopic. In that manner, the full set of functions from X to Y can then be divided into homotopy classes so that all functions that are homotopic to each other are in the same homotopy class.
As we will see later, the relevant maps with regard to Instantons are maps from the three-sphere S^3 into a gauge group SU(2). Topologically, SU(2) is equivalent to S^3, i.e. we actually need to consider maps from S^3 to S^3. However, maps from three-spheres onto three-spheres are difficult to visualize. Thus, in order to gain a visual understanding of homotopy classes (which will prove sufficient to discuss the Instanton solutions), we discuss a simplified example using circles. That is, consider maps from the circle S^1, parameterized by an angle $\theta \in [0, 2\pi)$, into the gauge group $U(1)$. As $U(1)$ is topologically equivalent to S^1 we are therefore considering maps from a circle onto another circle,

$$f(\theta) : S^1 \to S^1 \,. \tag{E.2.1}$$

In this case, the homotopy classes are the elements of a group, the so called first homotopy group,

$$\pi_1(S^1) = \mathbb{Z} \,. \tag{E.2.2}$$

Thus, the different homotopy classes are characterized by the set of integers $n = 0, \pm 1, \pm 2, \ldots$. The integer n, called the winding number, is a topological invariant and counts how many times the domain space wraps around the target space.
Moreover, it can be shown that every map $f(\theta)$ from S^1 to S^1 is homotopic to one the standard maps

$$f^{(0)}(\theta) = 1 \,, \tag{E.2.3}$$

$$f^{(1)}(\theta) = e^{i\theta} \,, \tag{E.2.4}$$

$$f^{(n)}(\theta) = e^{in\theta} \,. \tag{E.2.5}$$

This scenario is visualized in Fig. E.2 where the target space is represented by the dotted circle an and the domain space is shown as a solid line. A useful analogy is to imagine the domain space as a rubber band which is wrapped around the target circle. Smooth deformations allow us to deform the rubber band as long as we do not leave the plane of the rubber band. Thus, we can e.g. smoothly transform the map shown in Fig. E.2b into the trivial map shown in Fig. E.2a, i.e. both maps have winding number $n = 0$. However, there exists no smooth transformation that continously deforms any of the other maps into the trivial map. For example, the maps shown in Fig. E.2c and E.2d both wrap once around the circle, i.e. they have winding number $n = 1$ while the map shown in Fig. E.2e wraps twice around the circle, corresponding to winding number $n = 2$. On the other hand, the map shown in Fig. E.2f wraps once around the circle counterclockwise, corresponding to $n = -1$. Given any map $f(\theta)$, the corresponding winding number can be expressed as an integral formula,

$$n = \int_0^{2\pi} \frac{d\theta}{2\pi} \left[\frac{-i}{f(\theta)} \frac{df(\theta)}{d\theta} \right] . \tag{E.2.6}$$

Similar consideraions apply for maps from S^3 to S^3. In this case, the homotopy classes form the third homotopy group,

$$\pi_3(S^3) = \mathbb{Z} , \tag{E.2.7}$$

and again we find that the homotopy classes are characterized by an integer $n \in \mathbb{Z}$.

E.3 Yang-Mills Theory

Before we proceed with the discussion of the vacuum structure of YM theories and Instanton solutions, let us shortly set the notation which differs from the one used previously. For simplicity, we will restrict ourselves to pure YM theory with SU(2) as the gauge group. In the following, we will work with *anti-hermitian* generators of the Lie-Algebra,

$$\left[t^a, t^b\right] = \epsilon^{abc} t^c , \tag{E.3.1}$$

$$t^a = -\frac{i\sigma^a}{2} . \tag{E.3.2}$$

with the Cartan inner product given by

$$\left(t^a, t^b\right) = -2\mathrm{Tr}\left[t^a t^b\right] = \delta_{ab} . \tag{E.3.3}$$

Next, we define the gauge fields $A_\mu(x)$ and the field strength tensor $F_{\mu\nu}(x)$ as

$$A_\mu = g A^a_\mu t^a , \tag{E.3.4}$$

$$F_{\mu\nu} = \partial_\mu A_\nu - \partial_\nu A_\mu + [A_\mu, A_\nu] . \tag{E.3.5}$$

In euclidian space with $x^2 = x_0^2 + \vec{x}^2$, the Lagrangian $\mathcal{L}_E$ and the action S_E are therefore given by

$$\mathcal{L}_E = \frac{1}{4g^2} F_{\mu\nu}{}^a F_{\mu\nu}{}^a , \tag{E.3.6}$$

$$S_E = \int d^4x \frac{1}{4g^2} F_{\mu\nu}{}^a F_{\mu\nu}{}^a \sim \int d^4x \mathrm{Tr}\left[E_i E_i + B_i B_i\right] > 0\,, \tag{E.3.7}$$

where we did not distinguish between lower and upper indices since we are in euclidian space. Under a gauge transformation $U(x) = \exp\left(\lambda^a(x) t^a\right)$, they transform as

$$A_\mu \to A'_\mu = U^{-1} A_\mu U + U^{-1}\partial_\mu U \tag{E.3.8}$$

$$F_{\mu\nu} \to F_{\mu\nu}{}' = U^{-1} F_{\mu\nu} U\,. \tag{E.3.9}$$

Moreover, if $F_{\mu\nu}$ vanishes A_μ, is pure gauge, i.e. a gauge-transform of zero with

$$A_\mu^{PG} = U^{-1}\partial_\mu U\,. \tag{E.3.10}$$

Finally, the euclidian equations of motion are given by

$$\frac{\delta S_E}{\delta A_\nu} = D_\mu F_{\mu\nu} = 0\,, \tag{E.3.11}$$

where the covariant derivative is defined via

$$D_\lambda F_{\mu\nu} + [A_\lambda, F_{\mu\nu}]\,. \tag{E.3.12}$$

Although we focus on SU(2) in the following discussion, the results for SU(N) are exactly the same and require only the replacement of the Pauli matrices in (E.3.2) with the appropriate generators.

E.4 Vacuum Structure of Yang Mills Theories

In this section, our goal is to find the zero-energy states in YM theory. They are given by the minima of the euclidian action and therefore

$$F_{\mu\nu} = 0\,. \tag{E.4.1}$$

We will employ the gauge-fixing condition

$$A_0(x) = 0\,. \tag{E.4.2}$$

Under a gauge transformation U, we find that A_0 transforms as

$$A_0(x) \to A'_0(x) = \underbrace{U^{-1}(x) A_0(x) U(x)}_{=0} + U^{-1}(x)\partial_0(x) U(x)\,, \tag{E.4.3}$$

i.e. the condition (E.4.2) fixes the gauge only partially as we are still left with the freedom of time-independent gauge transformations,

$$A_0(x) \to A'_0(x) = U^{-1}(\vec{x})\partial_0(x) U(\vec{x}) = 0\,. \tag{E.4.4}$$

Thus, the vacuum configurations we are seeking are time-independent pure gauge potentials,

$$A_i(x) = A_i^{PG}(\vec{x}) = U^{-1}(\vec{x})\partial_i(x) U(\vec{x})\,, \tag{E.4.5}$$

and the gauge transformations $U(\vec{x})$ are now mappings $R^3 \to \mathrm{SU}(2)$. Next, we use the remaining gauge freedom to define a boundary condition at spatial infinity,

$$U(\vec{x}) = 1 \quad \text{as} \qquad |\vec{x}| \to \infty \,, \tag{E.4.6}$$

so that

$$A_i^{PG}(\vec{x}) = 0 \quad \text{as} \qquad |\vec{x}| \to \infty \,. \tag{E.4.7}$$

This boundary condition compactifies R^3 to the three-sphere S^3, i.e. the gauge transformations $U(\vec{x})$ are mappings from S^3 into the gauge group SU(2) which is topologically equivalent to S^3. Recalling our discussion in Sec. E.2, this implies that the gauge transformations $U(\vec{x})$ fall into different homotopy classes, characterized by an integer n,

$$U^{(n)}(\vec{x}) = \exp\left(\frac{i\pi\vec{x}\vec{\sigma}n}{\sqrt{|x|^2+\rho^2}}\right), \tag{E.4.8}$$

where ρ is an arbitrary parameter. In analogy to the previous discussion, we will refer to n as the winding number. In terms of pure gauge fields (E.4.5), the winding number n can be expressed as

$$n = -\frac{1}{24\pi^2}\int d^3x \epsilon_{ijk} \mathrm{Tr}\left[A_i^{PG}A_j^{PG}A_k^{PG}\right] \,. \tag{E.4.9}$$

Consequently, the gauge fields that minimize the euclidian action that are constructed from (E.4.5) and (E.4.8) are classified by the winding number n as well,

$$A_i^{(n)} = U^{(n)-1}(\vec{x})\partial_i(x)U^{(n)}(\vec{x}) \,. \tag{E.4.10}$$

We can further distinguish between small gauge transformations and large gauge transformations. Small gauge transformations do not change the winding number and are homotopic to the identity while large gauge transformations change the winding number and cannot be continously transformed into the identity. Thus, the gauge transformations in (E.4.8) with $n = 0$ are small gauge transformations while the gauge transformations with $n \neq 0$ are large gauge transformations. Considering e.g. a field with $A_i = 0$, under a small gauge transformation we have

$$A_i \to A_i' = 0 \,, \tag{E.4.11}$$

while a large gauge transformation with $n = 1$ results in

$$A_i \to A_i' = A_i^{(1)} = U^{(1)-1}(\vec{x})\partial_i(x)U^{(1)}(\vec{x}) \,. \tag{E.4.12}$$

Thus, given two fields $A_i^{(k)}, A_i^{(m)}$ of the form (E.4.10) in different homotopy classes, i.e. $k \neq m$, we can not continously deform $A_i^{(k)}$ into $A_i^{(m)}$ *unless* we leave pure gauge. If we leave pure gauge, we have $F_{\mu\nu} \neq 0$ and therefore a non-minimal euclidian action $S_E > 0$. In other words, we find that the vacuum of YM theories consists not of a single vacuum but of an infinite number of vacuum states, each classified by the winding number n, which are seperated by finite action barriers.

E.5 Instantons

In the previous section, we found the surprising result that the YM vacuum is degenerate. Thus, the natural question to ask next is if there occurs tunneling between these vacua. Recalling the discussion in (E.1), we know that the tunneling amplitude between classical vacua in the semiclassical approximation is dominated by stationary points of the action, i.e. solutions of the YM equation (E.3.11) . Moreover, we require that the action is finite since field configurations with infinite action are irrelevant in the semiclassical approximation, see (E.1.17). Finiteness of the action (E.3.7) implies that $F_{\mu\nu}$ goes to zero faster than $1/|x|^2$ as $|x| \to \infty$. Restricting ourselves to integer powers of $|x|$, we therefore have

$$F_{\mu\nu} \sim \mathcal{O}\left(\frac{1}{|x|^3}\,,\right) \tag{E.5.1}$$

$$F_{\mu\nu}|_{|x|\to\infty} = 0\,. \tag{E.5.2}$$

Thus, in the limit $|x| \to \infty$, the gauge field A_μ has to be a gauge transform of zero, i.e. pure gauge,

$$A_\mu|_{|x|\to\infty} = A_\mu^\infty = V^{-1}\partial_\mu V\,, \tag{E.5.3}$$

where V is a function of angular variables only and we stress that we are not in $A_0 = 0$ gauge. Thus, V is a map from the boundary S^3 of euclidian space into the gauge group $\mathrm{SU}(2) \sim S^3$. Consequently, the maps V and the corresponding finite action field configurations fall into different homotopy classes characterized by an integer which we will denote by ν,

$$V^{(\nu)} = \left(\frac{x_0 + i\vec{x}\vec{\tau}}{|x|}\right)^\nu\,, \tag{E.5.4}$$

$$A_\mu^{(\nu)} = V^{(\nu)-1}\partial_\mu V^{(\nu)}\,. \tag{E.5.5}$$

For reasons that will become clear later on, we will refer to ν as the topological charge.
Note that the topological arguments made here and in the previous section are related, but not identical. The maps $U^{(n)}$ given in (E.4.8) that are classified by the winding number n are time-independent maps from compactified S^3 into SU(2) and the gauge fields constructed from these maps are static pure gauge fields. On the other hand, the maps V are only defined in the limit $|x| \to \infty$ and therefore the corresponding gauge fields are only required to approach pure gauge at $|x| \to \infty$.
The topological charge ν can be expressed in terms of gauge fields as a gauge-invariant quantity,

$$\nu[A] = \frac{1}{21\pi^2}\int d^4x F_{\mu\nu}{}^a[A]\tilde{F}^a_{\mu\nu}[A]\,, \tag{E.5.6}$$

where $F_{\mu\nu}[A]$ fulfills (E.5.2) and (E.5.3). Defining the Chern-Simmons current K_μ as

$$\begin{aligned} K_\mu &= 2\epsilon_{\mu\nu\lambda\rho}\left(A^a_\nu\partial_\lambda A^a_\rho + \frac{1}{3}\epsilon^{abc}A^a_\nu A^b_\lambda A^c_\rho\right) \\ &= \epsilon_{\mu\nu\lambda\rho}\left(A_\nu, F_{\lambda\rho} - \frac{2}{3}A_\nu A_\lambda A_\rho\right) , \end{aligned} \tag{E.5.7}$$

we can write $F_{\mu\nu}{}^a\tilde{F}^a_{\mu\nu}$ as a total derivative,

$$\partial_\mu K_\mu = F_{\mu\nu}{}^a\tilde{F}^a_{\mu\nu} , \tag{E.5.8}$$

and transform (E.5.6) into an integral over the surface S^3 at infinity,

$$\nu[A] = \frac{1}{32\pi^2}\int d^4x\partial_\mu K_\mu[A] = \frac{1}{32\pi^2}\int_S d\sigma_\mu K_\mu[A] . \tag{E.5.9}$$

However, at infinity, $F_{\mu\nu}$ vanishes and $A_\mu \to A^\infty_\mu$ is purge gauge, see (E.5.3) and (E.5.2), and we find

$$\begin{aligned} \nu &= -\frac{1}{24\pi^2}\int_S d\sigma_\mu\epsilon_{\mu\nu\lambda\rho}\mathrm{Tr}\left[A^\infty_\nu A^\infty_\lambda A^\infty_\rho\right] \\ &= -\frac{1}{24\pi^2}\int_S d\sigma_\mu\epsilon_{\mu\nu\lambda\rho}\mathrm{Tr}\left[\left(V^{-1}\partial_\nu V\right)\left(V^{-1}\partial_\lambda V\right)\left(V^{-1}\partial_\rho V\right)\right] . \end{aligned} \tag{E.5.10}$$

We can now calculate the action of the Instanton in terms of the topological charge. With

$$\left(F_{\mu\nu} \pm \tilde{F}_{\mu\nu}\right)^2 = 2\left(F_{\mu\mu}F_{\mu\nu} \pm F_{\mu\mu}\tilde{F}_{\mu\nu}\right) \tag{E.5.11}$$

we find

$$S_E = \int d^4x\frac{1}{4g^2}\mathrm{Tr}\left[F_{\mu\nu}{}^aF_{\mu\nu}{}^a\right] = \mp\frac{1}{4g^2}\int d^4xF_{\mu\nu}{}^a\tilde{F}^a_{\mu\nu} + \frac{1}{8g^2}\int d^4x\left(F_{\mu\nu}{}^a \pm \tilde{F}^a_{\mu\nu}\right)^2 \tag{E.5.12}$$

$$= \mp\frac{8\pi^2\nu}{g^2} + \frac{1}{8g^2}\int d^4x\left(F_{\mu\nu}{}^a \pm \tilde{F}^a_{\mu\nu}\right)^2 . \tag{E.5.13}$$

Since

$$\int d^4x\left(F_{\mu\nu}{}^a \pm \tilde{F}^a_{\mu\nu}\right)^2 \geq 0 \tag{E.5.14}$$

we find

$$S_E \geq \frac{8\pi^2|\nu|}{g^2} . \tag{E.5.15}$$

and it is easy to see that (E.5.15) is minimized if

$$F_{\mu\nu} = \pm\tilde{F}_{\mu\nu} \tag{E.5.16}$$

holds. Clearly, configurations which satisfy (E.5.15) are finite-action solutions of the euclidian equations of motivation and have an action given by

$$S_\nu = \frac{8\pi^2|\nu|}{g^2}\,. \tag{E.5.17}$$

A non-trivial solution for $\nu = 1$ is given by

$$\begin{aligned} A_\mu(x) &= \left(\frac{|x|^2}{|x|^2+\rho^2}\right) V^{(0)-1}\partial_\mu V^{(0)}\,, \\ A_0(x) &= \frac{-i\vec{\tau}\vec{x}}{|x|^2+\rho^2}\,, \qquad A_i(x) = \frac{-i\left(\vec{\tau}x_0 + \vec{\tau}\times\vec{x}\right)}{|x|^2+\rho^2}\,, \end{aligned} \tag{E.5.18}$$

and is called the BPST Instanton with the Instanton size ρ and $V^{(0)}$ given by (E.5.4). In order to make the interpretation of Instantons as the tunneling solution between the vacua we found in the previous section transparent we need to transform the Instanton into the A_0 gauge. In this case, the only component of the Chern-Simmons current which contributes to the topological charge ν is K_0 and we can relate ν to the winding number n, (E.4.9), as

$$\nu = \int d^3x\,[K_0(x_0=\infty) - K_0(x_0=-\infty)] = n(x_0=\infty) - n(x_0=-\infty)\,. \tag{E.5.19}$$

Thus, an Instanton with a topological charge $\nu > 0$ interpolates between two topologically distinct vacua $n(\infty) \neq n(-\infty)$. Let us consider this more explicitly for the Instanton with $\nu = 1$. In order to express the solution given in (E.5.18) in $A_0 = 0$ gauge, i.e. we need to find a gauge transformation $U(x)$ so that

$$A_0'(x) = U^{-1}(x)A_0(x)U(x) + U^{-1}\partial_0 U(x) = 0\,. \tag{E.5.20}$$

A gauge transformation that fulfulls this condition is given by

$$U(x) = \exp\left(\frac{i\vec{x}\vec{\sigma}}{\sqrt{\vec{x}^2+\lambda}}\left[\arctan\left(\frac{x_0}{\sqrt{\vec{x}^2+\lambda}}\right) + \left(n+\frac{1}{2}\right)\pi\right]\right). \tag{E.5.21}$$

In the limit $x_0 \to \pm\infty$ we find

$$U(x_0\to-\infty) = U^{(n)}(\vec{x}) = \exp\left(\frac{i\vec{x}\vec{\sigma}}{\sqrt{\vec{x}^2+\lambda}}n\right), \tag{E.5.22}$$

$$U(x_0\to\infty) = U^{(n+1)}(\vec{x}) = \exp\left(\frac{i\vec{x}\vec{\sigma}}{\sqrt{\vec{x}^2+\lambda}}(n+1)\right) \tag{E.5.23}$$

and thus

$$A_i'(x_0\to-\infty,\vec{x}) = U^{(n)-1}(\vec{x})\partial_i U^{(n)}(\vec{x}) = A_i^{(n)}\,, \tag{E.5.24}$$

$$A_i'(x_0\to\infty,\vec{x}) = U^{(n+1)-1}(\vec{x})\partial_i U^{(n+1)}(\vec{x}) = A_i^{(n+1)}\,. \tag{E.5.25}$$

In this form, it is evident that the Instanton is the desired tunneling solution that interpolates between the different winding sectors with $\nu = (n+1) - n$.

E.6 Theta Vacua

The existence of degenerate vacua with tunneling solutions implies that the true ground state of the theory is given by a superposition of the $|n\rangle$ vacua. We can write the true vacuum, called θ vacuum, in terms of an angle $\theta \in [0, 2\pi)$ and the $|n\rangle$ vacua as

$$|\theta\rangle = \sum_n e^{in\theta} |n\rangle \ . \tag{E.6.1}$$

The transition amplitude between different θ vacua is then given by

$$\langle\theta'|e^{-H\tau}|\theta\rangle = \sum_{n,m} e^{im\theta'} e^{-in\theta} \langle m|e^{-H\tau}|n\rangle \tag{E.6.2}$$

$$= \sum_{n,m} e^{im(\theta'-\theta)} e^{-i(n-m)\theta} \langle m|e^{-H\tau}|n\rangle \tag{E.6.3}$$

$$= \sum_{\nu,m} e^{im(\theta'-\theta)} e^{-i(\nu)\theta} \int [dA_\mu]_\nu e^{-S_E} \tag{E.6.4}$$

$$= \delta(\theta'-\theta) \int [dA_\mu]_\nu e^{-S_E - \frac{i\theta}{32\pi^2}\int d^4x F_{\mu\nu}{}^a \tilde{F}^a_{\mu\nu}} \tag{E.6.5}$$

and we note that the existence of tunneling solutions between different winding sectors $n \neq m$ amounts to adding a term

$$\mathcal{L}_{E,\theta} = -\frac{i\theta}{32\pi^2} F_{\mu\nu}{}^a \tilde{F}^a_{\mu\nu} \tag{E.6.6}$$

to the Lagrangian in euclidian space. In order to discuss the physical relevance of this term, let us go back to Minkowski space and rescale the gauge fields according to the conventions used in 2.2, yielding

$$\mathcal{L}_\theta = \frac{g^2\theta}{32\pi^2} F_{\mu\nu}{}^a \tilde{F}^{a,\mu\nu} \ , \tag{E.6.7}$$

where g is the gauge coupling of SU(N). Although it is gauge invariant and therefore a viable contribution to the Lagrangian, it can be written as a total derivative. Since variations were assumed to vanish at the boundary, it was usually discarded. It became clear only once Instanton solutions were found that the surface term does not vanish if tunneling between different winding sectors takes place. Thus, this term can have physical consequences and should be considered as an additional term of the Lagrangian.

APPENDIX F

Boltzmann Equations

F.1 General Equations

Although the assumption that the Universe evolves through sequences of states close to thermal equilibrium proves reasonable, it is the intermedient departures of the particle content from equilibrium that invoke interesting effetcts. Thus, in order to study those deviations from equilibrium, we need a formalism that describes the evolution of the different particles species, taking both the expansion of the Universe and the interactions in the plasma into account. This is achieved by means of *Boltzmann equations*. For a particle species X it is of the form

$$\frac{dn_X}{dt} + 3\mathcal{H}n_X = -\sum_{\text{processes}} [Xa \leftrightarrow ij] \,. \tag{F.1.1}$$

Focusing on the LHS first, note that the term proportional to $\mathcal{H}$ takes the dilution of the number density due to the expansion of the Universe into account. Using (3.2.13), we can rewrite the LHS of (F.1.1) as

$$\frac{dn_X}{dt} + 3\mathcal{H}n_X = s\frac{dY_X}{dt} \,. \tag{F.1.2}$$

Moreover, it is convenient to introduce a new variable

$$z_X \equiv \frac{m_X}{\mathsf{T}} \tag{F.1.3}$$

and express the Boltzmann equations in terms of z_X rather than t. Thus, we need to derive a relation between the temperature T and time t. To that end, note that (3.1.21) in a radiation dominant Universe implies

$$\mathcal{H} = \frac{1}{2t} \,, \tag{F.1.4}$$

and further imposing that the Universe is flat, we find

$$\rho_c = \frac{3\mathcal{H}^2}{8\pi G} = \frac{3}{32\pi G t^2} \eqsim \rho_{\text{rel}} = \frac{\pi^2}{30} g_* \mathsf{T}^4 \,, \tag{F.1.5}$$

where we used (3.2.8). This yields the desired relation between T and t as

$$t = \left(\frac{90}{32\pi^3 G g_*}\right)^{\frac{1}{2}} \frac{1}{\mathsf{T}^2} \,, \tag{F.1.6}$$

and consequently (F.1.2) becomes

$$s\frac{dY_X}{dt} = s\mathcal{H}z_X\frac{dY_X}{dz_X}\,. \tag{F.1.7}$$

The RHS of (F.1.1) is the so called *collision term* where the sum runs over all interactions involving X. For simplicity, let us consider the collision term for a species X interacting only via $Xa \leftrightarrow ij$ which in the most general form is given by

$$\begin{aligned}[Xa \leftrightarrow ij] = &\int d\Pi_X d\Pi_a d\Pi_i d\Pi_j \,(2\pi)^4\,\delta^{(4)}\left(p_i + p_j - p_X + p_a\right)\\ &\times\left[|M|^2_{X+a\to i+j} f_X f_a\,(1\pm f_i)\,(1\pm f_j) - |M|^2_{i+j\to X+a} f_i f_j\,(1\pm f_X)\,(1\pm f_a)\right]\,,\end{aligned} \tag{F.1.8}$$

where

$$d\Pi_l \equiv \frac{g_l}{(2\pi)^2}\frac{d^3p_l}{2E_l}\,, \tag{F.1.9}$$

f_l are the phase space densities of a particle l and $|M|^2$ are the squared matrix elements averaged over intial and final state spins and include symmetry factors for identical particles in the intial or final states. The $(1\pm f_l)$ terms correspond to Bose enhancement ("+") and Pauli blocking ("−"). If elastic scatterings are fast, kinetic equilibrium holds and the phase space distributions are given by (3.2.1). Moreover, since the average energy per particle is given by $\langle E\rangle \approx 3\mathsf{T}$, we can approximate the Bose-Einstein and Fermi-Dirac distributions as Maxwell-Boltzmann distributions,

$$f_i \approx e^{\frac{\mu_i}{\mathsf{T}}}e^{-\frac{E_i}{\mathsf{T}}} = e^{\frac{\mu_i}{\mathsf{T}}}f_i^{\rm eq}\,, \tag{F.1.10}$$

and since $f_i \ll 1$, the Pauli blocking and Bose enhancement factors in (3.2.1) can be neglected, $1\pm f_i \approx 1$. Further defining

$$|M_\to|^2 \equiv |M|^2_{X+a\to i+j}\,, \qquad |M_\leftarrow|^2 \equiv |M|^2_{i+j\to X+a}\,, \tag{F.1.11}$$

these assumptions greatly simplify the collison term, resulting in

$$\begin{aligned}[Xa \leftrightarrow ij] = &\int d\Pi_X d\Pi_a d\Pi_i d\Pi_j \,(2\pi)^4\\ &\times\delta^{(4)}\left(p_i + p_j - p_X + p_a\right)\left[|M_\to|^2 f_X f_a - |M_\leftarrow|^2 f_i f_j\right]\,.\end{aligned} \tag{F.1.12}$$

Moreover, note that energy conservation $E_X + E_a = E_i + E_j$ implies

$$|M_\to|^2 f_X f_a - |M_\leftarrow|^2 f_i f_j = e^{-\frac{E_X+E_a}{\mathsf{T}}}\left(|M_\to|^2 e^{\frac{\mu_X+\mu_a}{\mathsf{T}}} - |M_\leftarrow|^2 e^{\frac{\mu_i+\mu_j}{\mathsf{T}}}\right)\,. \tag{F.1.13}$$

Since the chemical potential does not depend on p, we can write the number density of a species l as

$$n_l = e^{\frac{\mu_l}{\mathsf{T}}}n_l^{\rm eq}\,, \tag{F.1.14}$$

where the equilibrium number density is given by

$$n_l^{\rm eq} = g_l \int \frac{d^3 p_l}{(2\pi)^3} f_l^{\rm eq} = \frac{g_l m_l \mathsf{T}}{2\pi^2} \mathrm{K}_2\Big(\frac{m_l}{\mathsf{T}}\Big) \approx \begin{cases} g_l \frac{\mathsf{T}^3}{\pi^2}\,, & \mathsf{T} \gg m_l\,, \\ g_l \left(\frac{m_l \mathsf{T}}{2\pi}\right) \frac{3}{2} e^{-\frac{m_l}{\mathsf{T}}}\,, & \mathsf{T} \gg m_l\,, \end{cases} \tag{F.1.15}$$

and $K_n(x)$ is the modified Bessel function of the second kind. Rewriting (F.1.13) as

$$|M_{\rightarrow}|^2 f_X f_a - |M_{\leftarrow}|^2 f_i f_j = e^{-\frac{E_X + E_a}{\mathsf{T}}} \left(|M_{\rightarrow}|^2 \frac{n_X n_a}{n_X^{\rm eq} n_a^{\rm eq}} - |M_{\leftarrow}|^2 \frac{n_i n_j}{n_i^{\rm eq} n_j^{\rm eq}} \right)\,, \tag{F.1.16}$$

and defining the thermal rate as

$$\gamma^{\rm eq}\left(Xa \to ij\right) \equiv \int d\Pi_X d\Pi_a d\Pi_i d\Pi_j \left(2\pi\right)^4 \delta^{(4)}\left(p_i + p_j - p_X + p_a\right) |M|^2_{\rightarrow} f_X^{\rm eq} f_a^{\rm eq}\,, \tag{F.1.17}$$

the collision term can be written as

$$[Xa \leftrightarrow ij] = \left(\frac{n_X n_a}{n_X^{\rm eq} n_a^{\rm eq}} \gamma^{\rm eq}\left(Xa \to ij\right) - \frac{n_i n_j}{n_i^{\rm eq} n_j^{\rm eq}} \gamma^{\rm eq}\left(ij \to Xa\right) \right)\,. \tag{F.1.18}$$

Thus, putting everything together and using

$$\frac{n_l}{n_l^{\rm eq}} = \frac{Y_l}{Y_l^{\rm eq}} \equiv \delta_i\,, \tag{F.1.19}$$

the Boltzmann equation for the evolution of a particle X which interacts via $Xa \leftrightarrow ij$ reads

$$s\mathcal{H} z_X \frac{dY_X}{dz_X} = -\left(\delta_X \delta_a \gamma^{\rm eq}\left(Xa \to ij\right) - \delta_i \delta_j \gamma^{\rm eq}\left(ij \to Xa\right)\right)\,. \tag{F.1.20}$$

Moreover, if the process $Xa \leftrightarrow ij$ is $\mathcal{CP}$ invariant,

$$\gamma^{\rm eq}\left(Xa \to ij\right) \overset{\mathcal{CP}}{=} \gamma^{\rm eq}\left(ij \to Xa\right)\,, \tag{F.1.21}$$

we can simplify (F.1.20) further, yielding

$$s\mathcal{H} z_X \frac{dY_X}{dz_X} = -\left(\delta_X \delta_a - \delta_i \delta_j\right) \gamma^{\rm eq}\left(ij \leftrightarrow Xa\right)\,. \tag{F.1.22}$$

Note that the Boltzmann equation as given in (F.1.20) tracks the changes in particle abundances and is only valid when kinetic equilibrium holds.

F.2 Vanilla Leptogenesis

In this section, wederive the Boltzmann equations for VL, i.e. the Boltzmann equations that govern the evolution of the neutrino abundance and the lepton asymmetry, respectively, following [94]. For brevity, we will generally omit the index 1 in the following so that $\{N, M_N, \tilde{m}, \epsilon\} \equiv \{N_1, M_{N_1}, \tilde{m}_1, \epsilon_1\}$. In our discussion, we neglect thermal effects and scattering processes involving gauge bosons. Thus, the only processes relevant for

the neutrino evolution are decays and quark scatterings[1], see first row in Fig. 4.7, yielding the Boltzmann equation

$$\begin{aligned} s\mathcal{H}z_N\frac{\mathrm{d}Y_N}{\mathrm{d}z_N} =& -\left[N \leftrightarrow LH\right] - \left[N \leftrightarrow \overline{L}H^\dagger\right] - \left[NL \leftrightarrow Q_3U_3\right] - \left[N\overline{L} \leftrightarrow \overline{Q_3U_3}\right] \\ & - \left[N\overline{Q_3} \leftrightarrow L\overline{U_3}\right] - \left[N\overline{U_3} \leftrightarrow L\overline{Q_3}\right] - \left[NQ_3 \leftrightarrow \overline{L}U_3\right] - \left[NU_3 \leftrightarrow \overline{L}Q_3\right] . \end{aligned} \tag{F.2.1}$$

As discussed in 4.3.3.1, the N decays violate $\mathcal{CP}$ which can be parametrized as

$$\gamma_{N\to LH} \overset{\mathcal{CP}}{=} \gamma_{\overline{L}H^\dagger\to N} = \frac{\gamma_D}{2}\left(1+\epsilon\right) , \qquad \gamma_{N\to\overline{L}H^\dagger} \overset{\mathcal{CP}}{=} \gamma_{LH\to N} = \frac{\gamma_D}{2}\left(1+\epsilon\right) , \tag{F.2.2}$$

where the decay rate γ_D is given by

$$\gamma_D = n_N^{\mathrm{eq}}\frac{\mathrm{K}_1(z_N)}{\mathrm{K}_2(z_N)}\Gamma_D . \tag{F.2.3}$$

Further assuming that $N, L, \overline{L}$ can be out of equilibrium while the remaining fields follow equilibrium distributions with $Y_X = Y_X^{\mathrm{eq}}$, we find

$$\left[N \leftrightarrow LH\right] = \gamma_{N\to LH}\delta_N - \gamma_{LH\to N}\delta_L = \frac{\gamma_D}{2}\left[\left(1+\epsilon\right)\delta_N - \left(1-\epsilon\right)\delta_L\right] , \tag{F.2.4}$$

$$\left[N \leftrightarrow \overline{L}H^\dagger\right] = \gamma_{N\to\overline{L}H^\dagger}\delta_N - \gamma_{\overline{L}H^\dagger\to N}\delta_{\overline{L}} = \frac{\gamma_D}{2}\left[\left(1-\epsilon\right)\delta_N - \left(1+\epsilon\right)\delta_{\overline{L}}\right] , \tag{F.2.5}$$

and

$$\left[N\overline{U_3} \leftrightarrow L\overline{Q_3}\right] = \left[N\overline{Q_3} \leftrightarrow L\overline{U_3}\right] = \left(\delta_N - \delta_L\right)\gamma_{N\overline{U_3},L\overline{Q_3}} , \tag{F.2.6}$$

$$\left[NU_3 \leftrightarrow \overline{L}Q_3\right] = \left[NQ_3 \leftrightarrow \overline{L}U_3\right] = \left(\delta_N - \delta_{\overline{L}}\right)\gamma_{NU_3,\overline{L}Q_3} , \tag{F.2.7}$$

$$\left[NL \leftrightarrow Q_3U_3\right] = \left(\delta_N\delta_L - 1\right)\gamma_{NL,Q_3U_3} , \tag{F.2.8}$$

$$\left[N\overline{L} \leftrightarrow \overline{Q_3U_3}\right] = \left(\delta_N\delta_{\overline{L}} - 1\right)\gamma_{N\overline{L},\overline{Q_3U_3}} , \tag{F.2.9}$$

where we used $\gamma_{N\overline{U_3},L\overline{Q_3}} = \gamma_{N\overline{Q_3},L\overline{U_3}}$. Moreover, $\mathcal{CP}$ invariance results in

$$\gamma_{N\overline{U_3},L\overline{Q_3}} = \gamma_{NU_3,\overline{L}Q_3} , \qquad \gamma_{NL,Q_3U_3} = \gamma_{N\overline{L},\overline{Q_3U_3}} , \tag{F.2.10}$$

and we can define a total quark scattering rate as

$$\gamma_Q \equiv 2\gamma_{NU_3,\overline{L}Q_3} + \gamma_{NL,Q_3U_3} . \tag{F.2.11}$$

Putting everything together and using the approximation $Y_L + Y_{\overline{L}} \approx 2Y_L^{\mathrm{eq}}$, the Boltzmann equation for the neutrino evolution (F.2.1) finally becomes

$$s\mathcal{H}z_N\frac{\mathrm{d}Y_N}{\mathrm{d}z_N} = -\left(\delta_N - 1\right)\gamma_D - 2\gamma_Q\left(\delta_N - 1\right) . \tag{F.2.12}$$

The Boltzmann equation for the evolution of the lepton asymmetry $\Delta L'$ is conveniently derived from the evolutions of Y_L and $Y_{\overline{L}}$. Besides the $\Delta L' = 1$ decays and quark scatterings, it is essential to also take $\Delta L' = 2$ scattering proccesses into account (see second

[1] The relevant cross sections are given in App. G.2.1.

row in Fig. 4.7), yielding the Boltzmann equations

$$\begin{aligned} s\mathcal{H}z_N\frac{\mathrm{d}Y_L}{\mathrm{d}z_N} =& -\left[LH\leftrightarrow N\right]-\left[LH\leftrightarrow\overline{L}H^\dagger\right]-2\left[LL\leftrightarrow HH\right] \\ &-\left[LN\leftrightarrow Q_3U_3\right]-\left[L\overline{Q_3}\leftrightarrow N\overline{U_3}\right]-\left[L\overline{U_3}\leftrightarrow N\overline{Q_3}\right]\,, \end{aligned} \tag{F.2.13}$$

$$\begin{aligned} s\mathcal{H}z_N\frac{\mathrm{d}Y_{\overline{L}}}{\mathrm{d}z_N} =& -\left[\overline{L}H\leftrightarrow N\right]-\left[\overline{L}H^\dagger\leftrightarrow LH\right]-2\left[\overline{LL}\leftrightarrow H^\dagger H^\dagger\right] \\ &-\left[\overline{L}N\leftrightarrow\overline{Q_3U_3}\right]-\left[\overline{L}Q_3\leftrightarrow NU_3\right]-\left[\overline{L}U_3\leftrightarrow NQ_3\right]\,. \end{aligned} \tag{F.2.14}$$

Naively, the evolution of the lepton asymmetry is obtained by simply substracting (F.2.14) from (F.2.13). However, in this case the asymmetry would evolve as

$$s\mathcal{H}z_N\frac{\mathrm{d}Y_{\Delta L'}}{\mathrm{d}z_N} = \underbrace{\epsilon\gamma_D\left(\delta_N+1\right)}_{\equiv f(\delta_N)=-[LH\leftrightarrow N]+[\overline{L}H\leftrightarrow N]} -\left\{\left[LH\leftrightarrow\overline{L}H^\dagger\right]-\left[\overline{L}H^\dagger\leftrightarrow LH\right]+...\right\} \tag{F.2.15}$$

where the term in curly brackets is proportional to $\delta_{\Delta L'}$ and describes how the lepton asymmetry is washed out. Right now, its explicit form is irrelevant. The first term on the other hand is problematic: All quantities appearing in $f(\delta_N)$ are positive and even if neutrinos are in equilibrium, i.e. $\delta_N=1$, we have $f(1)>0$ and consequently, a lepton asymmetry would be generated. This clearly violates the Sakharov conditions. The reason for this is simple: The scattering rate for $LH\leftrightarrow\overline{L}H^\dagger$ contains both on-shell and off-shell contributions for s-channel N exchange, see Fig. 4.7. However, the on-shell contribution is already accounted for by successive (inverse) decays $LH\leftrightarrow N\leftrightarrow\overline{L}H^\dagger$ and therefore counted twice. In order to correct this, we need to substract the on-shell contribution from $\gamma_{LH,\overline{L}H^\dagger}$ and replace $\gamma_{LH,\overline{L}H^\dagger}$ with the off-shell contribution $\gamma^{off}_{LH,\overline{L}H^\dagger}$. Since the neutrino decays violate $\mathcal{CP}$, we need to consider both directions individually, i.e.

$$\gamma^{off}_{LH\to\overline{L}H^\dagger}=\gamma_{LH\to\overline{L}H^\dagger}-\gamma^{on}_{LH\to\overline{L}H^\dagger}\,,\qquad \gamma^{off}_{\overline{L}H^\dagger\to LH}=\gamma_{\overline{L}H^\dagger\to LH}-\gamma^{on}_{\overline{L}H^\dagger\to LH}\,, \tag{F.2.16}$$

where the on-shell contributions are given by

$$\gamma^{on}_{LH\to\overline{L}H^\dagger}=\gamma_{LH\to N}\mathrm{Br}_{N\to\overline{L}H^\dagger}=\frac{\gamma_D}{4}\left(1-\epsilon\right)^2\,, \tag{F.2.17}$$

$$\gamma^{on}_{\overline{L}H^\dagger\to LH}=\gamma_{\overline{L}H^\dagger\to N}\mathrm{Br}_{N\to LH}=\frac{\gamma_D}{4}\left(1+\epsilon\right)^2\,, \tag{F.2.18}$$

and $\mathrm{Br}_{N\to\overline{L}H^\dagger},\mathrm{Br}_{N\to LH}$ are the branching ratios,

$$\mathrm{Br}_{N\to LH}=\frac{1}{2}\left(1+\epsilon\right)\,,\qquad \mathrm{Br}_{N\to\overline{L}H^\dagger}=\frac{1}{2}\left(1-\epsilon\right)\,. \tag{F.2.19}$$

Consequently, we need to replace $\left[LH\leftrightarrow\overline{L}H^\dagger\right]$ and $\left[\overline{L}H^\dagger\leftrightarrow LH\right]$ in (F.2.15) with the correspnding off-shell contributions, given by

$$\left[LH\leftrightarrow\overline{L}H^\dagger\right]^{off}=\delta_L\gamma^{off}_{LH\to\overline{L}H^\dagger}-\delta_{\overline{L}}\gamma^{off}_{\overline{L}H^\dagger\to LH}=\delta_{\Delta L'}\left(\gamma_{LH,\overline{L}H^\dagger}-\frac{\gamma_D}{4}\right)+\epsilon\gamma_D\,, \tag{F.2.20}$$

$$\left[\overline{L}H^\dagger\leftrightarrow LH\right]^{off}=\delta_{\overline{L}}\gamma^{off}_{\overline{L}H^\dagger\to LH}-\delta_L\gamma^{off}_{LH\to\overline{L}H^\dagger}=-\delta_{\Delta L'}\left(\gamma_{LH,\overline{L}H^\dagger}-\frac{\gamma_D}{4}\right)-\epsilon\gamma_D\,. \tag{F.2.21}$$

It is evident that the additional contributions from the second terms in (F.2.20) and (F.2.21), respectively, to $f(\delta_N)$ result in

$$f(\delta_N) - 2\epsilon\gamma_D = \epsilon\gamma_D\left(\delta_N - 1\right) \tag{F.2.22}$$

which indeed vanishes when neutrinos are in equilibrium. The remaining scattering terms can be written as

$$\begin{aligned}
[LL \leftrightarrow HH] &= \left(\delta_L^2 - 1\right)\gamma_{LL,HH}\,, & \left[\overline{LL} \leftrightarrow H^\dagger H^\dagger\right] &= \left(\delta_{\overline{L}}^2 - 1\right)\gamma_{\overline{LL},H^\dagger,H^\dagger}\,,\\
[LN \leftrightarrow Q_3U_3] &= \left(\delta_L\delta_N - 1\right)\gamma_{LN,Q_3U_3}\,, & \left[\overline{L}N \leftrightarrow \overline{Q_3U_3}\right] &= \left(\delta_{\overline{L}}\delta_N - 1\right)\gamma_{\overline{L}N,\overline{Q_3U_3}}\,,\\
\left[N\overline{U_3} \leftrightarrow L\overline{Q_3}\right] &= \left(\delta_N - \delta_L\right)\gamma_{N\overline{U_3},L\overline{Q_3}}\,, & \left[NU_3 \leftrightarrow \overline{L}Q_3\right] &= \left(\delta_N - \delta_{\overline{L}}\right)\gamma_{NU_3,\overline{L}Q_3}\,,\\
\left[N\overline{Q_3} \leftrightarrow L\overline{U_3}\right] &= \left(\delta_N - \delta_L\right)\gamma_{N\overline{Q_3},L\overline{U_3}}\,, & \left[NQ_3 \leftrightarrow \overline{L}U_3\right] &= \left(\delta_N - \delta_{\overline{L}}\right)\gamma_{NQ_3,\overline{L}U_3}\,,
\end{aligned} \tag{F.2.23}$$

yielding the Boltzmann equation for the lepton asymmetry as

$$s\mathcal{H}z_N\frac{\mathrm{d}Y_{\Delta L'}}{\mathrm{d}z_N} = \epsilon\gamma_D\left(\delta_N - 1\right) - 2\delta_{\Delta L'}\left[\gamma_{\Delta L'=2} + \gamma_{N\overline{U_3},L\overline{Q_3}} + \frac{\delta_N}{2}\gamma_{LN,Q_3U_3}\right]. \tag{F.2.24}$$

Here we combined the thermal rates for the $\Delta L' = 2$ interactions, $\gamma_{\Delta L'=2} \equiv \gamma_{LH,\overline{L}H^\dagger} + 2\gamma_{LL,HH}$. Moreover, we can write $\gamma_{\Delta L'=2}$ in terms of on- and off-shell contributions as

$$\gamma_{\Delta L'=2} = \gamma^{off}_{\Delta L'=2} + \gamma^{on}_{\Delta L'=2} \approx \gamma^{off}_{\Delta L'=2} + \frac{\gamma_D}{4} \approx \frac{\gamma_D}{4}\,, \tag{F.2.25}$$

where in the last step, we used that the on-shell contribution $\gamma^{on}_{LH\leftrightarrow\overline{L}H^\dagger} = \gamma_D/4$ provides the dominant contribution to $\gamma_{\Delta L'=2}$, finally yielding the Boltzmann equation for the lepton asymmetry as

$$s\mathcal{H}z_N\frac{\mathrm{d}Y_{\Delta L'}}{\mathrm{d}z_N} = \epsilon\gamma_D\left(\delta_N - 1\right) - \delta_{\Delta L'}\left[\frac{\gamma_D}{2} + 2\gamma_{N\overline{U_3},L\overline{Q_3}} + \delta_N\gamma_{LN\leftrightarrow Q_3U_3}\right]. \tag{F.2.26}$$

F.3 Majoron+Triplet Model

In this section, we derive the Boltzmann equations relevant for leptogenesis in the MTM. Besides the lepton number violating neutrino decays and quark scatterings that already appear in VL, the Boltzmann equation for the neutrino evolution in the MTM receives contributions from interactions involving T, σ and J, see Fig. 6.1, yielding

$$\begin{aligned}
s\mathcal{H}z_N\frac{\mathrm{d}Y_N}{\mathrm{d}z_N} = s\mathcal{H}z_N\frac{\mathrm{d}Y_N^{\mathrm{VL}}}{\mathrm{d}z_N} &+ 2[NN \leftrightarrow \sigma] + 2\left[NN \leftrightarrow TT\right] + 2\left[NN \leftrightarrow \sigma\sigma\right]\\
&+ 2\left[NN \leftrightarrow JJ\right] + 2\left[NN \leftrightarrow \sigma J\right]\,,
\end{aligned} \tag{F.3.1}$$

where

$$s\mathcal{H}z_N\frac{\mathrm{d}Y_N^{\mathrm{VL}}}{\mathrm{d}z_N} = -\left(\delta_N - 1\right)\gamma_D - 2\gamma_Q\left(\delta_N - 1\right)\,, \tag{F.3.2}$$

as given in (4.3.59) and we assumed that N, L, T, σ and J can deviate from equilibrium. Similarly to the discussion in Sec. G.2.1, we need to substract the on-shell contributions

from $2 \to 2$ scattering processes if the on-shell process can take place, i.e.

$$[NN \leftrightarrow TT] = \left(\delta_N^2 - \delta_T^2\right) \gamma_{NN,TT}^{off}\,, \qquad [NN \leftrightarrow JJ] = \left(\delta_N^2 - \delta_J^2\right) \gamma_{NN,JJ}^{off}\,, \tag{F.3.3}$$

where the off-shell contributions are given by

$$\gamma_{NN,TT}^{off} = \gamma_{TT,NN}^{off} = \gamma_{NN,TT} - \mathrm{Br}_{\sigma,TT}\gamma_{\sigma,NN}\,, \tag{F.3.4}$$

$$\gamma_{NN,JJ}^{off} = \gamma_{JJ,NN}^{off} = \gamma_{NN,JJ} - \mathrm{Br}_{\sigma,JJ}\gamma_{\sigma,NN}\,. \tag{F.3.5}$$

The remaining terms in (F.3.1) are given by

$$[NN \leftrightarrow \sigma\sigma] = \left(\delta_N^2 - \delta_\sigma^2\right) \gamma_{NN,\sigma\sigma}\,, \qquad [NN \leftrightarrow \sigma] = \left(\delta_N^2 - \delta_\sigma\right) \gamma_{NN,\sigma}\,, \tag{F.3.6}$$

$$[NN \leftrightarrow \sigma J] = \left(\delta_N^2 - \delta_\sigma\delta_J\right) \gamma_{NN,\sigma J}\,. \tag{F.3.7}$$

Similarly, the Boltzmann equations for T, σ and J can be written as

$$\begin{aligned} s\mathcal{H}z_N \frac{\mathrm{d}Y_T}{\mathrm{d}z_N} &= 2\,[TT \leftrightarrow \sigma] + 2\,[TT \leftrightarrow NN] + 2\,[TT \leftrightarrow \sigma\sigma] + 2\,[TT \leftrightarrow JJ] \\ &\quad + 2\,[TT \leftrightarrow \sigma J] + 2\,[TT \leftrightarrow AA]\,, \end{aligned} \tag{F.3.8}$$

$$\begin{aligned} s\mathcal{H}z_N \frac{\mathrm{d}Y_\sigma}{\mathrm{d}z_N} &= [\sigma \leftrightarrow JJ] + [\sigma \leftrightarrow NN] + [\sigma \leftrightarrow TT] + 2\,[\sigma\sigma \leftrightarrow JJ] \\ &\quad + 2\,[\sigma\sigma \leftrightarrow NN] + 2\,[\sigma\sigma \leftrightarrow TT] + [\sigma J \leftrightarrow NN] + [\sigma J \leftrightarrow TT] \\ &\quad + [\sigma N \leftrightarrow JN] + [\sigma T \leftrightarrow JT]\,, \end{aligned} \tag{F.3.9}$$

$$\begin{aligned} s\mathcal{H}z_N \frac{\mathrm{d}Y_J}{\mathrm{d}z_N} &= [JJ \leftrightarrow \sigma] + 2\,[JJ \leftrightarrow \sigma\sigma] + 2\,[JJ \leftrightarrow TT] + 2\,[JJ \leftrightarrow NN] \\ &\quad + [\sigma J \leftrightarrow NN] + [\sigma J \leftrightarrow TT] + [JN \leftrightarrow \sigma N] + [JT \leftrightarrow \sigma T]\,. \end{aligned} \tag{F.3.10}$$

where

$$[TT \leftrightarrow \sigma] = \left(\delta_T^2 - \delta_\sigma\right) \gamma_{\sigma,TT}\,, \qquad [TT \leftrightarrow NN] = \left(\delta_T^2 - \delta_T^2\right) \gamma_{TT,NN}^{off}\,, \tag{F.3.11}$$

$$[TT \leftrightarrow \sigma\sigma] = \left(\delta_T^2 - \delta_\sigma^2\right) \gamma_{TT,\sigma\sigma}\,, \qquad [TT \leftrightarrow JJ] = \left(\delta_T^2 - \delta_J^2\right) \gamma_{TT,JJ}^{off}\,, \tag{F.3.12}$$

$$[TT \leftrightarrow \sigma J] = \left(\delta_T^2 - \delta_\sigma\delta_J\right) \gamma_{TT,\sigma J}\,, \qquad [TT \leftrightarrow AA] = \left(\delta_T^2 - \delta_A A^2\right) \gamma_{TT,AA} \tag{F.3.13}$$

for the evolution of T,

$$[\sigma \leftrightarrow JJ] = \left(\delta_\sigma - \delta_J^2\right) \gamma_{\sigma,JJ}\,, \qquad [\sigma \leftrightarrow NN] = \left(\delta_\sigma - \delta_N^2\right) \gamma_{\sigma,NN}\,, \tag{F.3.14}$$

$$[\sigma \leftrightarrow TT] = \left(\delta_\sigma - \delta_T^2\right) \gamma_{\sigma,TT}\,, \qquad [\sigma\sigma \leftrightarrow JJ] = \left(\delta_\sigma^2 - \delta_J^2\right) \gamma_{\sigma\sigma,JJ}\,, \tag{F.3.15}$$

$$[\sigma\sigma \leftrightarrow NN] = \left(\delta_\sigma^2 - \delta_N^2\right) \gamma_{\sigma\sigma,NN}\,, \qquad [\sigma\sigma \leftrightarrow TT] = \left(\delta_\sigma^2 - \delta_T^2\right) \gamma_{\sigma\sigma,TT}\,, \tag{F.3.16}$$

$$[\sigma J \leftrightarrow NN] = \left(\delta_\sigma\delta_J - \delta_N^2\right) \gamma_{\sigma J,NN}\,, \qquad [\sigma J \leftrightarrow TT] = \left(\delta_\sigma\delta_J - \delta_T^2\right) \gamma_{\sigma J,TT}\,, \tag{F.3.17}$$

$$[\sigma N \leftrightarrow JN] = \left(\delta_\sigma\delta_N - \delta_J\delta_N\right) \gamma_{\sigma N,JN}\,, \qquad [\sigma T \leftrightarrow JT] = \left(\delta_\sigma\delta_T - \delta_J\delta_T\right) \gamma_{\sigma T,JT}\,. \tag{F.3.18}$$

for the evolution of σ and

$$[JJ \leftrightarrow \sigma\sigma] = \left(\delta_J^2 - \delta_\sigma^2\right) \gamma_{JJ,\sigma\sigma}\,, \qquad [JJ \leftrightarrow TT] = \left(\delta_J^2 - \delta_\sigma\right) \gamma_{\sigma,JJ}\,, \tag{F.3.19}$$

$$[JJ \leftrightarrow NN] = \left(\delta_J^2 - \delta_N^2\right) \gamma_{JJ,NN}^{off}\,, \qquad [JJ \leftrightarrow TT] = \left(\delta_J^2 - \delta_T^2\right) \gamma_{JJ,TT}^{off}\,, \tag{F.3.20}$$

$$[\sigma J \leftrightarrow NN] = \left(\delta_J\delta_\sigma - \delta_N^2\right) \gamma_{\sigma J,NN}\,, \qquad [\sigma J \leftrightarrow TT] = \left(\delta_J\delta_\sigma - \delta_T^2\right) \gamma_{\sigma J,TT}\,, \tag{F.3.21}$$

$$[JN \leftrightarrow \sigma N] = (\delta_J\delta_N - \delta_\sigma\delta_N)\,\gamma_{JN,\sigma N}\,, \qquad [JT \leftrightarrow \sigma T] = (\delta_J\delta_T - \delta_\sigma\delta_T)\,\gamma_{JT,\sigma T} \tag{F.3.22}$$

for the evolution of J. Moreover,

$$\gamma^{off}_{TTJJ} = \gamma^{off}_{JJ,TT} = \gamma_{TT,JJ} - \mathrm{Br}_{\sigma,JJ}\gamma_{\sigma,TT}\,, \tag{F.3.23}$$

is the off-shell rate of $TT \leftrightarrow JJ$ and the Boltzmann equation for the triplet (F.3.8) is given for the sum of the components as $Y_T = Y_T^0 + Y_T^+ + Y_T^-$.
Defining

$$\delta_{sub} = \delta_\sigma - \delta_J^2\mathrm{Br}_{\sigma,JJ} - \delta_N^2\mathrm{Br}_{\sigma,NN} - \delta_T^2\mathrm{Br}_{\sigma,TT} \tag{F.3.24}$$

and

$$\begin{aligned}\rho \equiv{}& \left(1-\delta_J^2\right)\left(\gamma_{NNJJ} - \mathrm{Br}_{\sigma,JJ}\gamma_{\sigma,NN}\right) + \left(1-\delta_T^2\right)\left(\gamma_{NNTT} - \mathrm{Br}_{\sigma,TT}\gamma_{\sigma,NN}\right)\\ &+ \left(1-\delta_\sigma^2\right)\gamma_{NN\sigma\sigma} + \left(1-\delta_\sigma\delta_J\right)\gamma_{NN\sigma J} + \left(1-\delta_\sigma\right)\gamma_{\sigma,NN}\\ ={}& \left(1-\delta_J^2\right)\gamma_{NNJJ} + \left(1-\delta_T^2\right)\gamma_{NNTT} + \left(1-\delta_\sigma^2\right)\gamma_{NN\sigma\sigma} + \left(1-\delta_\sigma\delta_J\right)\gamma_{NN\sigma J}\\ &+ \left[\left(1-\delta_\sigma\right) - \left(1-\delta_J^2\right)\mathrm{Br}_{\sigma,JJ} - \left(1-\delta_T^2\right)\mathrm{Br}_{\sigma,TT}\right]\gamma_{\sigma,NN}\,,\end{aligned} \tag{F.3.25}$$

we can write the full set of coupled Boltzmann equations for N, T, σ and J in the form

$$\begin{aligned}s\mathcal{H}z_N\frac{\mathrm{d}Y_N}{\mathrm{d}z_N} &= \frac{\mathrm{d}Y_N^{\mathrm{VL}}}{\mathrm{d}z_N} - 2\left(\delta_N^2-\delta_T^2\right)\gamma_{NNTT} - 2\left(\delta_N^2-\delta_J^2\right)\gamma_{NNJJ} - 2\left(\delta_N^2-\delta_\sigma^2\right)\gamma_{NN\sigma\sigma}\\ &\quad - 2\left(\delta_N^2-\delta_J\delta_\sigma\right)\gamma_{NN\sigma J} + 2\delta_{sub}\gamma_{\sigma,NN}\\ &\equiv -\left(\delta_N-1\right)\gamma_D - 2\left(\delta_N-1\right)\gamma_Q - 2(\delta_N^2-1)\gamma_S - 2\rho\,,\end{aligned} \tag{F.3.26}$$

$$\begin{aligned}s\mathcal{H}z_N\frac{\mathrm{d}Y_T}{\mathrm{d}z_N} &= -2\left(\delta_T^2-\delta_N^2\right)\gamma_{TTNN} - 2\left(\delta_T^2-\delta_J^2\right)\gamma_{TTJJ} - 2\left(\delta_T^2-\delta_\sigma^2\right)\gamma_{TT\sigma\sigma}\\ &\quad - 2\left(\delta_T^2-\delta_\sigma\delta_J\right)\gamma_{TT\sigma J} - 2\left(\delta_T^2-1\right)\gamma_{T,gauge} + 2\delta_{sub}\gamma_{\sigma,TT}\,,\end{aligned} \tag{F.3.27}$$

$$\begin{aligned}s\mathcal{H}z_N\frac{\mathrm{d}Y_\sigma}{\mathrm{d}z_N} &= -2\left(\delta_\sigma^2-\delta_N^2\right)\gamma_{\sigma\sigma NN} - 2\left(\delta_\sigma^2-\delta_T^2\right)\gamma_{\sigma\sigma TT} - 2\left(\delta_\sigma^2-\delta_J^2\right)\gamma_{\sigma\sigma JJ}\\ &\quad - \left(\delta_\sigma\delta_J-\delta_T^2\right)\gamma_{\sigma JTT} - \left(\delta_\sigma\delta_J-\delta_N^2\right)\gamma_{\sigma JNN} - \left(\delta_N\delta_\sigma-\delta_N\delta_J\right)\gamma_{N\sigma NJ}\\ &\quad - \left(\delta_T\delta_\sigma-\delta_T\delta_J\right)\gamma_{T\sigma TJ} - \left(\delta_\sigma-\delta_N^2\right)\gamma_{\sigma,NN} - \left(\delta_\sigma-\delta_T^2\right)\gamma_{\sigma,TT}\\ &\quad - \left(\delta_\sigma-\delta_J^2\right)\gamma_{\sigma,JJ}\,,\end{aligned} \tag{F.3.28}$$

$$\begin{aligned}s\mathcal{H}z_N\frac{\mathrm{d}Y_J}{\mathrm{d}z_N} &= -2\left(\delta_J^2-\delta_N^2\right)\gamma_{JJNN} - 2\left(\delta_J^2-\delta_\sigma^2\right)\gamma_{JJ\sigma\sigma} - 2\left(\delta_J^2-\delta_T^2\right)\gamma_{JJTT}\\ &\quad - \left(\delta_J\delta_\sigma-\delta_N^2\right)\gamma_{J\sigma NN} - \left(\delta_J\delta_\sigma-\delta_T^2\right)\gamma_{J\sigma TT} - \left(\delta_J\delta_N-\delta_\sigma\delta_N\right)\gamma_{JN\sigma N}\\ &\quad - \left(\delta_J\delta_T-\delta_\sigma\delta_T\right)\gamma_{JT\sigma T} + 2\delta_{sub}\gamma_{\sigma,JJ}\,.\end{aligned} \tag{F.3.29}$$

APPENDIX G

Thermal Rates

G.1 General Expressions

For $\mathcal{CP}$ conserving scattering processes $ab \leftrightarrow ij$, the thermal rate (F.1.17) can be simplified to

$$\begin{aligned}\gamma_{ab,ij} &= \frac{\mathsf{T}}{64\pi^4}\int_{s_{min}}^{\infty} \mathrm{d}s\sqrt{s}\,\hat{\sigma}(s)\,\mathrm{K}_1\left(\frac{\sqrt{s}}{\mathsf{T}}\right) \\ &= \frac{M_X M_Y^3}{64\pi^4}\int_{x_{min}}^{\infty}\mathrm{d}x_Y\frac{\sqrt{x_Y}}{z_X}\,\hat{\sigma}(x_Y)\,\mathrm{K}_1\left(\frac{M_Y}{M_X}\sqrt{x_Y}z_X\right)\,,\end{aligned} \tag{G.1.1}$$

where

$$z_X = \frac{M_X}{\mathsf{T}}\,,\quad x_Y = \frac{s}{M_Y^2}\,, \tag{G.1.2}$$

$$s_{min} = \max\left[(M_a+M_b)^2,(M_i+M_j)^2\right]\,, \tag{G.1.3}$$

$$x_{min} = \max\left[\left(\frac{M_a+M_b}{M_Y}\right)^2,\left(\frac{M_i+M_j}{M_Y}\right)^2\right]\,. \tag{G.1.4}$$

Moreover, $\hat{\sigma}(s)$ is the reduced crossection defined as

$$\hat{\sigma}(s) = 2s\lambda(1,\frac{M_a^2}{s},\frac{M_b^2}{s})\sigma(s)\,,\quad \sigma(s) = \int_{-1}^{1}\mathrm{d}\cos\theta\frac{1}{32\pi s}|\overline{M}|^2\,, \tag{G.1.5}$$

where σ is the total cross section summed over initial and final spins and

$$\lambda(a,b,c) = (a-b-c)^2\,. \tag{G.1.6}$$

For $\mathcal{CP}$ conserving decays $a \leftrightarrow ij$, we can write the thermal rate as

$$\gamma_{a,ij} = n_a^{\mathrm{eq}}\frac{\mathrm{K}_1(z)}{\mathrm{K}_2(z)}\Gamma_a\,, \tag{G.1.7}$$

where Γ_a is the decay rate.

G.2 Cross Sections and Matrix Elements for Leptogenesis

G.2.1 Vanilla Leptogenesis

The reduced cross sections for neutrino interactions involvolving third generation quarks can e.g. be found in Ref. [179] and are given by

$$\sigma_{Q_3U_3NL} = \frac{3y_t^2}{4\pi}\frac{\tilde{m}_1 M_N}{v^2}\left(\frac{x_N-1}{x_N}\right)^2 \tag{G.2.1}$$

$$\sigma_{L\overline{Q_3}N\overline{U_3}} = \sigma_{L\overline{U_3}N\overline{Q_3}} = \frac{3yt^2}{4\pi}\frac{M_N\tilde{m}_1}{v^2}\frac{x-1}{x}\left(\frac{x-2+2a_r}{x-1+a_r}+\frac{1-2a_r}{x-1}\log\left(\frac{x_N-1+a_r}{a_r}\right)\right), \tag{G.2.2}$$

where $a_r \equiv \frac{m_h}{M_N}$.

G.2.2 Triplet Gauge Scatterings

The reduced cross section for scatterings of the triplet T involvolving gauge bosons, $TT \leftrightarrow AA, L\overline{L}, Q\overline{Q}, H\overline{H}$, is given by [183, 187, 274, 275]

$$\hat{\sigma}_{T,gauge} = \frac{6g_2^4}{72\pi}\left(\frac{45}{2}\beta - \frac{27}{2}\beta^3 - \left(9\left(\beta^2-2\right)^2+18\left(\beta^2-1\right)^2\right)\log\left[\frac{1+\beta}{1-\beta}\right]\right), \tag{G.2.3}$$

where $\beta = \sqrt{1-\frac{4}{x_T}}$.

G.2.3 Majoron+Triplet Model

Next, we present the cross sections and matrix elements that appear in the MTM. For convenience, we introduce the following abbreviations:

$$\overline{x} = x-1\,, \qquad \hat{x} = x+1\,, \qquad \tilde{x} = \left(x^2-1\right), \tag{G.2.4}$$

$$A = \sqrt{\frac{\left(M_N^2\overline{x}+m_\sigma^2\right)^2}{M_N^2 x}}\,, \qquad B = 4m_J^2 - M_N^2 x\,, \tag{G.2.5}$$

$$C = 4m_\sigma^2 - M_N^2 x\,, \qquad D = 4M_T^2 - M_N^2 x\,, \tag{G.2.6}$$

$$E = m_J^2 - M_N^2 x\,, \qquad F = m_\sigma^2 - M_N^2 x\,, \tag{G.2.7}$$

$$G = M_T^2 - M_N^2 x\,, \qquad H = \sqrt{\frac{M_N^4\overline{x}^2 - 2M_N^2 m_\sigma^2\hat{x} + m_\sigma^4}{M_N^2 x}}\,, \tag{G.2.8}$$

$$O = \sqrt{\frac{m_J^4 - 2m_J^2 M_N^2 \hat{x} + M_N^4 \overline{x}^2}{M_N^2 x}}\,, \qquad Q = \left(-m_J^2 + M_N^2 x + m_\sigma^2\right)^2\,, \tag{G.2.9}$$

$$R = M_N^2(x-4)\,, \qquad S = \left(M_N^2 x + m_\sigma^2\right)\,, \tag{G.2.10}$$

$$T = \left(x - c_\vartheta^2(x-4)\right)\,, \qquad U = \left(F^2 + \Gamma_\sigma^2 m_\sigma^2\right)\,. \tag{G.2.11}$$

The reduced cross sections for $NN \to TT$ can then be written as

$$\hat{\sigma}(NN \leftrightarrow TT) = \frac{3\sqrt{-D}g_T^2 g_N^2 \sqrt{R}\left(\frac{M_N^4 x^2}{E^2} - \frac{DR}{F^2+\Gamma_\sigma^2 m_\sigma^2}\right)}{8\pi M_N^2 x}\,. \tag{G.2.12}$$

For brevity, we only present the squared matrix elements (summed over initial and final spins) for the remaining interactions,

$$|\overline{M}(NN \leftrightarrow JJ)|^2 = \frac{g_N^2 R}{2} \times M_{NN}^{JJ}\,, \tag{G.2.13}$$

$$|\overline{M}(NTT \leftrightarrow JJ)|^2 = 3|\overline{M}(NN \leftrightarrow JJ)|^2\big|_{g_N \to g_T, M_N \to M_T} \tag{G.2.14}$$

$$|\overline{M}(NN \leftrightarrow \sigma J)|^2 = \frac{g_N^2}{E^2 M_N^2 x\left(c_\vartheta\sqrt{R}\sqrt{\frac{F^2+m_J^4-2m_J^2 S}{M_N^2 x}} + \sqrt{Q} - 2m_\sigma^2\right)^2} \times M_{NN}^{\sigma J}\,, \tag{G.2.15}$$

$$|\overline{M}(TT \leftrightarrow \sigma J)|^2 = 3|\overline{M}(NN \leftrightarrow \sigma J)|^2\big|_{g_N \to g_T, M_N \to M_T}\,, \tag{G.2.16}$$

$$|\overline{M}(\sigma N \leftrightarrow JN)|^2 = \frac{g_N^4 x\left(M_N^2 x\right)^{-7/2} \times \left(Ax M_N^2 M_{\sigma N,1}^{JN} + \sqrt{M_N^2 x} M_{\sigma N,2}^{JN}\right)}{\left(A(M_N^2\hat{x} - m_J^2) + (c_\vartheta HO - 2m_\sigma^2)\sqrt{M_N^2 x}\right)^2 (\overline{x}^2 M_N^2 + \Gamma_N^2)}\,, \tag{G.2.17}$$

$$|\overline{M}(\sigma T \leftrightarrow JT)|^2 = 3|\overline{M}(\sigma N \leftrightarrow JN)|^2|_{g_N \to g_T, M_N \to M_T}\,, \tag{G.2.18}$$

$$|\overline{M}(NN \leftrightarrow \sigma\sigma)|^2 = \frac{g_N^2 R}{2U\left(Cc_\vartheta^2 R + \left(M_N^2 x - 2m_\sigma^2\right)^2\right)^2} \times M_{NN}^{\sigma\sigma}\,, \tag{G.2.19}$$

$$|\overline{M}(TT \leftrightarrow \sigma\sigma)|^2 = 3|\overline{M}(NN \leftrightarrow \sigma\sigma)|^2\big|_{g_N \to g_T, M_N \to M_T}\,, \tag{G.2.20}$$

$$|\overline{M}(\sigma\sigma \leftrightarrow JJ)|^2 = \frac{k_\sigma^4}{m_\sigma^4 U\left(\left(M_N^2 x - 2m_\sigma^2\right)^2 - BCc_\vartheta^2\right)^2} \times M_{\sigma\sigma}^{JJ}\,, \tag{G.2.21}$$

where

$$
\begin{aligned}
M_{NN}^{JJ} &\equiv \frac{k_\sigma^2}{U} + \frac{4Bc_\vartheta^2 g_N M_N \left(Bg_N M_N T + \frac{2Fk_\sigma\left(4m_J^2 M_N^2 T - M_N^4 xT - 4m_J^4\right)}{U}\right)}{\left(-4m_J^2 M_N^2 T + M_N^4 xT + 4m_J^4\right)^2}\,, \\
M_{NN}^{\sigma J} &\equiv -c_\vartheta^2 R\left(E^2 g_N^2 - k_\sigma^2 M_N^2 x\right)\left(F^2 + m_J^4 - 2m_J^2 S\right) \\
&\quad - 2c_\vartheta k_\sigma M_N^3 \sqrt{R} x \sqrt{\frac{F^2 + m_J^4 - 2m_J^2 S}{M_N^2 x}} \left(2Eg_N\left(\sqrt{Q} - 2M_N^2 x\right) + k_\sigma M_N x\left(2m_\sigma^2 - \sqrt{Q}\right)\right) \\
&\quad + M_N^2 x\left\{E^2 g_N^2\left(m_J^4 - 2m_J^2 S + M_N^4 x(x+16) - 2M_N^2\left(8\sqrt{Q} + m_\sigma^2(x-8)\right) + m_\sigma^4\right)\right. \\
&\quad -4Eg_N k_\sigma M_N\left\{m_J^4 - 2m_J^2 S + M_N^4 x^2 - 2m_\sigma^2\sqrt{Q} + 6M_N^2 m_\sigma^2 x - 2\left(M_N^2 x\right)^{3/2}\sqrt{\frac{Q}{M_N^2 x}}\right. \\
&\quad \left.\left. + m_\sigma^4\right\} + k_\sigma^2 M_N^2 x\left(m_J^4 - 2m_J^2 S + M_N^4 x^2 + m_\sigma^2\left(2M_N^2 x - 4\sqrt{Q}\right) + 5m_\sigma^4\right)\right\}\,,
\end{aligned}
\tag{G.2.22}
$$

$$
\begin{aligned}
M_{NN}^{\sigma\sigma} &\equiv 2Cc_\vartheta^2\left(-2g_N^2\left(M_N^4(x-16)x - 4M_N^2 m_\sigma^2(x-8)\right)U\right. \\
&\quad +4g_N k_\sigma M_N\left(M_N^4 x^2 - 3M_N^2 m_\sigma^2 x + 2m_\sigma^4\right)\left(M_N^2(8-3x) + 2m_\sigma^2\right) + k_\sigma^2 R\left(M_N^2 x - 2m_\sigma^2\right)^2\Big) \\
&\quad + \left(M_N^2 x - 2m_\sigma^2\right)^2\left(64\Gamma_\sigma^2 g_N^2 M_N^2 m_\sigma^2 + \left(M_N^2 x(k_\sigma - 8g_N M_N) - 2m_\sigma^2(k_\sigma - 4g_N M_N)\right)^2\right) \\
&\quad - \left(c_\vartheta^4(x-4)\left(M_N^3 x - 4M_N m_\sigma^2\right)^2\left(-8Fg_N k_\sigma M_N + 4g_N^2 U - k_\sigma^2 R\right)\right)\,,
\end{aligned}
\tag{G.2.23}
$$

$$
\begin{aligned}
M_{\sigma\sigma}^{JJ} &\equiv 8m_\sigma^6\left(\Gamma_\sigma^2\left(2B^2 c_\vartheta^4 + 11Bc_\vartheta^2 M_N^2 x + 11M_N^4 x^2\right) - 2M_N^4 x^2\left(9Bc_\vartheta^2 + 17M_N^2 x\right)\right) \\
&\quad + 8M_N^2 m_\sigma^4 x\left(2M_N^2 x\left(B^2 c_\vartheta^4 + 6Bc_\vartheta^2 M_N^2 x + 6M_N^4 x^2\right) - \Gamma_\sigma^2\left(Bc_\vartheta^2 + M_N^2 x\right)\left(Bc_\vartheta^2 + 2M_N^2 x\right)\right) \\
&\quad + M_N^4 m_\sigma^2 x^2\left(\left(c_\vartheta^2 - 1\right)M_N^2 x - 4c_\vartheta^2 m_J^2\right)\left(8M_N^2 x\left(Bc_\vartheta^2 + 2M_N^2 x\right) - \Gamma_\sigma^2\left(Bc_\vartheta^2 + M_N^2 x\right)\right) \\
&\quad + 32m_\sigma^8\left(2M_N^2 x\left(Bc_\vartheta^2 + 6M_N^2 x\right) - 3\Gamma_\sigma^2\left(Bc_\vartheta^2 + 2M_N^2 x\right)\right) \\
&\quad + M_N^8 x^4\left(\left(c_\vartheta^2 - 1\right)M_N^2 x - 4c_\vartheta^2 m_J^2\right)^2 + 16m_\sigma^{10}\left(9\Gamma_\sigma^2 - 16M_N^2 x\right) + 64m_\sigma^{12}\,,
\end{aligned}
\tag{G.2.24}
$$

$$
\begin{aligned}
M^{JN}_{\sigma N,1} \equiv & \left(-\left(\left(3c_\vartheta^2+1\right)\overline{x}^3 M_N^6\right)+m_\sigma^2\overline{x}\left((7x+5)c_\vartheta^2-x+1\right)M_N^4+m_\sigma^4\left((1-5x)c_\vartheta^2+x-1\right)M_N^2+\left(c_\vartheta^2+1\right)m_\sigma^6\right)m_J^6\\
&+M_N^2\left(3\left(3c_\vartheta^2+1\right)\overline{x}^3\hat{x}M_N^6-m_\sigma^2\tilde{x}\left(3(7x+5)c_\vartheta^2+x+3\right)M_N^4+m_\sigma^2\left(m_\sigma^2\left(3\hat{x}(5x-1)c_\vartheta^2+5x^2+3\right)-2c_\vartheta HOx\hat{x}\right)M_N^2\right.\\
&\left.+2c_\vartheta Hm_\sigma^4 Ox-m_\sigma^6\left(3\hat{x}c_\vartheta^2+7x+3\right)\right)m_J^4+M_N^4\left(-\overline{x}^2\overline{x}\left(\left(9x^2+6x+9\right)c_\vartheta^2+x(7x+6)+3\right)\right.\\
&M_N^6+\left(\overline{x}\left((7x+5)(x(3x+2)+3)c_\vartheta^2+x(17x\hat{x}+11)+3\right)m_\sigma^2-4x^2(x+3)\Gamma_N^2-8c_\vartheta HOx^2\tilde{x}\right)M_N^4\\
&-m_\sigma^2\left(\left((5x-1)(x(3x+2)+3)c_\vartheta^2+x(x(25x+17)+3)+3\right)m_\sigma^2-4x^2\Gamma_N^2-4c_\vartheta HOx\left(4x^2+x+1\right)\right)M_N^2\\
&\left.-4c_\vartheta Hm_\sigma^4 Ox(2x+1)+m_\sigma^6\left((x(3x+2)+3)c_\vartheta^2+(3x+1)(5x+3)\right)\right)\\
&m_J^2+M_N^6\hat{x}\left(\overline{x}^3\left(3\overline{x}^2c_\vartheta^2+x(5x+2)+1\right)M_N^6+\left(4x^2\left((x+3)\Gamma_N^2+2c_\vartheta HO\tilde{x}\right)\right.\right.\\
&\left.-m_\sigma^2\overline{x}\left(\overline{x}^2(7x+5)c_\vartheta^2+(3x+1)(x(5x+2)+1)\right)\right)M_N^4+m_\sigma^2\left(m_\sigma^2\left(\overline{x}^2(5x-1)c_\vartheta^2+x+x^2(19x+11)+1\right)-\\
&\left.2x\left(2x\Gamma_N^2+c_\vartheta HO\left(7x^2+1\right)\right)\right)M_N^2+2c_\vartheta Hm_\sigma^4 Ox(3x+1)-m_\sigma^6\left(\overline{x}^2c_\vartheta^2+(3x+1)^2\right)\Big)\ ,\\
M^{JN,2}_{\sigma N} \equiv & \ m_\sigma^2\left(M_N^2\hat{x}-m_\sigma^2\right)\left(\left(c_\vartheta^2+1\right)\overline{x}^2M_N^4-2m_\sigma^2\left(\hat{x}c_\vartheta^2-x+1\right)M_N^2+\left(c_\vartheta^2+1\right)m_\sigma^4\right)m_J^6\\
&+M_N^2\left(4\left(c_\vartheta^2+1\right)\overline{x}^3x\hat{x}M_N^8-\overline{x}\left(m_\sigma^2\left(3\overline{x}^3+c_\vartheta^2(5x(3x\hat{x}+1)-3)\right)-c_\vartheta\left(c_\vartheta^2+3\right)HO\overline{x}^2x\right)M_N^6\right.\\
&+m_\sigma^2\left(m_\sigma^2\left(\hat{x}(x(21x+2)+9)c_\vartheta^2-5x+x^2(7-11x)+9\right)-2c_\vartheta HO\overline{x}x\left(\hat{x}c_\vartheta^2-2x+2\right)\right)M_N^4\\
&-m_\sigma^4\left(m_\sigma^2\left((x(13x+18)+9)c_\vartheta^2+x(10-3x)+9\right)-c_\vartheta\left(c_\vartheta^2-1\right)HO\overline{x}x\right)M_N^2-2c_\vartheta Hm_\sigma^6 Ox+m_\sigma^8\left(3\hat{x}c_\vartheta^2+7x+3\right)\Big)m_J^4\\
&-M_N^4\left(8\overline{x}^2x\hat{x}\left(\tilde{x}c_\vartheta^2+x(x+2)-1\right)M_N^8+\left(2x\hat{x}\left(c_\vartheta\left(c_\vartheta^2+3\right)HO\overline{x}^3+8x\Gamma_N^2\right)-m_\sigma^2\overline{x}\left(\hat{x}(x(x(27x+23)+17)-3)c_\vartheta^2\right.\right.\right.\\
&\left.\left.\left.+\overline{x}^2(x(7x+12)-3)\right)\right)M_N^6+m_\sigma^2\left(\left((33x^4+52x^3+30x^2+4x+9)c_\vartheta^2-4x+x^2(6-x(7x+4))+9\right)m_\sigma^2-4x^2(x+5)\Gamma_N^2\right.\\
&\left.-4c_\vartheta HOx\tilde{x}\left(\hat{x}c_\vartheta^2-x+2\right)\right)M_N^4-m_\sigma^4\left(\left(\hat{x}(x(17x+6)+9)c_\vartheta^2+x(x(9x+7)+23)+9\right)m_\sigma^2-4x^2\Gamma_N^2\right.\\
&\left.-2c_\vartheta HOx\left(\tilde{x}c_\vartheta^2+3x^2+1\right)\right)M_N^2-4c_\vartheta Hm_\sigma^6 Ox(2x+1)+m_\sigma^8\left((x(3x+2)+3)c_\vartheta^2+(3x+1)(5x+3)\right)\Big)\\
&m_J^2+M_N^6\left(4\left(\overline{x}^2c_\vartheta^2+\overline{x}^2\right)\overline{x}^3x\hat{x}M_N^8-\overline{x}\left(\left(\overline{x}^2(x(13x\hat{x}+7)-1)c_\vartheta^2+\overline{x}(x(x(x(5x-32)+2)-8)+1)\right)m_\sigma^2\right.\right.\\
&\left.+x\left(16x\hat{x}\Gamma_N^2-c_\vartheta HO\overline{x}\left(c_\vartheta^2\overline{x}^3+x(x(7x-17)-3)-3\right)\right)\right)M_N^6+\left(\hat{x}\left(\overline{x}^2(x(15x-2)+3)c_\vartheta^2+\overline{x}^2(x(3x+2)+3)\right)m_\sigma^4\right.\\
&\left.+2x\left(-2x(x(x+2)+5)\Gamma_N^2-c_\vartheta HO\tilde{x}\left(c_\vartheta^2\overline{x}^2+2\left(2x^2+x+1\right)\right)\right)m_\sigma^2\right.\\
&\left.+4c_\vartheta HO\overline{x}x^3\Gamma_N^2\right)M_N^4+m_\sigma^4\left(x\left(4x\hat{x}\Gamma_N^2+c_\vartheta HO\left(c_\vartheta^2\overline{x}^3+x+x^2(11x+19)+1\right)\right)\right.\\
&\left.-m_\sigma^2\left(\overline{x}^2(x(7x+6)+3)c_\vartheta^2+11x^4+28x^3+10x^2+12x+3\right)\right)M_N^2+m_\sigma^6\hat{x}\left(m_\sigma^2\left(\overline{x}^2c_\vartheta^2+(3x+1)^2\right)-2c_\vartheta HOx(3x+1)\right)\Big)\ .
\end{aligned}
$$

APPENDIX H

VLL-Scalar-SM Mixing Yukawa Terms

Here we give the Yukawa couplings relevant for (7.3.10):

$$g_{h^0}^{\mu\mu} = \frac{m_\mu}{v\cos\beta}U_{11}V_{\mu\mu}^2 + yU_{21}V_{\mu M}V_{\mu\mu} + y'U_{31}V_{\mu M}V_{\mu\mu}\,, \tag{H.0.1}$$

$$g_{h^0}^{MM} = \frac{m_\mu}{v\cos\beta}U_{11}V_{\mu M}^2 - yU_{21}V_{\mu M}V_{\mu\mu} - y'U_{31}V_{\mu M}V_{\mu\mu}\,, \tag{H.0.2}$$

$$g_{h^0,\mathtt{L}}^{\mu M} = -\frac{m_\mu}{v\cos\beta}U_{11}V_{\mu M}V_{\mu\mu} - yU_{21}V_{\mu M}^2 + y'U_{31}V_{MM}V_{\mu\mu}\,, \tag{H.0.3}$$

$$g_{h^0,\mathtt{R}}^{\mu M} = -\frac{m_\mu}{v\cos\beta}U_{11}V_{\mu M}V_{\mu\mu} + yU_{21}V_{\mu\mu}V_{\mu\mu} - y'U_{31}V_{\mu M}^2\,, \tag{H.0.4}$$

$$g_{H^0}^{\mu\mu} = \frac{m_\mu}{v\cos\beta}U_{12}V_{\mu\mu}^2 + yU_{22}V_{\mu M}V_{\mu\mu} + y'U_{32}V_{\mu M}V_{\mu\mu}\,, \tag{H.0.5}$$

$$g_{H^0}^{MM} = \frac{m_\mu}{v\cos\beta}U_{12}V_{\mu M}^2 - yU_{22}V_{\mu M}V_{\mu\mu} - y'U_{32}V_{\mu M}V_{\mu\mu}\,, \tag{H.0.6}$$

$$g_{H^0,\mathtt{L}}^{\mu M} = -\frac{m_\mu}{v\cos\beta}U_{12}V_{\mu M}V_{\mu\mu} - yU_{22}V_{\mu M}^2 + y'U_{32}V_{MM}V_{\mu\mu}\,, \tag{H.0.7}$$

$$g_{H^0,\mathtt{R}}^{\mu M} = -\frac{m_\mu}{v\cos\beta}U_{12}V_{\mu M}V_{\mu\mu} + yU_{22}V_{\mu\mu}^2 - y'U_{33}V_{\mu M}^2\,, \tag{H.0.8}$$

$$g_{S^0}^{\mu\mu} = \frac{m_\mu}{v\cos\beta}U_{13}V_{\mu\mu}^2 + yU_{23}V_{\mu M}V_{\mu\mu} + y'U_{33}V_{\mu M}V_{\mu\mu}\,, \tag{H.0.9}$$

$$g_{S^0}^{MM} = \frac{m_\mu}{v\cos\beta}U_{13}V_{\mu M}^2 - yU_{23}V_{\mu M}V_{\mu\mu} - y'U_{33}V_{\mu M}V_{\mu\mu}\,, \tag{H.0.10}$$

$$g_{S^0,\mathtt{L}}^{\mu M} = -\frac{m_\mu}{v\cos\beta}U_{13}V_{\mu M}V_{\mu\mu} - yU_{23}V_{\mu M}^2 + y'U_{33}V_{MM}V_{\mu\mu}\,, \tag{H.0.11}$$

$$g_{S^0,\mathtt{R}}^{\mu M} = -\frac{m_\mu}{v\cos\beta}U_{13}V_{\mu M}V_{\mu\mu} + yU_{23}V_{\mu\mu}^2 - y'U_{33}V_{\mu M}^2\,. \tag{H.0.12}$$

APPENDIX I

Higgs Decay Rates

Defining $\tau_i = 4m_i^2/m_h^2, i = V, f$, the diphoton decay width for a general model including spin-1 particles V and fermions f with electric charge Q_i coupling to the Higgs is given by [277]

$$\Gamma(h^0 \to \gamma\gamma) \propto \left| \frac{g_{hVV}}{m_V^2} Q_V^2 A_1(\tau_V) + \frac{2g_{hf\bar{f}}}{m_f} N_{c,f} Q_f^2 A_{1/2}(\tau_f) \right|^2 . \tag{I.0.1}$$

The $h^0 \to \gamma Z$ decay width for a general model including spin-1 particles V and fermions f coupling to the Higgs is given by [278]

$$\Gamma(h^0 \to \gamma Z) = \left| \frac{g_{hVV}}{m_V^2} g_{ZVV} A_1(\tau_V, \lambda_V) + N_{c,f} \frac{2g_{hf\bar{f}}}{m_f} (2Q_f)(g_{Zll}^f + g_{Zrr}^f) A_{1/2}(\tau_f, \lambda_f) \right|^2 , \tag{I.0.2}$$

where $\lambda_i = 4\frac{m_i^2}{m_Z^2}$ and

$$g_{Zkk}^f = \frac{1}{\sin\vartheta_W \cos\vartheta_W} (T_3^{(k,f)} - Q_f \sin\vartheta_W^2) , \qquad k = l, r \tag{I.0.3}$$

are the couplings of the Z to LH and RH particles with weak isospin $T_3^{k,f}$, respectively. The corresponding loop functions used in section 7.4.1 are given by [277]

$$A_1(x) = -x^2 \left(2x^{-2} + 3x^{-1} + 3(2x^{-1} - 1) f(x^{-1})\right) , \tag{I.0.4}$$

$$A_{\frac{1}{2}}(x) = 2x^2 \left(x^{-1} + \left(x^{-1} - 1\right) f(x^{-1})\right) , \tag{I.0.5}$$

$$A_1(x, y) = 4(3 - \tan^2\vartheta_W) I_2(x, y) + [(1 - \frac{2}{x}) \tan^2\vartheta_W - (5 + \frac{2}{x}] I_1(x, y) , \tag{I.0.6}$$

$$A_{1/2}(x, y) = I_1(x, y) - I_2(x, y) , \tag{I.0.7}$$

$$I_1(x, y) = \frac{xy}{2(x - y)} + \frac{x^2 y^2}{2(x - y)^2} [f(x^{-1}) - f(y^{-1})] + \frac{x^2 y}{(x - y)^2} [g(x^{-1}) - g(y^{-1})] , \tag{I.0.8}$$

$$I_2(x, y) = -\frac{xy}{2(x - y)} [f(x^{-1}) - f(y^{-1})] , \tag{I.0.9}$$

$$f(x) = \arcsin^2 \sqrt{x} , \tag{I.0.10}$$

$$g(x) = \sqrt{x^{-1} - 1} \arcsin \sqrt{x} . \tag{I.0.11}$$

APPENDIX J

Exemplary Data Sets for the AMM

In Tab. J.1, we present data sets that yield viable contributions to the AMM, see Chapter 7.5, displayed in Fig. 7.7.

Parameter	1	2	3	4	5	6	7	8	9
y'	-2.880	-1.783	-0.876	-0.491	-0.844	-1.019	-0.922	-1.318	-0.386
λ_1	0.559	0.387	0.311	0.456	0.616	0.456	0.616	0.559	0.311
λ_2	0.116	0.123	0.141	0.204	0.099	0.204	0.099	0.116	0.141
λ_3	0.093	0.945	0.731	0.828	0.665	0.828	0.665	0.093	0.731
λ_4	-0.101	-0.141	-0.702	0.168	-0.365	0.168	-0.365	-0.101	-0.702
λ_5	-0.074	-0.884	-0.099	-0.968	-0.402	-0.968	-0.402	-0.074	-0.099
λ_S	0.924	0.867	0.910	0.352	0.600	0.352	0.600	0.924	0.910
η_2	0.182	0.158	0.156	0.226	0.173	0.226	0.173	0.182	0.156
μ_1/GeV	41.982	42.672	46.821	102.293	22.346	102.293	22.346	41.982	46.821
μ_2/GeV	71.135	69.551	72.458	94.039	66.776	94.039	66.776	71.135	72.458
μ_S/GeV	98.904	94.206	91.722	95.987	99.757	95.987	99.757	98.904	91.722
v_1/GeV	102.562	119.174	129.687	142.845	96.180	142.845	96.180	102.562	129.687
v_2/GeV	223.600	215.206	209.039	200.278	226.419	200.278	226.419	223.600	209.039
v_S/GeV	26.778	42.620	41.949	19.861	42.840	19.861	42.840	26.778	41.949
m_{H^0}/GeV	90.749	88.633	89.541	139.698	86.112	139.698	86.112	90.749	89.541
m_{S^0}/GeV	28.652	45.074	47.940	8.761	26.970	8.761	26.970	28.652	47.940
c_{23}	0.977	0.934	0.954	0.999	0.916	0.999	0.916	0.977	0.954
c_{13}	0.994	0.985	0.985	0.995	0.985	0.995	0.985	0.994	0.985
c_{12}	0.700	0.661	0.588	0.484	0.723	0.484	0.723	0.700	0.588

Table J.1: Exemplary parameter sets used in Fig. 7.7.

Bibliography

[1] Tim Brune, Thomas W. Kephart, and Heinrich Päs. "Muon $g-2$ Anomaly from Vector-like Leptons in a 2-Higgs-doublet + Scalar Singlet Model". In: *The European Physical Journal C* 84.12 (Dec. 2024), p. 1254. DOI: 10.1140/epjc/s10052-024-13617-5. arXiv: 2205.05566 [hep-ph].

[2] Tim Brune. "Leptogenesis in Majoron Models without Domain Walls". In: *Physical Review D* 107.9 (May 2023), p. 096023. DOI: 10.1103/PhysRevD.107.096023. arXiv: 2201.12239 [hep-ph].

[3] Tim Brune. "Leptogenesis in a Majoron plus triplet model". In: *Phys. Rev. D* 111.11 (June 2025), p. 115001. DOI: 10.1103/tbsx-7ffr. arXiv: 2501.11529 [hep-ph].

[4] F. Englert and R. Brout. "Broken Symmetry and the Mass of Gauge Vector Mesons". In: *Physical Review Letters* 13.9 (Aug. 1964), pp. 321–323. DOI: 10.1103/PhysRevLett.13.321.

[5] Peter W. Higgs. "Broken Symmetries and the Masses of Gauge Bosons". In: *Physical Review Letters* 13.16 (Oct. 1964), pp. 508–509. DOI: 10.1103/PhysRevLett.13.508.

[6] G. Aad et al. "Observation of a New Particle in the Search for the Standard Model Higgs Boson with the ATLAS Detector at the LHC". In: *Physics Letters B* 716.1 (Sept. 2012), pp. 1–29. DOI: 10.1016/j.physletb.2012.08.020.

[7] The CMS Collaboration. "Observation of a New Boson at a Mass of 125 GeV with the CMS Experiment at the LHC". In: *Physics Letters B* 716.1 (Sept. 2012), pp. 30–61. DOI: 10.1016/j.physletb.2012.08.021. arXiv: 1207.7235 [hep-ex].

[8] Edwin Hubble. "A Relation between Distance and Radial Velocity among Extra-Galactic Nebulae". In: *Proceedings of the National Academy of Science* 15 (Mar. 1929), pp. 168–173. DOI: 10.1073/pnas.15.3.168.

[9] G. Lemaître. "Un Univers Homogène de Masse Constante et de Rayon Croissant Rendant Compte de La Vitesse Radiale Des Nébuleuses Extra-Galactiques". In: *Annales de la Société Scientifique de Bruxelles* 47 (Jan. 1927), pp. 49–59.

[10] Ralph A. Alpher and Robert Herman. "Evolution of the Universe". In: *Nature* 162.4124 (Nov. 1948), pp. 774–775. DOI: 10.1038/162774b0.

[11] A. A. Penzias and R. W. Wilson. "A Measurement of Excess Antenna Temperature at 4080 Mc/s." In: *The Astrophysical Journal* 142 (July 1965), pp. 419–421. DOI: 10.1086/148307.

[12] G. Gamow. "The Evolution of the Universe". In: *Nature* 162.4122 (Oct. 1948), pp. 680–682. DOI: 10.1038/162680a0.

[13] R. A. Alpher, H. Bethe, and G. Gamow. "The Origin of Chemical Elements". In: *Physical Review* 73.7 (Apr. 1948), pp. 803–804. DOI: 10.1103/PhysRev.73.803.

[14] G. Gamow. "The Origin of Elements and the Separation of Galaxies". In: *Physical Review* 74.4 (Aug. 1948), pp. 505–506. DOI: 10.1103/PhysRev.74.505.2.

[15] P. J. E. Peebles. "Primeval Helium Abundance and the Primeval Fireball". In: *Physical Review Letters* 16.10 (Mar. 1966), pp. 410–413. DOI: 10.1103/PhysRevLett.16.410.

[16] Robert V. Wagoner, William A. Fowler, and F. Hoyle. "On the Synthesis of Elements at Very High Temperatures". In: *The Astrophysical Journal* 148 (Apr. 1967), p. 3. DOI: 10.1086/149126.

[17] Tsung-Han Yeh et al. "Probing Physics Beyond the Standard Model: Limits from BBN and the CMB Independently and Combined". In: *Journal of Cosmology and Astroparticle Physics* 2022.10 (Oct. 2022), p. 046. DOI: 10.1088/1475-7516/2022/10/046. arXiv: 2207.13133 [astro-ph].

[18] N. Aghanim et al. “Planck 2018 Results. VI. Cosmological Parameters”. In: *Astron. Astrophys.* 641 (2020), A6. DOI: 10.1051/0004-6361/201833910.

[19] A. D. Sakharov. “Violation of CP Invariance, C Asymmetry, and Baryon Asymmetry of the Universe”. In: *Pisma Zh. Eksp. Teor. Fiz.* 5 (1967), pp. 32–35. DOI: 10 . 1070 / PU1991v034n05ABEH002497.

[20] K. Eguchi et al. “First Results from KamLAND: Evidence for Reactor Anti-Neutrino Disappearance”. In: *Phys. Rev. Lett.* 90 (2003), p. 021802. DOI: 10.1103/PhysRevLett.90.021802.

[21] Q. R. Ahmad et al. “Direct Evidence for Neutrino Flavor Transformation from Neutral Current Interactions in the Sudbury Neutrino Observatory”. In: *Phys. Rev. Lett.* 89 (2002), p. 011301. DOI: 10.1103/PhysRevLett.89.011301.

[22] Y. Fukuda et al. “Evidence for Oscillation of Atmospheric Neutrinos”. In: *Phys. Rev. Lett.* 81 (1998), pp. 1562–1567. DOI: 10.1103/PhysRevLett.81.1562.

[23] Peter Minkowski. “$\mu \to e\gamma$ at a Rate of One Out of 10^9 Muon Decays?” In: *Phys. Lett. B* 67 (1977), pp. 421–428. DOI: 10.1016/0370-2693(77)90435-X.

[24] M. Fukugita and T. Yanagida. “Baryogenesis Without Grand Unification”. In: *Phys. Lett. B* 174 (1986), pp. 45–47. DOI: 10.1016/0370-2693(86)91126-3.

[25] F. Zwicky. “Die Rotverschiebung von Extragalaktischen Nebeln”. In: *Helvetica Physica Acta* 6 (Jan. 1933), pp. 110–127.

[26] Douglas Clowe et al. “A Direct Empirical Proof of the Existence of Dark Matter”. In: *The Astrophysical Journal* 648.2 (Sept. 2006), pp. L109–L113. DOI: 10.1086/508162.

[27] Howard Georgi and S. L. Glashow. “Unity of All Elementary-Particle Forces”. In: *Physical Review Letters* 32.8 (Feb. 1974), pp. 438–441. DOI: 10.1103/PhysRevLett.32.438.

[28] Y. Chikashige, Rabindra N. Mohapatra, and R. D. Peccei. “Are There Real Goldstone Bosons Associated with Broken Lepton Number?” In: *Phys. Lett. B* 98 (1981), pp. 265–268. DOI: 10.1016/0370-2693(81)90011-3.

[29] Howard M. Georgi, Sheldon Lee Glashow, and Shmuel Nussinov. “Unconventional Model of Neutrino Masses”. In: *Nucl. Phys. B* 193 (1981), pp. 297–316. DOI: 10.1016/0550-3213(81)90336-9.

[30] J. Schechter and J. W. F. Valle. “Neutrino Decay and Spontaneous Violation of Lepton Number”. In: *Phys. Rev. D* 25 (1982), p. 774. DOI: 10.1103/PhysRevD.25.774.

[31] V. Berezinsky and J. W. F. Valle. “The KeV Majoron as a Dark Matter Particle”. In: *Phys. Lett. B* 318 (1993), pp. 360–366. DOI: 10.1016/0370-2693(93)90140-D.

[32] Tim Brune and Heinrich Päs. “Massive Majorons and Constraints on the Majoron-Neutrino Coupling”. In: *Phys. Rev. D* 99.9 (2019), p. 096005. DOI: 10.1103/PhysRevD.99.096005.

[33] Michele Frigerio, Thomas Hambye, and Eduard Masso. “Sub-GeV Dark Matter as Pseudo-Goldstone from the Seesaw Scale”. In: *Phys. Rev. X* 1 (2011), p. 021026. DOI: 10.1103/PhysRevX.1.021026.

[34] Lawrence J. Hall et al. “Freeze-In Production of FIMP Dark Matter”. In: *JHEP* 03 (2010), p. 080. DOI: 10.1007/JHEP03(2010)080.

[35] I. Z. Rothstein, K. S. Babu, and D. Seckel. “Planck Scale Symmetry Breaking and Majoron Physics”. In: *Nucl. Phys. B* 403 (1993), pp. 725–748. DOI: 10.1016/0550-3213(93)90368-Y.

[36] R. D. Peccei and Helen R. Quinn. “CP Conservation in the Presence of Pseudoparticles”. In: *Physical Review Letters* 38.25 (June 1977), pp. 1440–1443. DOI: 10.1103/PhysRevLett.38.1440.

[37] Steven Weinberg. “A New Light Boson?” In: *Physical Review Letters* 40.4 (Jan. 1978), pp. 223–226. DOI: 10.1103/PhysRevLett.40.223.

[38] F. Wilczek. "Problem of Strong P and T Invariance in the Presence of Instantons". In: *Physical Review Letters* 40.5 (Jan. 1978), pp. 279–282. DOI: 10.1103/PhysRevLett.40.279.

[39] Diego Aristizabal Sierra et al. "Leptogenesis with a Dynamical Seesaw Scale". In: *JCAP* 07 (2014), p. 052. DOI: 10.1088/1475-7516/2014/07/052.

[40] Pei-Hong Gu and Utpal Sarkar. "Leptogenesis Bound on Spontaneous Symmetry Breaking of Global Lepton Number". In: *Eur. Phys. J. C* 71 (2011), p. 1560. DOI: 10.1140/epjc/s10052-011-1560-2.

[41] Apostolos Pilaftsis. "Electroweak Resonant Leptogenesis in the Singlet Majoron Model". In: *Phys. Rev. D* 78 (2008), p. 013008. DOI: 10.1103/PhysRevD.78.013008.

[42] Pei-Hong Gu, Ernest Ma, and Utpal Sarkar. "Pseudo-Majoron as Dark Matter". In: *Physics Letters B* 690.2 (June 2010), pp. 145–148. DOI: 10.1016/j.physletb.2010.05.012. arXiv: 1004.1919 [hep-ph].

[43] B. Abi et al. "Measurement of the Positive Muon Anomalous Magnetic Moment to 0.46 Ppm". In: *Phys. Rev. Lett.* 126.14 (2021), p. 141801. DOI: 10.1103/PhysRevLett.126.141801.

[44] D. P. Aguillard et al. "Measurement of the Positive Muon Anomalous Magnetic Moment to 0.20 Ppm". In: *Phys. Rev. Lett.* 131.16 (2023), p. 161802. DOI: 10.1103/PhysRevLett.131.161802.

[45] T. Aoyama et al. "The Anomalous Magnetic Moment of the Muon in the Standard Model". In: *Phys. Rept.* 887 (2020), pp. 1–166. DOI: 10.1016/j.physrep.2020.07.006.

[46] Tatsumi Aoyama et al. "Complete Tenth-Order QED Contribution to the Muon g-2". In: *Phys. Rev. Lett.* 109 (2012), p. 111808. DOI: 10.1103/PhysRevLett.109.111808.

[47] Tatsumi Aoyama, Toichiro Kinoshita, and Makiko Nio. "Theory of the Anomalous Magnetic Moment of the Electron". In: *Atoms* 7.1 (2019), p. 28. DOI: 10.3390/atoms7010028.

[48] Andrzej Czarnecki, William J. Marciano, and Arkady Vainshtein. "Refinements in Electroweak Contributions to the Muon Anomalous Magnetic Moment". In: *Phys. Rev. D* 67 (2003), p. 073006. DOI: 10.1103/PhysRevD.67.073006.

[49] C. Gnendiger, D. Stöckinger, and H. Stöckinger-Kim. "The Electroweak Contributions to (g-2)_\mu after the Higgs Boson Mass Measurement". In: *Phys. Rev. D* 88 (2013), p. 053005. DOI: 10.1103/PhysRevD.88.053005.

[50] M. Davier et al. "A New Evaluation of the Hadronic Vacuum Polarisation Contributions to the Muon Anomalous Magnetic Moment and to $\alpha(m_Z^2)$". In: *Eur. Phys. J. C* 80.3 (2020), p. 241. DOI: 10.1140/epjc/s10052-020-7792-2.

[51] Alexander Keshavarzi, Daisuke Nomura, and Thomas Teubner. "Muon G-2 and $\alpha(m_Z^2)$: A New Data-Based Analysis". In: *Phys. Rev. D* 97.11 (2018), p. 114025. DOI: 10.1103/PhysRevD.97.114025.

[52] Gilberto Colangelo, Martin Hoferichter, and Peter Stoffer. "Two-Pion Contribution to Hadronic Vacuum Polarization". In: *JHEP* 02 (2019), p. 006. DOI: 10.1007/JHEP02(2019)006.

[53] Martin Hoferichter, Bai-Long Hoid, and Bastian Kubis. "Three-Pion Contribution to Hadronic Vacuum Polarization". In: *JHEP* 08 (2019), p. 137. DOI: 10.1007/JHEP08(2019)137.

[54] Alexander Keshavarzi, Daisuke Nomura, and Thomas Teubner. "G-2 of Charged Leptons, $\alpha(m_Z^2)$, and the Hyperfine Splitting of Muonium". In: *Phys. Rev. D* 101.1 (2020), p. 014029. DOI: 10.1103/PhysRevD.101.014029.

[55] Alexander Kurz et al. "Hadronic Contribution to the Muon Anomalous Magnetic Moment to Next-to-next-to-Leading Order". In: *Phys. Lett. B* 734 (2014), pp. 144–147. DOI: 10.1016/j.physletb.2014.05.043.

[56] Kirill Melnikov and Arkady Vainshtein. "Hadronic Light-by-Light Scattering Contribution to the Muon Anomalous Magnetic Moment Revisited". In: *Phys. Rev. D* 70 (2004), p. 113006. DOI: 10.1103/PhysRevD.70.113006.

[57] Pere Masjuan and Pablo Sanchez-Puertas. "Pseudoscalar-Pole Contribution to the (G_\mu-2): A Rational Approach". In: *Phys. Rev. D* 95.5 (2017), p. 054026. DOI: 10.1103/PhysRevD.95.054026.

[58] Gilberto Colangelo et al. "Dispersion Relation for Hadronic Light-by-Light Scattering: Two-Pion Contributions". In: *JHEP* 04 (2017), p. 161. DOI: 10.1007/JHEP04(2017)161.

[59] Martin Hoferichter et al. "Dispersion Relation for Hadronic Light-by-Light Scattering: Pion Pole". In: *JHEP* 10 (2018), p. 141. DOI: 10.1007/JHEP10(2018)141.

[60] Antoine Gérardin, Harvey B. Meyer, and Andreas Nyffeler. "Lattice Calculation of the Pion Transition Form Factor with $N_f = 2 + 1$ Wilson Quarks". In: *Phys. Rev. D* 100.3 (2019), p. 034520. DOI: 10.1103/PhysRevD.100.034520.

[61] Johan Bijnens, Nils Hermansson-Truedsson, and Antonio Rodriguez-Sanchez. "Short-Distance Constraints for the HLbL Contribution to the Muon Anomalous Magnetic Moment". In: *Phys. Lett. B* 798 (2019), p. 134994. DOI: 10.1016/j.physletb.2019.134994.

[62] Gilberto Colangelo et al. "Longitudinal Short-Distance Constraints for the Hadronic Light-by-Light Contribution to $g - 2_\mu$ with Large-N_c Regge Models". In: *JHEP* 03 (2020), p. 101. DOI: 10.1007/JHEP03(2020)101.

[63] Thomas Blum et al. "Hadronic Light-by-Light Scattering Contribution to the Muon Anomalous Magnetic Moment from Lattice QCD". In: *Phys. Rev. Lett.* 124.13 (2020), p. 132002. DOI: 10.1103/PhysRevLett.124.132002.

[64] Gilberto Colangelo et al. "Remarks on Higher-Order Hadronic Corrections to the Muon G\ensuremath-2". In: *Phys. Lett. B* 735 (2014), pp. 90–91. DOI: 10.1016/j.physletb.2014.06.012.

[65] Abdus Salam. "Weak and Electromagnetic Interactions". In: *World Scientific Series in 20th Century Physics*. Vol. 5. WORLD SCIENTIFIC, May 1994, pp. 244–254. ISBN: 978-981-02-1662-7 978-981-279-591-5. DOI: 10.1142/9789812795915_0034.

[66] Sheldon L. Glashow. "Partial-Symmetries of Weak Interactions". In: *Nuclear Physics* 22.4 (Feb. 1961), pp. 579–588. DOI: 10.1016/0029-5582(61)90469-2.

[67] Steven Weinberg. "A Model of Leptons". In: *Physical Review Letters* 19.21 (Nov. 1967), pp. 1264–1266. DOI: 10.1103/PhysRevLett.19.1264.

[68] Francis Halzen and Alan Douglas Martin. *Quarks and Leptons: An Introductory Course in Modern Particle Physics*. New York Chichester Brisbane [etc.]: J. Wiley & sons, 1984. ISBN: 978-0-471-88741-6.

[69] Heather E. Logan. *TASI 2013 Lectures on Higgs Physics within and beyond the Standard Model*. June 2022. arXiv: 1406.1786 [hep-ph].

[70] Palash B. Pal and Amitabha Lahiri. *A First Book of Quantum Field Theory*.

[71] Michael Edward Peskin and Daniel V. Schroeder. *An Introduction to Quantum Field Theory*. Reading (Mass.) Menlo Park (Calif.) Paris [etc.]: Addison-Wesley publ, 1995. ISBN: 978-0-201-50397-5.

[72] U. Sarkar. *Particle and Astroparticle Physics*. Series in High Energy Physics, Cosmology, and Gravitation. New York: Taylor & Francis, 2008. ISBN: 978-1-58488-931-1.

[73] Matthew Dean Schwartz. *Quantum Field Theory and the Standard Model*. New York: Cambridge University Press, 2014. ISBN: 978-1-107-03473-0.

[74] Mark Thomson. *Modern Particle Physics*. Cambridge: Cambridge university press, 2013. ISBN: 978-1-107-03426-6.

[75] Erick J. Weinberg. *Classical Solutions in Quantum Field Theory: Solitons and Instantons in High Energy Physics*. Cambridge Monographs on Mathematical Physics. Cambridge: Cambridge University Press, 2012. ISBN: 978-0-521-11463-9 978-1-139-57217-0.

[76] Nicola Cabibbo. "Unitary Symmetry and Leptonic Decays". In: *Physical Review Letters* 10.12 (June 1963), pp. 531–533. DOI: 10.1103/PhysRevLett.10.531.

[77] Makoto Kobayashi and Toshihide Maskawa. "C P -Violation in the Renormalizable Theory of Weak Interaction". In: *Progress of Theoretical Physics* 49.2 (Feb. 1973), pp. 652–657. DOI: 10.1143/PTP.49.652.

[78] C. Jarlskog. "Commutator of the Quark Mass Matrices in the Standard Electroweak Model and a Measure of Maximal CP Nonconservation". In: *Physical Review Letters* 55.10 (Sept. 1985), pp. 1039–1042. DOI: 10.1103/PhysRevLett.55.1039.

[79] A. Barroso et al. "Metastability Bounds on the Two Higgs Doublet Model". In: *Journal of High Energy Physics* 2013.6 (June 2013), p. 45. DOI: 10.1007/JHEP06(2013)045. arXiv: 1303.5098 [hep-ph].

[80] Jérémy Bernon et al. "Scrutinizing the Alignment Limit in Two-Higgs-Doublet Models. Part 1: $m_h = 125$ GeV". In: *Physical Review D* 93.3 (Feb. 2016), p. 035027. DOI: 10.1103/PhysRevD.93.035027. arXiv: 1507.00933 [hep-ph].

[81] Gautam Bhattacharyya and Dipankar Das. "Scalar Sector of Two-Higgs-Doublet Models: A Mini-Review". In: *Pramana* 87.3 (Sept. 2016), p. 40. DOI: 10.1007/s12043-016-1252-4. arXiv: 1507.06424 [hep-ph].

[82] G. C. Branco et al. "Theory and Phenomenology of Two-Higgs-doublet Models". In: *Phys. Rept.* 516 (2012), pp. 1–102. DOI: 10.1016/j.physrep.2012.02.002.

[83] Indrani Chakraborty and Anirban Kundu. *On the Scalar Potential of Two-Higgs Doublet Models*. Dec. 2015. DOI: 10.1103/PhysRevD.92.095023. arXiv: 1508.00702 [hep-ph].

[84] Lei Wang, Jin Min Yang, and Yang Zhang. *Two-Higgs-doublet Models in Light of Current Experiments: A Brief Review*. Apr. 2023. DOI: 10.1088/1572-9494/ac7fe9. arXiv: 2203.07244 [hep-ph].

[85] I. F. Ginzburg and K. A. Kanishev. "Different Vacua in 2HDM". In: *Physical Review D* 76.9 (Nov. 2007), p. 095013. DOI: 10.1103/PhysRevD.76.095013. arXiv: 0704.3664 [hep-ph].

[86] K. G. Klimenko. "On Necessary and Sufficient Conditions for Some Higgs Potentials to Be Bounded From Below". In: *Theor. Math. Phys.* 62 (1985), pp. 58–65. DOI: 10.1007/BF01034825.

[87] Lars Bergström and Ariel Goobar. *Cosmology and Particle Astrophysics*. 2. ed., reprinted. Springer Praxis Books in Astronomy and Planetary Science. Chichester, UK: Praxis Publ, 2008. ISBN: 978-3-540-32924-4.

[88] Scott Dodelson. *Modern Cosmology*. San Diego, Calif: Academic Press, 2003. ISBN: 978-0-12-219141-1.

[89] Edward Kolb. *The Early Universe*. Ed. by Edward W. Kolb and Michael S. Turner. 1st ed. CRC Press, Mar. 2018. ISBN: 978-0-429-49286-0. DOI: 10.1201/9780429492860.

[90] V. A. Rubakov. "Cosmology". In: *CERN Yellow Reports: School Proceedings* (July 2017), 239 Pages. DOI: 10.23730/CYRSP-2017-002.239.

[91] Mark Trodden and Sean M. Carroll. *TASI Lectures: Introduction to Cosmology*. Jan. 2004. arXiv: astro-ph/0401547.

[92] Alex Vilenkin and E. P. S. Shellard. *Cosmic Strings and Other Topological Defects*. Reprint. Cambridge Monographs on Mathematical Physics. Cambridge [u.a.]: Cambridge Univ. Press, 2001. ISBN: 978-0-521-65476-0 978-0-521-39153-5.

[93] Cosimo Bambi and Alexandre D. Dolgov. *Introduction to Particle Cosmology: The Standard Model of Cosmology and Its Open Problems*. UNITEXT for Physics. Berlin, Heidelberg: Springer, 2016. ISBN: 978-3-662-48077-9 978-3-662-48078-6. DOI: 10.1007/978-3-662-48078-6.

[94] G. F. Giudice et al. "Towards a Complete Theory of Thermal Leptogenesis in the SM and MSSM". In: *Nucl. Phys. B* 685 (2004), pp. 89–149. DOI: 10.1016/j.nuclphysb.2004.02.019.

[95] Alejandro Gangui. *Topological Defects in Cosmology*. Oct. 2001. arXiv: astro-ph/0110285.

[96] R. Rajaraman. *Solitons and Instantons: An Introduction to Solitons and Instantons in Quantum Field Theory*. North-Holland Personal Library. Amsterdam [etc.]: North-Holland, 1989. ISBN: 978-0-444-87047-6.

[97] Tanmay Vachaspati. *Kinks and Domain Walls: An Introduction to Classical and Quantum Solitons*. Cambridge: Cambridge University Press, 2006. ISBN: 978-0-521-83605-0 978-0-511-24657-9 978-0-511-24588-6.

[98] Tanmay Vachaspati. *Lectures on Cosmic Topological Defects*. Feb. 2001. arXiv: hep-ph/0101270.

[99] A. Vilenkin. "Gravitational Field of Vacuum Domain Walls and Strings". In: *Phys. Rev. D* 23 (1981), pp. 852–857. DOI: 10.1103/PhysRevD.23.852.

[100] T.W.B. Kibble. "Some Implications of a Cosmological Phase Transition". In: *Physics Reports* 67.1 (Dec. 1980), pp. 183–199. DOI: 10.1016/0370-1573(80)90091-5.

[101] T W B Kibble. "Topology of Cosmic Domains and Strings". In: *Journal of Physics A: Mathematical and General* 9.8 (Aug. 1976), pp. 1387–1398. DOI: 10.1088/0305-4470/9/8/029.

[102] Csaba Csáki et al. *Instanton NDA and Applications to Axion Models*. May 2024. arXiv: 2311.09285 [hep-ph].

[103] Anson Hook. *TASI Lectures on the Strong CP Problem and Axions*. Nov. 2023. arXiv: 1812.02669 [hep-ph].

[104] Masahiro Kawasaki and Kazunori Nakayama. "Axions : Theory and Cosmological Role". In: *Annual Review of Nuclear and Particle Science* 63.1 (Oct. 2013), pp. 69–95. DOI: 10.1146/annurev-nucl-102212-170536. arXiv: 1301.1123 [hep-ph].

[105] Jihn E. Kim. "Light Pseudoscalars, Particle Physics and Cosmology". In: *Physics Reports* 150.1-2 (June 1987), pp. 1–177. DOI: 10.1016/0370-1573(87)90017-2.

[106] Markus Kuster, Berta Beltrán, and Georg Raffelt, eds. *Axions: Theory, Cosmology, and Experimental Searches*. SpringerLink Bücher. Berlin, Heidelberg: Springer Berlin Heidelberg, 2008. ISBN: 978-3-540-73517-5 978-3-540-73518-2. DOI: 10.1007/978-3-540-73518-2.

[107] David J. E. Marsh. "Axion Cosmology". In: *Physics Reports* 643 (July 2016), pp. 1–79. DOI: 10.1016/j.physrep.2016.06.005. arXiv: 1510.07633 [astro-ph].

[108] Jérémie Quevillon and Christopher Smith. "Axions Are Blind to Anomalies". In: *The European Physical Journal C* 79.10 (Oct. 2019), p. 822. DOI: 10.1140/epjc/s10052-019-7304-4. arXiv: 1903.12559 [hep-ph].

[109] Pierre Sikivie. "Axion Cosmology". In: vol. 741. 2008, pp. 19–50. DOI: 10.1007/978-3-540-73518-2_2. arXiv: astro-ph/0610440.

[110] P. Sikivie. "Axions, Domain Walls, and the Early Universe". In: *Physical Review Letters* 48.17 (Apr. 1982), pp. 1156–1159. DOI: 10.1103/PhysRevLett.48.1156.

[111] Alexander Vilenkin and Allen E. Everett. "Cosmic Strings and Domain Walls in Models with Goldstone and Pseudo-Goldstone Bosons". In: *Physical Review Letters* 48.26 (June 1982), pp. 1867–1870. DOI: 10.1103/PhysRevLett.48.1867.

[112] Ia. B. Zeldovich, I. Iu. Kobzarev, and L. B. Okun. "Cosmological Consequences of a Spontaneous Breakdown of a Discrete Symmetry". In: *Zhurnal Eksperimentalnoi i Teoreticheskoi Fiziki* 67 (Jan. 1975), pp. 3–11.

[113] D. J. Fixsen. "The Temperature of the Cosmic Microwave Background". In: *The Astrophysical Journal* 707.2 (Dec. 2009), pp. 916–920. DOI: 10.1088/0004-637X/707/2/916. arXiv: 0911.1955 [astro-ph].

[114] Wayne Hu and Scott Dodelson. "Cosmic Microwave Background Anisotropies". In: *Annual Review of Astronomy and Astrophysics* 40.1 (Sept. 2002), pp. 171–216. DOI: 10.1146/annurev.astro.40.060401.093926. arXiv: astro-ph/0110414.

[115] Vera C. Rubin and W. Kent Ford Jr. "Rotation of the Andromeda Nebula from a Spectroscopic Survey of Emission Regions". In: *The Astrophysical Journal* 159 (Feb. 1970), p. 379. DOI: 10.1086/150317.

[116] Hong-Yee Chiu. "Symmetry Between Particle and Antiparticle Populations in the Universe". In: *Physical Review Letters* 17.13 (Sept. 1966), pp. 712–714. DOI: 10.1103/PhysRevLett.17.712.

[117] Ya.B. Zeldovic, L.B. Okun, and S.B. Pikelner. "Quarks, Astrophysical and Physico-Chemical Aspects". In: *Physics Letters* 17.2 (July 1965), pp. 164–166. DOI: 10.1016/0031-9163(65)90284-2.

[118] Ya. B. Zel'dovich. "The Hypothesis of Cosmological Magnetic Inhomogeneity." In: *Soviet Astronomy* 13 (Feb. 1970), p. 608.

[119] A. Arbey and F. Mahmoudi. "Dark Matter and the Early Universe: A Review". In: *Progress in Particle and Nuclear Physics* 119 (July 2021), p. 103865. DOI: 10.1016/j.ppnp.2021.103865. arXiv: 2104.11488 [hep-ph].

[120] L. Bergstrom. "Non-Baryonic Dark Matter - Observational Evidence and Detection Methods". In: *Reports on Progress in Physics* 63.5 (May 2000), pp. 793–841. DOI: 10.1088/0034-4885/63/5/2r3. arXiv: hep-ph/0002126.

[121] Gianfranco Bertone, Dan Hooper, and Joseph Silk. "Particle Dark Matter: Evidence, Candidates and Constraints". In: *Physics Reports* 405 (Jan. 2005), pp. 279–390. DOI: 10.1016/j.physrep.2004.08.031.

[122] Keith A. Olive. *TASI Lectures on Dark Matter*. Jan. 2003. arXiv: astro-ph/0301505.

[123] M. Sajjad Athar et al. "Status and Perspectives of Neutrino Physics". In: *Progress in Particle and Nuclear Physics* 124 (May 2022), p. 103947. DOI: 10.1016/j.ppnp.2022.103947. arXiv: 2111.07586 [hep-ph].

[124] Ziro Maki, Masami Nakagawa, and Shoichi Sakata. "Remarks on the Unified Model of Elementary Particles". In: *Progress of Theoretical Physics* 28.5 (Nov. 1962), pp. 870–880. DOI: 10.1143/PTP.28.870.

[125] Bruno Pontecorvo. "Inverse Beta Processes and Nonconservation of Lepton Charge". In: *Zh.Eksp.Teor.Fiz.* 34.247 (1957).

[126] Ivan Esteban et al. "NuFit-6.0: Updated Global Analysis of Three-Flavor Neutrino Oscillations". In: *Journal of High Energy Physics* 2024.12 (Dec. 2024), p. 216. DOI: 10.1007/JHEP12(2024)216. arXiv: 2410.05380 [hep-ph].

[127] M. Aker et al. "Direct Neutrino-Mass Measurement with Sub-Electronvolt Sensitivity". In: *Nature Phys.* 18.2 (2022), pp. 160–166. DOI: 10.1038/s41567-021-01463-1.

[128] GERDA collaboration et al. "Final Results of GERDA on the Search for Neutrinoless Double- β Decay". In: *Physical Review Letters* 125.25 (Dec. 2020), p. 252502. DOI: 10.1103/PhysRevLett.125.252502. arXiv: 2009.06079 [nucl-ex].

[129] Steven Weinberg. "Baryon- and Lepton-Nonconserving Processes". In: *Physical Review Letters* 43.21 (Nov. 1979), pp. 1566–1570. DOI: 10.1103/PhysRevLett.43.1566.

[130] T. P. Cheng and Ling-Fong Li. "Neutrino Masses, Mixings, and Oscillations in SU(2)×U(1) Models of Electroweak Interactions". In: *Physical Review D* 22.11 (Dec. 1980), pp. 2860–2868. DOI: 10.1103/PhysRevD.22.2860.

[131] W. Konetschny and W. Kummer. "Nonconservation of Total Lepton Number with Scalar Bosons". In: *Physics Letters B* 70.4 (Oct. 1977), pp. 433–435. DOI: 10.1016/0370-2693(77)90407-5.

[132] Rabindra N. Mohapatra and Goran Senjanović. "Neutrino Masses and Mixings in Gauge Models with Spontaneous Parity Violation". In: *Physical Review D* 23.1 (Jan. 1981), pp. 165–180. DOI: 10.1103/PhysRevD.23.165.

[133] J. Schechter and J. W. F. Valle. "Neutrino Masses in SU(2) ⊗ $U(1)$ Theories". In: *Physical Review D* 22.9 (Nov. 1980), pp. 2227–2235. DOI: 10.1103/PhysRevD.22.2227.

[134] G. Lazarides, Q. Shafi, and C. Wetterich. "Proton Lifetime and Fermion Masses in an SO(10) Model". In: *Nuclear Physics B* 181.2 (Apr. 1981), pp. 287–300. DOI: 10.1016/0550-3213(81)90354-0.

[135] R. Foot et al. "See-Saw Neutrino Masses Induced by a Triplet of Leptons". In: *Zeitschrift für Physik C Particles and Fields* 44.3 (Sept. 1989), pp. 441–444. DOI: 10.1007/BF01415558.

[136] E. Kh Akhmedov. *Neutrino Physics*. Jan. 2000. arXiv: hep-ph/0001264.

[137] Pasquale Di Bari. "An Introduction to Leptogenesis and Neutrino Properties". In: *Contemporary Physics* 53.4 (July 2012), pp. 315–338. DOI: 10.1080/00107514.2012.701096. arXiv: 1206.3168 [hep-ph].

[138] Carlo Giunti and Chung-Wook Kim. *Fundamentals of Neutrino Physics and Astrophysics*. Oxford: Oxford university press, 2007. ISBN: 978-0-19-850871-7.

[139] Alessandro Granelli. "Standard and Non-Standard Aspects of Neutrino Physics". In: *Universe* 10.4 (Mar. 2024), p. 164. DOI: 10.3390/universe10040164. arXiv: 2403.16308 [hep-ph].

[140] S. Pascoli. "Neutrino Physics". In: *CERN Yellow Reports: School Proceedings* Vol 6 (Nov. 2019), 213 Pages. DOI: 10.23730/CYRSP-2019-006.213.

[141] Yi Cai et al. *Lepton Number Violation: Seesaw Models and Their Collider Tests*. May 2018. arXiv: 1711.02180 [hep-ph].

[142] Yu Cheng et al. "Electroweak Precision Tests for Triplet Scalars". In: *Nuclear Physics B* 989 (Apr. 2023), p. 116118. DOI: 10.1016/j.nuclphysb.2023.116118. arXiv: 2208.06760 [hep-ph].

[143] Thomas Hambye, Martti Raidal, and Alessandro Strumia. "Efficiency and Maximal CP-asymmetry of Scalar Triplet Leptogenesis". In: *Physics Letters B* 632.5-6 (Jan. 2006), pp. 667–674. DOI: 10.1016/j.physletb.2005.11.007. arXiv: hep-ph/0510008.

[144] R. Primulando, J. Julio, and P. Uttayarat. "Scalar Phenomenology in Type-II Seesaw Model". In: *Journal of High Energy Physics* 2019.8 (Aug. 2019), p. 24. DOI: 10.1007/JHEP08(2019)024. arXiv: 1903.02493 [hep-ph].

[145] D. Aristizabal Sierra, Mikael Dhen, and Thomas Hambye. "Scalar Triplet Flavored Leptogenesis: A Systematic Approach". In: *Journal of Cosmology and Astroparticle Physics* 2014.08 (Aug. 2014), pp. 003–003. DOI: 10.1088/1475-7516/2014/08/003. arXiv: 1401.4347 [hep-ph].

[146] A. Abada et al. "$\mu \to e\gamma$ and $\tau \to \ell\gamma$ Decays in the Fermion Triplet Seesaw Model". In: *Physical Review D* 78.3 (Aug. 2008), p. 033007. DOI: 10.1103/PhysRevD.78.033007. arXiv: 0803.0481 [hep-ph].

[147] Abdesslam Arhrib et al. "Collider Signatures for the Heavy Lepton Triplet in the Type I + III Seesaw Mechanism". In: *Physical Review D* 82.5 (Sept. 2010), p. 053004. DOI: 10.1103/PhysRevD.82.053004.

[148] D. Aristizabal Sierra, Jernej F. Kamenik, and Miha Nemevsek. "Implications of Flavor Dynamics for Fermion Triplet Leptogenesis". In: *JHEP* 10 (2010), p. 036. DOI: 10.1007/JHEP10(2010)036.

[149] Roberto Franceschini, Thomas Hambye, and Alessandro Strumia. "Type-III See-Saw at LHC". In: *Physical Review D* 78.3 (Aug. 2008), p. 033002. DOI: 10.1103/PhysRevD.78.033002. arXiv: 0805.1613 [hep-ph].

[150] Tong Li and Xiao-Gang He. "Neutrino Masses and Heavy Triplet Leptons at the LHC: Testability of the Type III Seesaw Mechanism". In: *Physical Review D* 80.9 (Nov. 2009), p. 093003. DOI: 10.1103/PhysRevD.80.093003.

[151] Edison T. Franco. "Type I+III Seesaw Mechanism and CP Violation for Leptogenesis". In: *Physical Review D* 92.11 (Dec. 2015), p. 113010. DOI: 10.1103/PhysRevD.92.113010. arXiv: 1510.06240 [hep-ph].

[152] Pei-Hong Gu. "A Left-Right Symmetric Model with SU(2)-Triplet Fermions". In: *Physical Review D* 84.9 (Nov. 2011), p. 097301. DOI: 10.1103/PhysRevD.84.097301. arXiv: 1110.6049 [hep-ph].

[153] S. Navas et al. "Review of Particle Physics". In: *Phys. Rev. D* 110.3 (2024), p. 030001. DOI: 10.1103/PhysRevD.110.030001.

[154] Mu-Chun Chen. *TASI 2006 Lectures on Leptogenesis*. Apr. 2007. arXiv: hep-ph/0703087.

[155] Sacha Davidson, Enrico Nardi, and Yosef Nir. "Leptogenesis". In: *Physics Reports* 466.4-5 (Sept. 2008), pp. 105–177. DOI: 10.1016/j.physrep.2008.06.002. arXiv: 0802.2962 [hep-ph].

[156] Chee Sheng Fong, Enrico Nardi, and Antonio Riotto. "Leptogenesis in the Universe". In: *Advances in High Energy Physics* 2012 (2012), pp. 1–59. DOI: 10.1155/2012/158303. arXiv: 1301.3062 [hep-ph].

[157] Antonio Riotto. *Theories of Baryogenesis*. July 1998. arXiv: hep-ph/9807454.

[158] Alessandro Strumia. *Baryogenesis via Leptogenesis*. Aug. 2006. arXiv: hep-ph/0608347.

[159] C.G. Callan, R.F. Dashen, and D.J. Gross. "The Structure of the Gauge Theory Vacuum". In: *Physics Letters B* 63.3 (Aug. 1976), pp. 334–340. DOI: 10.1016/0370-2693(76)90277-X.

[160] Curtis G. Callan, Roger Dashen, and David J. Gross. "Toward a Theory of the Strong Interactions". In: *Physical Review D* 17.10 (May 1978), pp. 2717–2763. DOI: 10.1103/PhysRevD.17.2717.

[161] Sidney Coleman. "The Uses of Instantons". In: *Subnucl. Ser.* 15 (1979), p. 805.

[162] R. Jackiw and C. Rebbi. "Vacuum Periodicity in a Yang-Mills Quantum Theory". In: *Physical Review Letters* 37.3 (July 1976), pp. 172–175. DOI: 10.1103/PhysRevLett.37.172.

[163] A I Vaĭnshteĭn et al. "ABC of Instantons". In: *Soviet Physics Uspekhi* 25.4 (Apr. 1982), pp. 195–215. DOI: 10.1070/PU1982v025n04ABEH004533.

[164] Mikhail Shifman. *Advanced Topics in Quantum Field Theory: A Lecture Course*. Cambridge: Cambridge University Press, 2012. ISBN: 978-1-139-01335-2 978-1-139-22341-6.

[165] C. Abel et al. "Measurement of the Permanent Electric Dipole Moment of the Neutron". In: *Physical Review Letters* 124.8 (Feb. 2020), p. 081803. DOI: 10.1103/PhysRevLett.124.081803.

[166] Stephen L. Adler. "Axial-Vector Vertex in Spinor Electrodynamics". In: *Physical Review* 177.5 (Jan. 1969), pp. 2426–2438. DOI: 10.1103/PhysRev.177.2426.

[167] J. S. Bell and R. Jackiw. "A PCAC Puzzle: $\Pi^0 \to \gamma\gamma$ in the σ-Model". In: *Il Nuovo Cimento A* 60.1 (Mar. 1969), pp. 47–61. DOI: 10.1007/BF02823296.

[168] Kazuo Fujikawa. "Path-Integral Measure for Gauge-Invariant Fermion Theories". In: *Physical Review Letters* 42.18 (Apr. 1979), pp. 1195–1198. DOI: 10.1103/PhysRevLett.42.1195.

[169] Pavel Fileviez Pérez and Hiren H. Patel. "The Electroweak Vacuum Angle". In: *Physics Letters B* 732 (May 2014), pp. 241–243. DOI: 10.1016/j.physletb.2014.03.064.

[170] Andrew J. Long, Hiren H. Patel, and Mark Trodden. "The Electroweak Vacuum Angle at Finite Temperature and Implications for Baryogenesis". In: *Physical Review D* 92.4 (Aug. 2015), p. 043513. DOI: 10.1103/PhysRevD.92.043513. arXiv: 1507.00654 [hep-ph].

[171] G. 'T Hooft. "Symmetry Breaking through Bell-Jackiw Anomalies". In: *Physical Review Letters* 37.1 (July 1976), pp. 8–11. DOI: 10.1103/PhysRevLett.37.8.

[172] Michela D'Onofrio, Kari Rummukainen, and Anders Tranberg. "The Sphaleron Rate in the Minimal Standard Model". In: *Physical Review Letters* 113.14 (Oct. 2014), p. 141602. DOI: 10.1103/PhysRevLett.113.141602. arXiv: 1404.3565 [hep-ph].

[173] A Dolgov. "Non-GUT Baryogenesis". In: *Physics Reports* 222.6 (Dec. 1992), pp. 309–386. DOI: 10.1016/0370-1573(92)90107-B.

[174] Jeffrey A. Harvey and Michael S. Turner. "Cosmological Baryon and Lepton Number in the Presence of Electroweak Fermion-Number Violation". In: *Physical Review D* 42.10 (Nov. 1990), pp. 3344–3349. DOI: 10.1103/PhysRevD.42.3344.

[175] Edward W. Kolb and Stephen Wolfram. "Baryon Number Generation in the Early Universe". In: *Nucl. Phys. B* 172 (1980), p. 224. DOI: 10.1016/0550-3213(82)90012-8.

[176] V. A. Rubakov and M. E. Shaposhnikov. "Electroweak Baryon Number Non-Conservation in the Early Universe and in High Energy Collisions". In: *Physics-Uspekhi* 39.5 (May 1996), pp. 461–502. DOI: 10.1070/PU1996v039n05ABEH000145. arXiv: hep-ph/9603208.

[177] S. Yu. Khlebnikov and M. E. Shaposhnikov. "The Statistical Theory of Anomalous Fermion Number Nonconservation". In: *Nucl. Phys. B* 308 (1988), pp. 885–912. DOI: 10.1016/0550-3213(88)90133-2.

[178] Steve Blanchet and Pasquale Di Bari. "The Minimal Scenario of Leptogenesis". In: *New Journal of Physics* 14.12 (Dec. 2012), p. 125012. DOI: 10.1088/1367-2630/14/12/125012. arXiv: 1211.0512 [hep-ph].

[179] W. Buchmüller, P. Di Bari, and M. Plümacher. "Leptogenesis for Pedestrians". In: *Annals Phys.* 315 (2005), pp. 305–351. DOI: 10.1016/j.aop.2004.02.003.

[180] Michael Plümacher. "Baryogenesis and Lepton Number Violation". In: *Z. Phys. C* 74 (1997), pp. 549–559. DOI: 10.1007/s002880050418.

[181] Laura Covi, Esteban Roulet, and Francesco Vissani. "CP Violating Decays in Leptogenesis Scenarios". In: *Phys. Lett. B* 384 (1996), pp. 169–174. DOI: 10.1016/0370-2693(96)00817-9.

[182] Sacha Davidson and Alejandro Ibarra. "A Lower Bound on the Right-Handed Neutrino Mass from Leptogenesis". In: *Phys. Lett. B* 535 (2002), pp. 25–32. DOI: 10.1016/S0370-2693(02)01735-5.

[183] Thomas Hambye et al. "Constraints on Neutrino Masses from Leptogenesis Models". In: *Nucl. Phys. B* 695 (2004), pp. 169–191. DOI: 10.1016/j.nuclphysb.2004.06.027.

[184] Apostolos Pilaftsis and Thomas E. J. Underwood. "Resonant Leptogenesis". In: *Nuclear Physics B* 692.3 (Aug. 2004), pp. 303–345. DOI: 10.1016/j.nuclphysb.2004.05.029. arXiv: hep-ph/0309342.

[185] Riccardo Barbieri et al. "Baryogenesis through Leptogenesis". In: *Nucl. Phys. B* 575 (2000), pp. 61–77. DOI: 10.1016/S0550-3213(00)00011-0.

[186] Alejandro Ibarra. "Leptogenesis from Heavy Right-Handed Neutrino Decay". In: *Indian Journal of Physics* 97.11 (Sept. 2023), pp. 3287–3299. DOI: 10.1007/s12648-023-02648-5.

[187] Thomas Hambye. "Leptogenesis: Beyond the Minimal Type I Seesaw Scenario". In: *New J. Phys.* 14 (2012), p. 125014. DOI: 10.1088/1367-2630/14/12/125014.

[188] D. Aristizabal Sierra and I. de Medeiros Varzielas. "The Role of Lepton Flavor Symmetries in Leptogenesis". In: *Fortsch. Phys.* 61 (2013), pp. 645–665. DOI: 10.1002/prop.201200122.

[189] Fred Jegerlehner. *The Anomalous Magnetic Moment of the Muon*. 2nd ed. Springer Tracts in Modern Physics Ser v.274. Cham: Springer International Publishing AG, 2017. ISBN: 978-3-319-63577-4.

[190] Fred Jegerlehner and Andreas Nyffeler. "The Muon G-2". In: *Physics Reports* 477.1-3 (June 2009), pp. 1–110. DOI: 10.1016/j.physrep.2009.04.003. arXiv: 0902.3360 [hep-ph].

[191] Marc Knecht. *The Anomalous Magnetic Moment of the Muon: A Theoretical Introduction*. Vol. 629. 2004. DOI: 10.1007/b98411. arXiv: hep-ph/0307239.

[192] Michel Davier et al. "Reevaluation of the Hadronic Vacuum Polarisation Contributions to the Standard Model Predictions of the Muon G-2 and $\alpha(m_Z^2)$ Using Newest Hadronic Cross-Section Data". In: *Eur. Phys. J. C* 77.12 (2017), p. 827. DOI: 10.1140/epjc/s10052-017-5161-6.

[193] D. P. Aguillard et al. "Measurement of the Positive Muon Anomalous Magnetic Moment to 127 ppb". In: (June 2025). arXiv: 2506.03069 [hep-ex].

[194] R. Aliberti et al. "The anomalous magnetic moment of the muon in the Standard Model: an update". In: (May 2025). arXiv: 2505.21476 [hep-ph].

[195] Peter Athron et al. "New Physics Explanations of A_μ in Light of the FNAL Muon g-2 Measurement". In: *JHEP* 09 (2021), p. 080. DOI: 10.1007/JHEP09(2021)080.

[196] Dominik Stöckinger and Hyejung Stöckinger-Kim. "On the Role of Chirality Flips for the Muon Magnetic Moment and Its Relation to the Muon Mass". In: *Frontiers in Physics* 10 (Aug. 2022), p. 944614. DOI: 10.3389/fphy.2022.944614.

[197] Andrzej Czarnecki and William J. Marciano. "The Muon Anomalous Magnetic Moment: A Harbinger For "New Physics"". In: *Physical Review D* 64.1 (June 2001), p. 013014. DOI: 10.1103/PhysRevD.64.013014. arXiv: hep-ph/0102122.

[198] Julian Heeck and Hiren H. Patel. "The Majoron at Two Loops". In: *Physical Review D* 100.9 (Nov. 2019), p. 095015. DOI: 10.1103/PhysRevD.100.095015. arXiv: 1909.02029 [hep-ph].

[199] George Lazarides et al. "Spontaneous Breaking of Lepton Number and the Cosmological Domain Wall Problem". In: *Phys. Rev. Lett.* 122.15 (2019), p. 151301. DOI: 10.1103/PhysRevLett.122.151301.

[200] G. B. Gelmini and M. Roncadelli. "Left-Handed Neutrino Mass Scale and Spontaneously Broken Lepton Number". In: *Phys. Lett. B* 99 (1981), pp. 411–415. DOI: 10.1016/0370-2693(81)90559-1.

[201] Camilo Garcia-Cely and Julian Heeck. "Neutrino Lines from Majoron Dark Matter". In: *Journal of High Energy Physics* 2017.5 (May 2017), p. 102. DOI: 10.1007/JHEP05(2017)102. arXiv: 1701.07209 [hep-ph].

[202] Apostolos Pilaftsis. "Astrophysical and Terrestrial Constraints on Singlet Majoron Models". In: *Physical Review D* 49.5 (Mar. 1994), pp. 2398–2404. DOI: 10.1103/PhysRevD.49.2398. arXiv: hep-ph/9308258.

[203] J. A. Casas and A. Ibarra. "Oscillating Neutrinos and $\mu \to e, \gamma$". In: *Nuclear Physics B* 618.1-2 (Dec. 2001), pp. 171–204. DOI: 10.1016/S0550-3213(01)00475-8. arXiv: hep-ph/0103065.

[204] Lucien Heurtier and Yongchao Zhang. "Supernova Constraints on Massive (Pseudo)Scalar Coupling to Neutrinos". In: *Journal of Cosmology and Astroparticle Physics* 2017.02 (Feb. 2017), pp. 042–042. DOI: 10.1088/1475-7516/2017/02/042. arXiv: 1609.05882 [hep-ph].

[205] Kfir Blum, Yosef Nir, and Michal Shavit. "Neutrinoless Double-Beta Decay with Massive Scalar Emission". In: *Physics Letters B* 785 (Oct. 2018), pp. 354–361. DOI: 10.1016/j.physletb.2018.08.022. arXiv: 1802.08019 [hep-ph].

[206] E. N. Alekseev et al. "Possible Detection of a Neutrino Signal on February 23, 1987 with the Baksan Underground Scintillation Telescope of the Nuclear Research Institute of the Soviet Academy of Sciences". In: *Pisma v Zhurnal Eksperimentalnoi i Teoreticheskoi Fiziki* 45 (May 1987), pp. 461–464.

[207] E. N. Alekseev et al. "Properties of the Supernova 1987A Neutrino Signal Recorded by the Baksan Underground Scintillation Telescope". In: *Soviet Astronomy Letters* 14 (Feb. 1988), p. 41.

[208] R. M. Bionta et al. "Observation of a Neutrino Burst in Coincidence with Supernova 1987A in the Large Magellanic Cloud". In: *Physical Review Letters* 58 (Apr. 1987), pp. 1494–1496. DOI: 10.1103/PhysRevLett.58.1494.

[209] K. Hirata et al. "Observation of a Neutrino Burst from the Supernova SN1987A". In: *Physical Review Letters* 58.14 (Apr. 1987), pp. 1490–1493. DOI: 10.1103/PhysRevLett.58.1490.

[210] K. S. Hirata et al. "Observation in the Kamiokande-II Detector of the Neutrino Burst from Supernova SN1987A". In: *Physical Review D* 38.2 (July 1988), pp. 448–458. DOI: 10.1103/PhysRevD.38.448.

[211] NEMO-3 Collaboration et al. "Search for Neutrinoless Double-Beta Decay of $_{100}Mo$ with the NEMO-3 Detector". In: *Physical Review D* 89.11 (June 2014), p. 111101. DOI: 10.1103/PhysRevD.89.111101. arXiv: 1311.5695 [hep-ex].

[212] M. Doi, T. Kotani, and E. Takasugi. "Neutrinoless Double-Beta Decay with Majoron Emission". In: *Physical Review D* 37.9 (May 1988), pp. 2575–2589. DOI: 10.1103/PhysRevD.37.2575.

[213] GERDA Collaboration et al. "Results on $\beta\beta$ Decay with Emission of Two Neutrinos or Majorons in $_{76}Ge$ from GERDA Phase I: GERDA Collaboration". In: *The European Physical Journal C* 75.9 (Sept. 2015), p. 416. DOI: 10.1140/epjc/s10052-015-3627-y.

[214] A.A. Anselm and A.A. Johansen. "Baryon Nonconservation in Standard Model and Yukawa Interaction". In: *Nuclear Physics B* 407.2 (Oct. 1993), pp. 313–327. DOI: 10.1016/0550-3213(93)90060-3.

[215] A. A. Anselm and A. A. Johansen. "Can Electro-Weak θ-Term Be Observable ?" In: *Nuclear Physics B* 412.3 (Jan. 1994), pp. 553–573. DOI: 10.1016/0550-3213(94)90392-1. arXiv: hep-ph/9305271.

[216] Maximilian Berbig. "About electroweak domain walls in Majoron models". In: (June 2025). arXiv: 2506.02910 [hep-ph].

[217] Georges Aad et al. "Search for Type-III Seesaw Heavy Leptons in Leptonic Final States in Pp Collisions at $\sqrt{s} = 13$TeV with the ATLAS Detector". In: *Eur. Phys. J. C* 82.11 (2022), p. 988. DOI: 10.1140/epjc/s10052-022-10785-0.

[218] Albert M Sirunyan et al. "Search for Evidence of the Type-III Seesaw Mechanism in Multilepton Final States in Proton-Proton Collisions at $\sqrt{s} = 13$TeV". In: *Phys. Rev. Lett.* 119.22 (2017), p. 221802. DOI: 10.1103/PhysRevLett.119.221802.

[219] T. W. Kephart and H. Päs. "Muon Anomalous Magnetic Moment in String Inspired Extended Family Models". In: *Phys. Rev. D* 65 (2002), p. 093014. DOI: 10.1103/PhysRevD.65.093014.

[220] Andreas Crivellin, Martin Hoferichter, and Philipp Schmidt-Wellenburg. "Combined Explanations of $g-2_{\mu,e}$ and Implications for a Large Muon EDM". In: *Phys. Rev. D* 98.11 (2018), p. 113002. DOI: 10.1103/PhysRevD.98.113002.

[221] Andreas Crivellin and Martin Hoferichter. "Consequences of Chirally Enhanced Explanations of $(g-2)_\mu$ for $h \to \mu\mu$ and $Z \to \mu\mu$". In: *JHEP* 07 (2021), p. 135. DOI: 10.1007/JHEP07(2021)135.

[222] Giorgio Arcadi et al. "Comparing 2HDM + Scalar and Pseudoscalar Simplified Models at LHC". In: *Journal of High Energy Physics* 2020.6 (June 2020), p. 98. DOI: 10.1007/JHEP06(2020)098. arXiv: 2001.10540 [hep-ph].

[223] Nicole F. Bell, Giorgio Busoni, and Isaac W. Sanderson. "Self-Consistent Dark Matter Simplified Models with an s-Channel Scalar Mediator". In: *Journal of Cosmology and Astroparticle Physics* 2017.03 (Mar. 2017), pp. 015–015. DOI: 10.1088/1475-7516/2017/03/015. arXiv: 1612.03475 [hep-ph].

[224] Adam Falkowski, David M. Straub, and Avelino Vicente. "Vector-like Leptons: Higgs Decays and Collider Phenomenology". In: *Journal of High Energy Physics* 2014.5 (May 2014), p. 92. DOI: 10.1007/JHEP05(2014)092. arXiv: 1312.5329 [hep-ph].

[225] Albert M Sirunyan et al. "Evidence for Higgs Boson Decay to a Pair of Muons". In: *JHEP* 01 (2021), p. 148. DOI: 10.1007/JHEP01(2021)148.

[226] Albert M Sirunyan et al. "Measurements of Higgs Boson Production Cross Sections and Couplings in the Diphoton Decay Channel at $\sqrt{s} = 13$TeV". In: *JHEP* 07 (2021), p. 027. DOI: 10.1007/JHEP07(2021)027.

[227] Armen Tumasyan et al. "Search for Higgs boson decays to a Z boson and a photon in proton-proton collisions at $\sqrt{s} = 13$ TeV". In: *JHEP* 05 (2023), p. 233. DOI: 10.1007/JHEP05(2023)233. arXiv: 2204.12945 [hep-ex].

[228] A. M. Baldini et al. "Search for the Lepton Flavour Violating Decay $\mu^+ \to e\gamma$ with the Full Dataset of the MEG Experiment". In: *Eur. Phys. J. C* 76.8 (2016), p. 434. DOI: 10.1140/epjc/s10052-016-4271-x.

[229] Wilhelm H. Bertl et al. "A Search for Muon to Electron Conversion in Muonic Gold". In: *Eur. Phys. J. C* 47 (2006), pp. 337–346. DOI: 10.1140/epjc/s2006-02582-x.

[230] Bernard Aubert et al. "Searches for Lepton Flavor Violation in the Decays $\tau^\pm \to e^\pm\gamma$ and $\tau^\pm \to \mu^\pm\gamma$". In: *Phys. Rev. Lett.* 104 (2010), p. 021802. DOI: 10.1103/PhysRevLett.104.021802.

[231] P. Wintz. "Results of the SINDRUM-II Experiment". In: *Conf. Proc. C* 980420 (1998). Ed. by H. V. Klapdor-Kleingrothaus and I. V. Krivosheina, pp. 534–546.

[232] W. Bertl et al. "Search for the Decay $\mu^+ \to e^+e^+e^p$". In: *Nuclear Physics B* 260.1 (1985), pp. 1–31. DOI: 10.1016/0550-3213(85)90308-6.

[233] K. Hayasaka et al. "Search for Lepton Flavor Violating Tau Decays into Three Leptons with 719 Million Produced Tau+Tau- Pairs". In: *Phys. Lett. B* 687 (2010), pp. 139–143. DOI: 10.1016/j.physletb.2010.03.037.

[234] T. P. Cheng and Ling-Fong Li. "$\mu \to e\gamma$ in Theories With Dirac and Majorana Neutrino Mass Terms". In: *Phys. Rev. Lett.* 45 (1980), p. 1908. DOI: 10.1103/PhysRevLett.45.1908.

[235] A. Ilakovac and A. Pilaftsis. "Flavor Violating Charged Lepton Decays in Seesaw-Type Models". In: *Nucl. Phys. B* 437 (1995), p. 491. DOI: 10.1016/0550-3213(94)00567-X.

[236] R. Alonso et al. "Muon Conversion to Electron in Nuclei in Type-I Seesaw Models". In: *JHEP* 01 (2013), p. 118. DOI: 10.1007/JHEP01(2013)118.

[237] Stefan Bißmann et al. "Multi-Lepton Signatures of Vector-like Leptons with Flavor". In: *The European Physical Journal C* 81.2 (Feb. 2021), p. 101. DOI: 10.1140/epjc/s10052-021-08886-3. arXiv: 2011.12964 [hep-ph].

[238] Georges Aad et al. "Search for Third-Generation Vector-like Leptons in Pp Collisions at $\sqrt{s}$ = 13TeV with the ATLAS Detector". In: *JHEP* 07 (2023), p. 118. DOI: 10.1007/JHEP07(2023)118.

[239] Nilanjana Kumar and Stephen P. Martin. "Vectorlike Leptons at the Large Hadron Collider". In: *Phys. Rev. D* 92.11 (2015), p. 115018. DOI: 10.1103/PhysRevD.92.115018.

[240] Armen Tumasyan et al. "Search for Pair-Produced Vector-like Leptons in Final States with Third-Generation Leptons and at Least Three b Quark Jets in Proton-Proton Collisions at $\sqrt{s} = 13$TeV". In: *Phys. Lett. B* 846 (2023), p. 137713. DOI: 10.1016/j.physletb.2023.137713.

[241] Albert M Sirunyan et al. "Search for Vector-like Leptons in Multilepton Final States in Proton-Proton Collisions at $\sqrt{s}$ = 13TeV". In: *Phys. Rev. D* 100.5 (2019), p. 052003. DOI: 10.1103/PhysRevD.100.052003.

[242] Armen Tumasyan et al. "Inclusive Nonresonant Multilepton Probes of New Phenomena at $\sqrt{s}$ = 13TeV". In: *Phys. Rev. D* 105.11 (2022), p. 112007. DOI: 10.1103/PhysRevD.105.112007.

[243] Aram Hayrapetyan et al. "Review of Searches for Vector-like Quarks, Vector-like Leptons, and Heavy Neutral Leptons in Proton-Proton Collisions at $\sqrt{s} = 13$TeV at the CMS Experiment". In: (May 2024).

[244] P. Achard et al. "Search for Heavy Neutral and Charged Leptons in $e^+ + e^+$- Annihilation at LEP". In: *Phys. Lett. B* 517 (2001), pp. 75–85. DOI: 10.1016/S0370-2693(01)01005-X.

[245] Cesar Bonilla et al. "Collider Signatures of Vector-like Fermions from a Flavor Symmetric Model". In: *JHEP* 01 (2022), p. 154. DOI: 10.1007/JHEP01(2022)154.

[246] Palash B. Pal. "Dirac, Majorana and Weyl Fermions". In: *American Journal of Physics* 79.5 (May 2011), pp. 485–498. DOI: 10.1119/1.3549729. arXiv: 1006.1718 [hep-ph].

[247] R Slansky. "Group Theory for Unified Model Building". In: *Physics Reports* 79.1 (Dec. 1981), pp. 1–128. DOI: 10.1016/0370-1573(81)90092-2.

[248] F. Gursey, Pierre Ramond, and P. Sikivie. "A Universal Gauge Theory Model Based on E6". In: *Phys. Lett. B* 60 (1976), pp. 177–180. DOI: 10.1016/0370-2693(76)90417-2.

[249] Q. Shafi. "E(6) as a Unifying Gauge Symmetry". In: *Phys. Lett. B* 79 (1978), pp. 301–303. DOI: 10.1016/0370-2693(78)90248-4.

[250] Yoav Achiman and Berthold Stech. "Quark Lepton Symmetry and Mass Scales in an E6 Unified Gauge Model". In: *Phys. Lett. B* 77 (1978), pp. 389–393. DOI: 10.1016/0370-2693(78)90584-1.

[251] S. L. Glashow. "Trinification of All Elementary Particle Forces". In: *Fifth Workshop on Grand Unification*. July 1984.

[252] K. S. Babu, Xiao-Gang He, and Sandip Pakvasa. "Neutrino Masses and Proton Decay Modes in SU(3) X SU(3) X SU(3) Trinification". In: *Phys. Rev. D* 33 (1986), p. 763. DOI: 10.1103/PhysRevD.33.763.

[253] G. R. Dvali and Q. Shafi. "Gauge Hierarchy in SU(3)(C) x SU(3)(L) x SU(3)-R and Low-Energy Implications". In: *Phys. Lett. B* 326 (1994), pp. 258–263. DOI: 10.1016/0370-2693(94)91319-6.

[254] G. R. Dvali and Q. Shafi. "Gauge Hierarchy, Planck Scale Corrections and the Origin of GUT Scale in Supersymmetric SU(3)**3". In: *Phys. Lett. B* 339 (1994), pp. 241–247. DOI: 10.1016/0370-2693(94)90638-6.

[255] Thomas W. Kephart and Qaisar Shafi. "Family Unification, Exotic States and Magnetic Monopoles". In: *Phys. Lett. B* 520 (2001), pp. 313–316. DOI: 10.1016/S0370-2693(01)01187-X.

[256] S. Willenbrock. "Triplicated Trinification". In: *Phys. Lett. B* 561 (2003), pp. 130–134. DOI: 10.1016/S0370-2693(03)00419-2.

[257] Jihn E. Kim. "Trinification with $\sin^2\theta_W = 3/8$ and Seesaw Neutrino Mass". In: *Phys. Lett. B* 591 (2004), pp. 119–126. DOI: 10.1016/j.physletb.2004.04.017.

[258] J. Sayre, S. Wiesenfeldt, and S. Willenbrock. "Minimal Trinification". In: *Phys. Rev. D* 73 (2006), p. 035013. DOI: 10.1103/PhysRevD.73.035013.

[259] Thomas W. Kephart, Chin-Aik Lee, and Qaisar Shafi. "Family Unification, Exotic States and Light Magnetic Monopoles". In: *JHEP* 01 (2007), p. 088. DOI: 10.1088/1126-6708/2007/01/088.

[260] Christophe Cauet et al. "Trinification, the Hierarchy Problem and Inverse Seesaw Neutrino Masses". In: *Phys. Rev. D* 83 (2011), p. 093008. DOI: 10.1103/PhysRevD.83.093008.

[261] Jamil Hetzel and Berthold Stech. "Low-Energy Phenomenology of Trinification: An Effective Left-Right-Symmetric Model". In: *Phys. Rev. D* 91 (2015), p. 055026. DOI: 10.1103/PhysRevD.91.055026.

[262] Jamil Hetzel. "Phenomenology of a Left-Right-Symmetric Model Inspired by the Trinification Model". PhD thesis. U. Heidelberg (main), 2015. DOI: 10.11588/heidok.00018259.

[263] Giulio Maria Pelaggi, Alessandro Strumia, and Saverio Vignali. "Totally Asymptotically Free Trinification". In: *JHEP* 08 (2015), p. 130. DOI: 10.1007/JHEP08(2015)130.

[264] K. S. Babu, Sudip Jana, and Anil Thapa. "Vector Boson Dark Matter from Trinification". In: *JHEP* 02 (2022), p. 051. DOI: 10.1007/JHEP02(2022)051.

[265] K. S. Babu et al. "Trinification at the TeV Scale". In: *AIP Conf. Proc.* 1900.1 (2017). Ed. by Barbara Szczerbinska et al., p. 020002. DOI: 10.1063/1.5010106.

[266] Zhi-Wei Wang et al. "Safe Trinification". In: *Phys. Rev. D* 99.11 (2019), p. 115017. DOI: 10.1103/PhysRevD.99.115017.

[267] Digesh Raut, Qaisar Shafi, and Anil Thapa. "Monopoles, Exotic States and Muon g-2 in TeV Scale Trinification". In: *Eur. Phys. J. C* 82.9 (2022), p. 803. DOI: 10.1140/epjc/s10052-022-10727-w.

[268] Ta-Pei Cheng and Ling-Fong Li. *Gauge Theory of Elementary Particle Physics*. Reprinted with corrections. Oxford Science Publications. Oxford: Clarendon Press, 2011. ISBN: 978-0-19-851961-4.

[269] Hilmar Forkel. *A Primer on Instantons in QCD*. Nov. 2002. arXiv: hep-ph/0009136.

[270] Stefan Vandoren and Peter van Nieuwenhuizen. *Lectures on Instantons*. Feb. 2008. arXiv: 0802.1862 [hep-th].

[271] Ian Affleck. "On Constrained Instantons". In: *Nuclear Physics B* 191.2 (Nov. 1981), pp. 429–444. DOI: 10.1016/0550-3213(81)90307-2.

[272] A.A. Belavin et al. "Pseudoparticle Solutions of the Yang-Mills Equations". In: *Physics Letters B* 59.1 (Oct. 1975), pp. 85–87. DOI: 10.1016/0370-2693(75)90163-X.

[273] Eike Bick and Frank Daniel Steffen. *Topology and Geometry in Physics*. Lecture Notes in Physics volume 659. Berlin: Springer, 2005. ISBN: 978-3-540-23125-7.

[274] Marco Cirelli, Alessandro Strumia, and Matteo Tamburini. "Cosmology and Astrophysics of Minimal Dark Matter". In: *Nucl. Phys. B* 787 (2007), pp. 152–175. DOI: 10.1016/j.nuclphysb.2007.07.023.

[275] Alessandro Strumia. "Sommerfeld Corrections to Type-II and III Leptogenesis". In: *Nucl. Phys. B* 809 (2009), pp. 308–317. DOI: 10.1016/j.nuclphysb.2008.10.007.

[276] A. Denner et al. "Feynman Rules for Fermion-Number-Violating Interactions". In: *Nuclear Physics B* 387.2 (Nov. 1992), pp. 467–481. DOI: 10.1016/0550-3213(92)90169-C.

[277] John F. Gunion et al. *The Higgs Hunter's Guide*. Vol. 80. 2000.

[278] Marcela Carena, Ian Low, and Carlos E. M. Wagner. "Implications of a Modified Higgs to Diphoton Decay Width". In: *JHEP* 08 (2012), p. 060. DOI: 10.1007/JHEP08(2012)060.

Acronyms

2HDM *two-Higgs doublet model*

AMM *anomalous magnetic moment*

BAU *baryon asymmetry of the Universe*
BBN *Big Bang Nucleosynthesis*
BSM *beyond the Standard Model*

CKM *Cabibbo-Kobayashi-Masukawa*
CMB *Cosmic Microwave Background*

DI *Davidson-Ibarra*
DM *dark matter*
DW *domain wall*

EWSB *electroweak symmetry breaking*

FCNC *flavor changing neutral current*
FRW *Friedmann-Robertson-Walker*

GR *General Relativity*
GUT *grand unified theory,*

IA *initial abundance*
IH *inverse hierarchy*

LFV *lepton flavor violation*
LH *left-handed*

MTM *Majoron+Triplet model*

NH *normal hierarchy*

PMNS *Pontecorvo-Maki-Nakagawa-Sakata*

QFT *quantum field theory*

RH *right-handed*

SM *Standard Model*
SN *supernova*
SSB *spontaneous symmetry breaking*

TE *thermal equilibrium*

VEV *vacuum expectation value*
VL *vanilla leptogenesis*
VLL *vector-like lepton*

WO *washout*

YM *Yang-Mills*

Glossary

G	gravitational constant
H	Higgs doublet
Y_X	abundance of X
Y_X^{eq}	equilibrium abundance of X
$Y_{\Delta B'}$	baryon asymmetry
$Y_{\Delta L'}$	lepton asymmetry
$\eta_{B'}$	baryon-to-photon ratio
B'	baryon number
δ_i	relative deviation of Y_i from Y_i^{eq}
η	efficiency
$\mathcal{H}$	Hubble parameter
L'	lepton number
$\mathcal{A}$	anomaly factor
$\tilde{m}$	effective neutrino mass
μ_X	chemical potential of X
Y_N^0	normalization factor
ρ	energy density
ρ_c	critical energy density
T	temperature
a	scale factor
d_H	particle horizon
g	$\mathrm{SU}(2)_{\mathsf{L}}$ gauge coupling
g'	$U(1)_Y$ gauge coupling
g_*	effective number of degrees of freedom
g_s	$\mathrm{SU}(3)_C$ gauge coupling
k	curvature parameter
n_X	number density of X
s	entropy density
v_{SM}	SM VEV
z_X	$= \frac{m_X}{\mathsf{T}}$